MULTIAXIAL FATIGUE CRACK GROWTH IN RAIL STEEL

by

P.E.BOLD, B.Eng.

March 1990

A Thesis Submitted in Fulfilment of the Requirements of the Degree of Ph.D. of the University of Sheffield.

Mechanical and Process Engineering Department,
University of Sheffield,
Mappin Street,
Sheffield, S1 3JD.

SUMMARY.

In the introduction to a recent symposium on rolling contact fatigue, R.A.Smith stated that it was difficult to apply our greatly increased understanding of metal fatigue, to rolling contact fatigue, because of "the apparent lack of alternating tensile stresses to drive the cracks." He went on to say "alternating shear stresses are easily found, but the reproduction of continuous crack growth controlled by shear (Mode II in fracture mechanics terms), has proved to be near impossible." This project has demonstrated that under specific conditions this mode of growth does occur.

The project began by studying rolling contact fatigue defects, in particular the 'squat' defect in railway lines, and the stress analyses that have been performed on them. It was concluded that the largest stress cycle experienced by the cracks must be a shear stress. A series of tests were then performed that loaded a crack in pure shear, or a mixture of tension and shear, looking at the effects of using fully reversed shear loading, and the effects of applying tensile mean stresses to reduce the friction on the crack flanks. However these tests all produced less than one millimetre of mode II growth, before the cracks arrested or branched.

The final series of tests however applied a tensile load cycle before each shear load cycle. This time coplanar growth was produced, that is the crack grew in the direction of the maximum shear stress. This type of load cycle is a simplification of the load cycle calculated by Bower and Johnson of Cambridge University, where the tensile load is produced by fluid trapped in the crack.

Two crack growth rate formulae were produced that fitted the data, indicating that the growth rate was dependent on both the tensile and the shear parts of the cycle.

CONTENTS.

PREFACE.

This thesis is based on research carried out in the department of Mechanical and Process Engineering, University of Sheffield, between October 1986 and October 1989.

Except for commonly accepted concepts, and where specific reference is made to other work, the content of this thesis is original.

No part of this thesis has been submitted to any other university for the award of any degree.

ACKNOWLEDGEMENTS.

I would like to thank Dr. M.W.Brown, my supervisor, for many very helpful discussions, and his guidance in the whole project.

I would also like to thank Dr. R.Allen, Mr. R.Tomlinson and the other staff from British Rail Technical Centre for their assistance in the whole project.

The advice and guidance of Dr.A.Bower and Prof.K.L.Johnson of Cambridge University is gratefully acknowledged.

Thanks are also due to many of the technicians of Sheffield University's Mechanical Engineering department, especially to Mr.J.Smith, and to the members of computing services. I acknowledge too the assistance of Dr. B.Kenny, and Mr. J.Driver in making the photo-elastic specimen and testing it; and thank the postgraduate students and various members of staff of Sheffield University for their valuable discussions.

The finance for this project was provided by British Rail Research and the Science and Engineering Research Council in a CASE award.

I thank also Professors K.J.Miller and R.F.Boucher, past and present heads of the Department of Mechanical and Process Engineering at Sheffield University, for the use of the laboratory equipment.

NOMENCLATURE.

K_I	Mode I stress intensity factor.
K_{II}	Mode II stress intensity factor.
K_ε	Mode I strain intensity factor.
K_γ	Mode II strain intensity factor.
K_σ	Equivalent K_I in maximum tangential stress criterion.
K_τ	Equivalent K_{II} in maximum shear stress criterion.
R	Minimum load / maximum load
σ, τ	Applied tensile and shear stresses.
ε, γ	Tensile and shear strains.
r, θ	Polar coordinates from the tip of the crack.
x, y	Rectangular coordinates from the tip of the crack.
σ_{xx}, σ_{yy}	Tensile stresses across x and y planes respectively.
τ_{xy}	Shear stress across x and y planes.
a	Crack length.
N	Number of cycles.
C, m	Constants from Paris law.
ε_p	Plastic strain.

k,n	Constants defining the cyclic stress strain curve, being the cyclic strength coefficient and the strain hardening exponent respectively.
T	The tensile strength of a material.
μ	Coefficient of friction.
M	Bending moment.
Q	Shear force.
S_1, S_2	Distances of inner and outer supports from axis of asymmetry in four point bending.
S_0	Distance of crack from axis of asymmetry in four point bending.

INTRODUCTION.

In the introduction to a recent symposium on rolling contact fatigue, R.A.Smith stated that it was difficult to apply our greatly increased understanding of metal fatigue, to rolling contact fatigue, because of "the apparent lack of alternating tensile stresses to drive the cracks." He went on to say "alternating shear stresses are easily found, but the reproduction of continuous crack growth controlled by shear (Mode II in fracture mechanics terms), has proved to be near impossible" [1]. This project investigated the effects of alternating shear stresses, and more complex mixed mode loadings, in an attempt to resolve this dilemma.

The subject is perhaps an ideal one to study for a Ph.D. in engineering. On the one hand it looks at one of the great paradoxes of fatigue, and it therefore provides much fascination to the academic. Every calculation on the crack tip conditions in rolling contact fatigue has predicted that the crack is loaded predominantly in shear. When fatigue tests have been performed on cracks in pure shear though, they have branched into cracks growing perpendicular to the tensile stress field on one side.

On the other hand the subject is concerned with a very costly industrial problem, especially for the railway industry. Currently British Rail have to replace around 1000 lengths of rail each year, at a cost of around £1000 a rail, because of a rolling contact defect known as the 'squat'. If the rate of growth of these cracks could be calculated, then appropriate action might be taken to save considerable sums of money.

The starting point of this work was to look at what was known about the stresses at crack tips in rolling contact fatigue, and to compare that with the relevant literature on metal fatigue. The work of Bower and Johnson at Cambridge, which was finished during this project, has clarified the situation enormously. The aim of this work was then to perform fatigue tests to fill in the gaps in our understanding, and to reproduce continuous fatigue crack growth predominantly controlled by shear.

The majority of fatigue crack growth tests have involved the application of uniform cyclic tensile or shear loads to simple specimens. The general philosophy behind it has been that the resulting crack growth laws can be used in a wide variety of situations, by using the maximum

stress intensity ranges in any complex cycle. In recent years there has been an increased awareness of how plasticity, multiaxial stress fields, variable amplitude loadings, and the environment can effect the fatigue crack growth rate and direction. In this project it was discovered that the complex stress cycle experienced by a real rolling contact fatigue crack tip produced a completely different form of growth to the first approximation that was made to it.

Reference.

1. R.A.Smith. 'Contact Fatigue'. Cambridge University Engineering Department. 29 September 1988.

CHAPTER 1.

LITERATURE SURVEY.

1.1 The Problem of Failures in Rails.

1.1.1 The 'Squat' Failure In Rails.

There are 3 main types of failure in rails:

1. Bolt hole cracks. In jointed track, bolt holes act as stress concentrations, and have frequently led to fatigue cracks. However the use of continuously welded track, and a programme of bolt hole cold expansion, have or will reduce this problem enormously. The bolt hole expansion technique puts a compressive residual stress around the bolt hole, which inhibits fatigue crack growth.

2. 'Taches Ovales'. In some rails hydrogen embrittlement causes a crack to initiate from the centre of the rail head. British Steel now Vacuum de-gas the steel, so in modern lines this should be less of a problem. However at present there are still hundreds of miles of older track in use where such defects may be growing. In addition 'taches ovales' can start from inclusions, which do occur in modern rails.

3. 'Squats'. 'Squats' are rolling contact fatigue defects. Before 1975 they accounted for only about 3 failures per year. They now produce more than any other. Unlike the other failures they are not associated with one particular structural feature of rails, like bolt holes, but can occur almost anywhere. They have been found in all types of rail steel, and so are probably not associated with metallurgical defects. They occur most frequently on tracks with the highest speed trains and the highest annual tonnage, and are a particularly serious problem on the West Coast main line, and the London to Bristol line where the trains can travel at over 100 mph. 'Squats' are the subject of this work. [1-5].

1.1.2 Causes of the initiation of the 'Squat'

'Squats' tend to form on the high rails of curves, where the contact stresses are highest. These stresses produce plastic deformation involving metal flowing in the direction of motion of the train, and towards the

inside corner, the gauge corner, of the rail.

'Squats' are also associated with three features of the running surface:

1. Periodic holes. Indentations about 5mm across, can occur about every 3m on rails which subsequently form squats. The exact cause of these holes is not known but it is assumed that it is because of something picked up on a wheel. The series of holes may go on for some miles. Plastic deformation around these holes causes the lip of the hole to flow towards the centre, forming a starter crack for a squat.

2. Corrugations. Plastic deformation of rails leads to the running surface becoming corrugated. In the running on side, that is the uphill side from the trains point of view, 'squats' can form. The mechanism is not fully understood.

3. Welds. Welds often are the origins of 'squats'. The reasons are not fully understood, but the differential wear rates resulting from the increased hardness, and the possibility of weld defects may be involved, [1-5].

1.1.3 The Development of a 'Squat'.

'Squats' are three dimensional cracks, and the details of their geometry vary to a certain extent depending on how they start. Fig. 1.1 shows how they develop from an angled crack on the high rail of a curve, and Fig. 1.2 is a photograph of a section through a 'squat'. The 'squats' growing from these angled cracks, start by growing down into the rail head at an angle of about 10° to the upper surface, mainly growing away from the gauge corner, and in the direction of the traffic. They then break out again having grown across the rail. 'Squats' starting from indentations, corrugations, or welds also grow at this 10° angle to the surface, but their shapes are different.

In all the 'squats' these cracks then grow along the rail in both directions, but grow more quickly in the direction of motion of the train. Once they have reached a length of between 20 mm and about 100mm they start to form branch cracks at about 55° to the surface. The first 'squats' that were investigated seemed to branch later than more recent ones, though the reason for this is not known. The flatter crack can continue to

grow close to the surface, after a branch has formed. This crack is in itself not a great danger to trains as if it flakes off, then the worst that can happen is that the train will have a rougher ride. The 55° crack however will lead to catastrophic failure, if it is left to grow. The continued growth of the 10° crack will obscure the 55° crack from normal methods of ultrasonic detection. It is not known how long the whole process takes and therefore British Rail (B.R.) at the moment have a policy of removing all squats when they reach a size of about 25 mm, [1-5].

It appears that a large part of the life of a track is spent in the stage of growth where the crack is a few millimetres long. The very early growth may be quick because of the large scale plasticity under the contact loading of the wheel. When a crack starts to branch down, growth may be quick because the crack is long, and is subject to large bending forces. In the intermediate stage, where the crack is growing out of the high contact stress regime, the wear of the track, which removes some of the crack from the surface as it grows from the tip, may well be significant.

1.1.4 Possible Solutions to the Problem.

There are four main alternatives to inspection and rail replacement currently being considered, to try to reduce the occurrence of 'squats'.

1. Grinding. B.R. have for some time been grinding the surface of the track to remove corrugations, and so to give a smoother ride. It has been suggested that by grinding more of the track away, in areas susceptible to squats, then the squats might be removed before they reached any great depth. The problems associated with this method are basically concerned with the amount of metal that would need to be removed. 1/3 mm was tried and it was found that the squats were still there. It is possible that 1mm would need to be removed each time the rail is ground. This would involve an enormous amount of time, expense and inconvenience. It also has the problem of seriously reducing the life of the track, as a considerable quantity of the rail is removed.

2. Planing. It was thought that it might be better to plane away 1mm, rather than having to grind it all. However attempts so far have left an unacceptable surface finish, and so this method will probably be abandoned.

3. Reducing the Stresses. It is not possible to greatly reduce the weight of a diesel train, so the only way to reduce the stresses in the rails is to increase the area on which that weight is distributed. This might be done by using a lower modulus metal than steel in the tyre. Again this is being considered, but a suitable material has to be found. Alternatively a larger number of wheels might be used, though the dynamics of going round curves does create problems.

4. Changing the Steel. Rail steel is a fairly simple medium carbon steel. It would be possible to change all the rails for a higher strength steel. However this would be very expensive. Also it would not necessarily improve the situation because the higher yield strength would result in smaller contact patches, and therefore higher stresses, [1-5]

This work aimed to clarify the mechanics of 'squat' development, and thus provide insight into the best method of controlling the problem.

1.2 Theoretical Stress Analysis, and Fatigue Crack Growth.

1.2.1 Hertzian Contact Stresses.

The stresses between two curved surfaces in contact were first calculated by Hertz in 1881, for a purely elastic, static loading. Since then the theory has been expanded to consider the effects of friction in rolling and sliding contact, and the effects of plastic deformation, [6]. The application to the fatigue of rails is obvious, and much work has been done on the stresses in a rail due to wheels. The details of this work are beyond the scope of this report, but it should be noted that large plastic deformations occur in the rails [7-10]. These deformations almost certainly cause the initiation of some squats, and have made the analysis of the crack loading much more complicated than would have been the case if a purely elastic situation could have been considered.

1.2.2 Fracture Mechanics.

The basis of linear elastic fracture mechanics (LEFM) is that the in plane stresses around a crack tip, as shown in Fig. 1.3, can be expressed by the equations [11,12] :

$$\sigma_{yy} \simeq \frac{K_I}{\sqrt{(2\pi r)}} \cos\frac{\theta}{2}\left[1 + \sin\frac{\theta}{2}\sin\frac{3\theta}{2}\right] + \frac{K_{II}}{\sqrt{(2\pi r)}} \sin\frac{\theta}{2}\cos\frac{\theta}{2}\cos\frac{3\theta}{2}$$

$$\sigma_{xx} \simeq \frac{K_I}{\sqrt{(2\pi r)}} \cos\frac{\theta}{2}\left[1 - \sin\frac{\theta}{2}\sin\frac{3\theta}{2}\right] - \frac{K_{II}}{\sqrt{(2\pi r)}} \sin\frac{\theta}{2}\left[2 + \cos\frac{\theta}{2}\cos\frac{3\theta}{2}\right] \quad (1.1)$$

$$\tau_{xy} \simeq \frac{K_I}{\sqrt{(2\pi r)}} \sin\frac{\theta}{2}\cos\frac{\theta}{2}\cos\frac{3\theta}{2} + \frac{K_{II}}{\sqrt{(2\pi r)}} \cos\frac{\theta}{2}\left[1 - \sin\frac{\theta}{2}\sin\frac{3\theta}{2}\right]$$

Where $K_I = \sigma\sqrt{(\pi a)}$,

and $K_{II} = \tau\sqrt{(\pi a)}$

σ and τ are the applied normal and shear stresses acting on a plane parallel to the crack plane.

These equations are the first terms in a series expansion containing an infinite number of terms in increasing powers of r. They are derived from the theory of elasticity, and so assume that the material remains perfectly elastic everywhere. The terms $K_I/\sqrt{(2\pi r)}$ and $K_{II}/\sqrt{(2\pi r)}$ will tend towards infinity as r approaches zero, whereas terms in higher powers of r will tend to zero. The only exception is the T stress, a constant stress, independent of r which is added to the σ_{xx} stress. This will also be negligible compared to K_I and K_{II} very close to the crack tip. The terms K_I and K_{II}, called the stress intensity factors, can therefore be used to compare very different cracks. That is if two cracks have the same K_I and K_{II} then they will behave in a similar manner.

However, real materials will yield near the crack tip where the stress is above the yield stress, and so these equations are not accurate. The stress needs to be redistributed, as shown in Fig. 1.3. If the redistribution is small, 'small scale yielding', then the stress intensity factors will still enable cracks to be compared. But if the plastic zone is too large, then other parameters are required. Elastic plastic fracture mechanics is then used, which considers among other things the total

strain, with elastic and plastic components, and the size of the plastic zone. The T stress, and the other terms in higher powers of r will become significant as they affect the size of the plastic zone. Strictly LEFM only applies where the plastic zone, r_p, is less than 1/50 of the crack length a, and where the bulk stress, σ_b, is less than 1/3 of the yield stress σ_y. In reality LEFM has been found to work well up to when r_p is less than 1/20 of a, [12-14].

1.2.3 Fatigue Crack Growth Rates Under Proportional Loading.

LEFM was first applied to metal fatigue by Paris and Erdogan in 1961 [15]. They were looking at crack growth rates under sinusoidal tensile loading. In the direction of crack growth the value of K_I would have varied sinusoidally with the load, and the value of K_{II} would have been equal to zero. This is the simplest form of proportional loading. That is loading where the ratio between K_I and K_{II} is a constant. They produced the Paris law:

$$\frac{da}{dN}=C(\Delta K_I)^m \qquad (1.2)$$

where da/dN is the crack growth rate. C and m are material dependent constants derived from experimental crack growth tests.

This law describes a period of stable crack growth as shown in Fig. 1.4. At lower stress intensity factors the crack would not grow, and a threshold value of ΔK can be found ΔK_{th}. At higher values of ΔK_I, approaching ΔK_{IC} when fracture occurs, the growth rate accelerates more quickly. This is because of the formation of very large plastic zones, and a change in the mechanism of fatigue [13].

When the plastic zone size is too large, and LEFM is not applicable, various other laws of crack growth have been formulated [14]. One of the simplest methods is the strain intensity approach[16]. This is simply a modification of the stress intensity to take into account the amount of plasticity. The strain intensity for a uniaxial stress field is defined as:

$$K_\varepsilon = \varepsilon\sqrt{(\pi a)} \qquad (1.3)$$

in general the strain is calculated using von Mises yield theory. More details can be found in Appendix 5.

Alternatively, for highly plastic stresses, Tomkins [17] gives the

equation:

$$\frac{da}{dn} = \frac{\pi^2}{8}\left[\frac{k}{T}\right]^2 \Delta\varepsilon_p^{2n+1} a \qquad (1.4)$$

where: T is the tensile strength of the material,

and $\Delta\varepsilon_p$ is the plastic strain range.

Here k and n are constants that define the cyclic stress strain curve, being the cyclic strength coefficient and the strain hardening exponent respectively:

$$\sigma = k \ \Delta\varepsilon_p^{\ n} \qquad (1.5)$$

Crack growth laws have also been produced using the plastic zone size [18]. This has the advantage that it describes the conditions around a crack tip more directly than the other parameters, and it works well. However, calculating the size of the plastic zone is much more involved than the strain based approaches. Since these simpler approaches also appear to work well, they are much more widely used.

Another important factor in the estimation of crack growth rate is crack closure. So far it has been said that crack growth rate depends on the range of stress intensity factor, ΔK. However, if the crack is in compression there will be no stress intensity at the crack tip. One solution is to neglect the compressive part of the cycle. However this is not a perfect solution as plastic deformation [19], oxide formation [20], and roughness [21] can all cause the crack to be closed, when the bulk stress is tensile. Also, residual stresses may cause the crack to be open when the bulk stress is compressive.

Paris' work and the vast majority of the early work in fatigue was just concerned with the tensile mode of crack growth, mode I in fracture mechanics terms, under a uniaxial stress field. This was because the vast majority of the failures have occurred in mode I. However it is also possible to get at least limited amounts of growth in Modes II and III, shear and tearing modes, as defined in Fig. 1.5 [22,23]. All three modes may be involved in the squat failure in rails, but this project is primarily concerned with mixed modes I and II. This is because this two dimensional approximation needs to be understood before a three dimensional

representation can be considered.

Currently there are no established crack growth rate laws for modes II and III. The work that has been done suggests that a law of the same form as the Paris law might be appropriate for mode II, but the lack of experimental data has made it impossible to define one. The reasons for this will be discussed in section 1.4.

1.2.4 Direction Of Crack Growth in Proportional Loading.

A wide variety of theories exist that have been used to predict the direction of crack growth under mixed mode I and II loading, in fatigue and fracture. Generally they have only considered proportional loading, that is loading where the ratio between K_I and K_{II} is kept constant during a cycle. Mainly they involve the calculation of the maximum of a factor assumed to control the crack growth, and the assumption that the crack will grow in the direction of that maximum. In particular there are the maximum tangential stress [24], the maximum tangential principal stress [25], the maximum tangential strain [26], the maximum K_I [27], the maximum ΔK_I [27] and the maximum crack growth rate [27] criteria. There are also the minimum strain energy density theory [28], and $K_{II}=0$ criterion [27]. Various modifications have been suggested, and certain limitations found to individual theories, but in general reasonable agreement is found between them, and also reasonable agreement is found between them and the experimental data available. However, they all predict the direction of a mode I crack under whatever loading is used, [29-31].

Two theories exist in the literature that have been used to try to predict whether mode I or mode II growth should occur and the corresponding threshold or fracture loads. Firstly Otsuka et al [32-35] used a theory of the maximum shear stress, as well as the maximum tangential stress, saying that crack growth should occur when the critical stress is reached, and that the crack should grow in the mode whose critical value is reached first. The values are defined by:

$$K_\sigma = \sigma_\theta \sqrt{(2\pi r)} = \cos\frac{\theta}{2}\left[K_I \cos^2\frac{\theta}{2} - \frac{3}{2} K_{II} \sin\theta \right]$$

$$K_\tau = \tau_{r\theta} \sqrt{(2\pi r)} = \frac{1}{2}\cos\frac{\theta}{2}\left[K_I \sin\theta + K_{II}(3\cos\theta - 1) \right] \qquad (1.6)$$

Secondly Melin [36] looked at the fracture of plates under mixed mode I and II static loading, using the K_I and K_{II} factors at the tip of an infinitesimal branch crack at an angle θ to the main crack. He calculated these stress intensity factors for loadings from pure mode I to pure mode II based on the work of Khrapkov [37]. His theory was that if the ratio between K_{IC} and K_{IIC} were known, then the mode of crack growth, and the load at which it should occur, could be calculated for any mixed mode loading. Chatterjee [38] carried out similar calculations for only mode I stress intensities, using branch cracks of finite length. This may be useful as a basis for refining Melin's theory because near threshold microstructural effects might produce a small branch crack.

Fig. 1.6 shows that there is very little difference in the results obtained from these theories. From the point of view of fracture mechanics, Melin's approach would seem to have the more obvious theoretical base, but Otsuka's model is much simpler to use, because the calculations are much simpler. Both the theories however depend on the assumptions of LEFM. The local stresses under the wheel in a rail are highly plastic, however, and so an elastic plastic model of this type would be useful for further analysis.

A basis for this might be the theory used by Gao Hua et al [22] who looked at the size of the plastic zone, and fracture ductility for pure mode II and pure mode I loading. They said that the plastic zone size at threshold should be a constant, independent of the mode of loading, and using the fracture ductility's were able to calculate the loads at which this should occur. This however considers that the crack growth would occur in a mixed mode manner. It will be shown later that under proportional loading crack growth always appears to be either mode I, mode II or mode III, not some direction in between. However Gao Hua's theory could be modified to account for this.

1.2.5 Crack growth directions and rates under non-proportional loading.

When the ratio between K_I and K_{II} is not constant, then the above criteria run into problems. The maximum value of a factor may be in a different direction from the maximum change of that factor, but both the maximum value, and the range can affect the crack growth rate. In rails, the locomotive wheels which apply the driving force for the train, will produce a different stress cycle to the other wheels, and therefore a different crack growth direction. When the brakes are applied the stress cycle will change again. The only unambiguous approach used in such circumstances seems to be the maximum crack growth rate criterion, that is, presuming the crack will simply grow in which ever direction makes it grow fastest.

Pineau et al used this quite successfully to predict crack directions for mode I cracks under non-proportional loads [27]. He loaded cracks in a biaxial stress field so that the peak value of the maximum tangential stress criterion $K_{\sigma max}$ for a given cycle occurred at a different angle to the maximum range, $\Delta K_{\sigma max}$. He showed that neither $K_{\sigma max}$ nor $\Delta K_{\sigma max}$ alone could predict the crack angle, but rather that it was neccessary to find the combination of K_σ and ΔK_σ that would give the maximum growth rate, according to ordinary mode I crack growth laws. To apply this more generally however it would be necessary to develop non-proportional crack growth laws for the stress cycles involved.

Under the non-proportional loadings looked at so far, certain modifications have been made to the growth rate laws. Socie et al suggested that the extra strain hardening in non-proportional loading would produce different sized and shaped plastic zones, and different plastic strains [39]. M.C.Smith looking at mixed mode I and II, and Hay looking at torsion, both showed that friction can seriously reduce growth rates [40-42]. At the moment there is no widely accepted method for dealing with the very wide variety of non-proportional cycles that could be applied. It is hoped that this project will provide growth rate expressions for the loading occurring in 'squats', and therefore expressions that can be used in the maximum growth rate criterion to predict crack directions in 'squats'.

Crack growth laws also do not accurately predict growth rates under variable amplitude loading. A large tensile load cycle will tend to blunt a

crack tip, and leave a large residual plastic zone. Subsequent smaller load cycles may then propagate a crack more slowly than would be predicted by the Paris law. This is also an area where much work is needed if growth rates are to be calculated for the combined loadings of heavy locomotives with high tractive forces, heavy freight trucks with no tractive force, and light coaches.

1.3 Rolling Contact Fatigue and Wear.

1.3.1 Previous Experimental Work in Rolling Contact Fatigue.

In 1935 Way tested about 80 steel rollers in rolling contact fatigue, looking at the formation of pits [43]. Pits are like squats in that they form by cracks growing at a shallow angle to the surface, but rather than branching down into the roller they branch up, to leave a pit in the surface. He showed that for pits to form it was necessary for a lubricant to be present, and that the viscosity of the lubricant had to be less than a critical viscosity, μ_{cr}. The value of μ_{cr} was less than the viscosity that would stop metal to metal contact, ie for pits to form there was always metal to metal contact, but if there was metal to metal contact, pits did not necessarily grow. The conclusion he came to was that for the cracks to grow they had to be filled with lubricant. If there was no lubricant, or if the lubricant was too viscous, then the cracks could not be filled and so no pits formed. Recent work by Dawson [44], and Hill and Clayton [45] has confirmed this. The same appears to be true of 'squats' in rails: in Japan in the mid 1950's, the railway operators started putting water on the tracks to try to improve the fuel economy. They then suffered great problems with 'squat' like defects, until they stopped putting water on the track [3]. In Britain, with a temperate climate, this solution is unfortunately not possible.

Hahn et al have carried out a series of experiments on rolling contact fatigue in Aluminium where the roller is shrunk onto a cylinder before testing so that the surface of the roller is always in tension [46]. This was to imitate the loading found in the inner race of an aircraft bearing. Sometimes the fatigue cracks turned into the roller like 'squats', rather than just forming pits. This suggests that the tension found in the

bearing race, and also that required in rails to stop them buckling, is necessary for the cracks to turn inwards.

There are other features of rolling contact fatigue worthy of a mention at this point, which any satisfactory theory has to explain. Firstly the pitting cracks or squats only grow in the driven roller, not the driver, even if the driver is made out of a less fatigue resistant material. This is because cracks will not propagate under a braking force, ie the force experienced by the driver, rather than because they will not start to grow in the first place. This was shown by Nakajima et al, who performed a disk machine experiment in which they first subjected a disk to a driving traction, and then reversed the tractive force when pits appeared. No more pits were formed after the forces were reversed, [47].

Secondly, the cracks always grow more quickly in the direction of motion of the driver, ie the direction in which the train is moving [47,48]. Fig. 1.2 shows this for a 'squat'.

Finally experiments have shown that large residual shear plastic deformations occur in the surface of the rollers under driving traction, suggesting that the predominant loading of rolling contact fatigue cracks is mode II, when they are growing at a shallow angle to the surface [46].

1.3.2 The Application of Fracture Mechanics To Rolling Contact Fatigue.

Much work has been done on the theoretical stress analysis of surface cracks under Hertzian contact stresses. The earlier work, which ignored potential effects of fluid in the cracks, calculated that the cracks were predominantly loaded in mode II [46,49,50]. However attempts to grow mode II cracks in laboratories, in steel and under simple mode II loading, have only produced very limited quantities of mode II growth, followed by mode I branch cracks. Details of these experiments are given later in section 1.4.2. Murakami et al, and Bower then performed similar calculations but included the effects of the lubricant [51,52].

The most detailed work was done by Bower and Johnson, at Cambridge University, and so we will discuss that in more detail here. They used the method of distributed dislocations to look at experimental rolling contact fatigue, with simple rollers. Their analysis was purely elastic, and they

modelled the crack face interactions as coulomb friction with a coefficient of friction, μ. They considered three possible effects of water, Fig. 1.7.

Firstly the water might simply lubricate the crack so that the ΔK_{II} value is only moderately reduced by friction, Fig. 1.7a. For this they used a value of μ of 0·1 instead of 0·25 that they used elsewhere. The details of one of the load cycles calculated are given in Fig. 1.8, which shows the mode II cycle. The notation is explained in Fig 1.9. It should be noted that this notation is different from that used elsewhere in this thesis, with a being the contact patch radius rather that the crack length, and c being the crack length. With no fluid pressure, no significant mode I load is generated. If the maximum tangential stress (MTS) and maximum shear stress (MSS) criteria are applied to this loading, then three possible crack directions are predicted. Fig. 1.10 is a radial plot showing the relative magnitudes and directions of these maxima with respect to the crack. The method used to calculate the values in this plot was to first find the minimum value of K_φ, as defined in equation 1.6, that occurred during the cycle, for angles from −180° to +180° to the crack. The minimum of K_φ was set to zero as a negative value could be found for all directions, and as the approximation was made that when the value was negative, no stress intensity occurred. The maximum range of K_φ and K_τ was then found for each point in the cycle, by calculating the range for each direction in turn.

If the crack grows in mode I then the maximum tangential stress has two maxima, one for a crack growing up and one for it going down. The reason that there are two maxima is that the mode II loading is approximately fully reversed, and so in one half of the cycle one crack flank is in tension and the other in compression, and in the other half it is the opposite way round. If the crack grows in mode II, then the maximum shear stress predicts coplanar crack growth. The two mode I branch directions fit well with the two possible branch crack directions in rolling contact fatigue, either branching up to remove a flake of material as happens in normal pit formation, or branching down through the specimen as happens in 'squats'. The shallow angled growth would fit with the mode II growth direction if it is in some way possible to grow mode II cracks.

The maxima are found in fixed directions throughout the cycle because there is only mode II loading applied. If there is both mode II and

mode I loading, and the ratio between them is not kept constant during a cycle, ie the loading is non-proportional, then the direction of the maxima will vary during the cycle, and the loci of the instantaneous maxima will be a loop of some sort.

The second possible effect of water that they considered, was that the water might pressurise the crack so that the internal pressure was equal to the Hertzian contact pressure, Fig. 1.7 b. This produced very high values of ΔK_I, which would have given growth rates much higher than are found in experiments. It therefore had to be rejected as a model.

The third possible effect was that the water might be trapped inside the crack when the crack mouth shuts, giving a mode I loading, Fig. 1.7 c. This gave a complicated non-proportional cycle, as shown in Fig. 1.11. Fig. 1.12 shows the MTS and MSS criteria. The two branching directions and the coplanar growth direction are again predicted by the tangential and shear stress maxima. The fact that the maxima occur in different directions during the cycle is due to the non-proportionality.

Bower concluded both the lubrication and the fluid entrapment models give load cycles consistent with what is known about rolling contact fatigue growth rates. Also both predict that the crack would grow more quickly in the direction of motion of the loading as is observed in practice. The practical difficulty of growing mode II cracks under simple mode II loading led him to reject model the lubrication model as a likely explanation, and he suggested that model the fluid entrapment model required a better understanding of non-proportional loading before it could be properly evaluated. The next section will discuss the relevant types of fatigue tests that have been performed, their results, and will compare the load cycles with the more complicated cycles predicted by the lubrication and fluid entrapment models.

For completeness, it should be mentioned that Hahn et al also used fracture mechanics to try to predict crack growth rates under rolling contact fatigue [46]. Their model was much simpler, ignoring friction and possible effects of a lubricant. However they were looking at Aluminium for which mode II crack growth data have been produced [30-33]. Their results were of the right order of magnitude, in spite of the simplicity of their model.

1.3.3 Wear.

Wear is the process by which material is removed from a surface, due to the action of another surface sliding against it. The material is removed in small thin fragments. Various workers [53-57] have tried to use fracture mechanics to describe wear, using the delamination theory of wear. It is generally believed that the process is dominated by mode II loading, though the actual cycle under gone by a wear crack will be different from a rolling contact fatigue cycle. The lack of mode II experimental data inhibits the analysis.

1.4 Mixed Mode Fatigue.

1.4.1 Methods of Loading In Mixed Mode Fatigue.

There are many methods of loading in mixed mode fatigue, but there are three main types that are relevant to this work.

1.4.1.1. The Angled Crack in a Tensile Specimen.

Most of the early work on mixed mode fatigue or fracture was done on this type of specimen, Fig. 1.13 a, [24,58,59]. The mixed mode loading changes from being pure mode I when the crack is perpendicular to the applied tensile stress, to mixed mode I and II as the angle θ increases. As θ approaches 90°, the loading approaches pure mode II, but the magnitude approaches zero, as shown by the Mohr's circle in Fig 1.13 b. Fig. 1.14 shows the maximum tangential stress and maximum shear stress criteria plotted radially for these specimens, as was done earlier for Bower and Johnson's rolling contact fatigue calculations. The loading used is for θ = 45°, giving K_I/K_{II} = 1·0. This predicts two possible growth directions. If the crack propagates in mode I then a branch would form growing at an angle of about 53° to the crack. If it propagates in mode II, a branch would grow at about 16° to the crack on the other side. The ratio between the maxima, K_τ/K_σ = 0·60. Because the loading is proportional the maxima are at constant angles throughout the cycle.

1.4.1.2. Mixed mode Specimens.

A wide variety of specimens have been designed so that the crack is situated where there is pure mode II loading. The simplest is perhaps the asymmetric 4 point bend specimen [22,60-63], as shown in Fig 1.15. The crack can be placed in a position of zero bending moment for pure mode II loading, though it does need to be positioned very accurately with respect to the grips. Moving the specimen slightly to one side gives a mixed mode condition. The magnitude of the stress intensity factors can be calculated from M and Q using simple bending theory as shown, with the calculations of Wang et al [64]. Here M and Q are the bending moment and shear force respectively. The Mohr's circle representation, and the maximum tangential and shear stress criteria are plotted in Figs. 1.16 and 1.17 respectively.

Fig. 1.17 shows that in asymmetric four point bending there are also two possible growth directions, predicted by the MTS and MSS criteria. If the crack propagates in mode II, it will continue in the same direction. If it grows in mode I it will form a branch crack at about 70°. The ratio between K_τ and K_σ is this time equal to 0·87, so the mode II growth should be more likely to occur in these specimens than in angled crack ones.

However, if the loading arrangement is further refined to allow fully reversed loading, the MTS and MSS radial plot has three maxima as shown in Fig. 1.18.

There are two MTS maxima because both the tensile and the compressive parts of the loading produce peaks; one for each crack flank, the other crack flank being in compression at that point. It also gives two MSS maxima, which are both coplanar. Adding them together to give the range of K_τ gives the maxima twice the size of the ordinary four point bending prediction. This is much closer to the loading predicted by Bower, as shown in Figs. 1.10 and 1.12. The ratio between ΔK_τ and ΔK_σ now becomes 1·74. This is an over estimation of the likelihood of mode II occurring compared to the ordinary asymmetric four point bending, because it ignores the fact that each mode I maximum will have an associated compressive stress cycle. Under simple mode I loading this extra compressive load would increase the growth rate. However this effect will only modify the criterion, and does not change the point that mode II growth is more likely in fully reversed mode II loading than in unreversed loading.

A wide variety of other specimens, as shown in Fig 1.19, work on the

same principle as the asymmetric four point bending. They all place the crack in a plane of zero bending moment [66-71]. If carefully enough machined, and if deformations are negligible, they should all give pure mode II loading, and a limited number of other mixed mode conditions.

Torsional loading of thin walled tubes has also been used to produce mode II loading [72,73], which is a simple method but it has the problem that the specimen distorts when the crack reaches a finite size. Cox and Field also loaded a square sectioned bar in combined bending and torsion, giving predominantly mode I loading at the corners, and mode II loading at the centre [74].

Mode II loading may also be obtained by loading through pins [24,75]. However this seriously limits the load that can be applied, and perhaps does not produce a simple mode II load because of the effects of loading through a point.

1.4.1.3. Biaxial Specimens.

Biaxial Specimens allow more complicated stress fields to be created for non-proportional loading experiments, Fig. 1.20. Type A [61,62,76,77] will give an equibiaxial stress field if both axes are in tension, or a pure shear field if one is in tension and the other in compression. If a crack is at 45° to the axes in the pure shear field, then it will be in pure mode II loading. It is possible therefore to obtain all the types of stress field produced by the mode II specimens mentioned so far, and a wide range of others. It is possible to give a mode I cycle followed by a mode II cycle; or cyclic mode II loading with static mode I superimposed. The former type of loading is of interest because Bower's fluid entrappment model [51] predicted that a mode I load would be applied before a mode II load. The latter cycle is of interest because it opens the the crack, allowing the mode II displacement to reach the crack tip rather than being reduced by friction, in the same way as Bower suggested that the fluid in the rolling contact fatigue cracks might reduce friction.

However this cycle does not merely reduce the friction, but it also increases the MTS maxima because the static K_I loading keeps K_σ positive for more of the cycle. For example a specimen loaded under cyclic shear with a mean stress large enough to keep the applied loads tensile all the

time, allowing the mode II load to reach the crack tip, also brings the ratio of ΔK_τ to ΔK_σ back down to 1·12 from 1·74.

The types of non-proportional cycle that can be applied to type A specimens are still limited hpowever, because the principal stress axes are fixed. For example to attempt to produce mode II growth, a cyclic shear load, with a static uniaxial tensile stress perpendicular to the crack, is desirable. This would open the crack, and affect the MTS values in the same way as an equibiaxial load, but the stress intensity of branch cracks of finite length would be lower because they would be growing at an angle to the mean stress rather than perpendicular to it. However with this specimen, that is not possible. The tensile load has to be an equibiaxial load, not a uniaxial one. This puts a mean tensile stress across the branch cracks as well as across the initial crack.

Type B [32-35,40,41] allows similar loading to A, and the actual specimen is much cheaper to manufacture. The mode II load is applied using just one axis, as in a conventional mode II specimen, while the mode I load is applied by the other axis. The mode I load this time is a uniaxial load, not an equibiaxial one. However type B specimens have the disadvantages that the stress field is not so pure, due to the stress distribution in bending specimens, and that there is not so much room for crack growth. Also type B is not nearly as good for investigating branch crack growth, because the stress state will change as soon as the crack has moved outside the plane of the original crack.

1.4.2 Mixed Mode Fracture.

Experiments have been carried out on the fracture of PMMA, a near perfectly elastic material, using axially loaded plates with central and edge cracks at an angle to the loading axis [24]; using point loading through pins [24], and using other mode II specimens [65,66,71]. In all of these experiments only mode I branch crack growth was recorded.

Melin compared his theory with some of the PMMA mixed mode fracture data [36], and found reasonable agreement, Fig. 1.21. The MTS criterion works equally well. He suggested that the reason that no mode II growth was found in those experiments was that the ratio between K_{Ic} and K_{IIc} is about 1, This makes mode I more favourable, because even under pure mode

II loading, a mode I stress intensity is formed at an angle of about 70° to the crack, 1·15 times the magnitude of the mode II stress intensity. See sections 1.2.4 and 1.4.1.

Gao Hua et al tested a high strength steel, GC-4, a medium strength rotor steel, 30Cr2MoV, and nodular cast iron using asymmetric three point and four point bend specimens [60]. Again only mode I branch crack growth was produced, but this time the mode I branch crack load was much higher than predicted by the MTS criterion or Melin's theory, as shown in Fig. 1.22. The reason suggested by Gao Hua et al was that the plastic zones, and displacements near the crack tip were very different from those under pure mode I loading, and so it was unreasonable to use the same fracture criterion. Alternatively it may have been due to frictional effects reducing the true stress intensity at the crack tip.

1.4.3 Mixed Mode Fatigue Crack Growth Behaviour in Steel.

Gao Hua, and Mao et al carried out mixed mode fatigue tests under pure mode II, and mixed mode I and II using asymmetric 4 point bending, and biaxial loading of a cruciform specimen with an angled crack [22,61,62]. They were looking for thresholds, by starting at a load that produced no growth, and increasing the load in 10% steps. The general behaviour that they recorded was that a mode II crack would grow for up to 400 μm, that it would then arrest, and that the crack would then only start to grow again at a much higher load after it had branched into mode I, Fig. 1.23. The ratio of $K_{II_{th}}/K_{I_{th}}$ was found to be about 0·6. The MTS and MSS analysis in section 1.4.1.2 would suggest that mode II growth should occur, given this ratio of $K_{II_{th}}/K_{I_{th}}$. However it does not explain why the mode II growth arrests. Also it can be seen from Fig. 1.24, that the mode I branch crack occurs at a load much higher than that predicted by the theory.

Gao Hua et al suggested that these effects are caused by crack closure. They suggested that the formation of oxide and wear debris in the crack during the mode II growth would wedge it shut, that this would prevent the mode II load from reaching the crack tip, and that this would also reduce the mode I loading on the crack flanks making the real stress intensity range lower than that predicted by the MTS criterion. This is

supported by their observation of oxide appearing at the sides of the crack, and also by the fact that the mode I branch line moved closer to the theoretical line as the R ratio increased, ie as the closure effects were reduced. The branching load is very important to an understanding of 'squat' failures, because the branching down into the rail, causing rail fracture, appears to be a transition from an essentially mode II crack extension mechanism to a mode I one. See section 1.3.2.

M.C.Smith [40,41] carried out similar tests using a mode II specimen designed by Richard [65], Fig. 1.19 a. He was investigating the effects of crack face friction. He pre-cracked his specimens using a constant value of ΔK_I, so that the crack path should be as straight as possible, and therefore should reduce friction effects to a minimum. He showed that friction locked the crack tip up when the loading was pure mode II, and so it would reduce the effective ΔK_{II} at the crack tip to zero, and prevent mode II growth. He observed no mode II growth, in spite of using a specimen that does give a reasonably pure mode II load, and in spite of deliberately looking for this type of growth.

His results appear therefore to contradict Gao Hua's. However the difference is probably just that Smith's method produced greater locking effects, and so locked the faces before any measurable mode II growth occurred, rather than after a fraction of a millimetre. This may have been because Gao Hua tested under a mixed mode condition, with a small positive mode I component, whereas Smith looked at pure mode II. Another difference between these two types of experiment was that Smith prepared his specimens by pre-cracking at a constant ΔK value, whereas Gao Hua et al pre-cracked by reducing the load down to threshold, as is normal in threshold tests. At threshold the residual plastic zone at the crack tip is as small as it can be, and so it should have a minimal effect on subsequent crack growth.

R.A.Smith also examined mixed mode threshold behaviour in steel. He was looking at ball bearing steel, a very hard steel, and like M.C.Smith he observed no mode II growth [63].

M.C.Smith also carried out some mode II tests at high loads and produced around 500μm of mode II growth before branching occurred [40,41]. The higher load would have been able to overcome greater frictional forces

than the near threshold tests, so this result supports the crack locking arguments put forward so far.

1.4.4 The Effects of Non-Proportional Loading on the Fatigue of Steel.

All the tests that have been described so far have been proportional loading tests. However Bower's calculations predict that 'squats' are loaded non-proportionally. Two types of non-proportional load are of particular interest.

Firstly, where the mean load applied is different to the cyclic load applied. For example a static mode I load across a crack, and a cyclic mode II load, might produce mode II growth otherwise stopped by crack closure effects. In 'squats' this might be equivalent to the effect of a fluid lubricating the crack, or to the effect of the tensile load in the rail.

M.C.Smith tested with a static mode I load, using a modified version of the specimen designed by Richard [65], as shown in Fig. 1.20. However he observed no mode II growth at all [40,41]. In his specimens cracks branched straight into mode I, and stayed there. As mentioned before, he pre-cracked at a constant ΔK, and was loading under LEFM conditions. He was also only using positive R ratios, ie his rig was only producing tensile loads, so that the shear loading was not fully reversed.

Otsuka et al tested mild steel and structural steel, using asymmetric four point bending with a static end load, and a specimen similar to M.C.Smith's, as shown in Fig. 1.20 [32-35]. With this they produced continuous mode II growth. However the growth rate did not accelerate with crack length, as occurs under mode I crack growth in steels.

Pascoe and Smith [76,77] used a cruciform specimen to produce a similar form of loading, on HY100 steel, a high yield, ductile, weldable steel, under EPFM conditions. The only difference was that the static stress field was equibiaxial rather than uniaxial. They were testing at loads well above threshold in the EPFM region. They produced some continuous mode II growth, though it sometimes branched into mode I, and sometimes branched back to mode II, as shown in Fig. 1.25, at B,C and A,e respectively.

The second type of non-proportional loading of interest involves much more complicated basic cycles, for example a mode I cycle followed by a

mode II cycle, as calculated by Bower for 'squats' [51]. It might be that a small mode I cycle would open a crack enabling mode II crack extension in the mode II cycle. No experiments of this kind have been found in the literature, and so it is impossible to predict the results. Nayeb-Hashemi however looked at the effects of a single mode II overload on mode I growth, and showed that such an overload could increase the crack growth rate by a factor of up to 2, over an increase in crack length of less than the mode II plastic zone size [78].

1.4.5 Torsion Testing.

Torsional tests on solid cylindrical specimens are also mixed mode loadings. Cracks growing circumferentially or longitudinally extend by mode II at the surface, and mode III as they grow towards the centre of the specimen. Cracks growing at 45° are mode I. There is not room here to discuss the extensive research that has been done in full, but certain points should be noted because of their relevance to mixed mode I and II loadings, or because of their relevance to the three dimensional aspect of 'squat' growth.

Firstly, shear mode growth generally occurs at higher stress levels, and at higher plastic strain ranges, while tensile mode growth occurs at lower loads [23,39,79-81]. This is perhaps most clearly shown by Socie and various workers who have studied torsional loading quite extensively, and have produced damage maps for fatigue failures in two steels, AISI 304 stainless and AISI 1045 steel, and in Inconel 718, a Nickel alloy, in both tension and torsion tests, Fig. 1.26 [79]. The mode of crack growth was not merely dependent on geometrical and loading characteristics, but also on the material itself. In Socie's work Fig. 1.26 shows that Inconel is most likely to grow in shear mode, followed by AISI 1045, with AISI 304 stainless most likely to fail by mode I. This suggests that shear mode growth may also be more likely to occur in mixed mode I and II situations at higher loads, and also that mixed mode fatigue results from one steel may be very different to those from another.

Secondly, in torsional fatigue the growth rate can be affected by friction on the crack faces. For example Hay found that a tensile end load on solid torsional specimens could increase the growth rate of cracks

under torsional loading by a factor of up to 100 [42,82]. Without the end load the nominal ΔK_{III} value was not sufficient to correlate the growth rate. For the same ΔK_{III} value a long crack with a low torque grew much more slowly than a short crack with a high torque. The use of static mode I loads, to separate the crack flanks in mode II loading, will also affect the growth rate.

The mode III crack growth is also relevant to the study of 'squats' because 'squats' are not 2 dimensional cracks. Parts of the crack are loaded predominantly in mode III rather than mode II, and so the mode II growth, and the interaction of the mode III with the mode II growth, must be understood before the growth direction and rate of 'squats' can be accurately predicted. Zachariah, for example, looked at the fatigue of hollow cylinders in torsion. He found that cracks started to grow in shear, and then branched into mode I cracks at about the time when they became through cracks [83]. The reason for this behaviour is not fully understood, but it may be that the mode III displacements in some way restrained the crack keeping it in a shear plane. When the crack became a through crack the change in geometry may then have changed the restraints allowing the crack to branch more easily.

1.4.6 Mixed Mode Fatigue and Fracture of Aluminium Alloys.

So far the fatigue of steel has been looked at, and it has been shown that mode II has only been produced for fractions of a millimetre under elastic proportional loading, and for a few millimetres by only Pascoe and Smith, and then only under elastic plastic non-proportional loading. However mode II growth has been produced in Aluminium and its alloys more frequently. Though these results cannot be used directly in this study, the loading conditions used in Aluminium do indicate where mode II growth is more likely to be produced in steel.

Otsuka and various co-workers have studied mode II growth in Aluminium quite extensively [32-35]. They used a static mode I end load to reduce frictional effects on the crack faces, in most of their tests. Mode II growth was then produced under cyclic mode II loading. Some alloys always grew in mode II under this loading, some grew in mode I at lower stress amplitudes, and mode II at higher stresses. They showed that mode

II growth was favoured by a sharp pre-fatigue crack, whereas mode I growth was favoured by a blunt notch.

1.4.7 Short Cracks.

For completeness, it should also be mentioned that it is generally accepted that mode II fatigue crack growth occurs in the first stage of the fatigue of plain specimens. The cracks grow on the plane of maximum shear stress, for one or two grain sizes, and then either stop growing, or slow down until a mode I branch crack can grow, Fig. 1.27. It is thought that the cracks stop because they reach a micro-structural barrier [84-86]. Gao Hua's work in stainless steel showed about 200μm of mode II growth, about 5 grain diameters, so it seems unlikely that the reason for the arrest of those mode II cracks is the same.

1.5. Discussion.

From the experiments recorded above, various factors can be picked out that may affect the type of growth that occurs under mixed mode loading:

1. The amount of plasticity. Generally it seems that the greater the cyclic plasticity experienced by a specimen, the greater the chance that more mode II growth will occur. This is shown in that no mode II growth has been recorded in PMMA, and in the very hard steels used by R.A.Smith, and none when M.C.Smith was testing at low stress levels near threshold; and yet Pascoe and Smith, and M.C.Smith at high loads both recorded at least some mode II growth.

2. The type of pre-cracking carried out. One of the differences between Gao Hua's proportional mixed mode tests, and M.C.Smith's was that Gao Hua pre-cracked her specimens by reducing the load down to threshold, whereas M.C.Smith pre-cracked at constant ΔK. It might be therefore that the larger residual mode I plastic zone in M.C.Smith's specimens, with its associated compressive residual stress near the crack tip, inhibited mode II growth. This is the opposite of Smith's equally logical argument that the larger residual opening left by pre-cracking at a higher value of ΔK might be expected to reduce the friction and so assist mode II crack

growth.

3. Closure or locking effects. Gao Hua et al commented that the reason the mode I branch load was so high might be a closure effect. It might also be the reason that mode II cracks stop, ie they start being open, but wear debris formed during the limited mode II growth might then wedge the crack shut, until a mode I branch crack can form. Also closure might be the reason for the difference between Gao Hua's results and M.C.Smith's. Gao Hua tested under a mixed mode condition in most of her tests, with a small positive ΔK_I component, whereas M.C.Smith tested under approximately pure mode II loading. It seems likely that the unstable mode of crack growth found by Pascoe and E.Smith is because of the lack of closure in their experiments. They tested with a static mode I load to open the crack, so the mode I threshold line might be brought down to about the theoretical position. The mode I and mode II lines would then be close together so that cracks could jump between one mode of growth and another.

A lack of closure might be the reason why mode II cracks grow in 'squats'. As mentioned earlier, Way showed that a fluid was necessary for the propagation of rolling contact fatigue cracks. Bower et al have suggested that the role of water might be that it would lubricate the crack, and/or produce a mode I loading in the crack due to hydrostatic pressure, reducing any closure effects.

4. Non-proportional loading. The effect of small mode I cycles followed by mode II cycles is at the moment unknown. It may be that the mode I cycle will open the crack, reducing the locking effects, and thus enabling mode II crack extension. However, as mentioned in point 2, a residual mode I plastic zone may under some circumstances inhibit mode II growth instead.

5. Mean Stress effects. The type of mean stress field may also be of great importance. Otsuka produced continuous mode II growth by using a four point bending rig with a static end load, giving a uniaxial tensile load perpendicular to the crack, and a slightly compressive load parallel to the crack. Pascoe and Smith used a cruciform specimen giving a mean tensile load in all directions. It may be that the equibiaxial tensile load tends to give unstable mode I/mode II growth because the mode I cracks at an angle to the original crack are kept open, whereas in Otsuka's set up they were closed some of the time. In 'squats', it may be that the crack

tip will experience some compression, because of the compressive contact loading, but be kept open by the fluid inside. Mode II growth might then be possible, while mode I growth is inhibited by the compressive stress.

6. Fully reversed shear loading. Gao Hua, M.C.Smith, and R.A.Smith all tested at positive R ratios. Pascoe and E.Smith tested at R=-1. The experimental results and the MTS / MSS analysis described in section 1.4.1 both predict that testing at R=-1 favours mode II growth, and Bower's analysis suggests that the loading on a 'squat' may be approximately fully reversed.

7. Geometry Effects. In all the mixed mode tests in asymmetric four point bending specimens, and ordinary mode II specimens like M.C.Smith's, mode I branch cracks never branched back to mode II cracks. In cruciform specimens like Pascoe and Smith's they did. This is because in the mode II specimens the cracks are situated in a position of pure mode II loading, and then experience mode I loading as soon as they move away from the original crack plane. In cruciform specimens there is a uniform stress across the working section, so the same does not happen.

8. Material differences. Socie et al have shown that under the same loading conditions in torsion, one steel can grow in shear mode, while another can grow in mode I. The same is probably true in mixed mode I and II loading.

1.6 Conclusions and the Test Programme.

The above discussion shows that mode II growth has been produced in limited quantities in the fatigue of steel, but that the conditions that will produce it are not well established. Slight differences in loading methods and materials have produced different results. Mode II growth laws have not been produced that could be applied to 'squats', and the effects of the non-proportional loads calculated by Bower are unknown. The following test programme was formulated to attempt to clarify the loading conditions under which mode II growth will be produced in rail steel, if it can be produced at all.

The first series of experiments was designed to look at the proportional mixed mode loading of rail steel, by using asymmetric four

point bending, Fig. 1.15. The series looked at the effects of fully reversed loading, as opposed to testing at a positive R ratio, and looked at the effects of pre-cracking by reducing the load to threshold, as opposed to pre-cracking at a constant value of ΔK_I. The tests also provided a useful link with the previous work using asymmetric four point bending, showing the similarities and differences between rail steel and the other materials used.

The second and third series of tests looked at the effects of combining mode I stresses to open the crack, with cyclic mode II stresses to propagate it. They also looked at the effects of plasticity by performing similar tests at different load levels. The first of these looked at the effect of applying a mean equibiaxial tensile stress to the cyclic mode II loading by using cruciform specimens. If mode II growth could have been produced by this method, confirming the results of Pascoe and Smith (section 1.4.4), then the aims of the project would have been mainly fulfilled. Branching conditions and growth rate laws could have been produced in terms of the applied mode I and II loadings and the length of crack, and compared with Bower's calculations. The cruciform specimen was chosen for these tests, as opposed to the other types of non-proportional biaxial specimens, because of its suitability for collecting a wide range of crack growth data in one test, and because of its suitability for finding branching conditions. A similar series of tests using one of the other types of specimen, and the different load cycles that it could produce, would make another useful research programme in the future.

The third series of tests then looked at the effects of applying cyclic mode I and fully reversed mode II loads sequentially, to more closely resemble the more complicated non-proportional loads calculated by Bower, sections 1.3.2, and 1.4.4. Again growth rates, branching conditions, and crack directions at different load levels were examined. The details of the cycles looked at are discussed at the beginning of chapter 4.

References.

1. M.B.P.Allery. 'Characteristics of "Squat" Type Defects in BS11 Steel Rails.'
British Railways Board, Research and Development Division, Track Group, Technical Note TN MET 1. 1976.

2. M.B.P.Allery. 'Rail Failures.'
Lecture at British Rail Technical Centre. 3 June 1987.

3. M.B.P.Allery, P Clayton. 'A Review of Recent Work On Rolling Contact Fatigue Defects (Squats) In Rails and Crossings.'
British Railways Board, Research and Development Division, Technical Note TN MET 20. Sept. 1979.

4. P Clayton, M.B.P.Allery. 'Metallurgical Aspects of Surface Damage Problems In Rails'
British Rail, Research Report Reference MR MF1.
Canadian Metallurgical Quarterly, 21(1), pp31-46, 1982.

5. P Clayton, M.B.P.Allery, P.J.Bolton. 'Surface Damage Phenomena In Rails.'
International Symposium On Contact Mechanics and Wear of Rail/Wheel Systems. University of British Columbia, Vancouver, Canada, July 6-9, 1982.
British Rail Research Report Reference MR MF3.

6. K.L.Johnson. 'One Hundred Years of Hertz Contact.'
Institution Of Mechanical Engineers, Tribology Group,
Proceedings 1982, Vol. 196 No. 39, pp363-378

7. K.L.Johnson. 'Plastic Flow, Residual Stress, and Shakedown in Rolling Contact.'
International Symposium On Contact Mechanics and Wear of Rail/Wheel Systems. University of Rhode Island. July 8-11 1986.

8. A.D.Hearle. 'Deformation, Shakedown, and Fatigue in Rolling Contact.'
PhD. Thesis. Department of Mechanical Engineering, University of Cambridge, December 1984.

9. A.D.Hearle, K.L. Johnson. 'Cumulative Plastic Flow in Rolling and Sliding Line Contact.'
J. Applied Mechanics, ASME Trans. Vol. 54, pp1-5. 1987.

10. A.F.Bower. 'The Influence of Strain Hardening on the Cumulative Plastic Deformation Caused by Repeated Rolling and Sliding Contact.'
Cambridge University Eng. Dept Report. CUED / C-Mech / TR 39. 1987

11. M.L.Williams. 'On the Stress Distribution at the Base of a Stationary Crack.'
Transactions of the ASME. Journal of Applied Mechanics Vol. 24, 109-114. 1957

12. J.F.Knott. 'Fundamentals of Fracture Mechanics.'
Butterworths. 1973.

13. K.J.Miller. 'An Introduction to Fracture Mechanics.'
'Mechanical and Thermal Behaviour of Metallic Materials.' pp97-119.
Soc. Italiana di Fisica - Bologna - Italy. 1982.

14. K.J.Miller. 'Elastic-Plastic Fracture Mechanics.'
'Mechanical and Thermal Behaviour of Metallic Materials.' pp120-132.
Soc. Italiana di Fisica - Bologna - Italy. 1982.

15. P.C.Paris, F.Erdogan. 'A Critical Analysis of Crack Propagation Laws.'
J. of Basic Engineering. Ser. D, Vol. 85, pp528. 1963.

16. R.P.Skelton. 'Growth of Short Cracks During High Strain Fatigue and Thermal Cycling.'
'Low-Cycle Fatigue and Life Prediction.' ASTM STP 770. Eds. C.Amzallag, B.N.Leis, and P.Rabbe. pp337-381. 1982.

17. B.Tomkins. 'Fatigue Crack Growth - An Analysis.'
Philosophical Magazine. Vol. 18, pp1041-1066. 1968

18. M.W.Brown, K.J.Miller. 'Mode I Fatigue Crack Growth Under Biaxial Stress at Room and Elevated Temperature.'
'Multiaxial Fatigue.' ASTM STP 853. Ed K.J.Miller, M.W.Brown. pp135-152. 1985.

19. W.Elber. 'Fatigue Crack Closure Under Cyclic Tension.'
Engineering Fracture Mechanics. Vol.2, pp37-45. 1970.

20. P.C.Paris, R.J.Bucci, E.T.Wessel, W.G.Clark, T.R.Mager. 'Extensive Study of Low Fatigue Crack Growth Rates in A533 and A508 Steels.'
Stress Analysis and The Growth of Cracks, Proceedings of the 1971 National Symposium on Fracture Mechanics, Part 1, ASTM STP 513. pp141-176.

21. N.Walker, C.J.Beevers. 'A Fatigue Crack Closure Mechanism in Titanium.'
Fatigue of Engineering Materials and Structures, Vol. 1, p135-148. 1979

22. Gao Hua, M.W.Brown, K.J.Miller. 'Mixed Mode Fatigue Crack Thresholds.'
Fatigue of Engineering Materials and Structures. Vol.5, No.1, pp1-17. 1982.

23. R.O.Ritchie, F.A.McClintock, H.Nayeb-Hashemi, M.A.Ritter. 'Mode III Fatigue Crack Propagation in a Low Alloy Steel.'
Metallurgical Transactions A. Vol.13A. pp101-110. 1982.

24. F.Erdogan, G.C.Sih. 'On the Crack Extension in Plates Under Plane Loading and Transverse Shear.'
J. of Basic Engineering. No.85, pp519-525. 1963.

25. S.K.Maiti, K.S.R.K.Prasad. 'A Study on the Theories of Unstable Crack Extension for the Prediction of Crack Trajectories.'
International Journal of Solids and Structures. Vol. 16, pp653-574. 1980.

26. H.-C. Wu. 'Dual Failure Criterion For Plain Concrete'
Journal of Engineering Mechanics, Division ASCE, Vol. 100, pp1167-1181. 1974.

27. F.Hourlier, H.d'Hondt, M.Truchon, A.Pineau. 'Fatigue Crack Path Behaviour Under Polymodal Fatigue.'
'Multiaxial Fatigue.' ASTM STP 853. Ed K.J.Miller, M.W.Brown. pp228-247. 1985.

28. G.C.Sih. 'Some Basic Problems in Fracture Mechanics and New concepts.'
Engineering Fracture Mechanics. Vol. 5, pp365-373. 1973.

29. S.K.Maiti, R.A.Smith. 'Theoretical and Experimental Studies on the Extension of Cracks Subjected to Concentrated Loading Near Their Faces To Compare Criteria For Brittle Fracture.'
Journal of Mechanical Physics and Solids. Vol.31, No.5, pp389-403. 1983.

30. S.K.Maiti, R.A.Smith. 'Comparison of the Criteria for Mixed Mode Brittle Fracture Based on the Pre-instability Stress-Strain Field.
Part I. Slit and Elliptical Cracks Under Uniaxial Tensile Loading.'
Int. Journal of Fracture. Vol. 23, pp281-295. 1983.

31. S.K.Maiti, R.A.Smith. 'Comparison of the Criteria for Mixed Mode Brittle Fracture Based on the Pre-instability Stress-Strain Field.
Part II. Pure Shear and Uniaxial Compressive Loading.'
Int. Journal of Fracture. Vol. 24, pp5-22. 1984.

32. A.Otsuka, K.Mori, T.Ohshima, S.Tsuyama. 'Mode II Fatigue Crack Propagation in Aluminium Alloys and Mild Steel.'
Proceedings of the 5th International Conference on Fracture, Cannes.
Vol.4, pp1851-1859. 1981

33. A.Otsuka, K.Mori, T.Miyata. 'The Condition of Fatigue Crack Growth in Mixed Mode Condition.'
Engineering Fracture Mechanics. Vol.7, pp429-439. 1975.

34. A.Otsuka, K.Tohgo, T.Kiba, S.Yamada. 'Mode II Fatigue Crack growth Characteristics and Mechanism I Aluminium Alloy 7N01-T4 Weldments Under Mode II Loading.'
Proceedings of the 6th International Conference on Fracture, New Delhi, India. pp1671. 1984.

35. A.Otsuka, K.Mori, K.Tohgo. 'Mode II Fatigue Crack Growth In Aluminium Alloy.'
'Current Research On Fatigue Cracks.' The Society of Material Science. Japan. MRS1 pp127. 1984.

36. S.Melin. 'Fracture From A Straight Crack Subject To Mixed Mode Loading.'
International Journal of Fracture. 32. pp257-263. 1986.

37. A.A.Khrapkov. 'The First Basic Problem For a Notch at the Apex of an Infinite Wedge.'
International Journal of Fracture. Vol. 7, No. 4, pp373-382. 1971

38. S.N.Chatterjee. 'The Stress Field in the Neighbourhood of a Branch Crack in an Infinite Elastic Sheet.'
International Journal of Solids and Structures. Vol.11, pp521. 1975.

39. A.Fatemi, D.F.Socie. 'A Critical Plane Approach to Multiaxial Fatigue.'
Fatigue and Fracture of Engineering Materials and Structures. Vol.11, No.3, pp149-165. 1988.

40. M.C.Smith. 'Some Aspects of Mode II Fatigue Crack Growth.'
PhD Thesis, Churchill College/Department of Engineering,
University of Cambridge. 1984.

41. M.C.Smith, R.A.Smith. 'Towards an Understanding of Mode II Fatigue Crack Growth.'
Basic Questions in Fatigue: Volume 1. ASTM STP 924, Eds. J.T.Fong, R.J.Fields. 1988. pp260-280.

42. E.Hay. 'Fatigue at Notches Subjected to Torsion and Axial Loading.'
PhD Thesis. Eng. Dept. University of Sheffield. 1983.

43. S.Way. 'Pitting due To Rolling Contact.'
Trans. ASME. J. of Applied Mechanics. Vol.57, ppA49-A58. 1935.

44. P.H.Dawson. 'The Pitting of Lubricated Gear Teeth and Rollers.'
Power Transmission, April and May, 1961.

45. P.Clayton, D.N.Hill. 'Rolling Contact Fatigue of a Rail Steel.'
Proc. of the 2nd International Symposium on Contact Mechanics and Wear of Rail/Wheel Systems, University of Waterloo Press, pp361-378. 1986.

46. G.T.Hahn, V.Bhargava, H.Yoshimura, C.Rubin. 'Analysis of Rolling Contact Fatigue and Fracture.'
6th International Conference on Fracture. New Delhi, India. Dec. 1984.

47. Y.Nakajima, K.Ichimaru, F.Hirano, M.Nishimura. 'Effects of Combination of Rolling Direction and Sliding Direction on Pitting of Rollers.'
JSLE International, Vol. 4, pp94-98. 1983.

48. K.Fujita, A.Yoshida. 'The Effect of Changing the Rolling Direction on the Rolling Contact Fatigue Lives of Annealed and Case Hardened Steel Rollers.'
Wear, Vol. 43, pp315-327. 1977.

49. L.M.Keer, M.D.Bryant, G.K.Haritos. 'Subsurface and Surface Cracking due to Hertzian Contact.'
J. of Lub. Tech. Vol.104, pp347. 1982.

50. L.M.Keer, M.D.Bryant. 'A Pitting Model for Rolling Contact Fatigue.'
Journal of Lubrication Technology, Vol. 105, pp198-205. 1983

51. A.F.Bower. 'The Influence of Crack Face Friction and Trapped Fluid on Surface Initiated Rolling Contact Fatigue Cracks.'
Trans. ASME, J. of Lubrication Tech, Vol.110, pp704-711. 1988.

52. Y.Murakami, M.Kaneta, H.Yatsuzuka. 'Analysis of Surface Crack Propagation in Lubricated Rolling Contact.' ASLE Trans. Vol. 28, pp60-68. 1985.

53. N.P.Suh. 'An Overview of the Delamination Theory of Wear.'
Wear. Vol.44, pp1-16. 1977.

54. H.C.Sin, N.P.Suh. 'Subsurface Crack Propagation Due To Surface Traction in Sliding Wear.'
Trans. ASME. J. of Applied Mechanics. Vol.51, pp317-323. 1984

55. S.Jahanmir, N.P.Suh. 'Mechanics of Subsurface Void Nucleation in Delamination Wear.'
Wear, Vol. 44, pp17-38. 1977.

56. J.R.Fleming, N.P.Suh. 'Mechanics of Crack Propagation In Delamination Wear.'
Wear, Vol. 44, pp39-56. 1977.

57. J.R.Fleming, N.P.Suh. 'The Relationship Between Crack Propagation Rates and Wear Rates.'
Wear. Vol. 44, pp57-64. 1977.

58. K.Tanaka. 'Fatigue Crack Propagation From a Crack Inclined to the Tensile Axis.'
Engineering Fracture Mechanics. Vol.6, pp493-507. 1974

59. S.Iida, A.S.Kobayashi. 'Crack Propagation Rate in 7075-T6 Plates Under Cyclic Tensile and Transverse Shear Loadings.'
Transactions of ASME. J. of Basic Engineering. Vol.91. pp764-769. 1969

60. Kao Hua, Wang Zhiqiang, Yang Chenshou. 'An Investigation On the Brittle Fracture of K_I-K_{II} Composite Mode Cracks.'
Acta Metallurgica Sinica. Vol. 15, pp380-391. 1979.

61. Gao Hua, N.Alagok, M.W.Brown, K.J.Miller. 'Growth of Fatigue Cracks Under Combined Mode I and II Loads.'
'Multiaxial Fatigue.' ASTM STP 853. Ed K.J.Miller, M.W.Brown. pp184-202. 1985.

62. Mao Yilin, N.Alagok. 'Mixed Mode Fatigue Crack Growth Thresholds in Three Metallic Materials.'
Dept. of Mechanical Engineering, University of Sheffield,
Research Report No. 115. 1983.

63. R.A.Smith. 'Fatigue Crack growth in Hard Steels.'
'Fracture Control of Engineering Structures.' ECF6. Eds. H.C.Von Elst, A.Bakker.
Pub. EMAS. pp1353-1363. 1986.

64. K.J.Wang C.L.Hsu, Kao Hua. 'Calculation of Stress Intensity Factors for Combined Mode Bend Specimens.'
Proc. ICF 4, Vol. 4, pp123-133. 1977.

65. H.A.Richard. 'A New Compact Shear Specimen.'
International Journal of Fracture. Vol. 17, ppR105-R107. 1981.

66. H.A.Richard. 'Bruchvorhersagen bei Uberlagerter Normal- und Schubbeanspruchung sowie reiner Shubbelastungvon Rissen.'
Habilitionsschrift Universitat, Kaiserslauten. 1984.

67. L.P.Pook. 'An Observation on Mode II Fatigue Crack Growth Threshold Behaviour.'
International J. of Fracture. Vol.13, pp867-869. 1977.

68. R.J.Buzzard, B.Gross, J.E.Srawley. 'Mode II Fatigue Crack Growth Specimen Development.'
ASTM STP 905. Fracture Mechanics. 17th Volume. Ed. Underwood, Chait, Smith, Wilhelm, Andrews, Newman. pp329-346. 1986.

69. D.L.Jones, D.B.Chrisholm. 'An Investigation into the Edge Sliding Mode in Fracture Mechanics.'
Engineering Fracture Mechanics. Vol.7, pp261-270. 1975.

70. J.Royer. 'A Specimen Geometry For Plane Mixed Modes.'
Engineering Fracture Mechanics. Vol.23, No.4, pp763-775. 1986.

71. L.Bank-Sills, M.Arcan. 'A Compact Mode II fracture Specimen.'
ASTM STP 905. Fracture Mechanics. 17th Volume. Ed. Underwood, Chait, Smith, Wilhelm, Andrews, Newman. pp347-363. 1986.

72. T.Yokobori, A.T.Yokobori, K.Sato, M.Omotani. 'The Effects of Ferrite Grain Size on Fracture of Low Carbon Steel Under Mixed Mode Loading.'
Engineering Fracture Mechanics. Vol.17, pp75-85. 1982.

73. T.Yokobori, A.Kamei, A.T.Yokobori. 'Fatigue Crack Propagation Under Mode II Loading.'
International J. of Fracture, Vol.12, pp158-160. 1976.

74. H.L.Cox, J.E.Field. 'The Initiation and Propagation of Fatigue Cracks in Mild Steel Pieces of Square Section.'
Aeronautical Quarterly. Aug. 1952

75. R.Roberts, J.J.Kibler. 'Mode II Crack Propagation.'
J. of Basic Engineering. Vol.93(D) pp671-680. 1971.

76. E.W.Smith, K.J.Pascoe. 'Fatigue Crack Initiation and Growth In a High Strength Ductile Steel Subject to In Plane Biaxial Loading.'
Multiaxial Fatigue. ASTM STP 853. Eds. K.J.Miller, M.W.Brown. pp111-134. 1985.

77. E.W.Smith, K.J.Pascoe. 'Fatigue Crack Initiation and Growth In HY100 Steel Subject to In Plane Biaxial Loading.'
Cambridge University Eng. Dept. Report CUED/C-MAT/TR95. 1982.

78. H.Nayeb-Hashemi, M.E.Taslim. 'Effects of the Transient Mode II on the Steady State Crack Growth in Mode I.'
Eng. Fract. Mech. Vol.26, No.6, pp789-807, 1987.

79. D.F.Socie. 'Fatigue Damage Maps.'
Fatigue '87. 3rd Int. Conf. on Fatigue and Fatigue Thresholds. University of Virginia. Eds. R.O.Ritchie, E.A.Starke Jr. Vol.2. pp599-616. 1987.

80. D.F.Socie. 'Multiaxial Fatigue Damage Models.'
J. of Eng. Materials and Technology. Vol.109, pp293-298. 1987.

81. C.T.Hua, D.F.Socie. 'Fatigue Damage in 1045 Steel under Variable Amplitude Biaxial Loading.'
Fat. and Fract. of Eng. Materials and Structures. Vol.8, No.2, pp101-114. 1985.

82. R.O.Ritchie, F.A.McClintock, E.K.Tschegg, H.Nayeb-Hashemi. 'Mode II Fatigue Crack Growth Under Combined Torsional and Axial Loading.'
'Multiaxial Fatigue.' ASTM STP 853. Ed K.J.Miller, M.W.Brown. pp203-227. 1985.

83. K.P.Zachariah. 'Fatigue Crack Initiation and Stage I Propagation.'
PhD Thesis. Mech. Eng. Dept. University of Sheffield. 1974.

84. P.J.E.Forsyth. 'A Two Stage Process of Fatigue Crack Growth.'
Symp. Crack Propagation, Cranfield, U.K. pp76-94. 1961.

85. M.W.Brown. 'Interfaces Between Short, Long, and Non-Propagating Cracks.'
'The Behaviour of Short Fatigue Cracks.' EGF Publication No. 1.
Eds. K.J.Miller, E.R.de Los Rios. Mech. Eng. Publications Ltd. London.
pp423-439. 1986.

86. P.D.Hobson, M.W.Brown, E.R.de Los Rios. 'Two Phases of Short Crack Growth in a Carbon Steel.'
'The Behaviour of Short Fatigue Cracks.' EGF Publication No. 1.
Eds. K.J.Miller, E.R.de Los Rios. Mech. Eng. Publications Ltd. London.
pp441-459. 1986.

Figures for chapter 1.

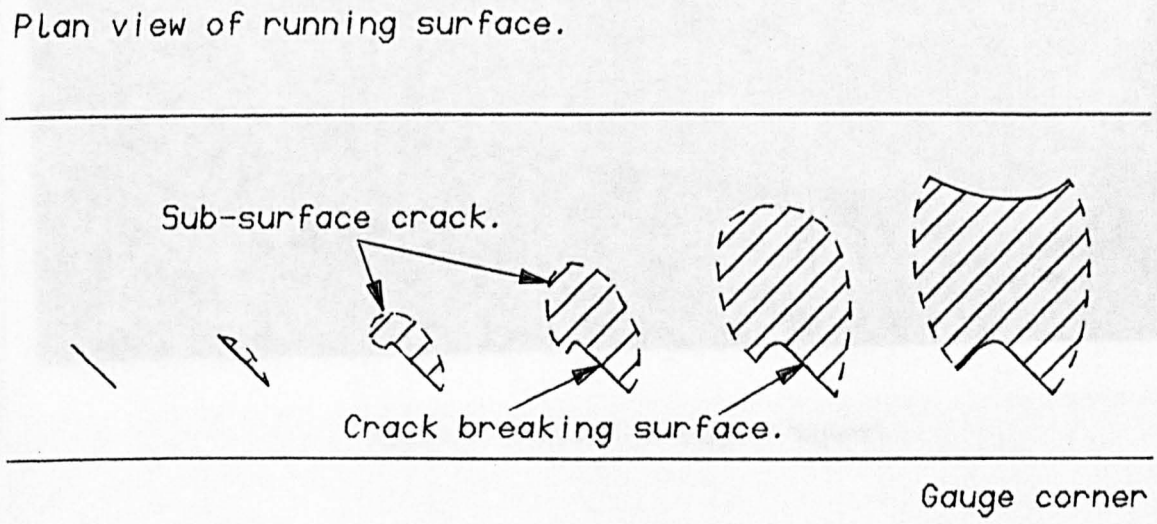

Fig. 1.1 'Squat' Development from a Slant Crack on a Curve.

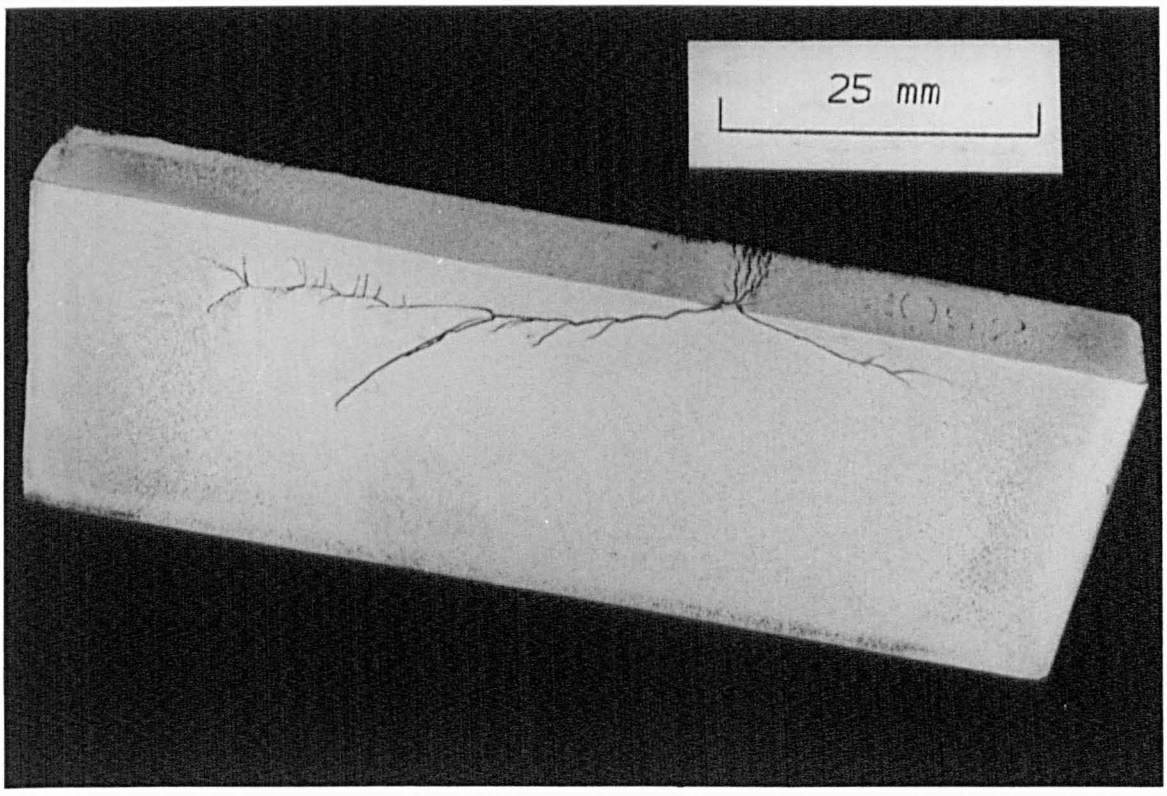

Fig. 1.2 Section through a 'squat'.

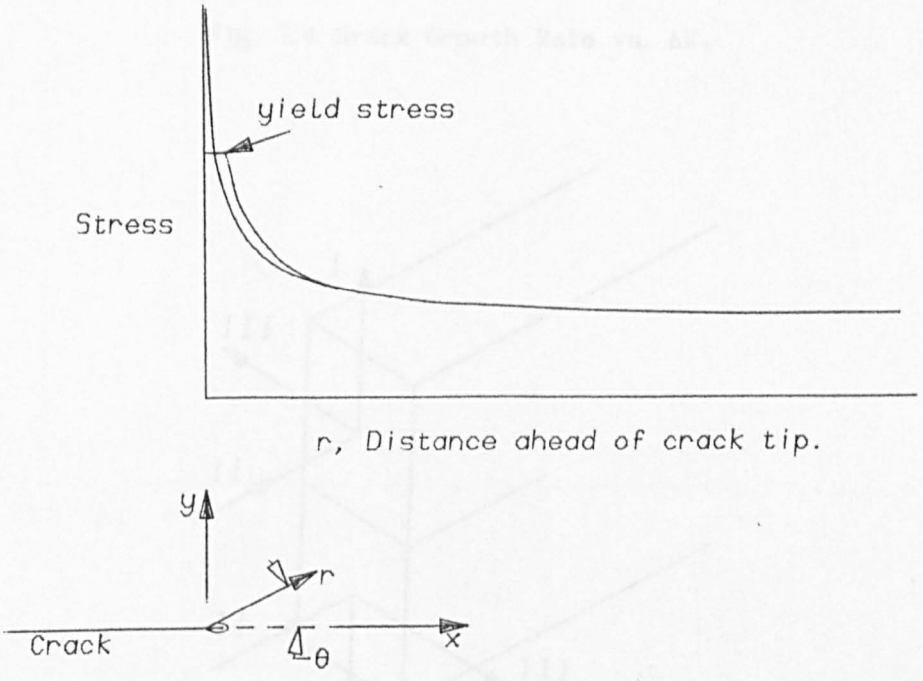

Fig. 1.3 Stress Distribution Near a crack Tip.

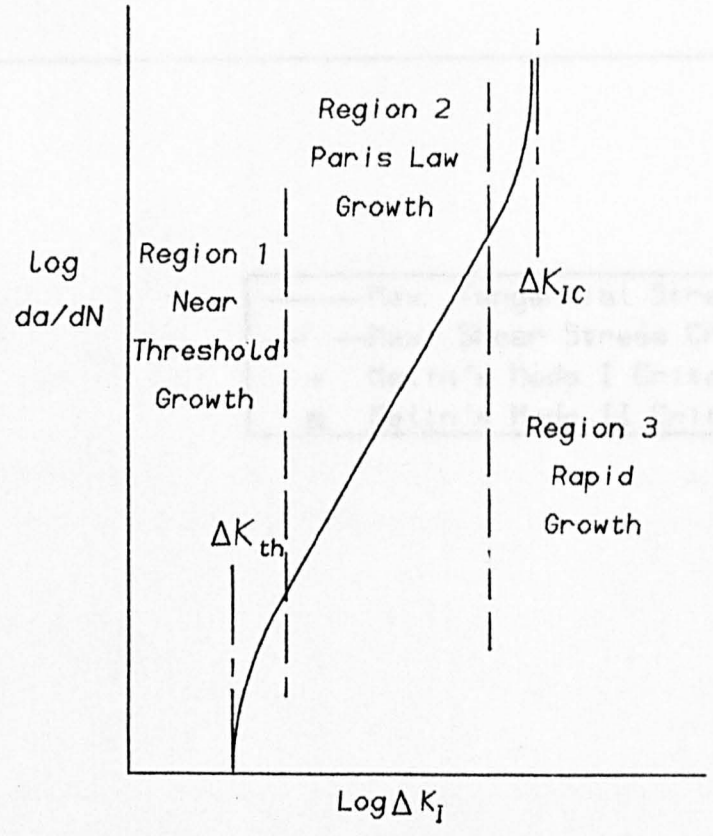

Fig. 1.4 Crack Growth Rate vs. ΔK_I

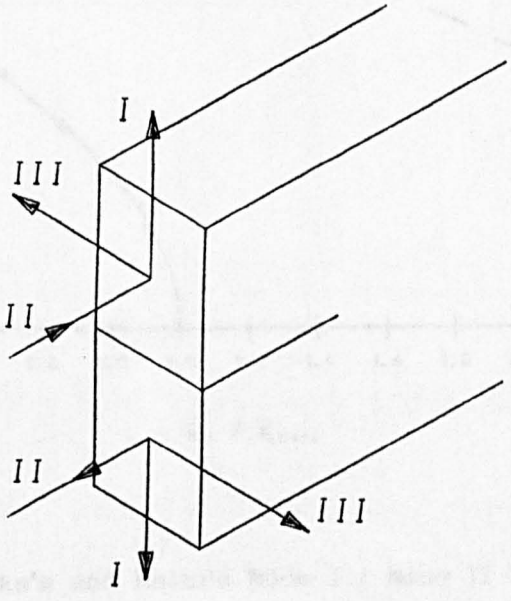

Fig. 1.5 Modes of Loading in Fatigue and Fracture.

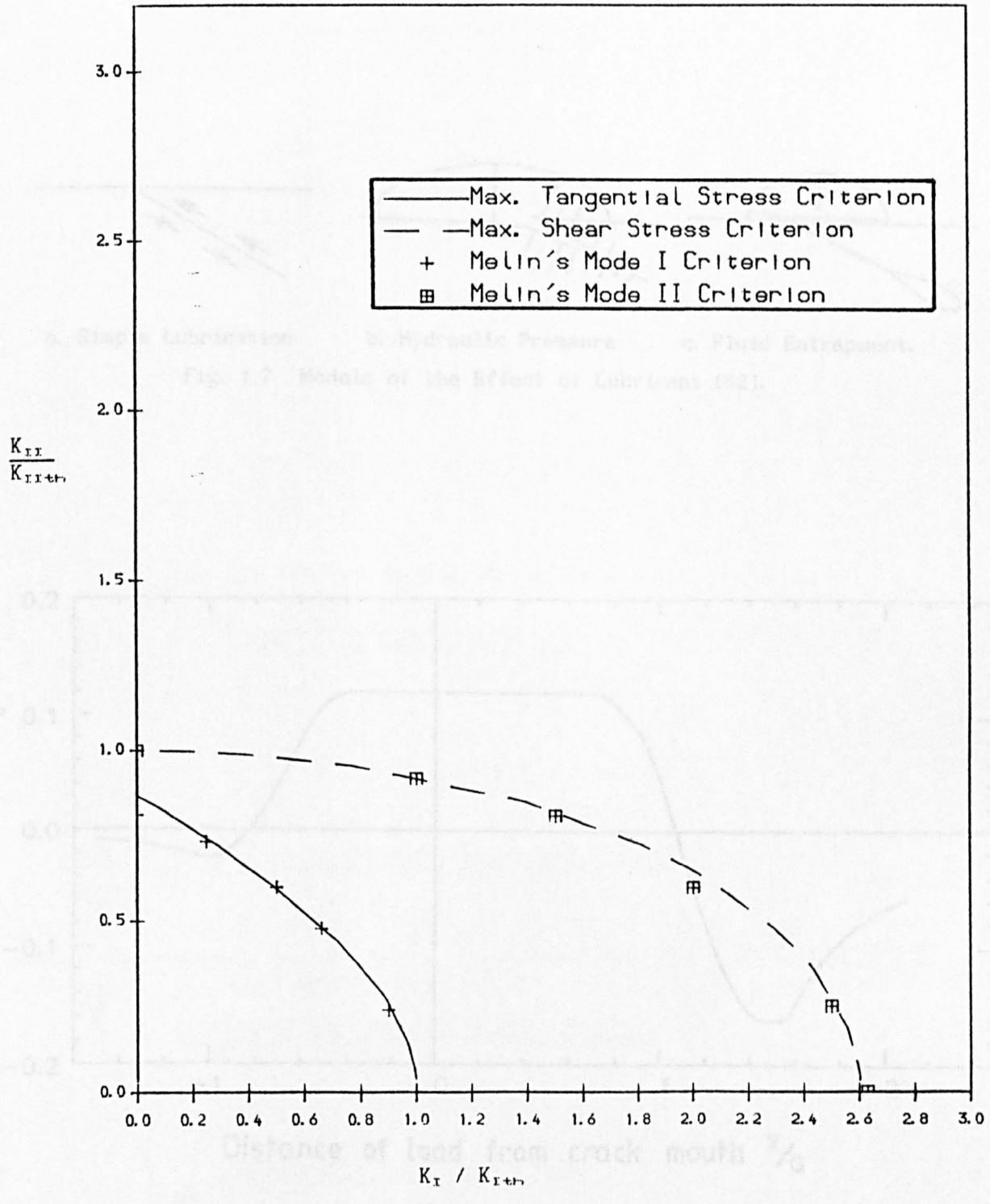

Fig. 1.6 Otsuka's and Melin's Mode I / Mode II Threshold or Fracture Criteria Assuming $K_{I th} = K_{II th}$ [32-36]

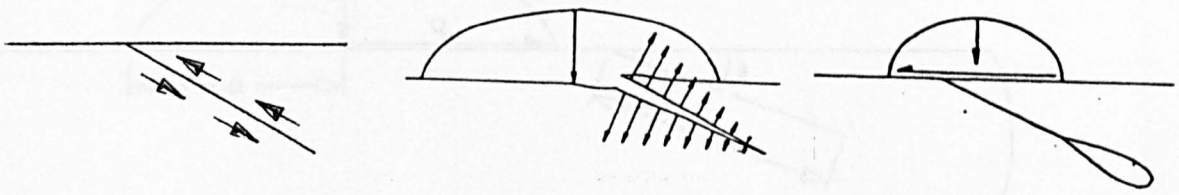

a. Simple Lubrication. b. Hydraulic Pressure c. Fluid Entrapment.

Fig. 1.7 Models of the Effect of Lubricant [52].

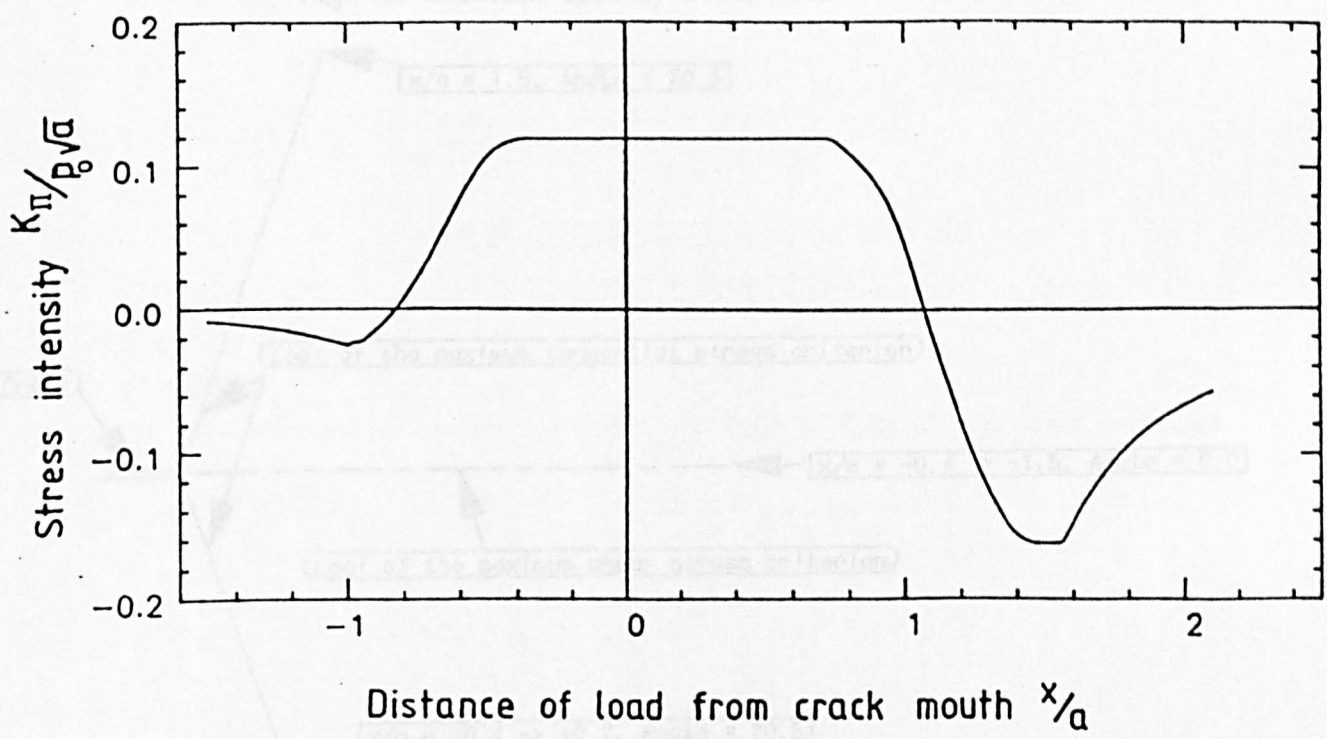

Fig. 1.8 K_{II} for a Lubricated Crack Under Rolling Contact.
$c/a = 0{\cdot}5$, $q_\infty/p_\infty = -0{\cdot}05$, $\beta = 25°$, $\mu = 0{\cdot}1$ [52].

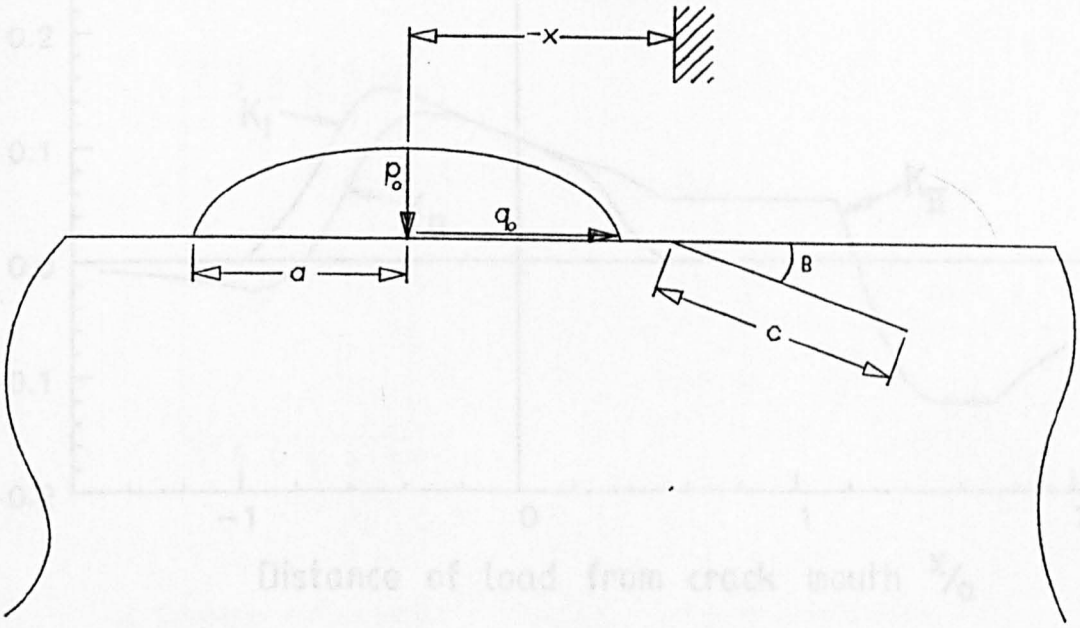

Fig. 1.9 Notation Used By Bower [52].

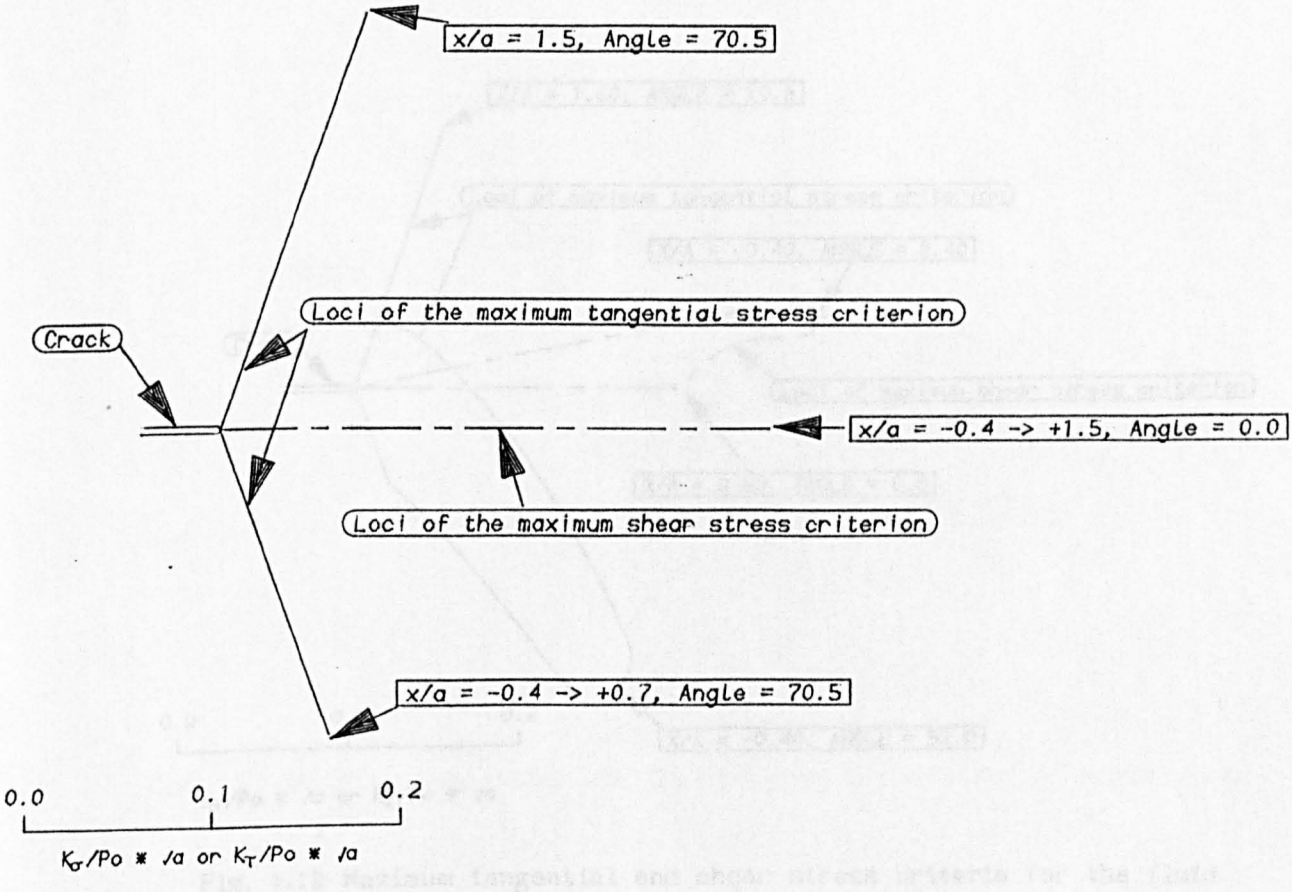

Fig. 1.10 Maximum tangential and shear stress criteria for a lubricated crack under rolling contact.

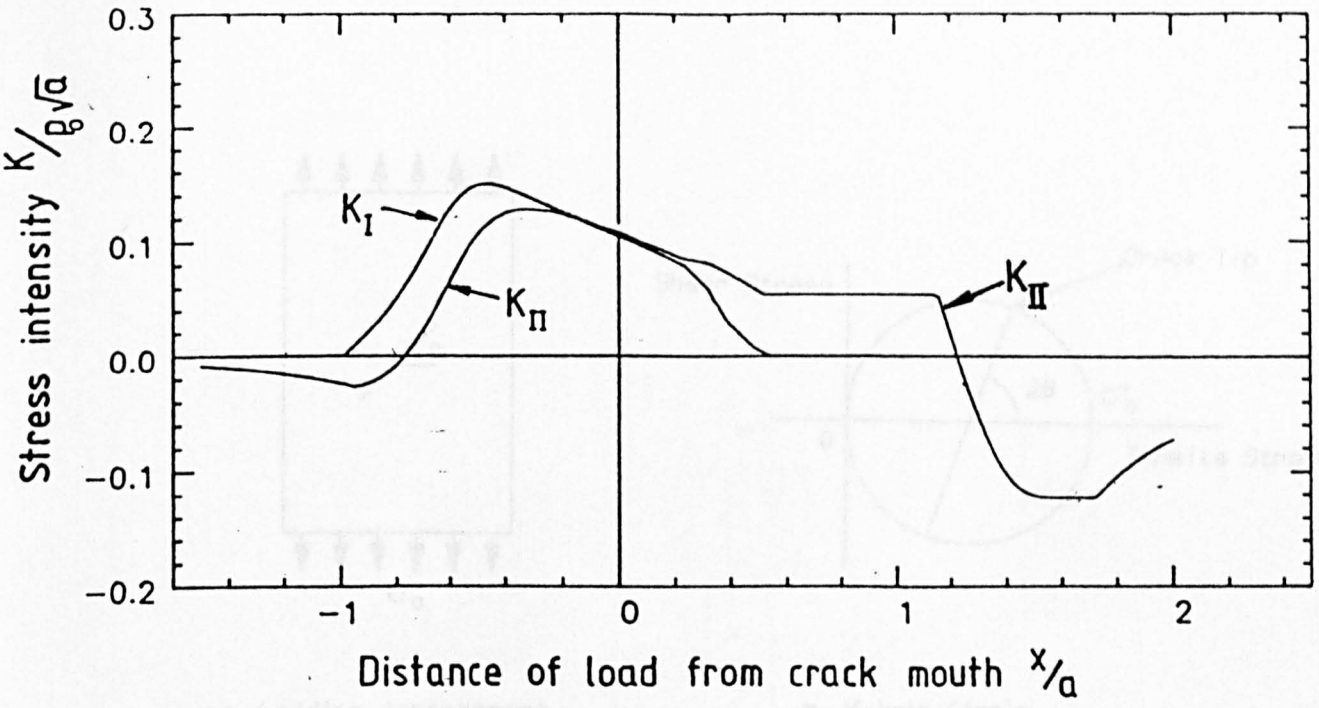

Fig. 1.11 K_I and K_{II} for Fluid Entrapment Mechanism [52].

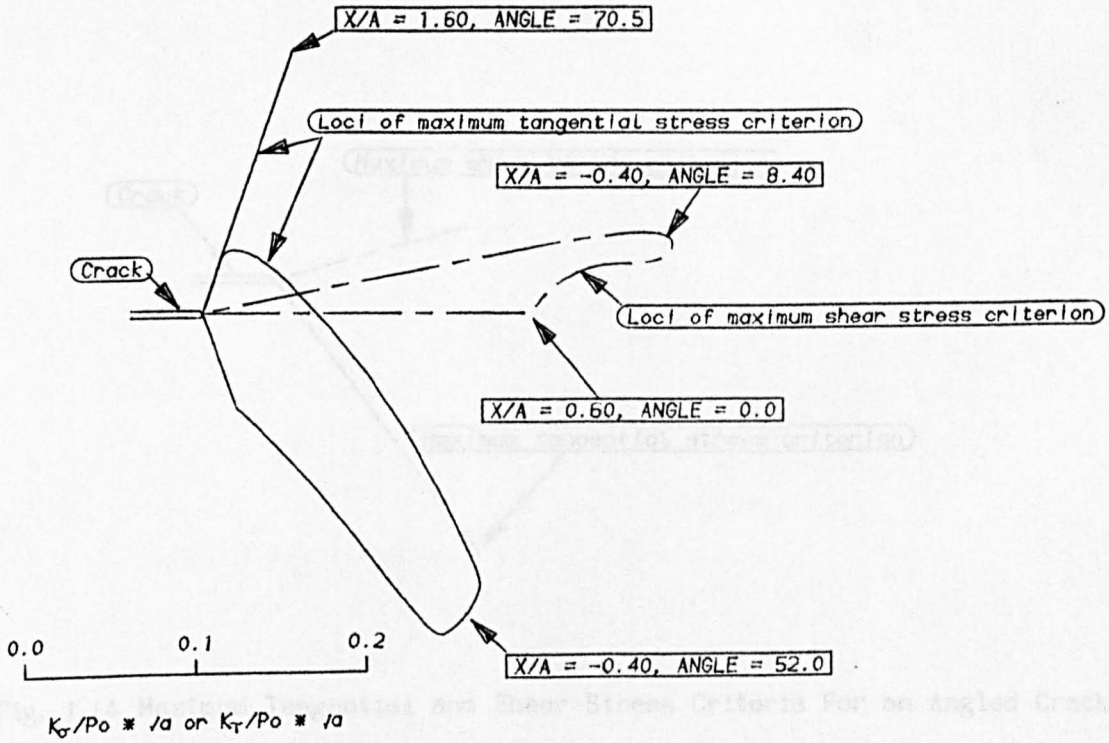

Fig. 1.12 Maximum tangential and shear stress criteria for the fluid entrapment mechanism.

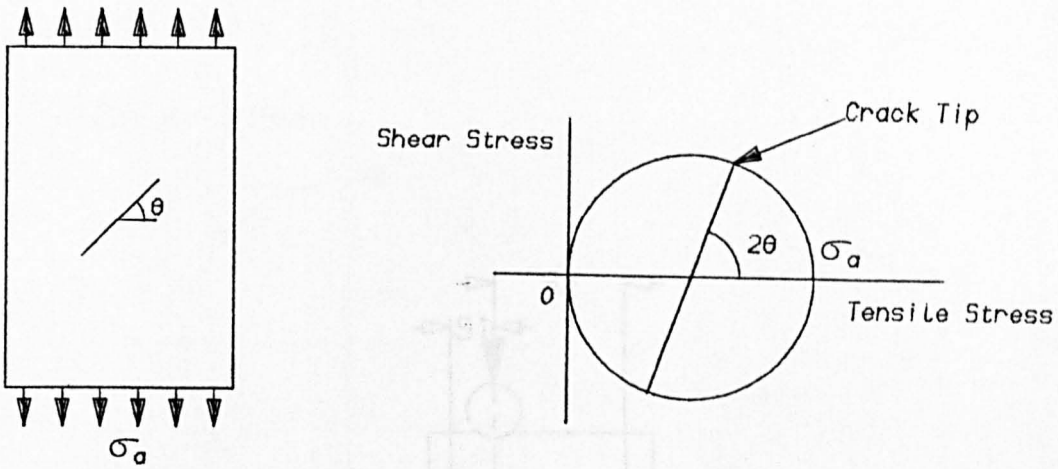

a. Loading Arrangement. b. Mohr's Circle.

Fig. 1.13 The Angled Crack Specimen.

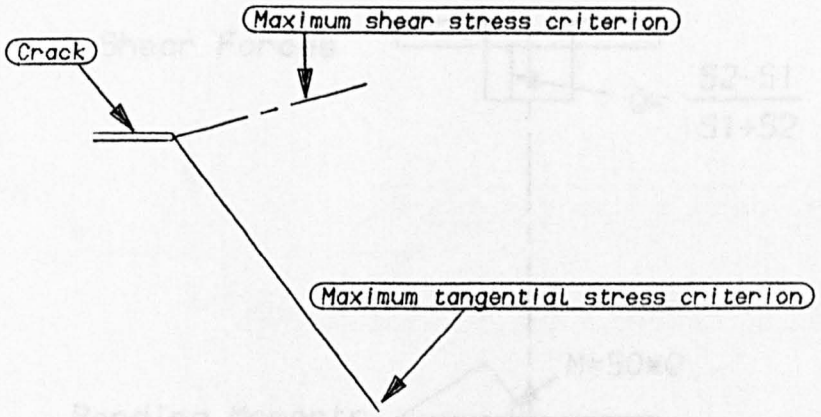

Fig. 1.14 Maximum Tangential and Shear Stress Criteria For an Angled Crack.

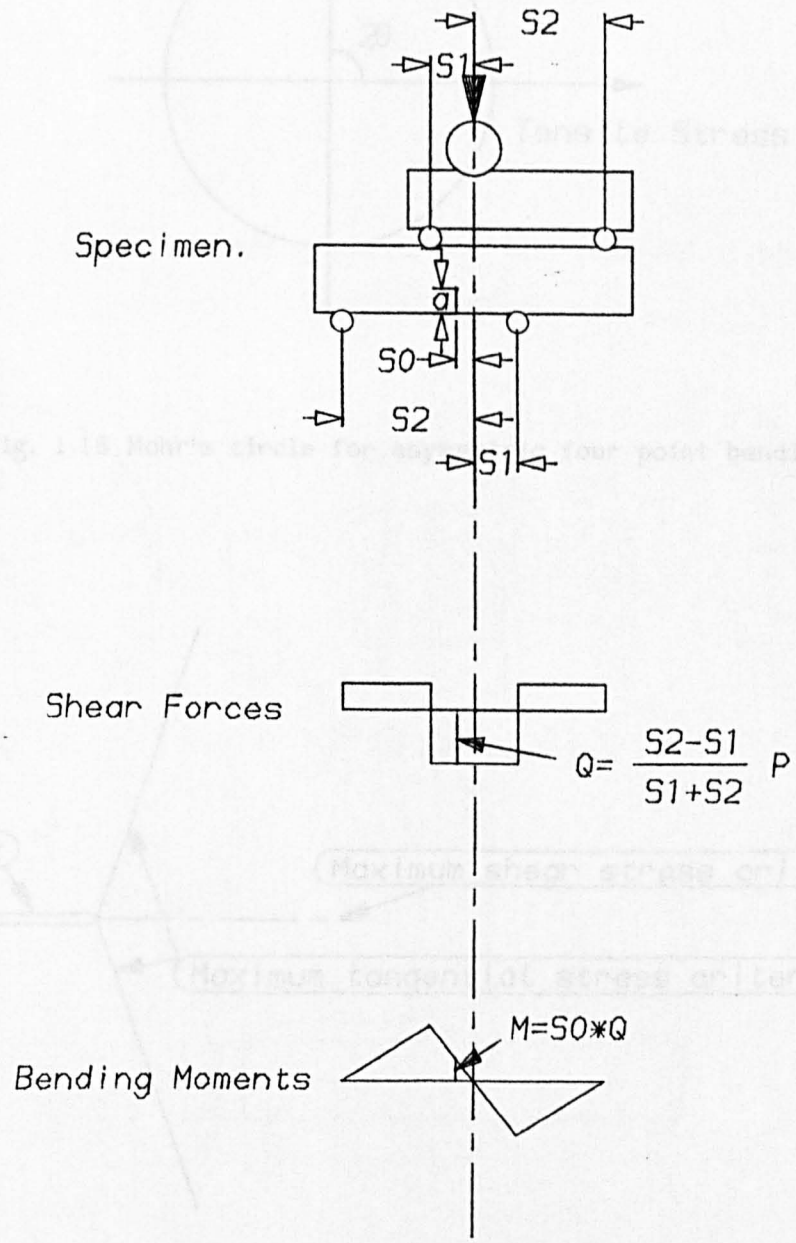

Fig. 1.15 Asymmetric Four point Bending.

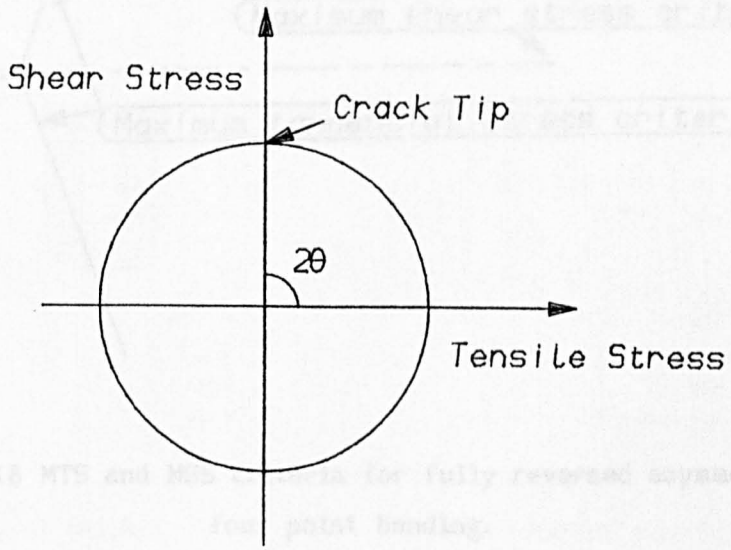

Fig. 1.16 Mohr's circle for asymmetric four point bending.

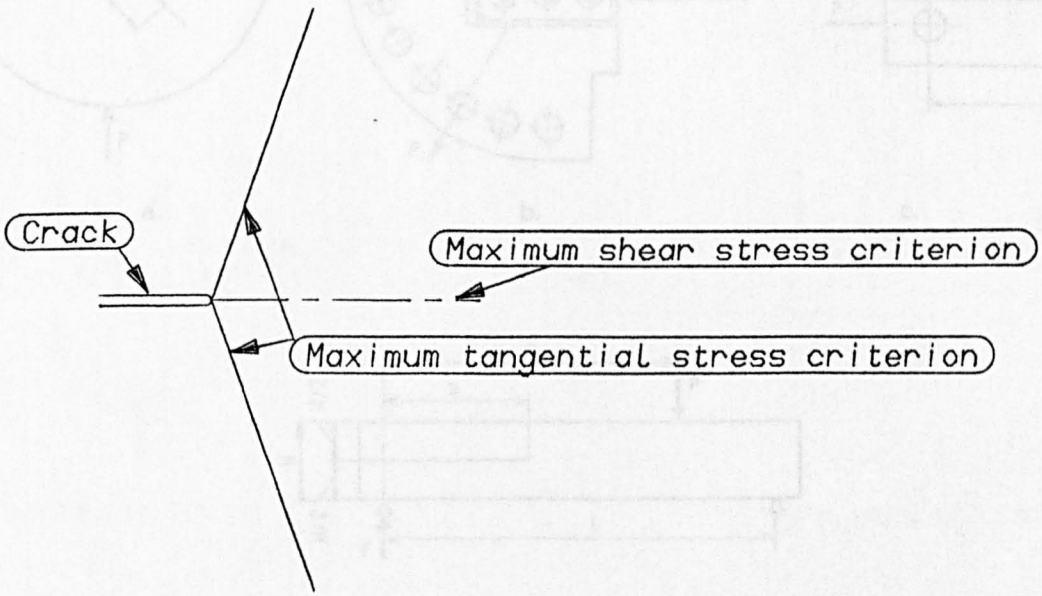

Fig. 1.17 MTS and MSS for asymmetric four point bending.

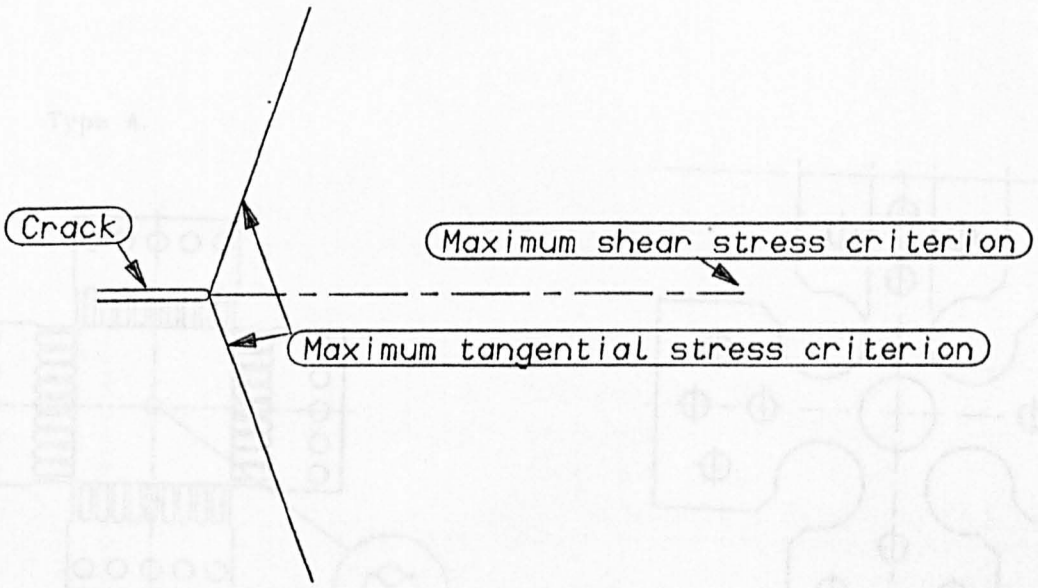

Fig. 1.18 MTS and MSS criteria for fully reversed asymmetric four point bending.

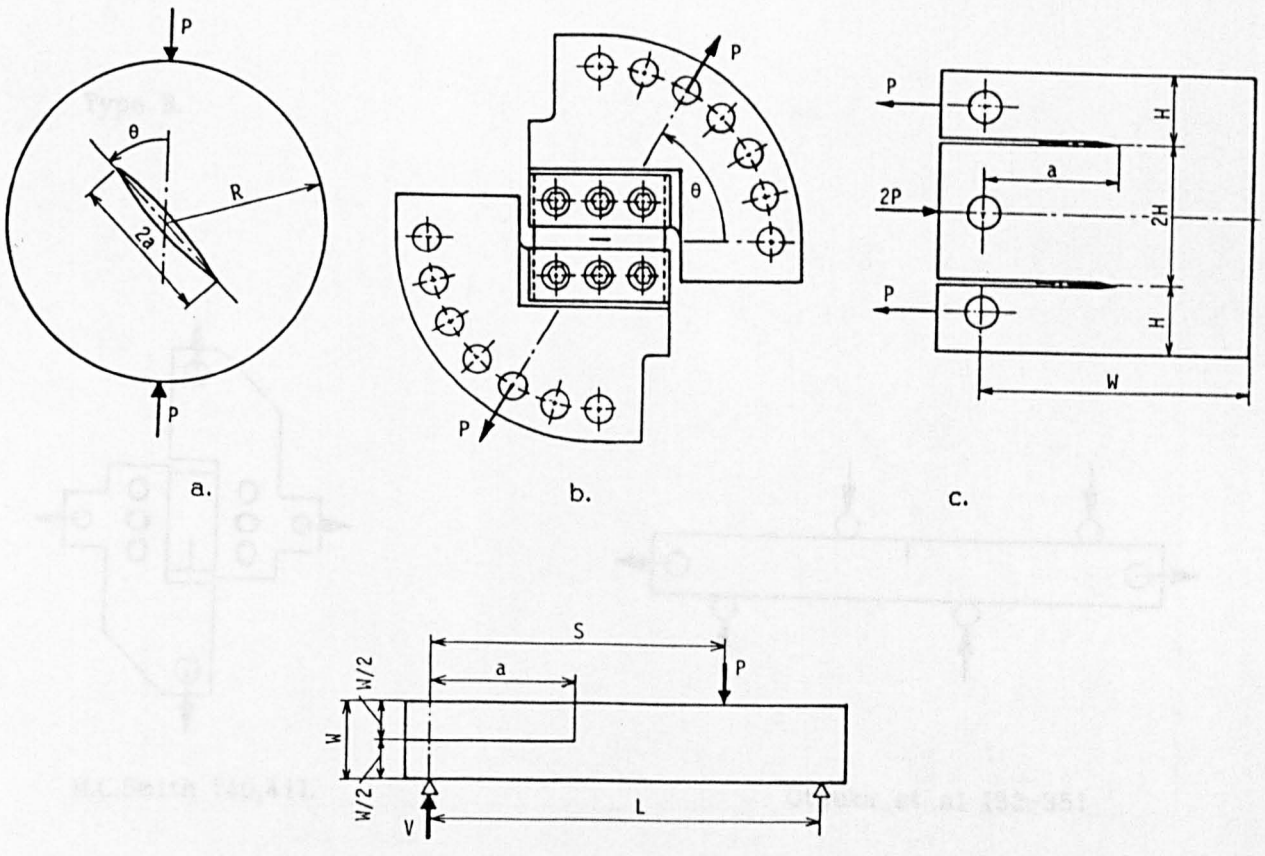

Fig. 1.19 Mode II Specimens.

Type A.

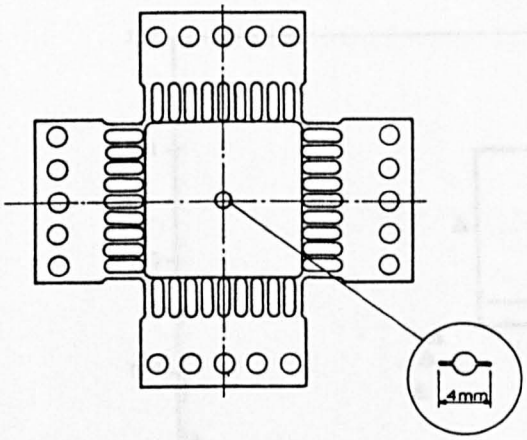

Gao Hua et al [61,62].

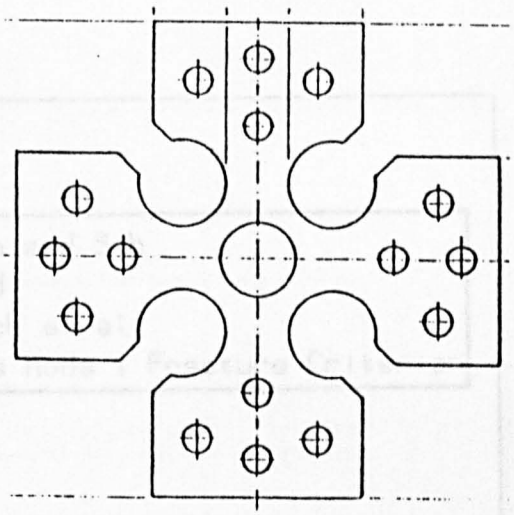

Pascoe and Smith [76,77].

Type B.

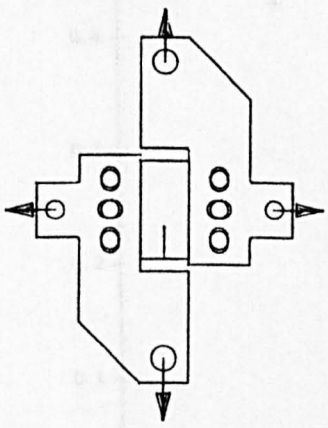

M.C.Smith [40,41].

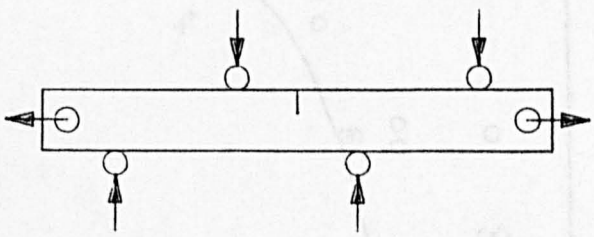

Otsuka et al [32-35]

Fig. 1.20 Biaxial Specimens.

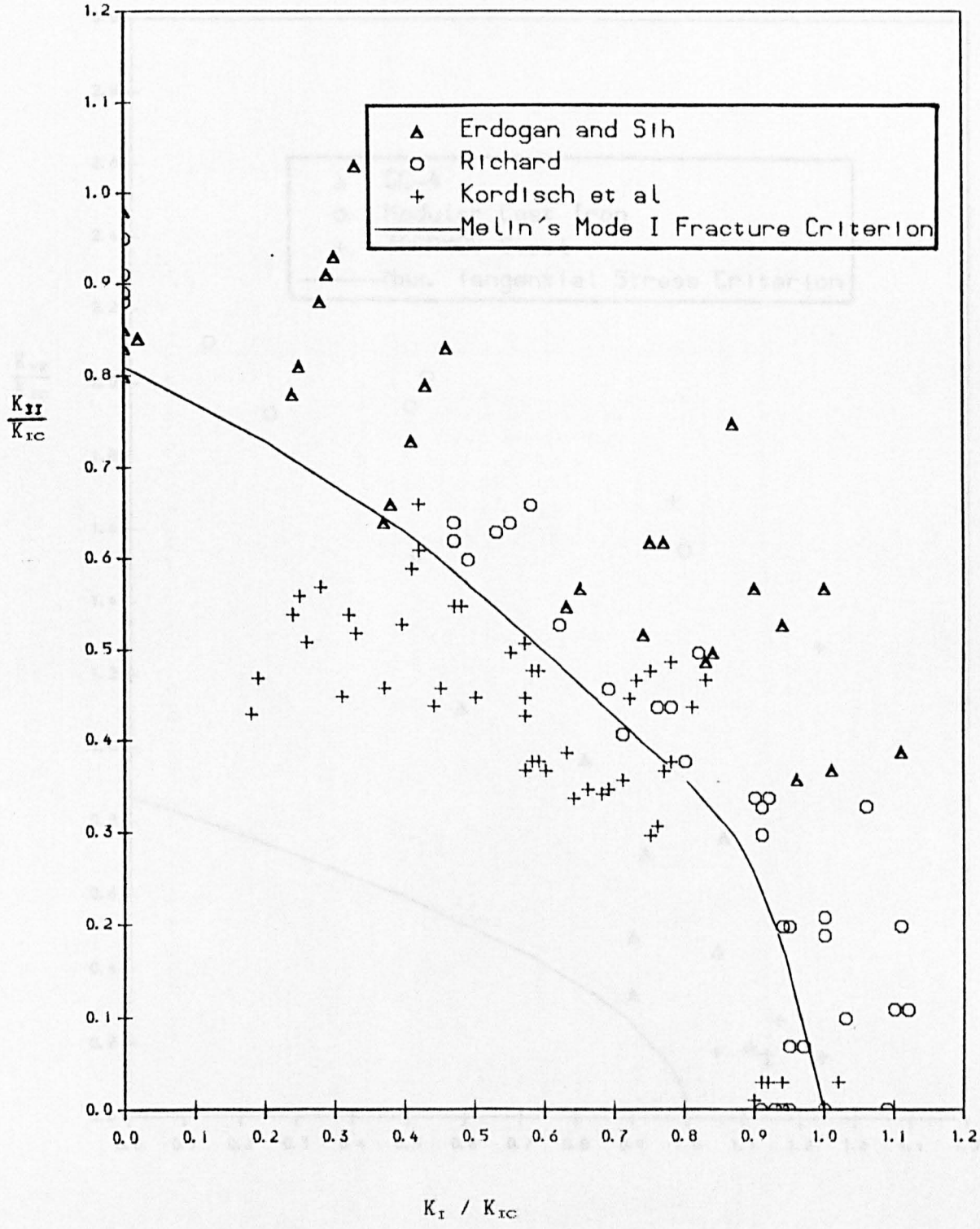

Fig. 1.21 Mixed Mode Fracture of PMMA [36].

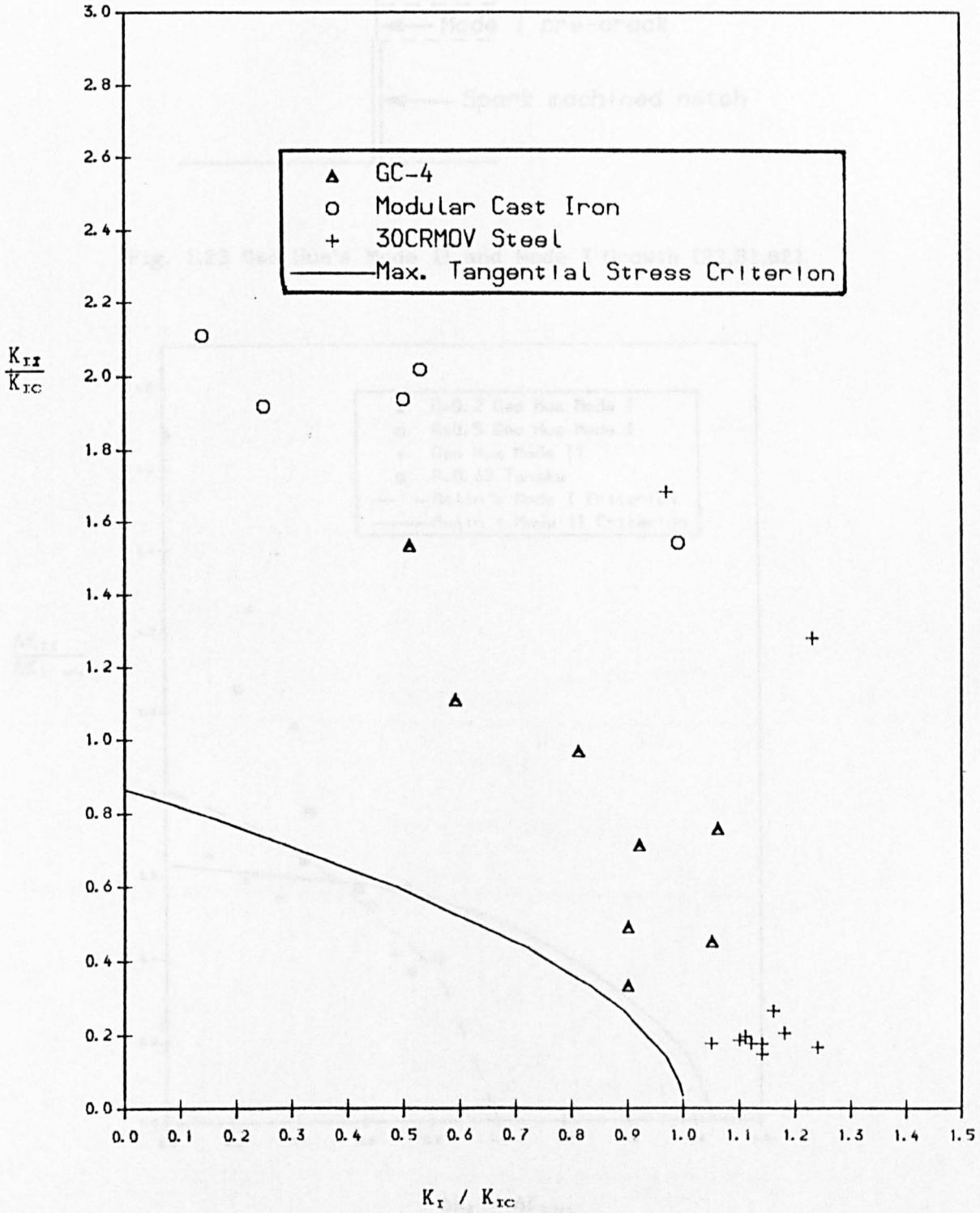

Fig. 1.22 Mixed Mode Fracture of Steel [60].

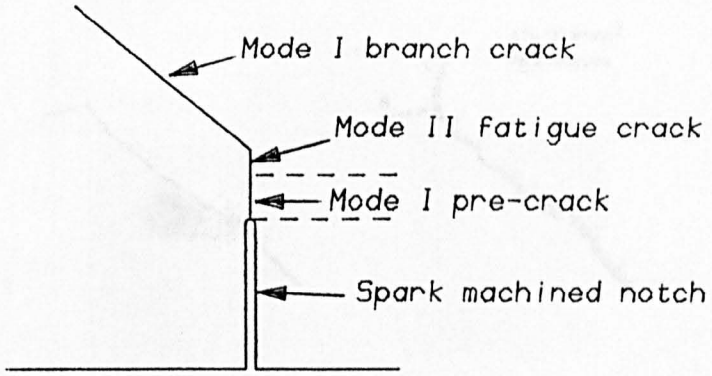

Fig. 1.23 Gao Hua's Mode II and Mode I Growth [22,61,62].

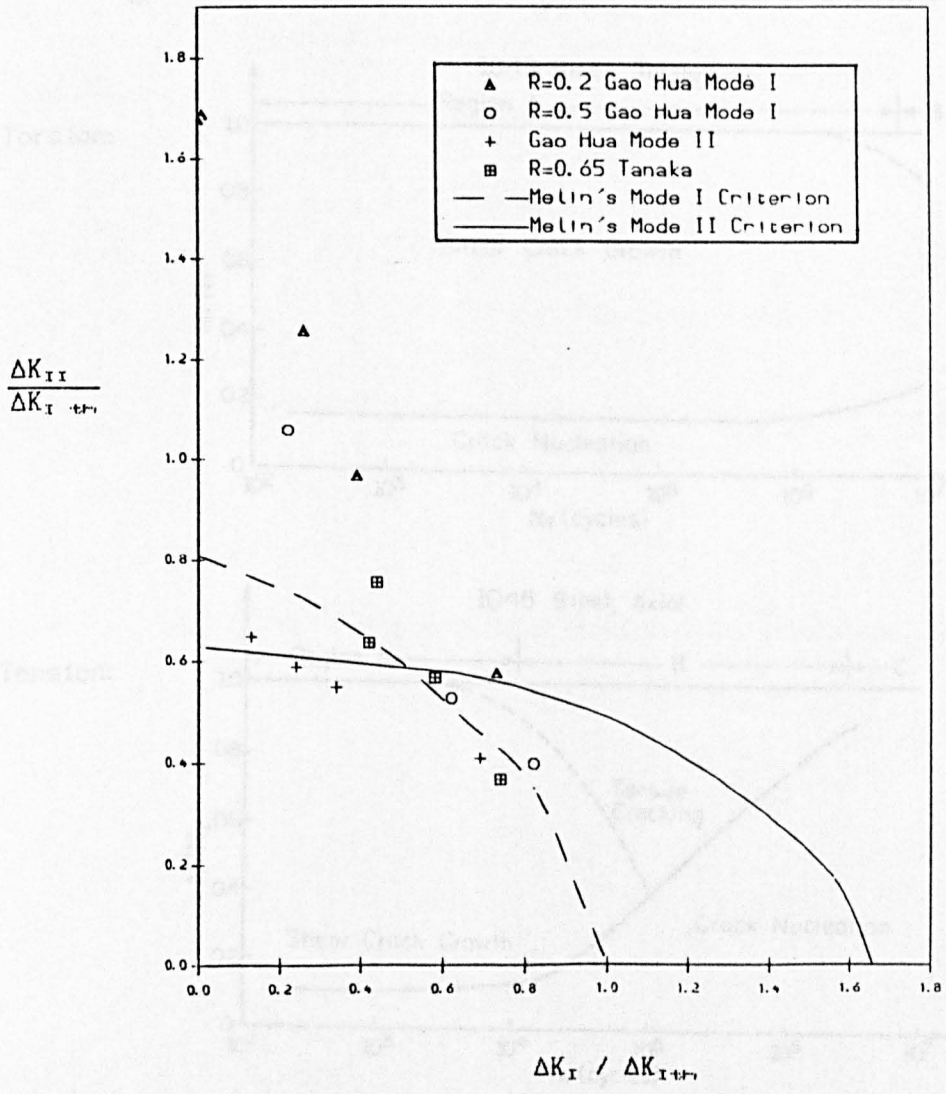

Fig. 1.24 Gao Hua's Mode I and Mode II Thresholds [22,61,62].

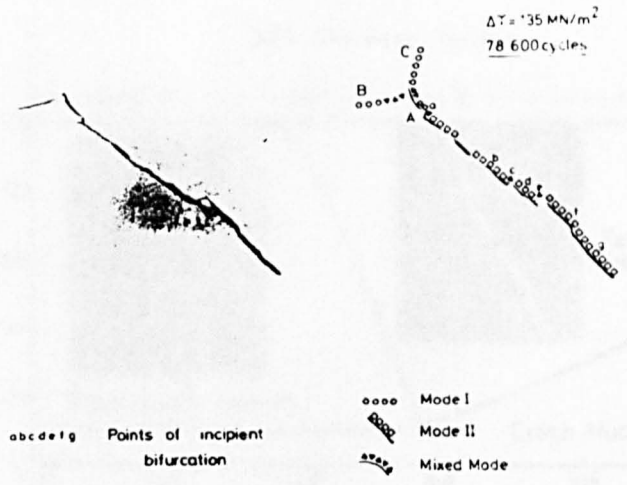

Fig. 1.25 Pascoe and Smith's Mode I and Mode II Growth [76,77].

Torsion:

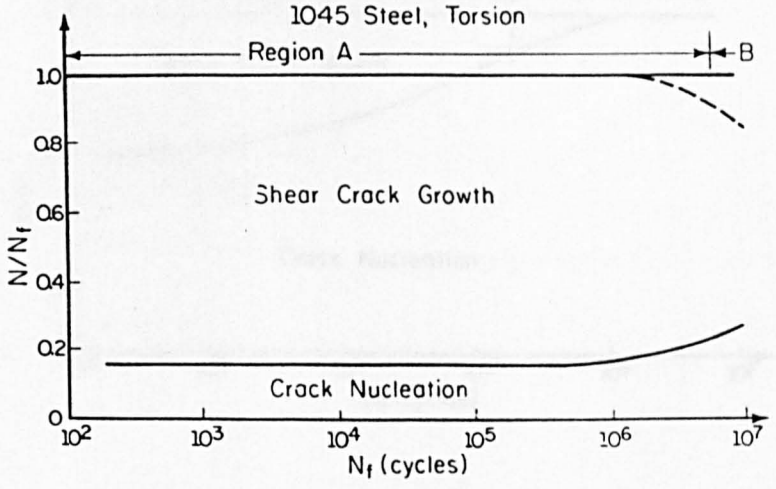

Tension:

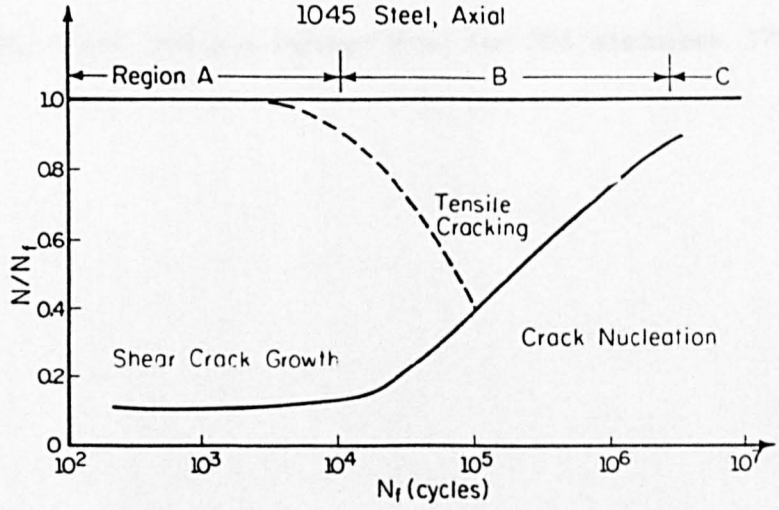

Fig. 1.26a. Fatigue Damage Maps for 1045 Steel. [79]

Torsion:

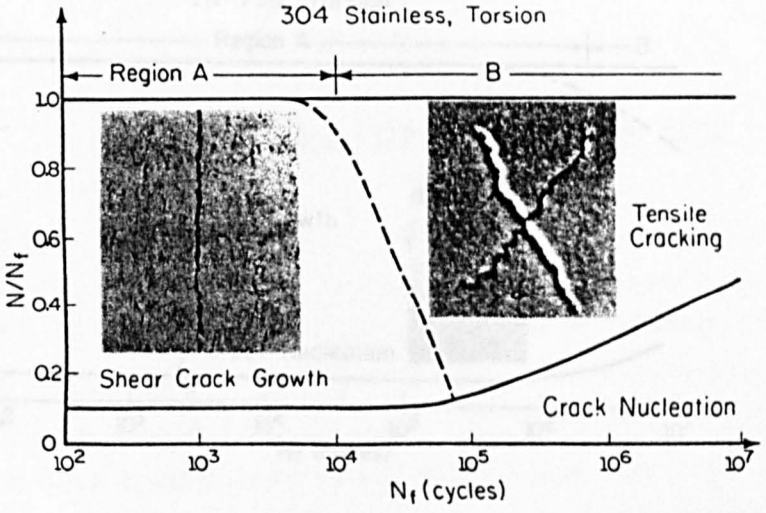

Tension:

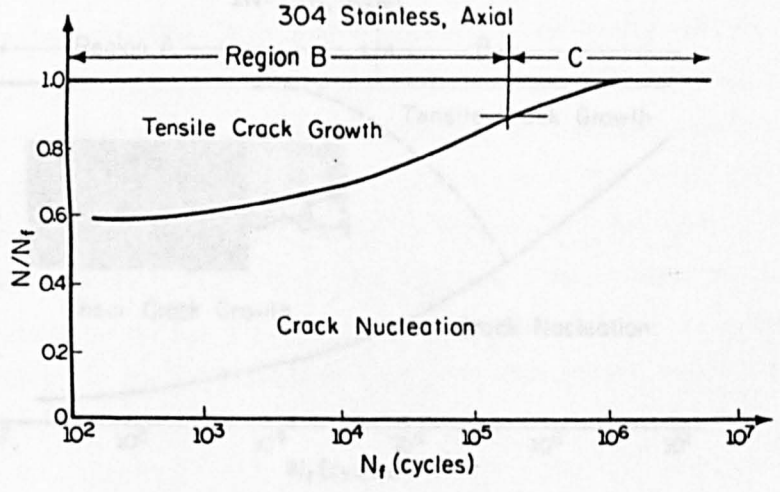

Fig. 1.26b. Fatigue Damage Maps for 304 stainless. [79]

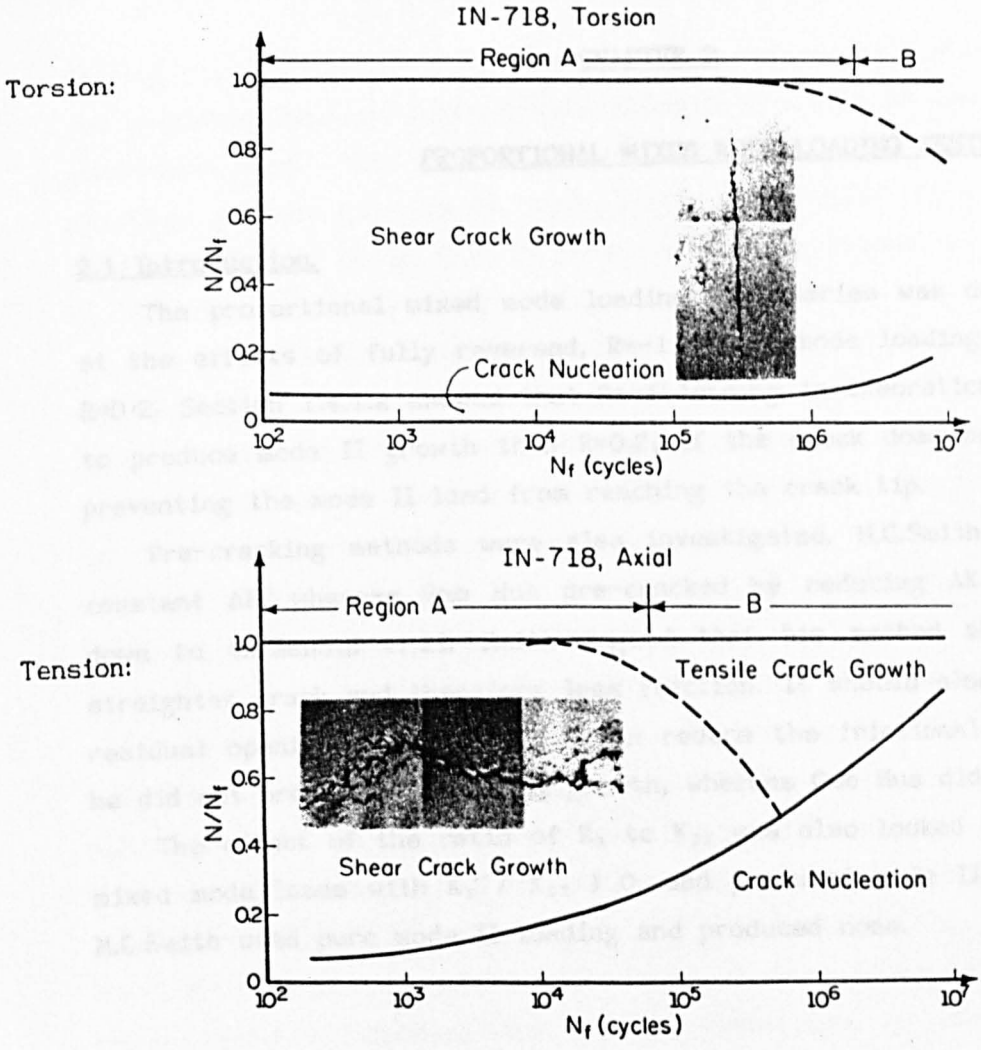

Fig. 1.26c. Fatigue Damage Maps for Inconel. [79]

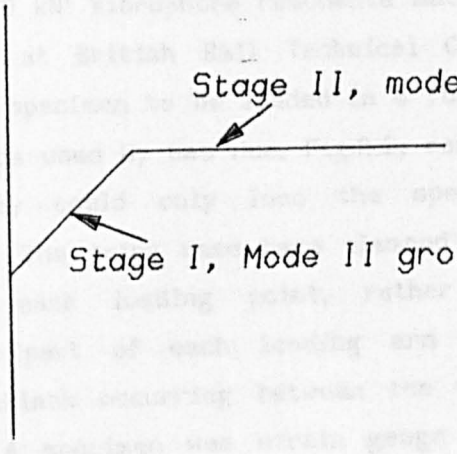

Fig. 1.27 Stages of Plane Specimen Fatigue.

CHAPTER 2.

PROPORTIONAL MIXED MODE LOADING TESTS.

2.1 Introduction.

The proportional mixed mode loading test series was designed to look at the effects of fully reversed, R=-1, mixed mode loading, as opposed to R=0·2. Section 1.4.1.2 showed that R=-1 loading is theoretically more likely to produce mode II growth than R=0.2, if the crack does not lock, thereby preventing the mode II load from reaching the crack tip.

Pre-cracking methods were also investigated. M.C.Smith pre-cracked at constant ΔK, whereas Gao Hua pre-cracked by reducing ΔK in 10 % steps down to threshold [1,2]. Smith argued that his method should produce a straighter crack and therefore less friction. It should also leave a larger residual opening, which should again reduce the frictional forces. However he did not produce any mode II growth, whereas Gao Hua did.

The effect of the ratio of K_I to K_{II} was also looked at. Gao Hua used mixed mode loads with $K_I / K_{II} > 0$, and produced mode II growth, whereas M.C.Smith used pure mode II loading and produced none.

2.2 The Testing Method.

All but one of the tests in this series were done using the asymmetric four point bending method, as described in section 1.4.1.2. Three different rigs were used:

1. A '100 kN' Vibrophore resonance machine was used for all the tests carried out at British Rail Technical Centre Derby. The grips on this enabled the specimen to be loaded in a fully reversed manner, Fig. 2.1. The type of grips used by Gao Hua, Fig.2.2, restricted the cyclic load to R > 0 because they could only load the specimen when the grips were in compression. The grips used here clamped the specimen on the top and the bottom at each loading point, rather than merely pushing it. The compressive part of each loading arm included a wedge mechanism to prevent backlash occurring between the tensile and compressive parts of the cycle. A specimen was strain gauge tested by British Rail when the grips were first used to check that no residual stress was applied in

setting up. The machine unfortunately could not run at 100 kN, in spite of its specification, and instead only managed about 15 kN under the loading conditions used. The specimen dimensions are given in Fig. 2.3. The specimen was designed to be much longer and thinner than the specimens used by Gao Hua et al [2], in order to obtain reasonably high values of K_{II}. The frequency was about 56 Hz.

The crack length was measured with a potential drop system using a single pair of leads, and using optical microscopes on the front and back faces of the specimen. Two different microscopes were used, one could resolve a change in crack length of about 0·05 mm, the other about 0·02 mm. The potential difference system could also theoretically measure a 0·02 mm change. Details of the potential difference equipment and calibrations are given in Appendix 3.

2. A 100 kN Schenck servo hydraulic testing rig was used at Sheffield, using ordinary asymmetric four point bending grips that restricted the load to $R > 0$, Fig. 2.2. The crack was again measured using a potential drop system but this time using three pairs of leads, for greater accuracy. Two pairs of leads measured the potential dropped across the crack. The mean of these two was then taken. The other pair of leads also measured the potential dropped across the crack, but from 20 mm either side of the crack. The ratio between the two was then used to calculate the crack length. This gave a calibration that was independent of the current through the specimen, and the resistivity of the specimen, both of which will vary with temperature.

An optical microscope was also used, capable of resolving 0·02 mm of crack growth. The specimen dimensions are given in Fig. 2.4. These specimens were shorter thicker and wider, so that higher loads were required to grow the cracks. These were chosen because servo-hydraulic machines do not work well when only a small percentage of their load capacity is used. The testing frequency varied between 10 and 20 Hz.

3. The other test used a cruciform specimen, in one of the Sheffield servo-hydraulic biaxial testing machines. The specimen, grips, and machine are described in Appendices 1 and 2. Again the crack length was measured using a potential drop system, this time with two pairs of leads. Both pairs again measured the potential across the crack, one from close to the crack, one from points 20mm away so that the crack length calculation was

not affected by temperature. The crack length was also measured using one optical microscope capable of resolving 0·02 mm of crack growth.

In all these tests the initial mixed mode load was chosen to be below threshold. The load was then increased in 10 % steps until failure occurred. The load was only increased after 200 000 cycles during which no growth was observed. This enabled a crack growth rate of 1×10^{-10} m/cycle to be detected. One definition of threshold is $2{\cdot}5\times10^{-10}$ m/cycle, which is approximately one atomic spacing per cycle [2], so it was assumed that 200 000 cycles would be enough to detect this.

Mode I threshold and crack growth data was also collected for use in the analysis. The mode I thresholds were given by:

$$R = 0{\cdot}44,\ \Delta K_{I\,th} = 6{\cdot}0\ \text{MPa}\sqrt{\text{m}}$$

$$R = 0{\cdot}22,\ \Delta K_{I\,th} = 9{\cdot}4\ \text{MPa}\sqrt{\text{m}}$$

$$R = -1{\cdot}0,\ \Delta K_{I\,th} = 18{\cdot}3\ \text{MPa}\sqrt{\text{m}}$$

The threshold values for R = 0·44, and R = -1·0 came from just one test each and so their repeatability is unknown. However the pre-cracking down to threshold was done at R = 0·2, and a mode I growth test was performed starting just above threshold, as well as the test designed to find the threshold accurately. These gave thresholds varying from 8·0 to 12·1 MPa$\sqrt{\text{m}}$, and a mean of 9·4 MPa$\sqrt{\text{m}}$. The test designed to give the threshold accurately gave 8·34 MPa$\sqrt{\text{m}}$. The details of these tests and the data, and comments on this scatter can be found in Appendix 4.

2.3 The Effect of Pre-cracking Methods on Mode II Thresholds and Growth.

Four tests were carried out under $K_{II}/K_I = 2$, and R = 0·2. Two of these tests used specimens pre-cracked at a constant ΔK_I of 18 MPa$\sqrt{\text{m}}$, two used specimens pre-cracked by reducing the load in 10 % steps down to threshold, growing at least 0.5 mm each step. Both pre-cracking methods grew the crack about 5 mm from a 5 mm starter notch, the specimen height being 25 mm.

The two specimens pre-cracked at constant ΔK_I produced no mode II growth, according to both the PD unit, and the microscopes, whereas the two pre-cracked by reducing the load to threshold, grew 0.15 mm and 0.17 mm in Mode II, prior to branching into mode I, according to the microscopes.

The PD unit did not give an accurate reading during these latter two tests because it picked up some electrical noise at the time when the growth occurred. The potential drop across the crack varied in this system with temperature, and because there was only one set of leads in these tests, it was not possible to obtain an accurate crack growth value from readings before and after the noise occurred.

All four tests produced branch crack growth at mode II stress intensities varying from 10·1 to 11·75 MPa$\sqrt{m}$, as shown in Table 2.1. The pre-cracking method apparently made no difference to this.

2.4 The Effects of R ratio and K_I to K_{II} ratio.

Two tests were performed under R=-1 loading, using fully reversed asymmetric four point bending. Both used the load reducing pre-cracking technique, as described in section 2.3. One used K_{II}/K_I = 2, the other used K_{II}/K_I = 8. Both produced mode II growth, the first produced 0·05 mm, the second produced 0·15 mm, as shown in Table 2.1. Another test was also done at R=-1, but using a cruciform specimen. Again the load reducing technique was used in pre-cracking, but this time the starter notch was only 0·18 mm wide having been cut by spark erosion using a 0.1 mm wire. This meant that the pre-cracking could begin at a lower stress, so a shorter pre-crack, 1·5 mm long was produced. The notch half length was 2 mm. This time K_I/K_{II} was zero. No mode II growth was observed.

Two tests were also performed using asymmetric four point bending at R=0·2, with K_{II}/K_I = 8, pre-cracked by the load reducing method. No mode II growth that could be detected.

The mode I branch crack loading could not be produced by the Vibrophore for the R=-1 tests. The load was increased after the mode II cracks had arrested, but no growth occurred. The maximum theoretical values of K_{II} were 14·5 and 16·8 Mpa$\sqrt{m}$. In the cruciform test, with R=-1 loading and K_I/K_{II}=0.0, mode I branch crack growth did occur, but it did not start from the crack tip. Instead it started from the notch tip, forming four branches, two from each end. The true branching load for the crack was therefore not attained.

Fig. 2.5 also shows the maximum theoretical K_I reached in each of these R=-1 tests, and compares them with the maximum tangential stress

criterion and Melin's theory. Both predict that branching should have occurred at lower loads than the highest ones applied.

The R=0.2 tests also all gave branch crack loads much higher than the theoretical predictions of Melin, or the maximum tangential stress criterion, Fig. 2.6. Test No.6 at K_{II}/K_I = 8 did not produce branch crack growth from the crack tip but from a point 2 mm before the tip, as shown in Fig. 2.7.

Test No.	R	Pre-Cracking Method	$\frac{\Delta K_I}{\Delta K_{II}}$	Mode II Threshold ΔK_{II}	Mode II Growth	Branching Threshold ΔK_{II}	Test Rig
				MPa√m	mm	MPa√m	
1	0.2	Const. ΔK	0.5	-	0·00	10.5	Vibrophore
2	0.2	Const. ΔK	0.5	-	0·00	11.75	Vibrophore
3	0.2	Red. Load	0.5	5.1	0.15	10.1	Vibrophore
4	0.2	Red. Load	0.5	5.3	0.17	11.3	Vibrophore
5	0.2	Red. Load	0.125	-	0·00	16.7	Schenck
6	0.2	Red. Load	0.125	-	0·00	>12.9	Schenck
7	-1.0	Red. Load	0.5	8.1	0·05	>14.5	Vibrophore
8	-1.0	Red. Load	0.125	10.2	0.15	>16.8	Vibrophore
9	-1.0	Red. Load	0·0	-	0·00	>19.8	Biaxial

Table 2.1 Results of Proportional Mixed Mode Tests.

2.5 Fracture Surfaces.

Fig.2.8 shows a scanning electron microscope image of the fracture surface of test No.4. There was no clear difference between the mode I pre-crack region and the mode II growth region. Both have large areas that have been smoothed by the crack faces rubbing together. A magnified view of this is given in Fig. 2.9. This surface damage was less extensive nearer the branching point, where the mode II growth took place, but it was not possible to distinguish a boundary between the pre-crack and the mode II.

Gao Hua et al [2] did see a difference between the mode II growth and the mode I growth. They described the mode II growth as being crystallographic, that is that the crack grew along crystallographic slip planes, rather than just growing on one flat plane. The difference may simply be because rail steel is fully pearlitic and so the grains do not have the same highly favourable slip planes.

2.6 Discussion.

The results of the investigation into pre-cracking are quite interesting. In the first place it offers one explanation as to why M.C.Smith recorded no mode II growth in his threshold experiments (1.4.3), when he was looking for it, and was using a good specimen. The implications are more far reaching than this though. One of the reasons that the method of pre cracking at a constant ΔK value was used, was that it was thought that the larger residual opening of the crack tip, and the straighter crack path, would reduce the friction on the crack faces, and therefore that it would increase the mode II growth. It was thought that friction attenuating the mode II loading at the crack tip was one of the major reasons for the arrest of mode II cracks. This may well be true, but it appears that removing the friction by giving the crack a residual opening prevents mode II growth for some other reason. The residual stress left by the pre-crack would be compressive, and this might inhibit the growth. However the process of mode II crack growth is not understood well enough to give a definitive answer.

The investigation into the effect of using fully reversed mode II loading was inconclusive. It was thought that the fully reversed cycle should make mode II growth more favourable than a cycle at a positive R ratio. However the crack apparently locked up so much that the mode II loading did not reach the crack tip, and therefore the theoretical arguments, about mathematical frictionless cracks, have very little to do with the reality.

The ratio between the mode II thresholds, and the mode I thresholds in ordinary mode I tests at the same load ratio, is about 0·5. This is similar to the ratio found by Gao Hua et al [2]. The mode II threshold at R=-1 is probably higher than the threshold at R=0·2 because the crack is completely locked for half the cycle at R=-1.

The mode I branch crack load was always much higher than the MTS criterion or the theoretical calculations of Melin predict. This, and the fact that the branch formed away from the crack tip in one specimen, support the theory that crack locking also has a very large effect on mode I branch loads, as explained in section 1.5.

2.7 Conclusions.

In conclusion it can be said that Rail Steel behaves in a similar manner to the other materials tested in asymmetric four point bending, producing around 0·1 mm of mode II growth, and forming a mode I branch crack at much higher loads. The mode II crack arrest, and the very high mode I branch crack loads are apparently caused by the crack locking up because of friction between the crack flanks. The extensive crack growth that occurs in 'squats' under a predominantly mode II load cannot be produced by asymmetric four point bending, and therefore more complicated non-proportional loading methods need to be investigated. The tests on pre-cracking methods showed that the residual plastic zone and the residual stress left by a pre-crack could retard or prevent mode II crack growth. Pre-cracks should therefore be produced by methods that leave plastic zones which are smaller than those produced in the first cycle of a test.

References.

1. M.C.Smith, R.A.Smith. 'Towards an Understanding of Mode II Fatigue Crack Growth.'
Basic Questions in Fatigue: Volume 1. ASTM STP 924, Eds. J.T.Fong, R.J.Fields. 1988. pp260-280.

2. Gao Hua, M.W.Brown, K.J.Miller. 'Mixed Mode Fatigue Crack Thresholds.'
Fatigue of Engineering Materials and Structures. Vol.5, No.1, pp1-17. 1982.

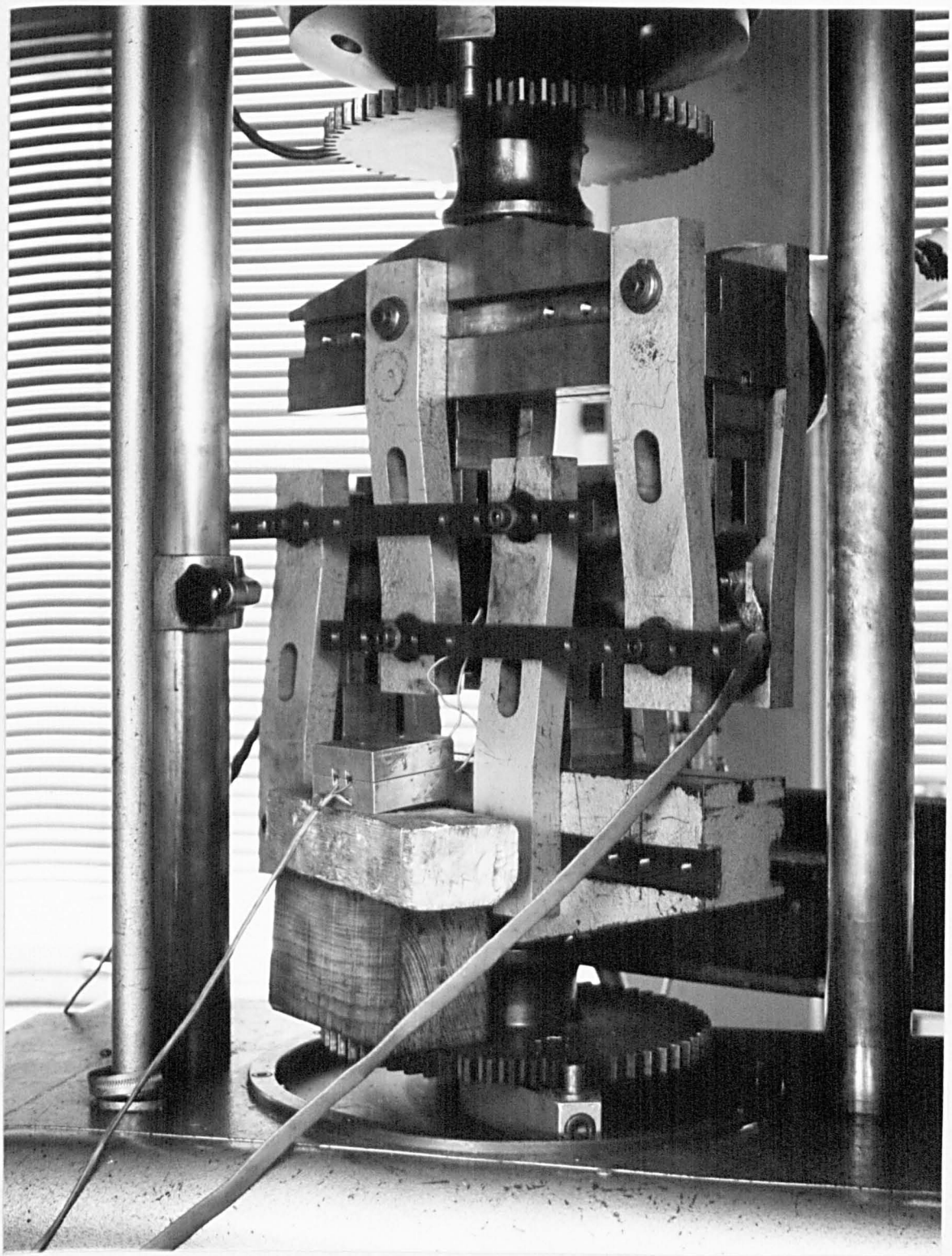

Fig. 2.1 The Vibrophore Grips For Fully Reversed Loading.

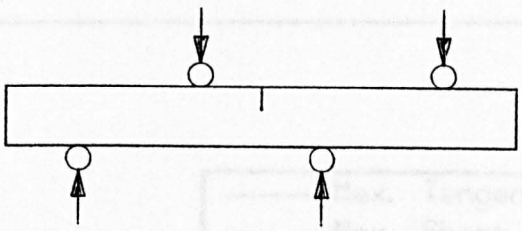

Fig.2.2 Ordinary Asymmetric Four Point Bending.

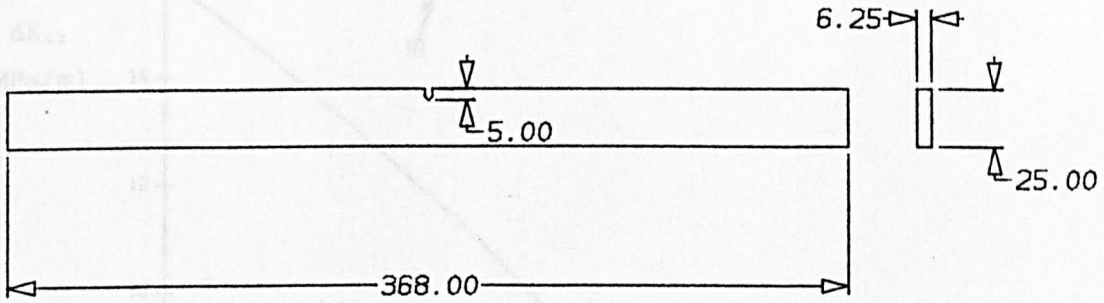

Fig.2.3 Specimen for the Vibrophore.
Dimensions in mm.

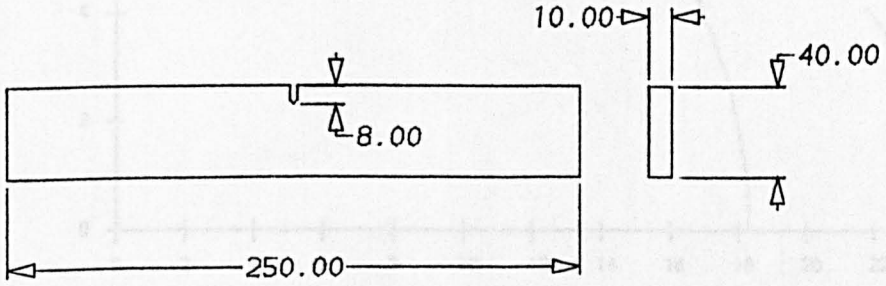

Fig.2.4 Specimen for the Schenck
Dimensions in mm.

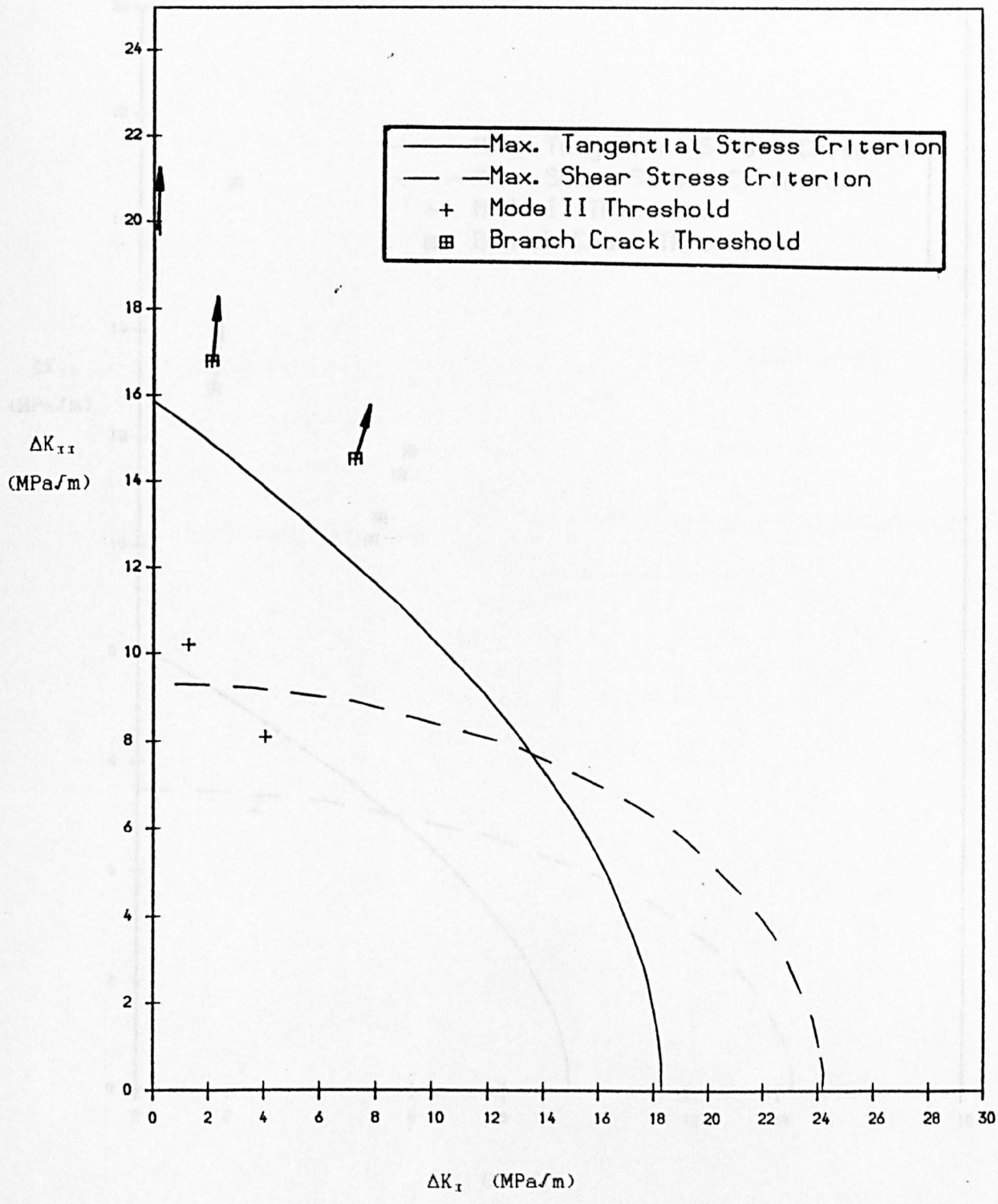

Fig. 2.5 Mixed Mode Thresholds at R = -1.0

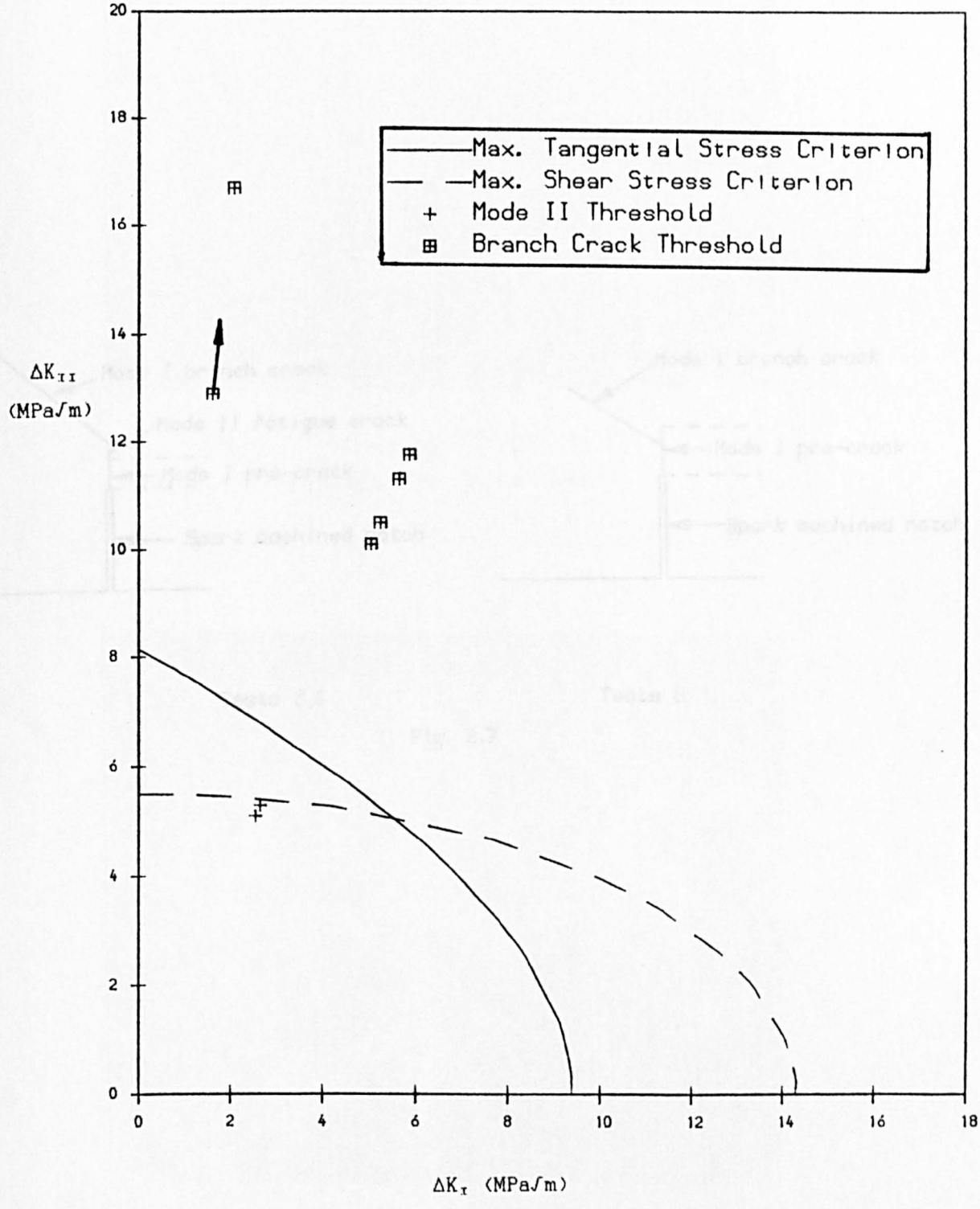

Fig. 2.6 Mixed Mode Thresholds at R = 0·2

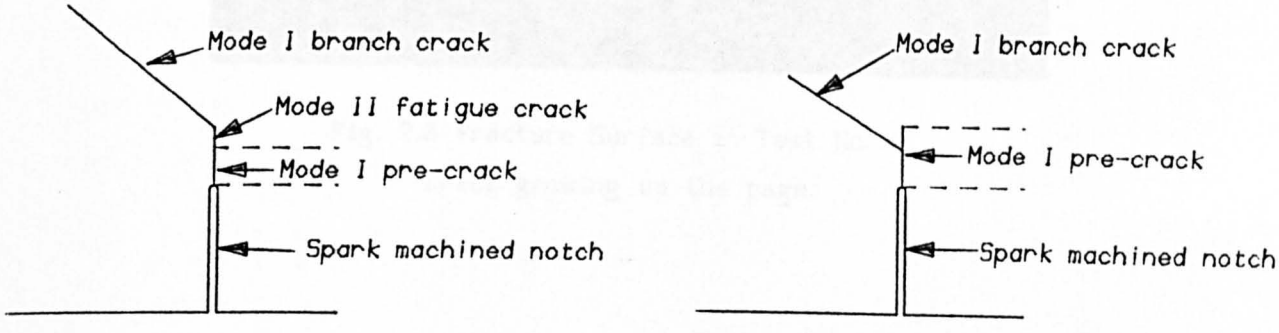

Tests 3,4

Tests 6

Fig. 2.7

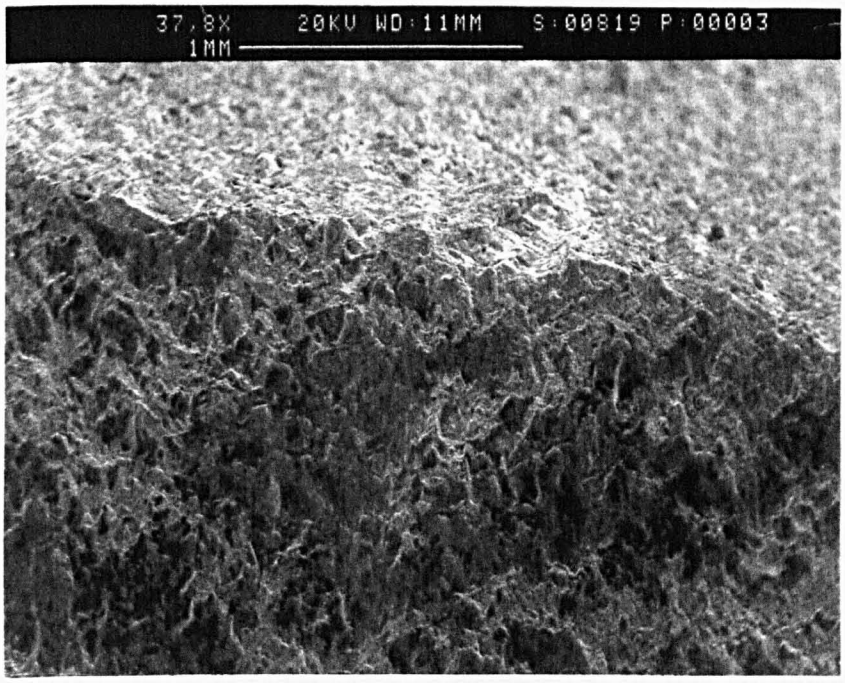

Fig. 2.8 Fracture Surface in Test No. 4.
Crack growing up the page.

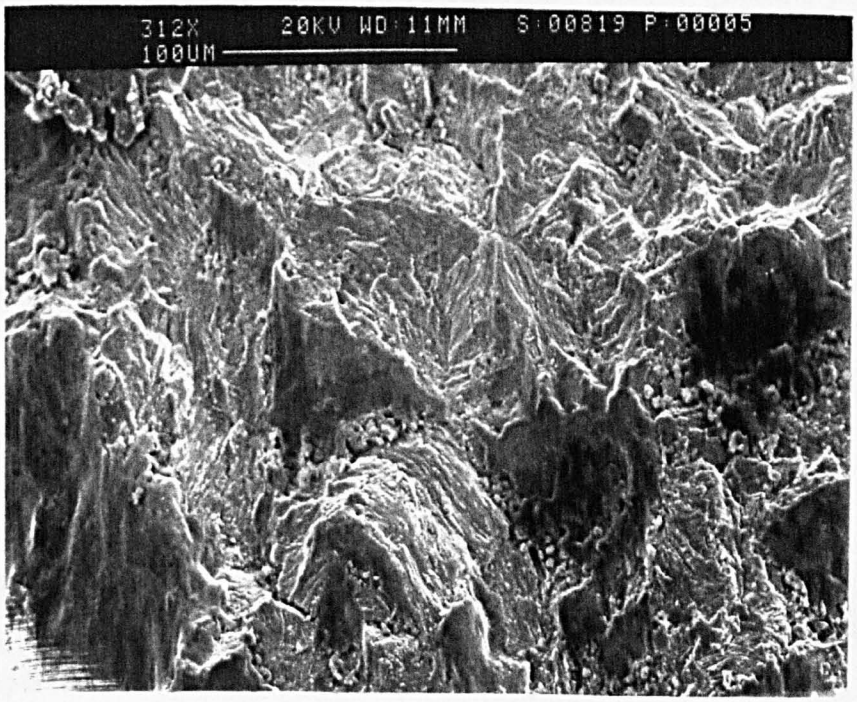

Fig. 2.9 Magnified View of Surface Rubbing Damage.
Crack growing up the page.

CHAPTER 3.

EFFECTS OF EQUIBIAXIAL MEAN STRESS AND STRESS RANGE ON FULLY REVERSED MIXED MODE FATIGUE.

3.1 Introduction.

This series of tests investigated three of the factors mentioned in the literature survey, that were thought to be important in deciding whether mode II rather than mode I crack growth occurred. See section 1.5.

The first factor is the effect of mode I mean stresses. The crack face roughness, oxide formation, and the formation of wear debris can all act to close, and therefore lock the crack. This would prevent any applied mode II load reaching the crack tip and producing a stress intensity [1]. The application of a mode I mean stress should unlock the crack. (However a mode I load may also make mode I branch crack growth more likely. See section 1.4.1.2.)

The second factor is the load range. From the experimental evidence available it appears that higher loads, or higher stress intensities at the crack tip tend to favour mode II rather than mode I growth. In particular Socie et al have shown that shear mode growth normally occurs in torsional fatigue at higher stresses [2].

The third factor is the effect of fully reversed loading. The MTS and MSS criteria combine to predict that mode II growth is more likely if the mode II loading is fully reversed, see section 1.4.1.2. Pascoe and Smith produced mode II growth by using fully reversed loading, with a mode I load to open the crack, and at high stresses [3].

The tests in this series were all conducted with fully reversed loading, looking at the effects of the other two factors.

3.2 Testing Method.

The tests were all carried out on Sheffield University's Mayes biaxial servo hydraulic test rigs. Details of these rigs can be found in Appendix 1. They use cross or cruciform shaped specimens, loaded by four servo hydraulic actuators. The capacity of the machines is +/- 200kN. For these tests the equibiaxial mean stress was applied by using the built in static

load control, and the cyclic shear stress was applied by using a signal generator. A tensile load on one axis, with an equal and opposite compressive load on the other, produce pure mode II loading on a crack at 45°.

A new specimen design was required for these tests, because the design used in previous tests on these machines was too large to be made out of a rail. It was also prone to failing from the edge of the working section, and was very expensive to manufacture. The new design is smaller, cheaper to manufacture, and should not fail at the edges under normal circumstances. The details can be found in Appendix 2.

The specimens were all made from one of two rails, from the same cast of rail steel. The same rail was employed for the tests described in chapters 2 and 4. The average chemical composition, monotonic, and cyclic stress strain properties of rail steel are given in Appendix 4. The chemical composition, and mode I threshold and fatigue crack growth data for the cast used are also listed in Appendix 4.

The crack lengths were measured on the front face by using a travelling microscope, capable of resolving 0·02 mm of crack growth. The crack lengths were also measured by using a direct current potential drop technique, with two pairs of leads, as described in Appendix 3. The two pairs of leads allow the crack lengths to be measured independently of the actual current, which varies with temperature. Theoretically this should allow a change in crack length of 0·02 mm to be resolved. This method has the advantage that it gives a measure of the average crack length across the crack front, rather than merely the crack length at the surface. The system also has the advantage that the crack lengths can be measured automatically, by using a data logger.

Both types of crack measurement gave a measure of the distance between the crack tips, rather than an absolute measurement. In the PD system this is because in the calibration it is necessary to assume that the crack is symmetrical. With the microscope it is because the centre of the specimen is not kept exactly still during the test, and so absolute crack lengths would require extra readings and calculations. The cracks were near enough symmetrical that this was not thought to be worthwhile. All crack lengths and growth rates calculated are therefore average crack lengths and growth rates.

3.3 Threshold Tests.

Two tests were carried out in which the specimens were loaded in cyclic mode II with a static mode I load, starting below threshold, and increasing in 10 % steps until growth occurred. About 1 000 000 cycles were done between load steps. The optical microscopes used had a resolution of approximately 0·02 mm, so that in 1 000 000 cycles a growth rate of 2×10^{-11} m/cycle could be detected. One definition of threshold is $2{\cdot}5\times10^{-10}$ m/cycle, which is approximately equal to 1 atomic spacing per cycle, so 1 000 000 cycles should easily identify this, [4]. The specimens were all pre-cracked by reducing the load down to threshold in 10 % steps. Again about 1 000 000 cycles were left before it was decided that the threshold had been reached, and the crack was allowed to grow at least 0·2mm between load increments to grow it through the previous load's plastic zone. The frequency was 20 Hz.

In the first test, RSB1, the equibiaxial mean stress was equal to 1/16 of the cyclic yield stress of the material, which was taken as 800 MPa. This corresponded to an initial K_I value of 6 MPa$\sqrt{m}$. ΔK_{th} at R = 0·44 was found to be 6·0 MPa$\sqrt{m}$, at R = 0·22 it was 9·4 MPa$\sqrt{m}$, and at R = -1·0 it was 18·6 MPa$\sqrt{m}$. It is possible to estimate a rough crack opening stress intensity, K_{op}, by assuming that the only effect of mean stress on threshold is to remove closure effects, and that at R = 0·44 no closure effects occur. This is essentially assuming that K_{op} is less than or equal to 4·7 MPa$\sqrt{m}$ in the R = 0·44 test. The result at R = 0·22 would then suggest a value of K_{op} equal to 6 MPa$\sqrt{m}$, and the result at R = -1·0 a value of K_{op} of 3·2 MPa$\sqrt{m}$. As the maximum value of K_I in the R = 0·44 threshold test is less than the maximum K_I for R=0·22 threshold test, this variation in the value of K_{op} is to be expected, and it can only be stated that the value is likely to be between 3 and 6 MPa$\sqrt{m}$.

Mode II growth occurred for about 0·03mm, at ΔK_{II} = 4·0 MPa$\sqrt{m}$, and then arrested. A further 0.02mm occurred at 4·8 MPa$\sqrt{m}$, and then no growth occurred until the load had been increased to ΔK_{II} = 6·3 MPa$\sqrt{m}$. Mode I branch cracks then formed, but rather than growing to failure as occurred in the asymmetric four point bending tests recorded in the previous chapter, they arrested. Small quantities of growth occurred again at 7·6 MPa$\sqrt{m}$, and 9·2 MPa$\sqrt{m}$, before continuous branch crack growth occurred at ΔK_{II} = 11·2 MPa$\sqrt{m}$, leading to failure, as shown in Fig. 3.1.

The second test, RSB2, had an equibiaxial mean stress equal to 1/3 of the cyclic yield stress, or 267MPa, corresponding to an initial K_I of 32 MPa$\sqrt{m}$. This time 0·08mm of mode II growth occurred at ΔK_{II} = 4·4 MPa$\sqrt{m}$, and branches formed at 4·9 MPa$\sqrt{m}$. These branches also arrested, but grew continuously to failure at 5·9 MPa$\sqrt{m}$. The crack path is shown in Fig. 3.2.

The threshold values are shown in Table 3.1 and are compared with the threshold from test RSB7. This test, recorded in the last chapter, was another cruciform test with fully reversed mode II loading, but it had no mean stress.

Table 3.1

The effect of mean stress on mode II and branch thresholds.

Test No.	Mean Stress	Mode II Growth	Mode II Threshold ΔK_{II}	Branch Crack Threshold ΔK_{II}	R ratio at branching load
	(MPa)	(mm)	(MPa$\sqrt{m}$)	(MPa$\sqrt{m}$)	
RSB7	0·0	0·00	-	>19·8	-1·0
RSB1	50·0	0·05	4·0	6·3 → 11·2	0·5 → 0·03
RSB2	267·0	0·08	4·4	4·9 → 5·9	0·85 → 0·83

The branch crack mode I growth rates were calculated and are shown in Fig. 3.3 and are compared with mode I growth rates in three point bending tests. Details of the K_I calibration are given in Appendix 6. It should be noted however that the calibration is not exact. A calibration was only available for cracks growing at 45° to the original crack, as opposed to growing initially at about 70° after branching, and then bending round towards 45°. The calibration predicts that initially the value of K_{II} will decrease as the crack length increases, but the magnitude of this decrease was not found accurately.

3.4 Discussion of the Threshold Tests.

It was suggested in the introduction that the static mode I load and the fully reversed mode II loading might provide conditions under which continuous mode II growth would occur. The simple part of this discussion is to say that they do not. A fraction of a millimetre of mode II growth was produced, which is more than occurred in test RSB7 which had no mean

stress, but the cracks arrested as occurred in the mixed mode asymmetric bending tests recorded in the last chapter. The mode II growth threshold in the bending tests was found to be about 10 MPa$\sqrt{m}$, for the fully reversed mixed mode tests, in which the crack was probably locked for about half the cycle, and about 5 MPa$\sqrt{m}$ for the R = 0·2 tests, where the crack was probably open for most of the cycle. The mode II growth threshold found here of around 4 MPa$\sqrt{m}$ for a crack that should be open all the time, is therefore in agreement.

The mode I branch load was very different from the branch loads in the bending tests, and in the pure mode II test on a cruciform specimen without a mean stress. In all the bending tests branching occurred at a mode II load of 10 MPa$\sqrt{m}$ or greater, and these tests all had a mode I stress intensity as well. The pure mode II loading in the cruciform specimen had not produced a branch crack at 19·8 MPa$\sqrt{m}$. The equibiaxial mean loads looked at in this chapter, reduced the initial branching loads to 6·3 MPa$\sqrt{m}$ and 4·9 MPa$\sqrt{m}$. The maximum tangential stress criterion predicts that branching should occur at a mode II load of 5·2 MPa$\sqrt{m}$, for a mode I threshold of 6·0 MPa$\sqrt{m}$. The mode I threshold for R = 0·44 was found to be 6·0 MPa$\sqrt{m}$, though the uncertainty in the threshold values might be as much as +/- 2 MPa$\sqrt{m}$, see Appendix 4. The main reason for the difference between the two types of test must be that the equibiaxial mean load prevents the crack locking. This then means that the MTS criterion can be applied.

These arguments seem relatively straight forward, but in fact there is a problem. The work so far has assumed that the reason that the mode II cracks arrest, and the reason why the mode I thresholds were higher than the MTS criterion predicted, was that the cracks locked. The mean stresses unlock the cracks, and bring the mode I threshold down to the MTS prediction, but they do not stop the mode II growth arresting. A definitive answer cannot be given without a better knowledge of crack growth mechanisms and crack tip deformations.

One part of the answer though, may be given by the work of Kfouri and Miller [5]. They used elastic plastic finite element analysis to model the growth of a crack from a starter crack that was opened by a large mode I load, where this mode I load was kept constant. Their model predicted that the new part of the crack would not open up to the same extent as the

starter crack. See Fig. 3.4. Some friction might therefore begin to attenuate the load at the crack tip, causing the growth to arrest. The relatively small increases in load might then allow mode I cracks to start to grow from just behind the crack tip.

Another feature of these tests that initially seemed surprising, was that the mode I branches arrested. Three factors may be involved in causing this crack arrest. Firstly the K_I calibration predicts that the value of K_I will actually decrease as the crack extends. The calibration, shown in Appendix 6, is not accurate, but it predicted that the value would decrease by 6 % as the branch grew to 0·1 times the starter crack half length, and that it would then increase. Secondly the crack extension might cause the crack flanks to touch and so reduce the load by friction, and form oxide and wear debris that would increase this friction. When the crack extended further the mode I opening displacement would prevent the faces touching. Thirdly any increase in load decreased the R ratio in this test, because the mean stress was kept constant. This would not actually cause a crack arrest, but it would make the necessary increase in load higher because the threshold increases as the R ratio decreases. In RSB2 with its 267 MPa mean stress only the first point applies, suggesting that the real decrease in K_I with branch crack length may be around 10% or 15%.

The use of mode I stress intensity factors, to correlate the branch crack growth in the threshold tests worked well when the branches were about half the length of the starter crack or greater. Fig. 3.3 shows that RSB1, at an R ratio of 0·03 grew at the same rate as the equibiaxial mode I test with a load ratio of 0·0. RSB2 with a load ratio of 0·83 grew at a rate in the middle of the bending test growth rates, whose load ratios varied from 0·22 to 0·44.

3.5 Tests with large scale plasticity.

Four tests were then performed under mode II cyclic loading under much higher loads, with a variety of mode I mean stresses. Pre-cracking for these tests was carried out using a stress intensity lower than the initial stress intensity of the mixed mode part of the test. It was assumed that there was no point reducing the load down to threshold, when the first cycle would wipe out the effects of a higher stress intensity.

The frequency used in the first test, RSB3, was 2 Hz, and in the others was 0·5 Hz.

The first two tests had a positive mean stress. The mean stress and the cyclic stress range in test RSB3 were both equal to 1/3 of the uniaxial cyclic yield stress, that is 267 MPa, for which Von Mises yield theory predicts a plastic strain range of 0·02 %, see Appendix 5. Test RSB4 had a mean stress of 133 MPa, with a stress range of 450 MPa. Von Mises predicts that this gives a cyclic plasticity of 0·23 %. Both tests produced about 1 mm of mode II crack growth before mode I branch crack growth took over. The crack paths are shown in Figs. 3.5 and 3.6.

Observation through a microscope while the test was running, showed that sometimes mode I and mode II cracks were growing at the same time. However the mode I crack relieves the stress at the mode II crack tip, and the mode II crack relieves the stress at the mode I crack tip. In these cases the mode I cracks ended up dominating.

The third test, RSB5, had no mean stress, and a shear stress range equal to 452 MPa. Initially mode II and mode I growth occurred together, the mode II growth branched to mode I, and the mode I growth at one time branched back to mode II. See Fig. 3.7. After the first millimetre of growth however the mode I became dominant, and grew until the test had to be stopped because of cracks growing from the edges.

The fourth test, RSB6, had a compressive mean stress of 133 MPa, and a cyclic shear stress of 452 MPa. This time about 0·15 mm of mode II growth occurred at one end and none from the other. Mode I growth then dominated, but the cracks did not accelerate. Instead they arrested, while other cracks started to grow from further up the pre-crack, as shown in Fig. 3.8. This time the test had to be stopped because the central section of the specimen began to buckle under the compressive stress.

3.6. Mode I Branch Crack Growth.

The branch crack growth data from these tests is plotted in Fig. 3.9, and is compared with the mode I data produced by British Rail at Derby in three point bending, and at Sheffield using cruciform specimens, see Appendix 4. The crack length used at all times was the crack length perpendicular to the loading axis. Only the microscope readings from these

tests were used, because in the first two tests the cracks branched parallel to the current, and in the second two tests the readings were meaningless because of shorting across the crack. The growth rates were calculated by using the seven point fitting routine given in ASTM E647, and the ΔK_I values calculated by using the calibration given in Appendix 6. The accuracy of this calibration is uncertain for short branch lengths, but the ASTM routine does not calculate growth rates for the first three measured points so stress intensities at these short lengths were ignored.

Fig. 3.9 shows that the branch crack growth data does not directly overlap with the mode I crack growth data. However it does suggest that the growth rates are too high for the given values of ΔK_I, and the given load ratios, apart from test RSB3 which had the lowest stress range. Test RSB6, where R = -3·8, is growing faster than test RSB14, where R = -1·0. Test RSB5 with R = -1·0 is growing faster than test RSB13 where R = 0·0. Also the branch crack growth in test RSB4, with R = -0·33, is faster than the branch crack growth in test RSB3 where R = 0·33. This is not surprising as LEFM no longer describes the crack tips at these loads. A mode I stress intensity of 50 MPa$\sqrt{m}$ has a plastic zone of about 2·5 mm. At the onset of branch crack growth the cracks had half lengths of only about 5 mm.

The branch crack growth data was therefore re-plotted, but this time against ΔK_ε. ΔK_ε is an elastic plastic fracture mechanics term which is relatively simple to calculate, but still takes into account the amount of plasticity, see section 1.2.3, and Appendix 5. This plot is given in Fig. 3.10. The effect of using ΔK_ε is to move the higher plasticity test data points to the right, because they have higher ΔK_ε values. RSB6 now is below and to the right of the other tests, as one would expect. The use of ΔK_ε is seen to improve the correlation of the data, however it is still an approximation. The branch cracks actually change their mechanism of growth from mode I to mode III in the branches, see Fig. 3.11. Also the effect of the finite width of the specimen has not been accurately modelled. However from an engineering point of view, this is not very relevant, as any component with a crack growing at anywhere near 1×10^{-8} m/cycle needs to be removed from service fast.

3.7. Discussion.

The results of this series of tests were in some ways rather surprising. When Pascoe and Smith tested HY100 steel cruciform specimens, under elastic-plastic cyclic shear loading, and with an equibiaxial mean stress they did produce continuous mode II growth. These results suggest that in rail steel this does not occur, but that instead the cracks will always branch into mode I. In section 1.4.5 it was noted that in torsion under the same loading conditions, some steels will grow in shear while others will grow in mode I [1]. The difference between Pascoe and Smith's work, and the results reported in this chapter is presumably therefore a similar difference in the normal behaviour of the materials.

These results do show that the fully reversed elastic plastic shear loading, with an equibiaxial mean stress, does produce more mode II growth than any of the tests done at lower stresses, or the two tests at a high load without a positive mean stress. The behaviour is in some ways similar to the behaviour of 'squats' where a number of mode I branches can form, growing in competition with the shallow angled crack, before one of the branches manages to grow fast enough to dominate. See Fig. 1.1, in chapter 1. However this loading does not produce the continuous shear mode growth that apparently occurs in 'squats'.

The fact that mode I and mode II cracks were sometimes growing at the same time and in competition, suggests that the use of the maximum tangential stress and the maximum shear stress criteria to decide which mode a crack should grow in may be inappropriate. These criteria depend purely on the stress intensities, and ignore the effects of mean stresses. As well as unlocking the crack, an equibiaxial mean stress opens the branch cracks. A uniaxial mean stress, perpendicular to the initial crack would only open the initial crack, and a compressive mean stress parallel to the starter crack could close the branch cracks. However it is not possible to apply this sort of loading to the cruciform specimens, and so this could not be investigated further in this project.

3.8 Conclusions.

In conclusion it appears that no combination of fully reversed mode II cyclic loading and equibiaxial mean stresses, at low or high stress levels, will produce continuous mode II growth in Rail steel. Near threshold the mode II cracks arrest and then mode I branch cracks form. At higher stresses a competition occurs between the mode I and the mode II cracks, but the mode I cracks always win. The maximum da/dN criterion, for deciding the direction of crack growth, see section 1.2.5, is therefore a good method for deciding which direction will dominate, if it can be applied over a finite crack length, and take into account the interactions of the different cracks.

Tests with a uniaxial mean stress perpendicular to the crack, might produce continuous mode II growth, because the branch cracks would not be kept open in the way they are by an equibiaxial mean stress.

A large equibiaxial mean stress appears to open the crack, so that the branch crack thresholds and growth rates can be predicted by normal mode I growth rate and threshold criteria. However it was also expected to stop the mode II cracks arresting, and this did not occur, the reasons for which are not fully understood.

References.

1. M.C.Smith, R.A.Smith. 'Towards an Understanding of Mode II Fatigue Crack Growth.'
Basic Questions in Fatigue: Volume 1. ASTM STP 924, Eds. J.T.Fong, R.J.Fields. 1988. pp260-280.

2. D.F.Socie. 'Fatigue Damage Maps.'
Fatigue '87. 3rd Int. Conf. on Fatigue and Fatigue Thresholds. University of Virginia. Eds. R.O.Ritchie, E.A.Starke Jr. Vol.2. pp599-616.

3. E.W.Smith, K.J.Pascoe. 'Fatigue Crack Initiation and Growth In a High Strength Ductile Steel Subject to In Plane Biaxial Loading.'
Multiaxial Fatigue. ASTM STP 853. Eds. K.J.Miller, M.W.Brown. pp111-134. 1985.

4. Gao Hua, M.W.Brown, K.J.Miller. 'Mixed Mode Fatigue Crack Thresholds.'
Fatigue of Engineering Materials and Structures. Vol.5, No.1, pp1-17. 1982.

5.. A.P.Kfouri, K.J.Miller. 'Crack Separation Energy Rates in Elastic-Plastic Fracture Mechanics.'
Proc. I. Mech. E. Applied Mechanics Group. Vol.190 48/76. pp571-584. 1976.

Figures.

Test RSB1. Threshold test, σ_{mean} = 50 MPa.

Fig. 3.1.

Test RSB2. Threshold test, σ_{mean} = 267 MPa.

Fig. 3.2.

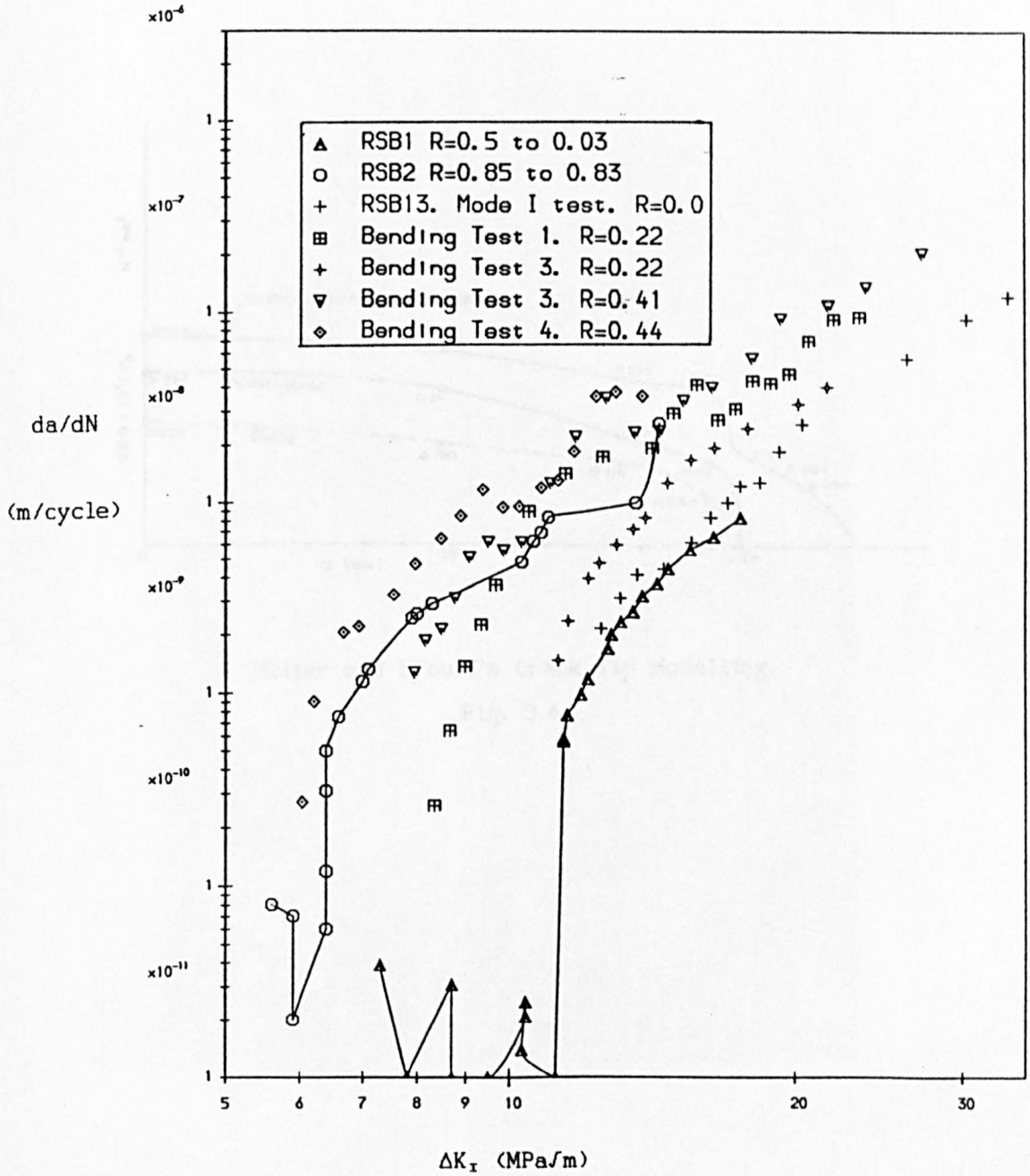

Branch crack growth data from threshold tests.

Fig. 3.3.

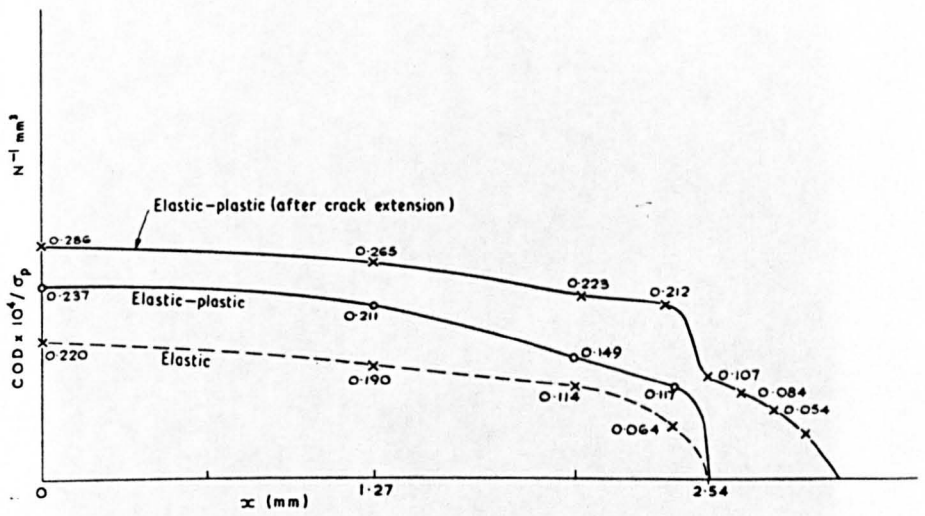

Miller and Kfouri's Crack Tip Modelling.

Fig. 3.4.

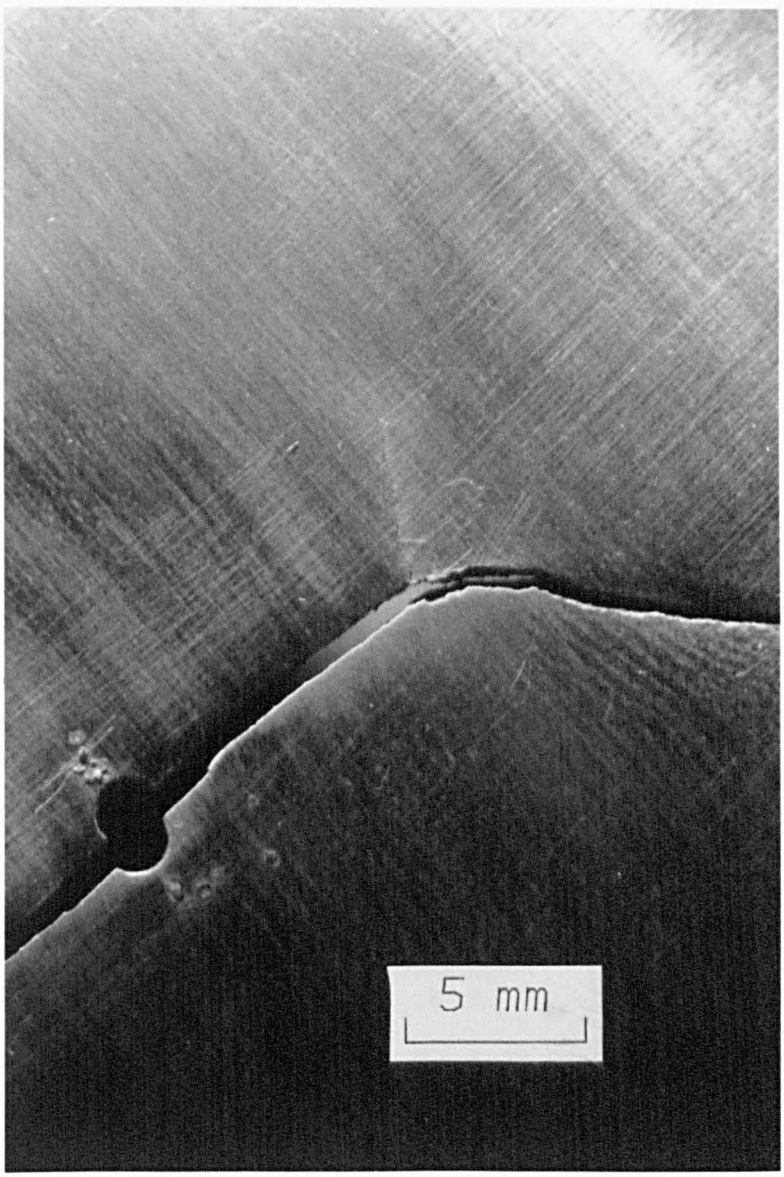

Test RSB3. $\Delta\sigma$ = 267 MPa, σ_{mean} = 267 MPa.

Fig. 3.5.

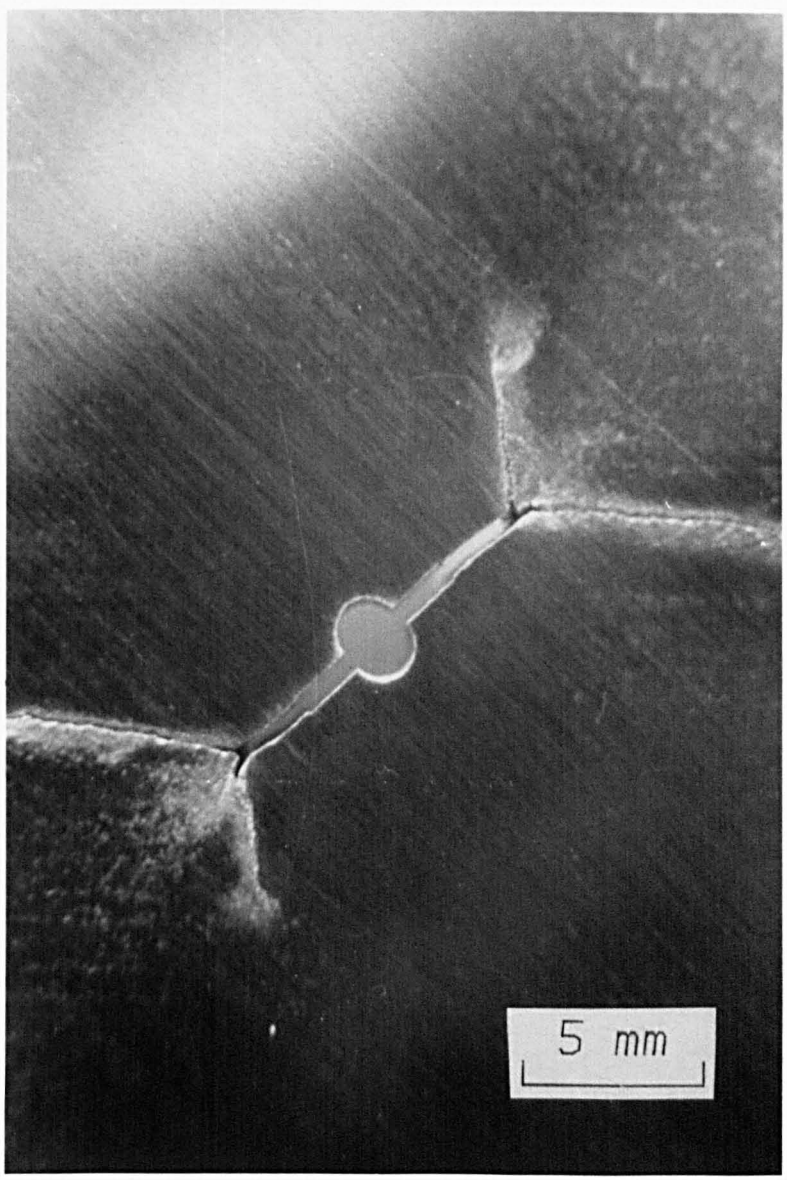

Test RSB4. $\Delta\sigma$ = 450 MPa, σ_{mean} = 133 MPa.

Fig. 3.6.

Test RSB5. $\Delta\sigma$ = 452 MPa, σ_{mean} = 0 MPa.

Fig. 3.7.

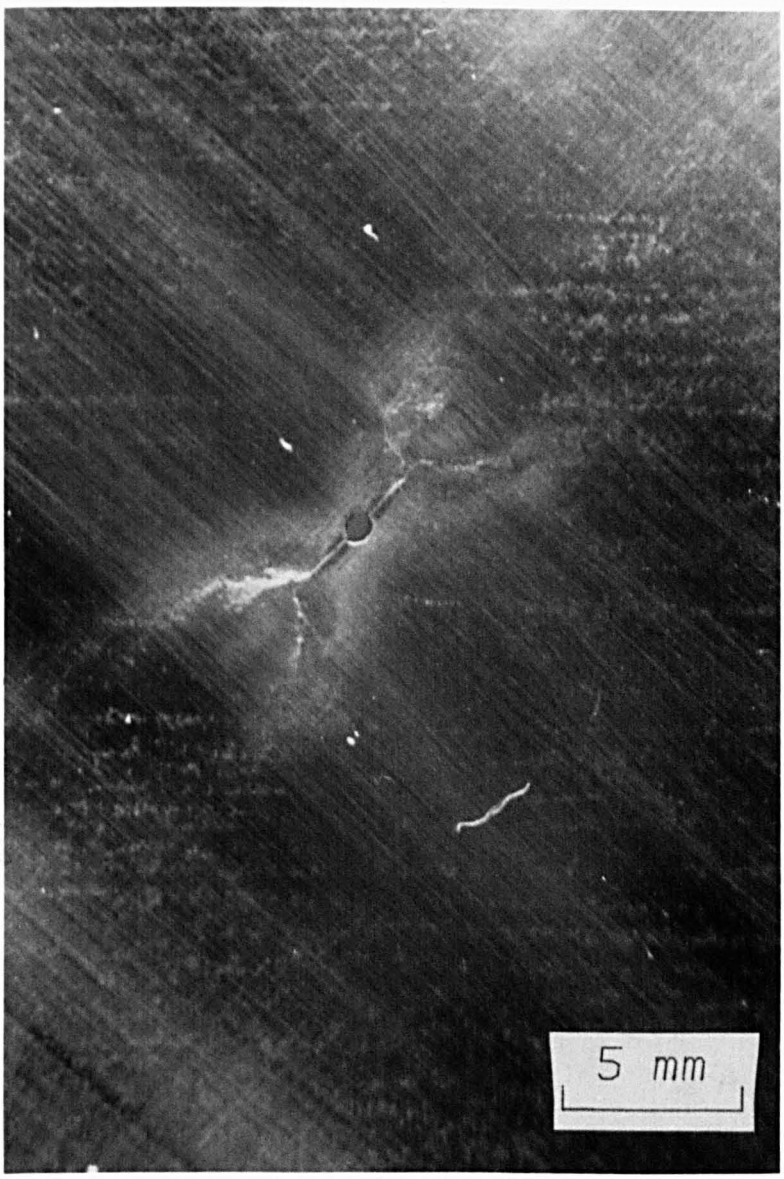

Test RSB6. $\Delta\sigma$ = 452 MPa, σ_{mean} = -133 MPa.

Fig. 3.8.

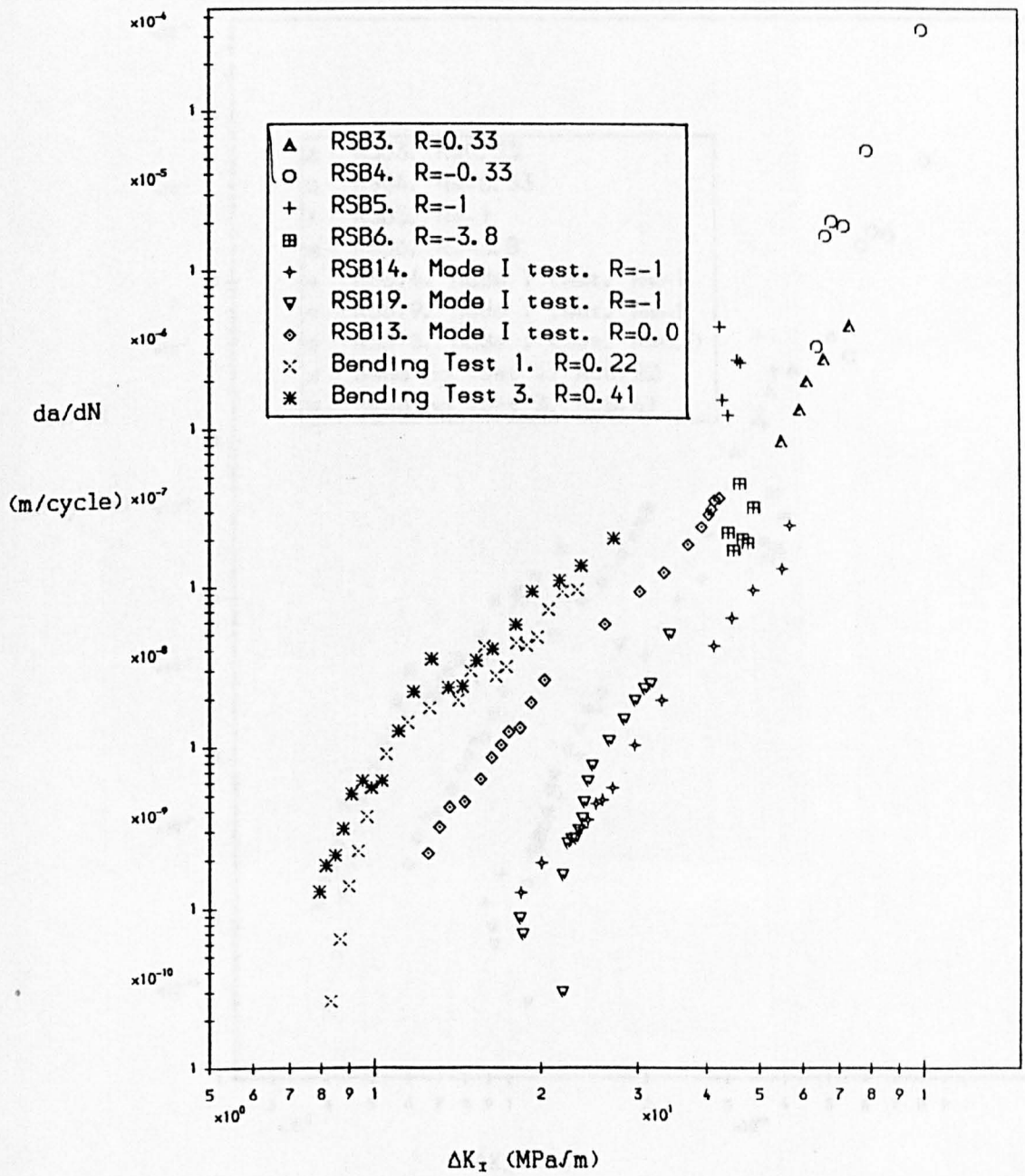

Branch Crack Growth Data from the High Stress Tests.

Fig. 3.9.

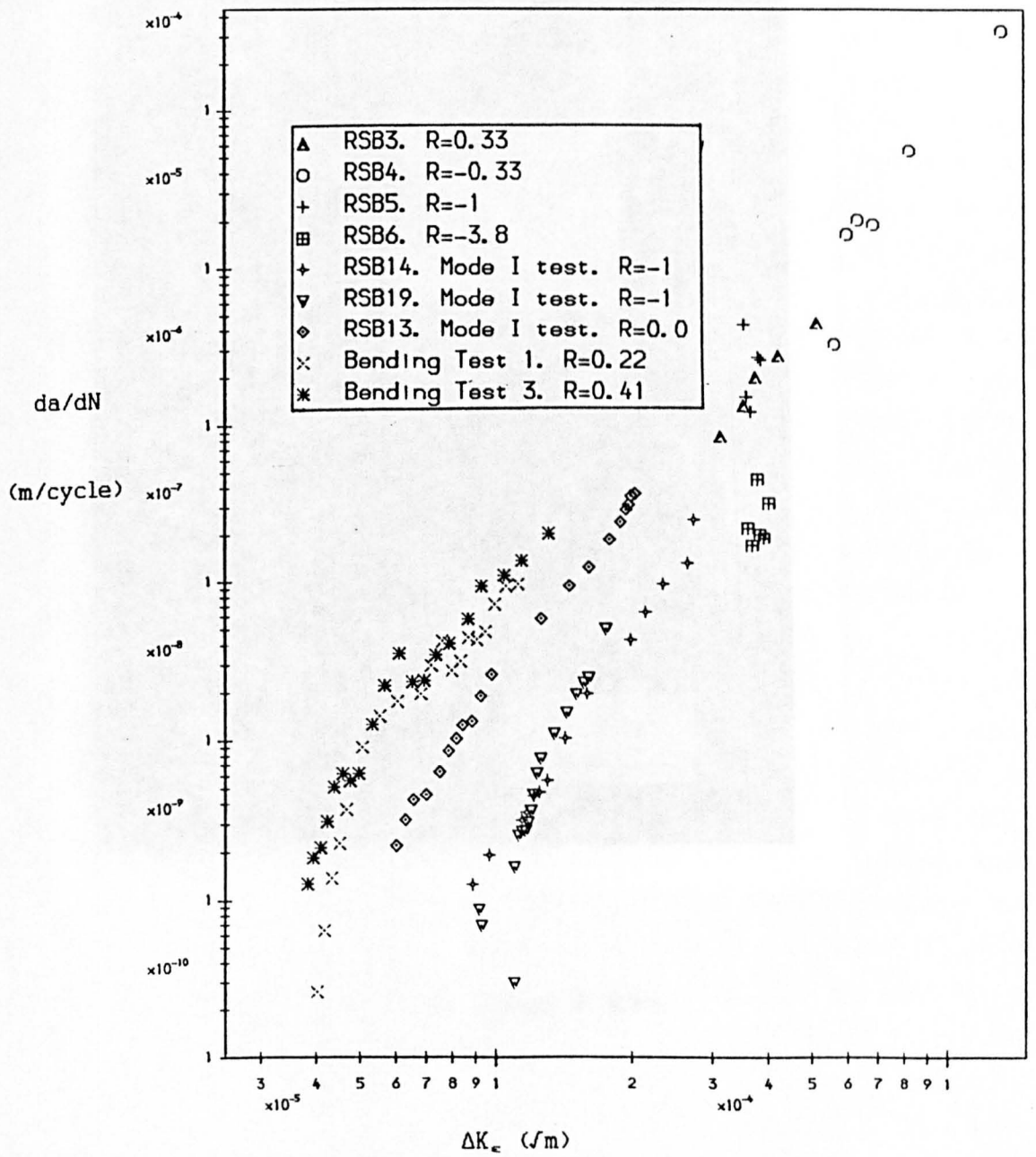

Branch Crack Data Plotted with ΔK_{eff}.

Fig. 3.10.

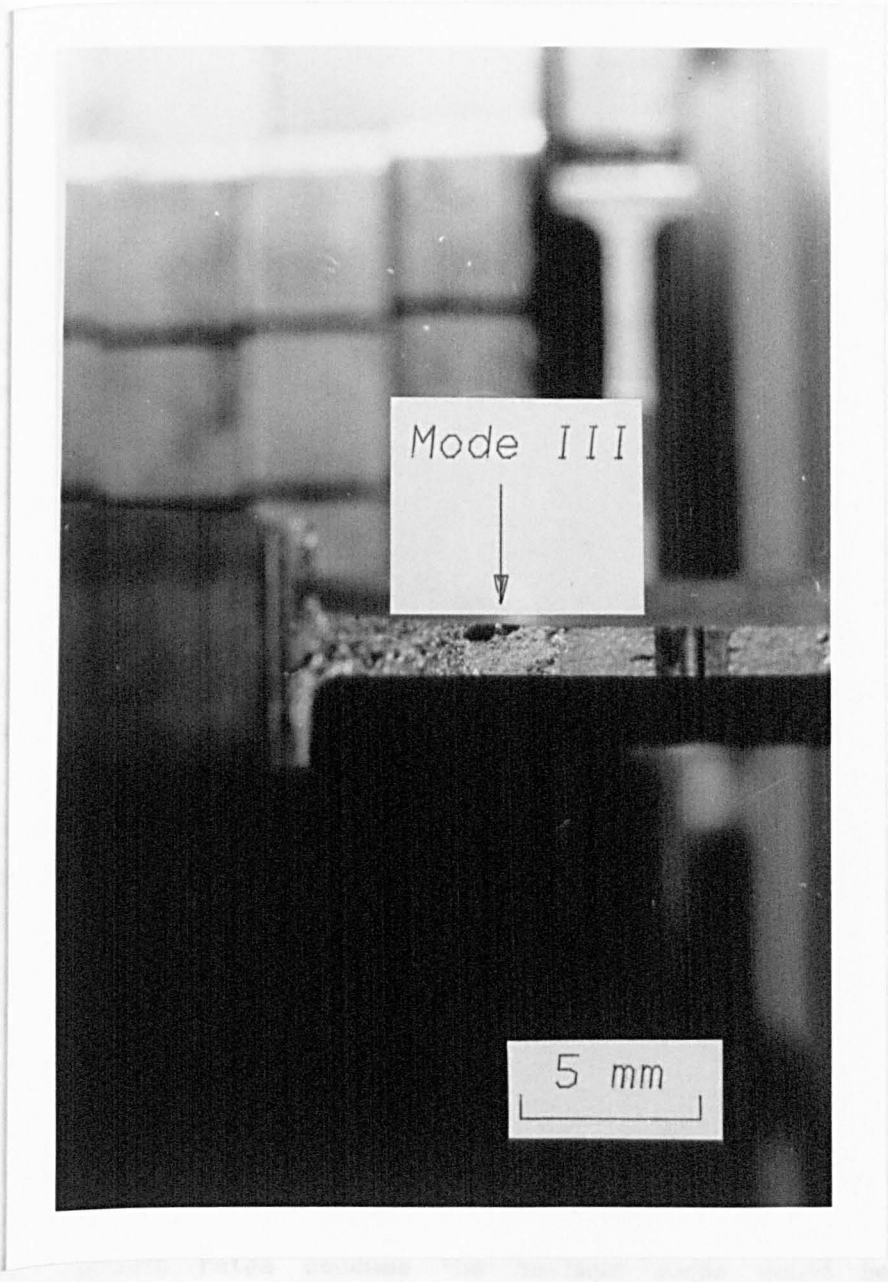

Mode I to Mode III Change in RSB4.

Fig. 3.11

CHAPTER 4.

SEQUENTIAL MODE I AND MODE II TESTS.

4.1 Introduction.

The mode II tests with a static mode I mean load reported in the previous chapter, showed that the coplanar crack growth found in squats could not be produced by a simple mode II cycle, even with a mode I load superimposed to open the crack. A series of tests was therefore carried out that more closely resembled the crack tip conditions calculated by Bower [1]. Details of his results can be found in section 1.3.2. He suggested that fluid, which must be present if rolling contact fatigue cracks are to grow, might be trapped inside the crack, and might pressurise the crack tip. This would produce a mode I load at the crack tip just before the mode II load reached the crack tip, Fig. 4.1. No tests using load sequences of this type could be found in the literature.

Two types of cycle were used in this series in an attempt to understand the interactions between the mode I and mode II cycles applied sequentially. In the first, type A, the mode I load is applied and removed before the fully reversed mode II cycle is applied, Fig. 4.2. In the second, type B, the mode I load is held constant at its maximum value while the mode II load is applied, and then removed, Fig. 4.3.

In type A it was anticipated that the mode I part of the cycle might leave a large enough residual opening for the mode II stress intensity to reach the crack tip. However it was thought that friction could still attenuate that stress intensity. Type B was expected to produce much higher growth rates because the maximum loads would be higher, and because the crack should be open for the whole of the mode II cycle. However it was also thought that branch crack growth might be dominant in type B, because of the tensile mean load on the crack flanks during the mode II part of the cycle, see section 1.4.1.3.

4.2. Experimental Method.

The tests used the Sheffield Mayes Biaxial servo hydraulic rigs, and the new cruciform specimen, as in the previous chapter. They are described

in Appendices 1 and 2. The command signal was produced using a Viglen I PC compatible computer, and a Blue Chip Technology digital to analogue output card. The details can also be found in Appendix 1. The tests all used a frequency of 2 Hz, which was slow enough to produce well defined stress cycles. The shape of the load waveform was checked by using a 2 channel storage oscilloscope. All the tests were carried out under load control. The stress ranges for the mode I and and mode II parts of the cycle were kept constant during the tests, so that the stress intensities were dependent on the constant tensile and shear stress ranges, $\Delta\sigma$ and $\Delta\tau$, and on the variable crack lengths as defined in Appendix 6.

A spark eroded 45° starter notch was put in the cruciform specimen, and it was then pre-cracked using equibiaxial mode I loading. The load was reduced during pre-cracking in 10% steps until a fatigue crack growth rate of less than 10^{-9} m/cycle was reached. This was to reduce the residual plastic zone size to less than that produced by the first cycle of the test.

The crack length was measured by both a travelling microscope, capable of resolving 0·02 mm of crack growth, and the automatic potential drop system as described in Appendix 3. As in the previous chapter, two pairs of potential drop leads were used to cancel out the effects of temperature changes. Theoretically this should also allow a change in the crack length, a, of 0·02 mm to be resolved. Unfortunately the potential drop system had problems when co-planar crack growth occurred, because of shorting across the crack in the early stages of growth. The optical microscope readings therefore had to be used for all the early growth, and the potential drop only used in the later stages where it was observed to agree with the optical readings.

4.3 Results.

Five out of the seven type A tests grew as co-planar cracks. The growth direction therefore corresponded to a pure mode II direction for the mode II part of the cycle. The other two branched into mode I fatigue cracks growing approximately perpendicular to one of the loading axes. Table 4.1 shows that the tests that branched were the tests where the ratio between the mode I and mode II parts of the cycle was smallest.

Three type B tests were performed all of which produced only branch crack growth. The details are again given in Table 4.1

Table 4.1
Details of the Sequential Loading Tests

Test No.	Test Type	$\Delta\sigma$	$\Delta\tau$	Initial Crack Length	Growth Type
		(MPa)	(MPa)	(mm)	
RSB12	A	104	156	6·2	Coplanar
RSB18	A	156	156	6·4	Coplanar
RSB9	A	52	208	7·0	Branch
RSB8	A	104	208	5·7	Coplanar
RSB10	A	156	208	5·7	Coplanar
RSB11	A	104	312	5·0	Branch
RSB20	A	156	312	5·0	Coplanar
RSB15	B	104	208	5·0	Branch
RSB16	B	156	208	5·8	Branch
RSB17	B	104	104	4·9	Branch

When the co-planar cracks in tests RSB18 and RSB20 were about 45 mm long, the mode I part of the cycle was reduced in 10% steps until branching occurred. In RSB18 the crack was allowed to grow about 0·3 mm between unloading increments. This was sufficient to ascertain whether the crack was branching or not, and it allowed the crack to grow through the mode I plastic zone of the previous load. In RSB20 the crack began branching after the first unloading increment. In neither test was there a simple swap from co-planar growth to branch crack growth. Instead branches would appear and start to grow in competition with the co-planar cracks. Some of the branch cracks arrested as shown in Fig. 4.4 from test RSB20, but new branches formed at the new co-planar crack tip, and eventually the branch cracks dominated. The stress intensities at which this transition to branching occurred are given by:

RSB18: ΔK_{II} = 39·8 MPa$\sqrt{m}$, ΔK_I= 17·8 MPa$\sqrt{m}$.

RSB20: ΔK_{II} = 82.0 MPa$\sqrt{m}$, ΔK_I= 36.9 MPa$\sqrt{m}$.

Fig. 4.5 shows these results graphically in the form of a fatigue map. The four branch crack points show the initial loading that immediately produced branch crack growth in tests RSB9 and RSB11, and the stress intensities at which the transition to branching took place in tests RSB18 and RSB20. The coplanar points show both the initial conditions and the loads at various points afterwards in tests RSB8, RSB10, RSB12, RSB18, and RSB20 that produced co-planar growth. The figure shows that for a cycle of

type A coplanar growth will occur if the ratio of mode I to mode II stress range is about 0·5 or greater. Otherwise branch crack growth will occur.

Two features of this co-planar growth are worthy of a mention at this point. Firstly large quantities of oxide were produced by the rubbing of the surfaces during the mode II part of the cycle. This oxide could easily be seen with the naked eye as it fell out of the crack. Fig. 4.6 shows some of the fracture surface from the co-planar part of test RSB20. It has been worn flat by the rubbing.

The second interesting feature was that at times the crack path was much straighter and smoother than occurs in ordinary mode I tests, as shown in Fig. 4.7. This figure is from test RSB8 which showed the most extensive growth of this type. In general it occurred most frequently in the tests where the mode I load was smallest.

4.4 Discussion.

The co-planar growth produced in these tests is very significant. Until now rolling contact fatigue had seemed confusing because the shallow angled cracks were thought to be predominantly loaded in mode II, and yet nearly all the laboratory tests performed with mode II loading had only produced very small quantities of mode II growth before branching into mode I. What is more, when the tests of Pascoe and Smith who had produced mode II growth were repeated in this project, only branch crack growth occurred, see section 3.7. Bower's results predicted that there might be a mode I load before the mode II load in rolling contact, and yet it was not known how to interpret this sequential loading. These tests have shown that the sequential application of mode I and mode II loads can produce co-planar growth, even when the mode II stress range is twice the mode I stress range.

However these tests cover only two types of cycle, and only a few different load ranges. It is necessary to try to produce more generalised crack growth laws and branching conditions if Bower's results, and the results of other non-proportional loading calculations are to be interpreted.

4.4.1. Coplanar Growth Rates.

As a first step in the investigation of the co-planar crack growth rate, the growth rate was plotted against ΔK_{II} as shown in Fig. 4.8. This shows that the growth rate does increase with ΔK_{II}, but that the mode I load also causes an increase in growth rate.

The first attempt to model this behaviour used the approximation that the growth rate is simply the addition of the growth due to the mode I part of the cycle and the growth due to the mode II part, and that the rates are independent. The growth due to the mode I part of the cycle can then be predicted by the Paris law derived from the mode I crack growth test at R=0·0 recorded in Appendix 4. This mode I growth rate was subtracted from each data point, and the resulting mode II growth rates were plotted against ΔK_{II}, Fig. 4.9. The growth rates then fell much nearer to a single straight line than in Fig. 4.8.

However test RSB20 now appeared to be at a higher growth rate than the other tests. This was not surprising as ΔK_{II} was still being used. This is a linear elastic parameter, and yet the cyclic plasticity in test RSB20 was around 0·02%. The graph was therefore re-plotted using a shear strain intensity factor, ΔK_{γ}, see Appendix 5. Fig. 4.10 shows that RSB20 is now on approximately the same line as the other tests.

There are still differences in the growth rate of a factor of about 5, for some values of ΔK_{γ}, but this is mainly due to the scatter in individual tests. For example both RSB10 and RSB18 start at a growth rate above the mean value for that ΔK_{γ}, and then drop down to it. Also tests RSB10 and RSB12 have three or four points beneath the mean value, part way through each test. Both of these features could be attributable to frictional or crack locking effects. At the start of a test there will be less oxide and wear debris between the crack faces, because there has not been any crack face rubbing due to the mode II displacements. As a result there would be smaller frictional forces reducing the mode II loading at the crack tip, and the growth rate would therefore be higher than that of an established crack. The reduced growth rates in RSB10 and RSB12 can be explained by saying that sometimes during the co-planar growth the crack would kink slightly as shown in Fig. 4.11. This would in turn increase the frictional forces, and therefore reduce the growth rate. Fig 4.11 shows the kink that occurred at a crack length of 13 mm in test RSB10, corresponding

to the dip in the growth rate curve at $\Delta K_\gamma = 5{\cdot}8 \times 10^{-4}\ \sqrt{m}$. The feature was more distinctive during the test, before it was worn away by the sliding displacements.

There is also a factor of 2 difference between the growth rates of RSB8 and RSB18. These two tests had the same applied shear stress, but RSB18 had twice as large an equibiaxial tensile stress. As RSB18 has the larger growth rate the difference may again be attributed to frictional effects. The larger mode I load would leave a larger residual opening, and should therefore reduce the frictional losses and increase the growth rate.

This last point, and the fact that in the previous tests in this project coplanar growth was not produced, shows that the growth rate from the mode II part of the cycle cannot be completely independent of the mode I part.

A general mode I mechanism growth law including the interactions of the previous mode II load, might be of the form:

$$\left(\frac{da}{dN}\right)_I = C_I \Delta K_\varepsilon^{m_I} \left(\frac{\Delta K_\gamma}{\Delta K_\varepsilon}\right)^{n_I}$$

And similarly a mode II law might be of the form:

$$\left(\frac{da}{dN}\right)_{II} = C_{II} \Delta K_\gamma^{m_{II}} \left(\frac{\Delta K_\varepsilon}{\Delta K_\gamma}\right)^{n_{II}}$$

These laws suggest that the increase in growth rate or the increase in effective stress intensity at the crack tip is proportional to the strain intensity of the previous part of the cycle, to an unknown power. This is equivalent to saying that the increase in growth rate is dependent on the plastic zone size, or the crack tip opening displacement, of the previous cycle, as both are proportional to the strain intensity squared.

Various values of n_I and n_{II} might be suggested, but without a better understanding of the crack growth process, no definitive answer can be given. Also with four exponents, and two coefficients a complex curve fitting process would be required to determine them from the available data. This was not considered to be worthwhile because of the limited time available in the project, and because the scatter in the results would probably make any improvement negligible.

Instead it was noted that if $m_I = m_{II} = 2n_I = 2n_{II}$, then the crack

growth law becomes:

$$\left(\frac{da}{dN}\right)_{Tot} = \left(\frac{da}{dN}\right)_{I} + \left(\frac{da}{dN}\right)_{II}$$

$$= C_I . \Delta K_\varepsilon^{n_I} . \Delta K_\gamma^{n_I} + C_{II} . \Delta K_\gamma^{n_I} . \Delta K_\varepsilon^{n_I}$$

$$= C' . \Delta K_\varepsilon^{n_I} . \Delta K_\gamma^{n_I}$$

da/dN was plotted against $(\Delta K_\varepsilon . \Delta K_\gamma)$ on log-log axes and a straight line was produced with less scatter than any of the other laws used so far, Fig. 4.12. This suggests that the above simplification is not unreasonable. The slope of the graph, which is equal to n_I, is about 1·74.

It should be noted that the growth rate rule is quite limited. As ΔK_ε or ΔK_γ tend to zero this law would precict that the growth rate went to zero. However the actual cycle would tend to a pure mode I or pure mode II cycle, so a transition needs to be made either to the Paris law, or to the proportional mode II loading behaviour involving predominantly branch crack growth. At this point it is not possible to identify where that transition would take place.

It was observed that at some points during the co-planar growth the crack grew in a very straight path, quite unlike normal mode I growth, while at other times the crack path was rough like a normal mode I crack. This suggests that two different mechanisms may produce the co-planar growth. However the growth rate curves do not show an obvious change in angle associated with this change in crack appearance, and so the significance of this observation cannot be evaluated.

4.4.2 Branch Crack Growth Rates.

The branch cracks in the type A tests undergo a stress intensity cycle consisting of a large fully reversed mode I cycle from the mode II loading, followed by a smaller mode I cycle at R=0 from the mode I loading. As the growth rate from the smaller cycles would be lower than that of the larger cycles by a factor of about 10 under constant amplitude loading, and as it would be further reduced by the residual plastic zones and the residual stresses of the larger cycle, the growth rates were plotted against the larger ΔK_ε only. ΔK_ε was used instead of ΔK_I because again

LEFM was beginning to break down in the higher load tests. The results are shown in Fig. 4.13, where they are also compared with the growth rate from tests RSB14 and RSB19, mode I tests under fully reversed equibiaxial tension and fully reversed shear loading, as described in Appendix 4.

The graph shows that the branch crack growth rates from tests RSB9 and RSB11 lie on the same line as the mode I data within the experimental scatter. The RSB18 data are below the line. RSB18 was initially a co-planar crack test, but the mode I part of the cycle was reduced at the end to find the branching condition. The data are therefore taken from a longer initial crack than the other branch crack tests, and are for relatively short branch crack lengths. The data may be lower because of inaccuracies in the K calibration for short branch cracks, see Appendix 6 and the discussion in section 3.4. Alternatively the real mode II load may be reduced by friction on the crack flanks, which is likely to be more significant in this test than in the others, because of the length of the crack and the relatively low stresses.

Test RSB20 also appears to be below the line through the mode I data, probably for similar reasons to RSB18, but the growth rates are so much higher than the rest of the data that a direct comparison cannot be made.

The branch cracks of type B tests undergo a stress intensity cycle of the form shown in Fig. 4.14a. To compare the data with conventional mode I test data, this cycle was considered to be equivalent to a simple sine wave cycle with the same amplitude, as shown in Fig. 4.14b. The growth rates are plotted against ΔK_I in Fig. 4.15, and against ΔK_ϵ in Fig.4.16. In this case the conversion to ΔK_ϵ makes no noticeable difference to the shape of the graph because the plasticity is so low, but the figure was drawn for comparison with the rest of the work. The figures both show that the branch crack growth data fall on top of the mode I data. The K_I calibration is again given in Appendix 6.

4.4.3 A Branching Criterion.

In section 1.2.5 it was suggested that the crack growth direction under non-proportional loading might best be calculated by the 'maximum crack growth rate criterion'. In other words a crack would propagate by whichever mechanism, and in whichever direction it would grow most quickly.

In these tests then the boundary between the loads that cause branching to occur and the loads that cause co-planar crack growth should be given by a loading condition that would cause them to grow at equal rates. For the type A tests two different growth rate laws have been suggested for the co-planar growth, and one for the branch crack growth:

The sequential growth rule:

$$\left(\frac{da}{dN}\right)_{\text{Co-planar}} = 1{\cdot}83\times10^{4}\ (\Delta K_{\gamma})^{3.44} + 2{\cdot}60\times10^{8}\ (\Delta K_{\varepsilon})^{4{\cdot}03}\ \text{m/cycle}$$

The interactive growth rule:

$$\left(\frac{da}{dN}\right)_{\text{Co-planar}} = 4{\cdot}85\times10^{5}\ (\Delta K_{\gamma}\Delta K_{\varepsilon})^{1{\cdot}74}\ \text{m/cycle}$$

Branch Crack Rule:

$$\left(\frac{da}{dN}\right)_{\text{Branch}} = 3{\cdot}07\times10^{7}\ (\Delta K_{\varepsilon})^{4{\cdot}01}\ \text{m/cycle}$$

ΔK_{ε} for the branch cracks is related to ΔK_{γ} in the co-planar growth equation by the K_I calibration. This predicts that for an infinitesimal crack:

$$\Delta K_{\varepsilon} = 1{\cdot}15\ \Delta K_{\gamma} / 2(1 + \nu)$$

For a branch length of 0·1 times the co-planar crack half length:

$$\Delta K_{\varepsilon} = 1{\cdot}08\ \Delta K_{\gamma} / 2(1 + \nu)$$

The calibration is only approximate for finite branch lengths however.

As the relation between ΔK_{ε} and ΔK_{γ} varies with crack length, a boundary condition is not easy to define. It might be that initially a branch crack would grow faster, but when the crack has grown a fraction of a millimetre the co-planar crack would grow faster. In RSB20 this sort of behaviour was observed with co-planar and branch cracks growing concurrently. The branch cracks and coplanar cracks will also interact, by reducing the stress intensity at the other cracks' tips.

Figs. 4.17 and 4.18 show the type A loadings that have produced co-planar growth and the loads that have produced branches, and show the boundary condition where the growth rates should be equal for infinitesimal cracks and for finite cracks. Fig. 4.17 uses the sequential co-planar crack growth law, and Fig. 4.18 uses the interactive crack growth law. The sequential law predicts that no ΔK_{ε} is required until ΔK_{γ} is greater than $5{\cdot}2\times10^{-4}\ \sqrt{m}$, and then predicts that the required value

increases with ΔK_y more quickly than was observed.

The interactive growth law however appears to work well in calculating the branching condition at ΔK_y levels below 8×10^{-4} $\sqrt{m}$, but then gives too high a value of ΔK_x. This is not surprising as the branch crack growth rate rule that was based on data from mode I tests, does not fit the branch crack growth rates for tests RSB18 and RSB20, the tests with the highest ΔK_y values. The infinitesimal branch length criterion also fits the data better than the finite length criterion, for the lower ΔK_y values.

4.4.4. Growth Rates and Directions Under Different Cycles.

The aim of a series of tests such as these is not just to collect knowledge about one particular set of loading conditions. Rather it is to expand the understanding of fatigue so that eventually predictions of growth rates and directions from a wider variety of cycles can be made without resorting to such expensive tests. That point has not been reached yet, but a general approach to growth rate and direction calculations for other cycles may be suggested.

Firstly any complicated sequence of loads should be examined to find peaks and troughs in the applied stresses, and in the maximum tangential and shear stress criteria. The peaks should correspond to possible growth directions. The sequence should then be split up into a number of discrete simplified cycles, like the two parts of the type A cycles, or into larger cycles like the approximation made to the branch loads in the type B cycles, Fig. 4.14. For each of the possible growth directions the growth rate may then be estimated by using one of the growth rate rules.

The sequential rule is probably by far the easiest to use, as the interactions between different loads in different series of cycles are not understood. Further testing on different types of load sequences should enable refinements to be made to the laws, and therefore improve the accuracy of any prediction. The rainflow technique for mode I growth uses an algorithm enabling a computer to produce these cycles [2,3]. This project however, points out that in rolling contact fatigue at least, a purely mode I based algorithm will not work.

For example the approach may be used for the type B tests to try to predict whether co-planar growth should occur. Two different possible

growth directions exist. Firstly if the crack remains co-planar, it will experience a mode I cycle with R = 0.0, then a mode II cycle with an equibiaxial mean stress, as shown in Fig. 4.19. Alternatively the crack might branch at about 45° to the original crack. This time the loading could be simplified to one large mode I cycle at R = 0.0, as shown in Fig. 4.14b. The sequential growth law was used for the co-planar growth. This assumes that the mode II growth is independent of the mode I growth. This is not true in general because friction reduces the effective mode II load, however in the type B tests the mode II load was always accompanied by a mode I load to open the crack, so the frictional effects should be low. The interactive law was not used because the mean stress must change any interactions upon which the law is based. The results are shown in Table 4.2. The table shows that the criteria predict that branch crack growth should occur at RSB16 and RSB17 as it did, and that RSB15 is on the border, with the infinitesimal crack length criterion predicting branch growth, and the finite length criterion predicting co-planar growth.

Table 4.2
Predicted Coplanar and Branch Crack Growth Rates for Type B Cycles.

Test No.	$\Delta\sigma$	$\Delta\tau$	Coplanar Growth Rate	Branch Growth Rate.	
				Small Branch	Finite Branch
	MPa	MPa	m/cycle	m/cycle	m/cycle
RSB15	104	208	$6{\cdot}46\times10^{-9}$	$7{\cdot}52\times10^{-9}$	$6{\cdot}46\times10^{-9}$
RSB16	156	208	$45{\cdot}3\times10^{-9}$	$82{\cdot}4\times10^{-9}$	$100{\cdot}9\times10^{-9}$
RSB17	104	104	$1{\cdot}23\times10^{-9}$	$2{\cdot}27\times10^{-9}$	$1{\cdot}85\times10^{-9}$

4.5 Conclusions.

This chapter has shown that a simplified form of the stress cycles calculated by Bower [1] for rolling contact fatigue can produce crack growth in all three possible directions in rolling contact. In particular it has shown that co-planar cracks can be produced from a crack loaded predominantly in shear, corresponding to the shallow angled crack in 'squats' and other rolling contact fatigue defects. It has shown that the small mode I load produced by fluid trapped inside the crack is necessary for this growth to take place, as is observed in rolling contact fatigue experiments. Two branch crack laws have been formulated that agree with the co-planar crack growth data that was collected. The sequential law

suggested that the growth rate may be derived from adding together the growth rates from the individual parts of the cycle, whereas the interactive law suggested that it is necessary to modify those growth rates to account for the effects of the previous part of the cycle. It was not possible to investigate the actual mechanism further within these tests, or to establish the values of the exponents and coefficients of the interactive law. However a simplified version of the law provided a good fit to the data.

These two formulae were then used in conjunction with the maximum crack growth rate criterion to predict the branching condition in the tests, and the interactive law was again a better fit to the data. However it was also noted that the sequential law would be more appropriate to use in finding a first approximation to the growth rates and directions in different types of tests, where the interactions between the cycles will be different.

References.

1. A.F.Bower. 'The Influence of Crack Face Friction and Trapped Fluid on Surface Initiated Rolling Contact Fatigue Cracks.'
Trans. ASME, J. of Lubrication Tech, Vol.110, pp704-711. 1988.

2. M.Matsuishi, T.Endo. 'Fatigue of Metals Subject to Varying Stresses.'
Presented at the Japanese Society of Mechanical Engineers, Fukuoka, Japan, 1968.

3. Dowling,N.E. 'Fatigue Failure Predictions for Complicated Stress-Strain Histories.'
J. of Materials, JMLSA, Vol. 7, No.1, pp71-87. 1972

Figures.

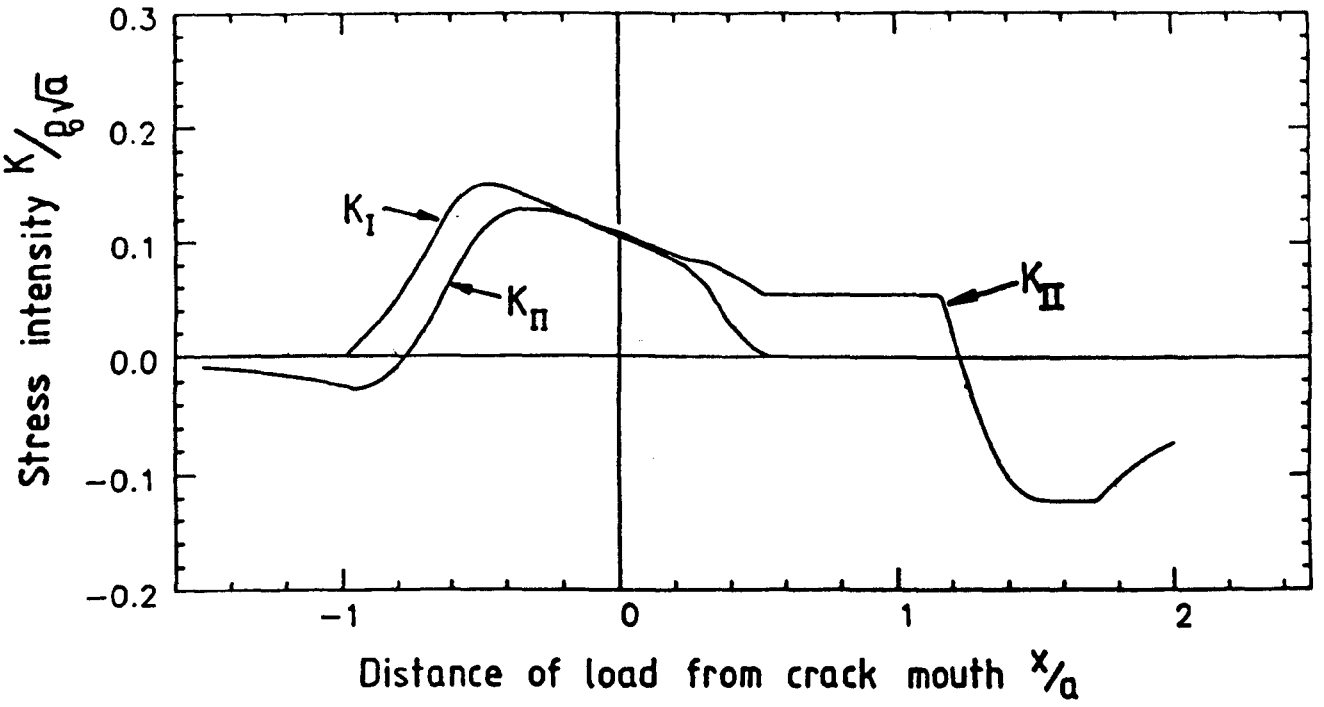

Fig. 4.1 Bower's Calculations [1].

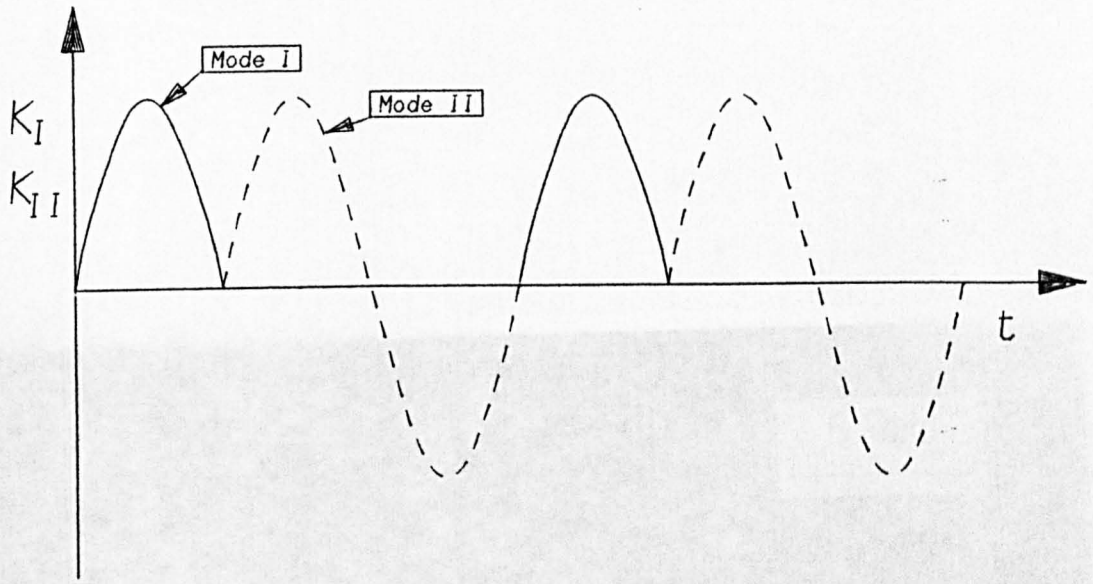

Fig. 4.2 Type A cycle.

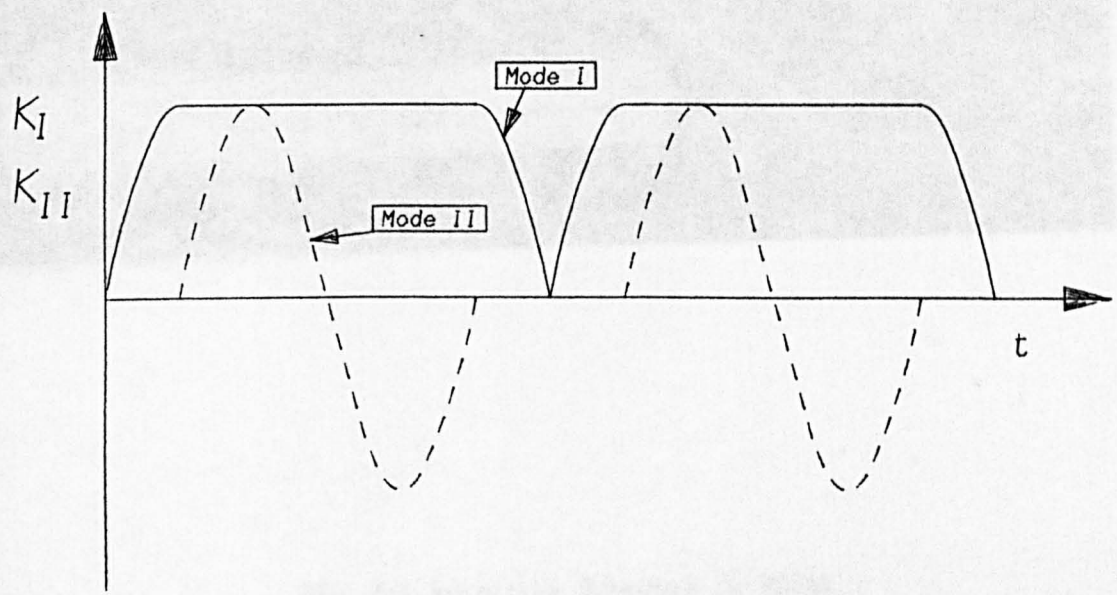

Fig. 4.3 Type B cycle.

Fig. 4.4 Arresting Branches in RSB20.

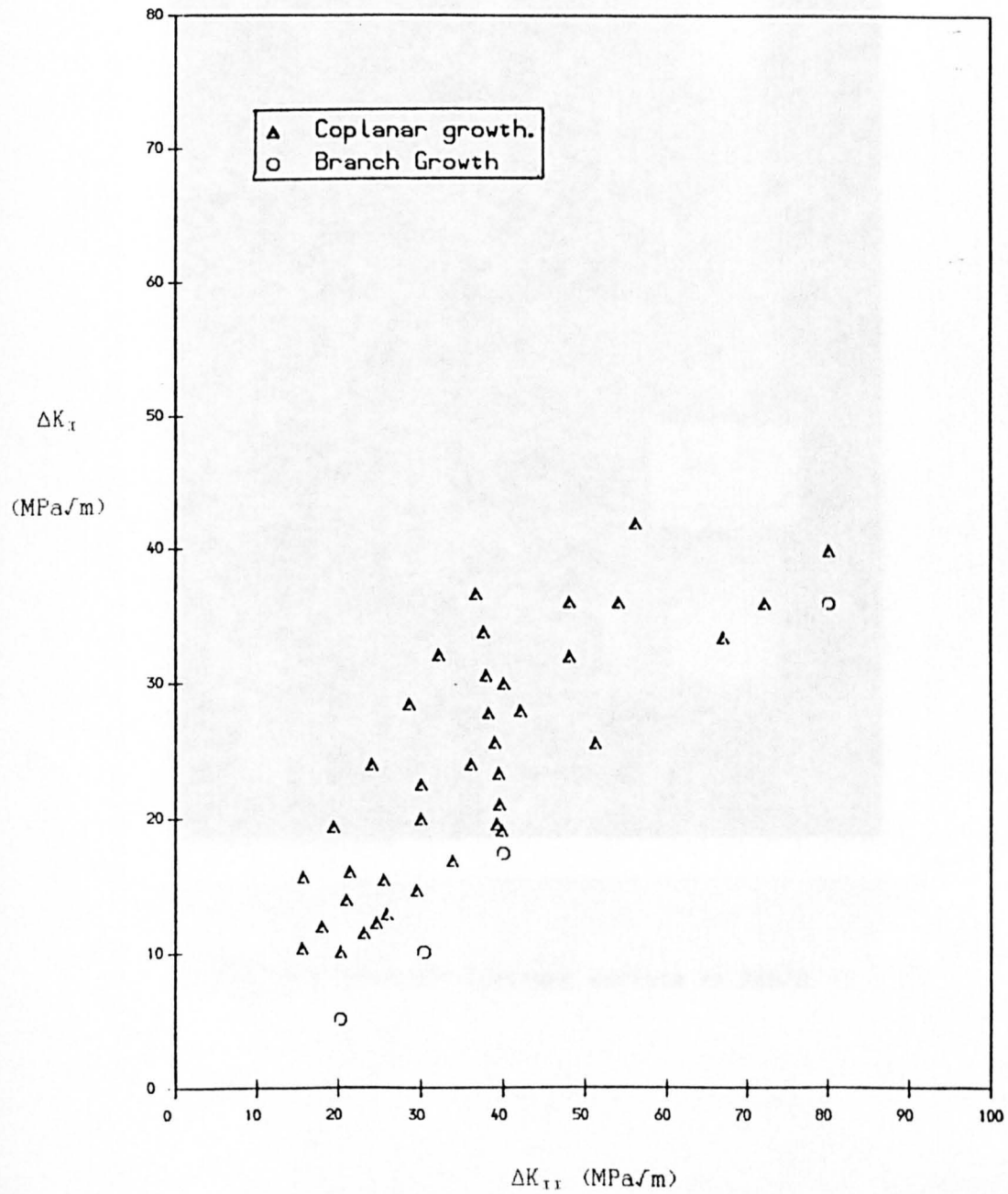

Fig. 4.5 Type A fatigue map.

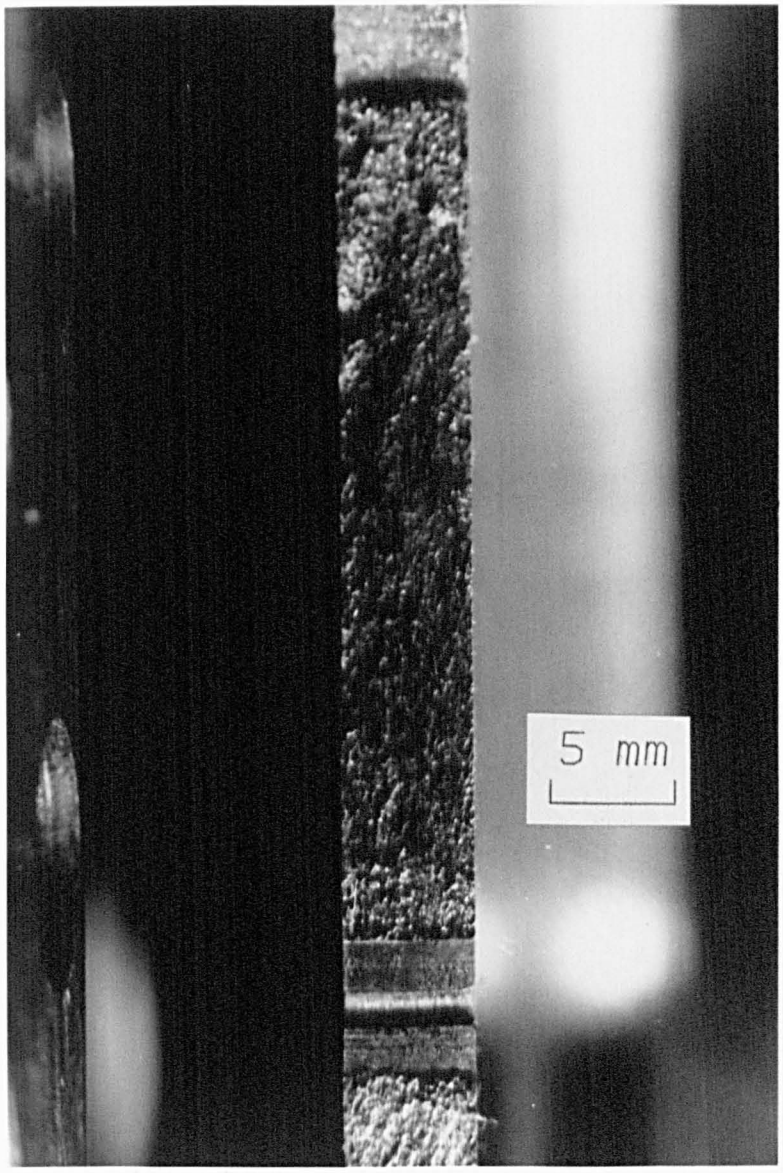

Fig. 4.6 Smoothed fracture surface in RSB20.

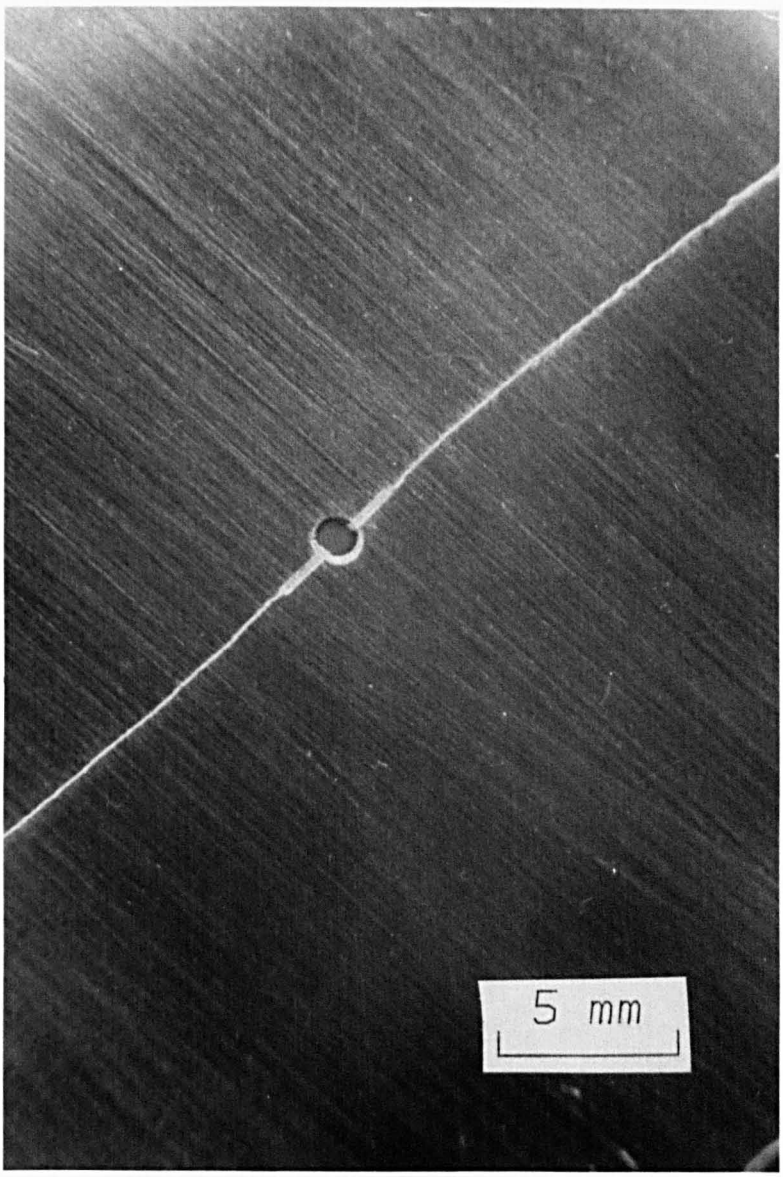

Fig. 4.7 Straight crack path in RSB8.

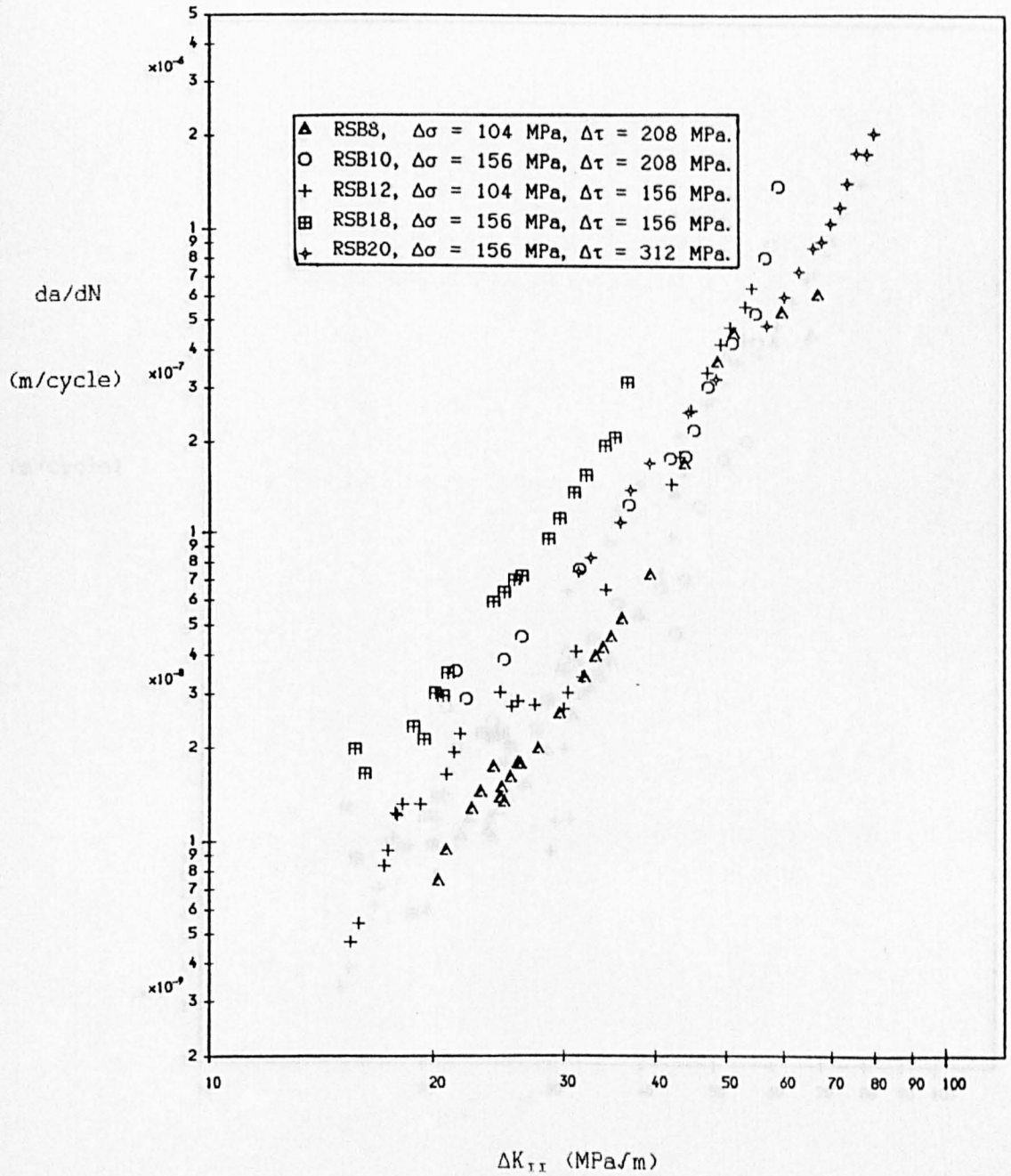

Fig. 4.8 Co-planar Fatigue Crack Growth Data.

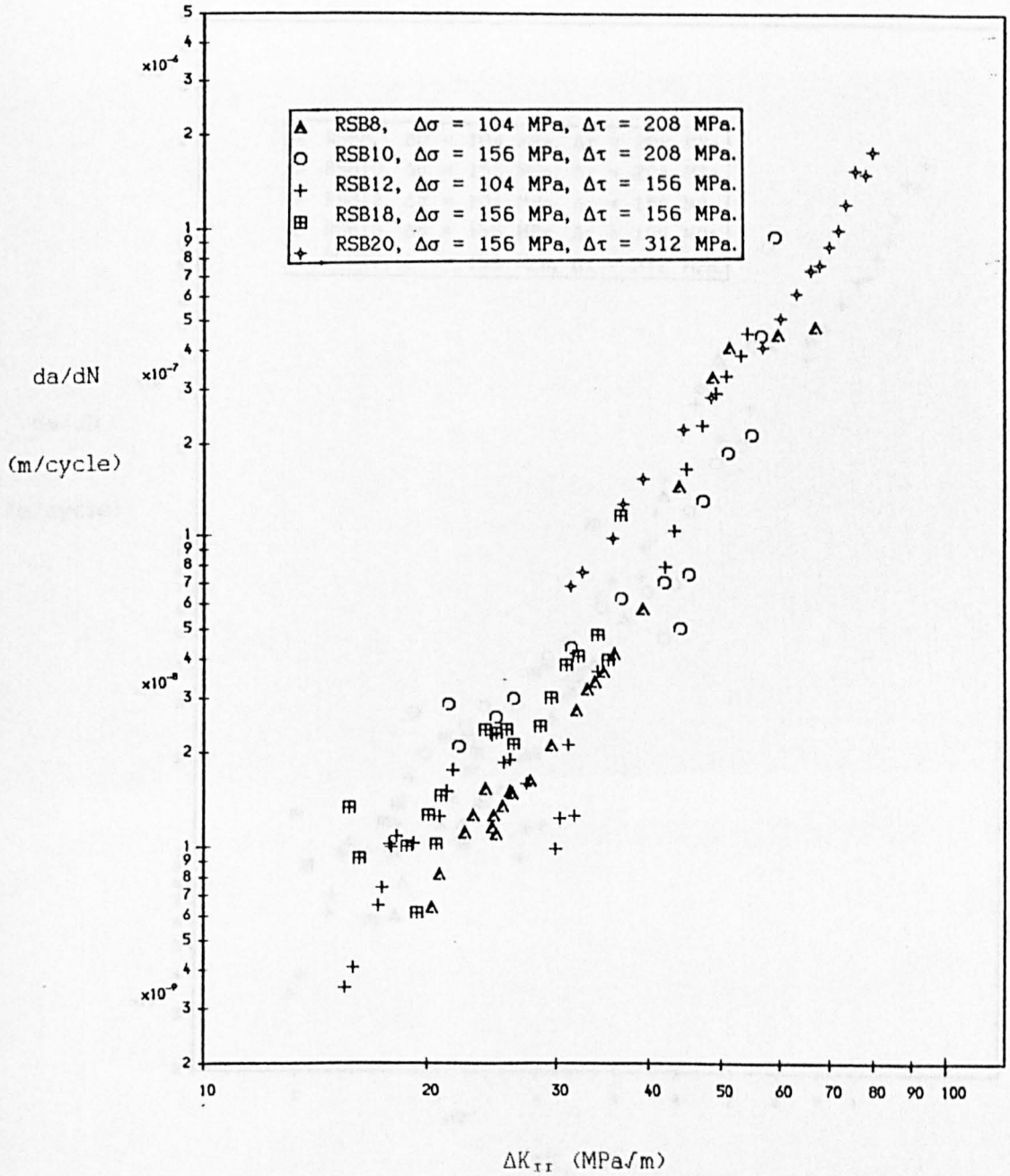

Fig. 4.9 Co-planar Fatigue Crack Growth Data Minus Mode I Component.

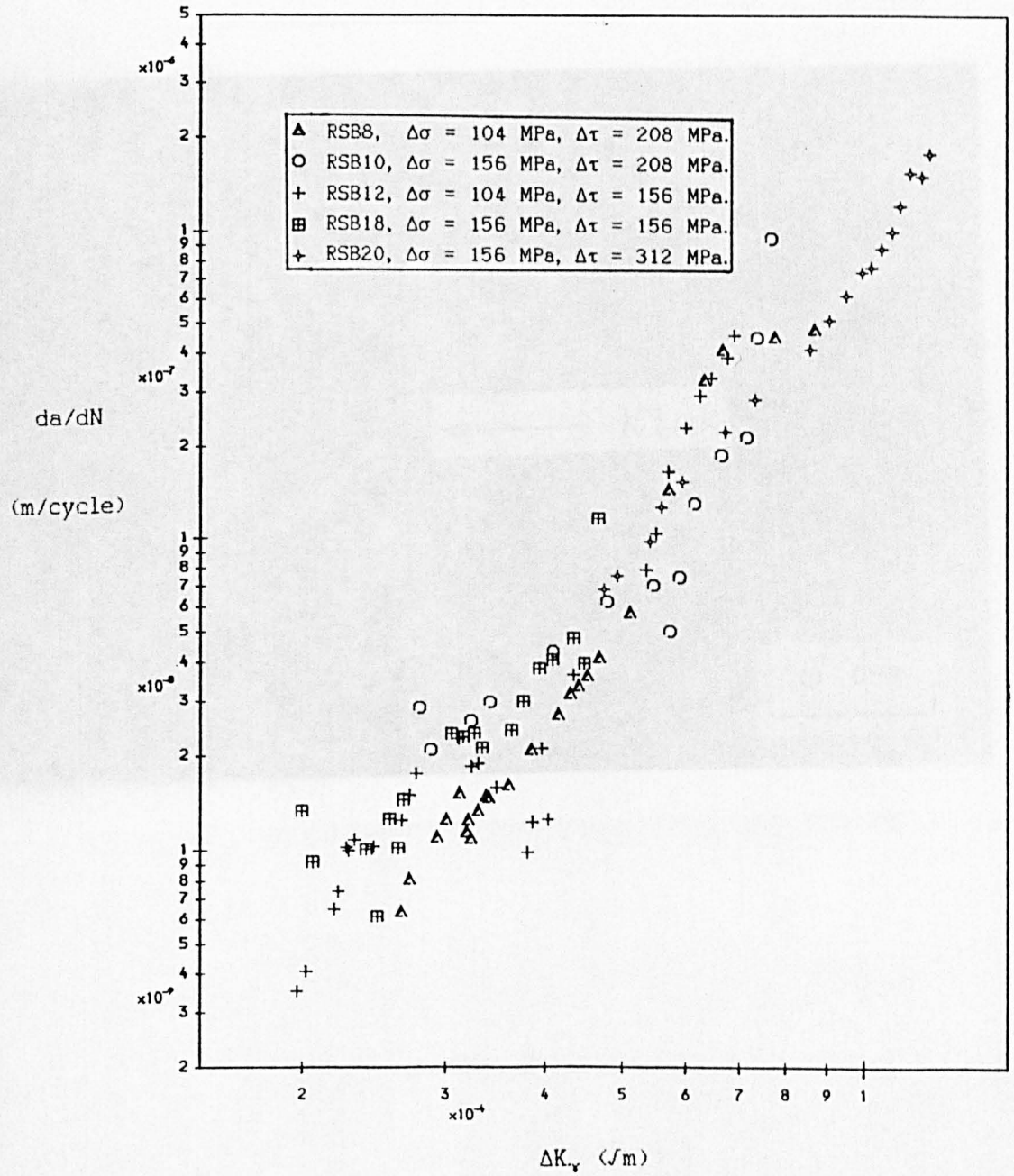

Fig. 4.10 Co-planar Fatigue Crack Growth Data, Minus Mode I Component.

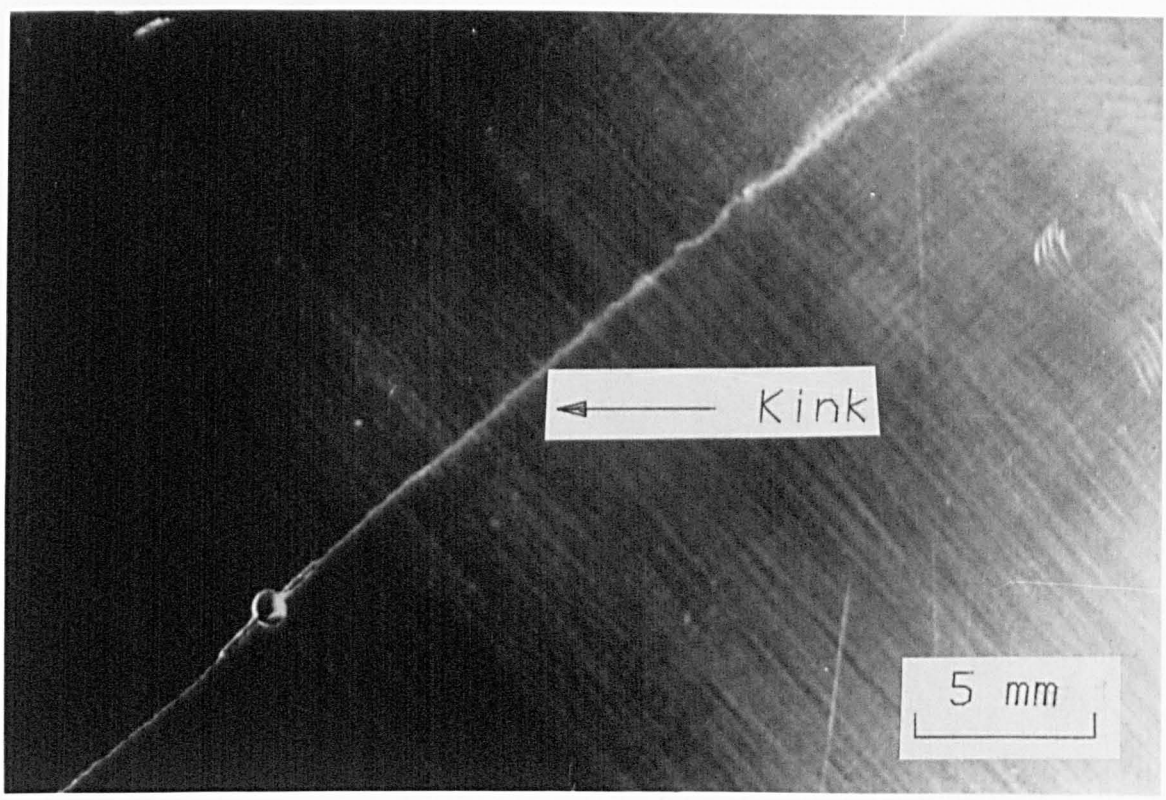

Fig. 4.11 Kink in co-planar growth

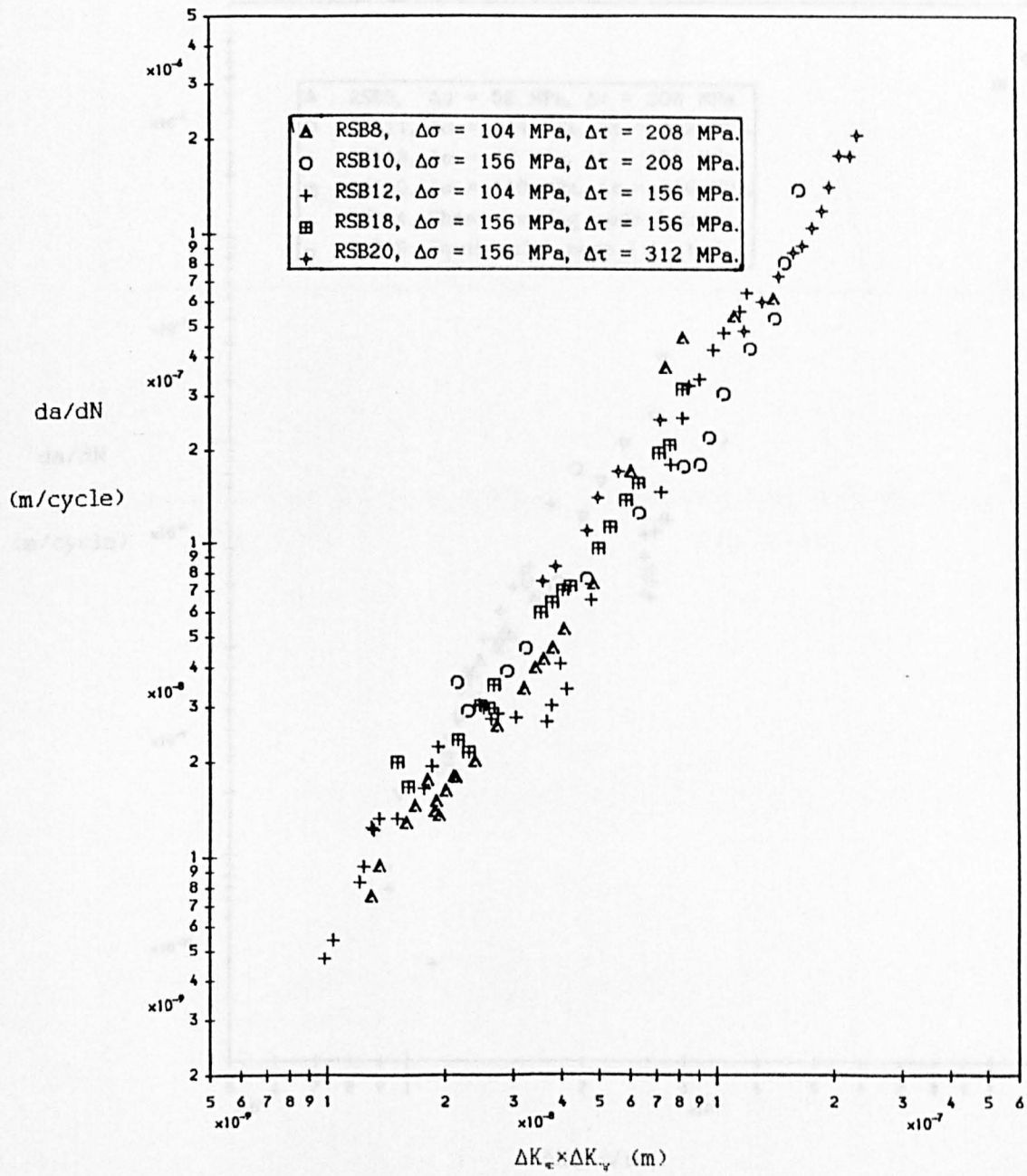

Fig. 4.12 Co-planar Fatigue Crack Growth Data Based on Interactive Rule.

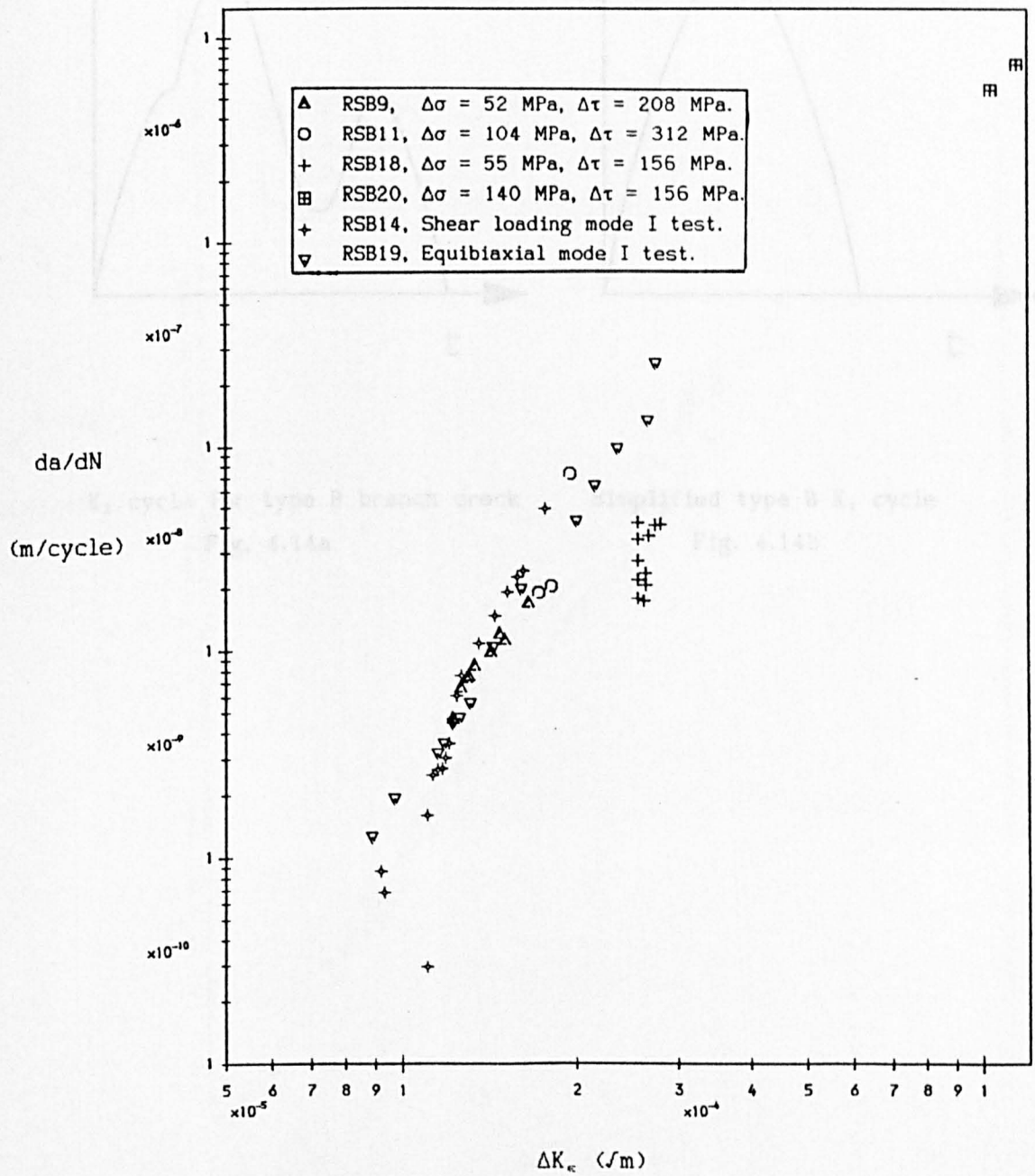

Fig. 4.13 Type A Branch Crack Growth Data.

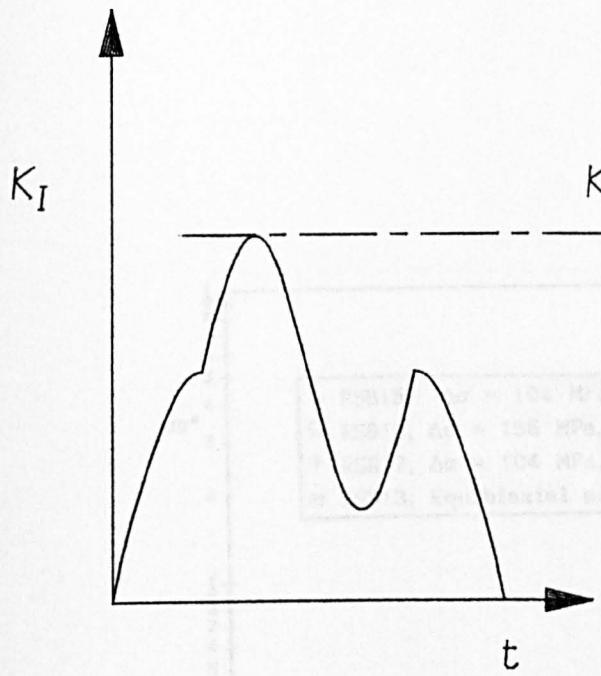

K_I cycle for type B branch crack

Fig. 4.14a

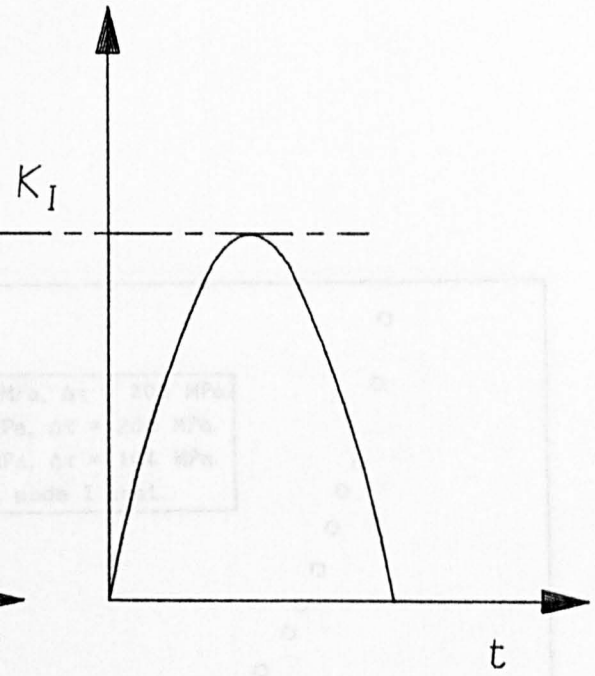

Simplified type B K_I cycle

Fig. 4.14b

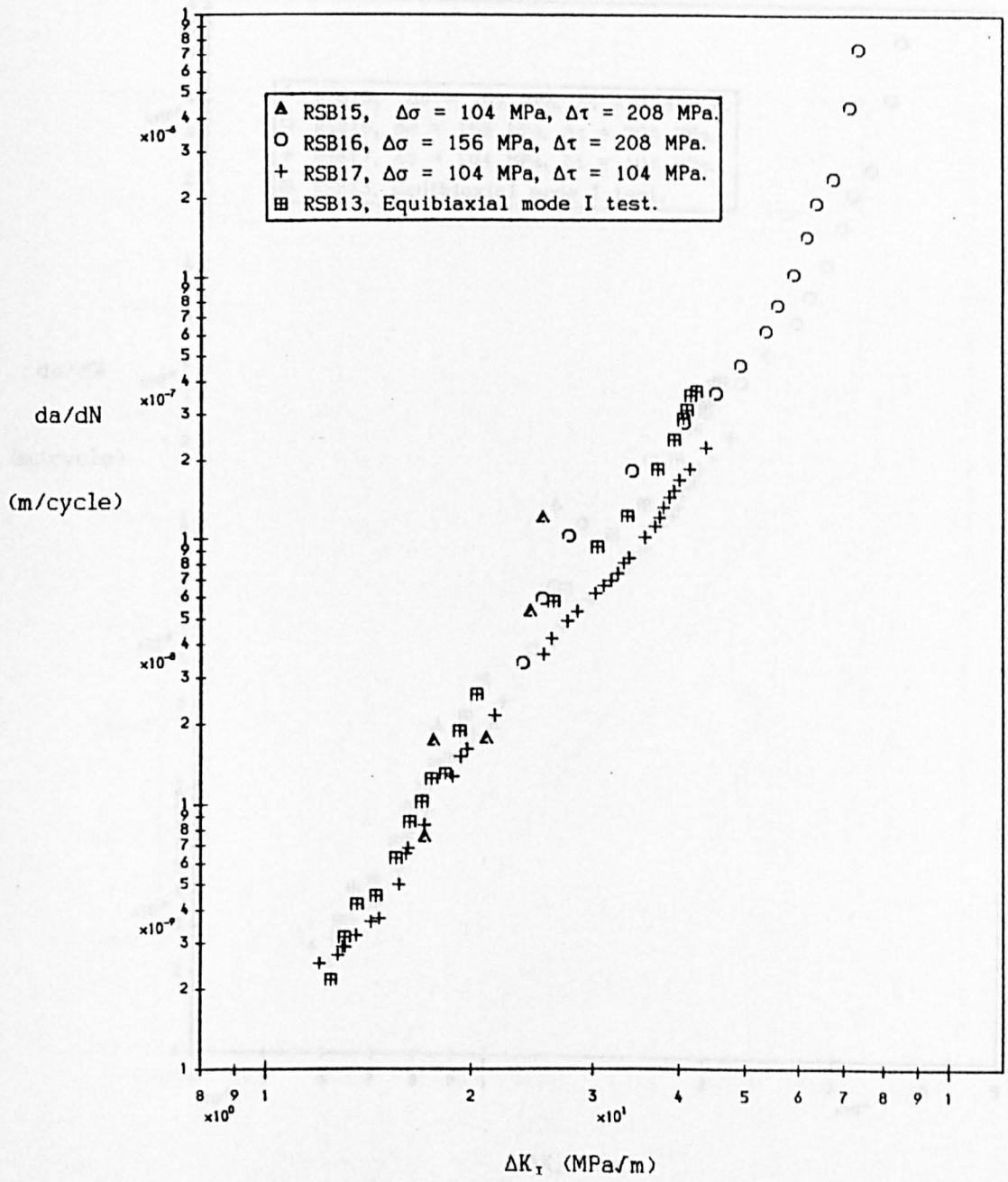

Fig. 4.15 Type B Branch Crack Growth Rates vs. ΔK_I.

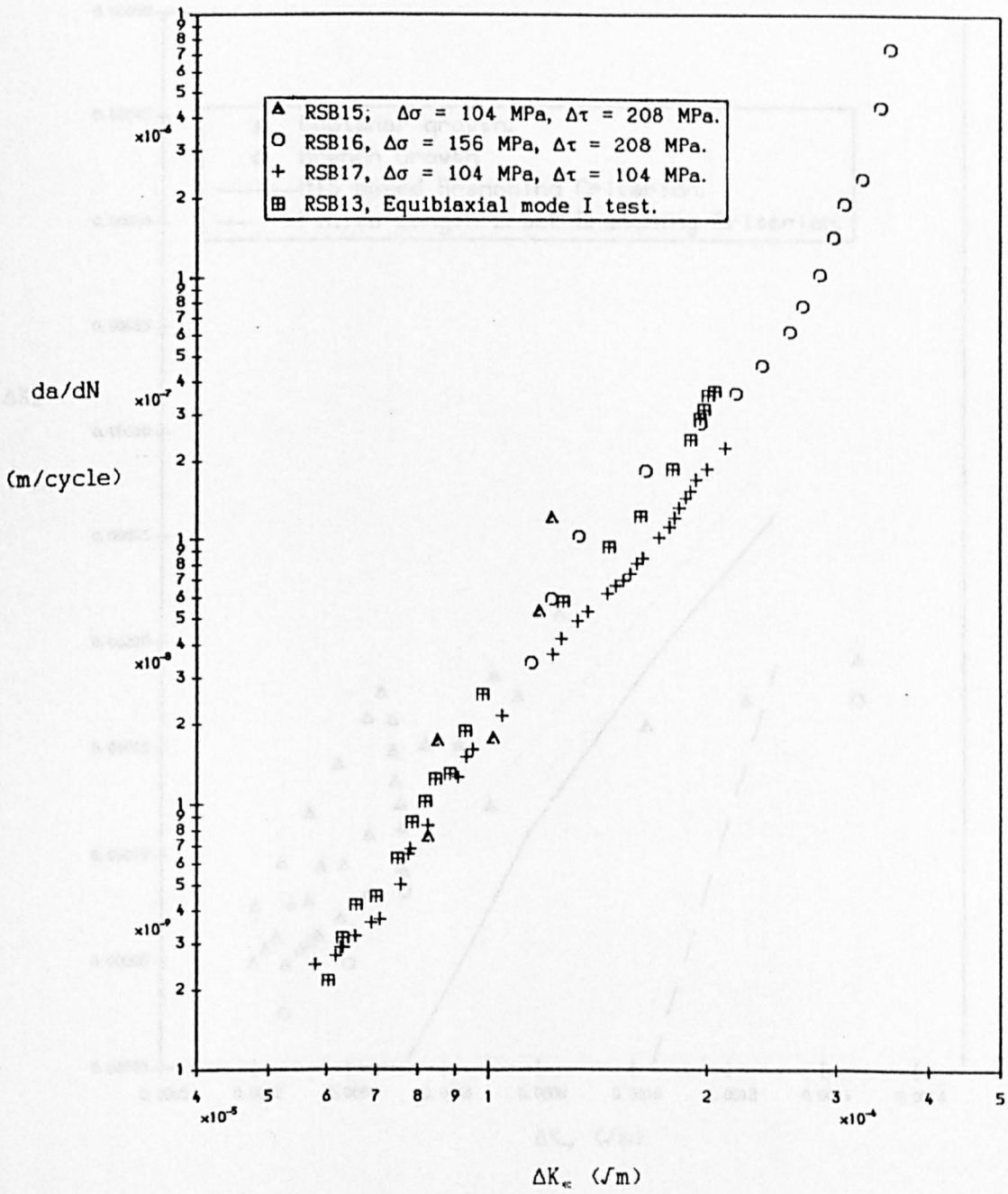

Fig. 4.16 Type B Branch Crack Growth Rates vs. ΔK_{ϵ}.

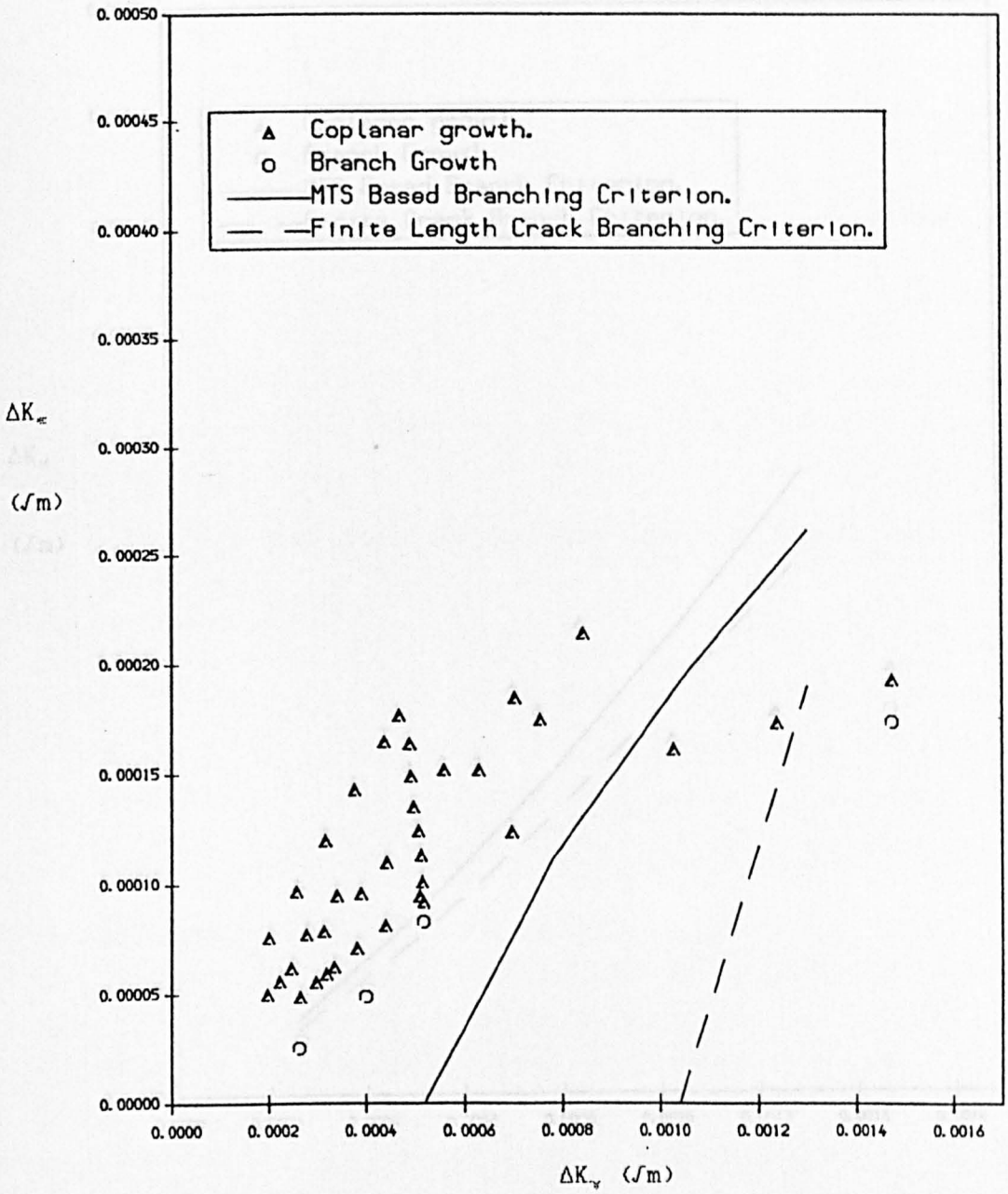

Fig. 4.17 Fatigue Map With Sequential Growth Rule Based Branching Criterion.

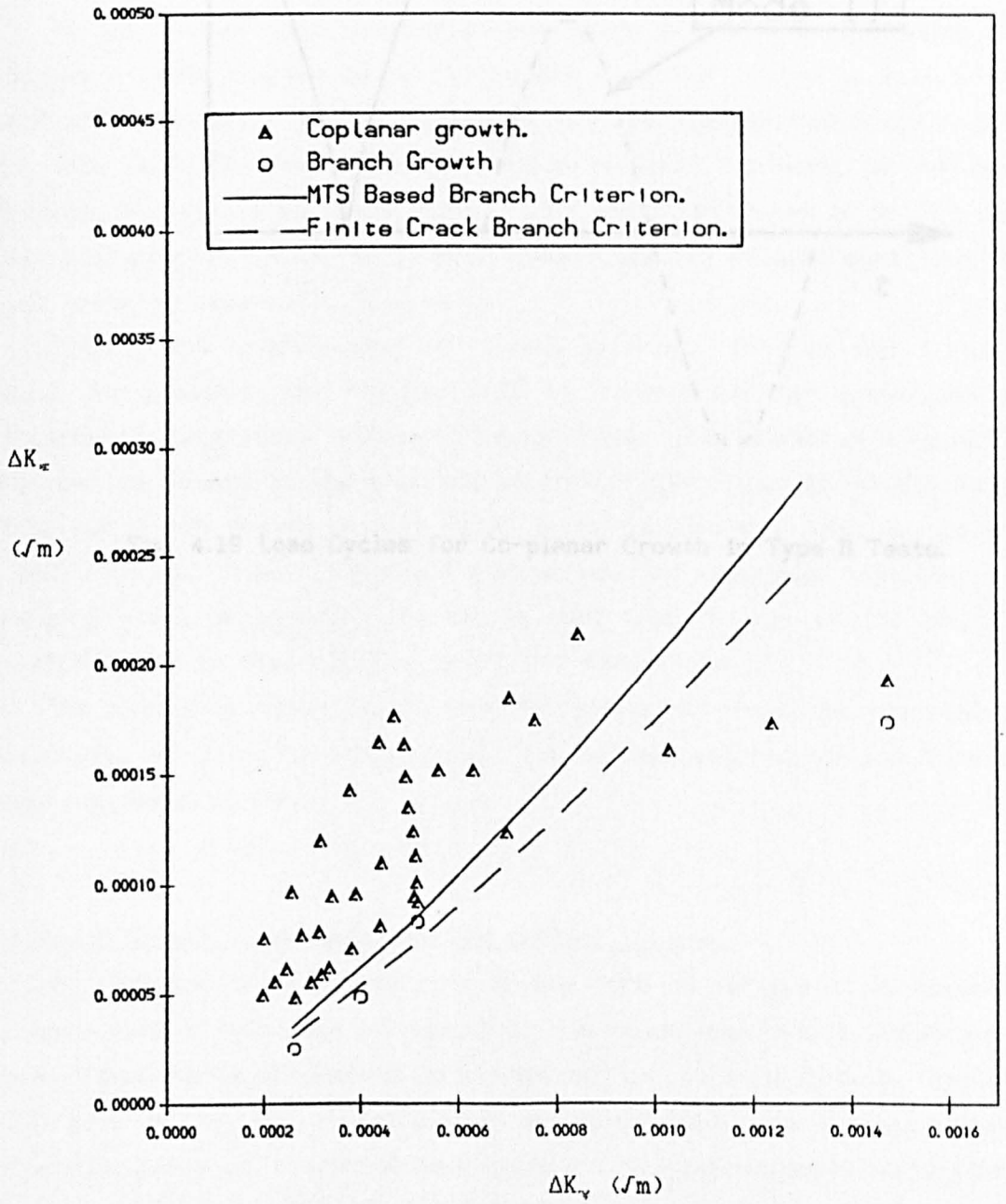

Fig. 4.18 Fatigue Map With Interactive Growth Rule Based Branching Criterion.

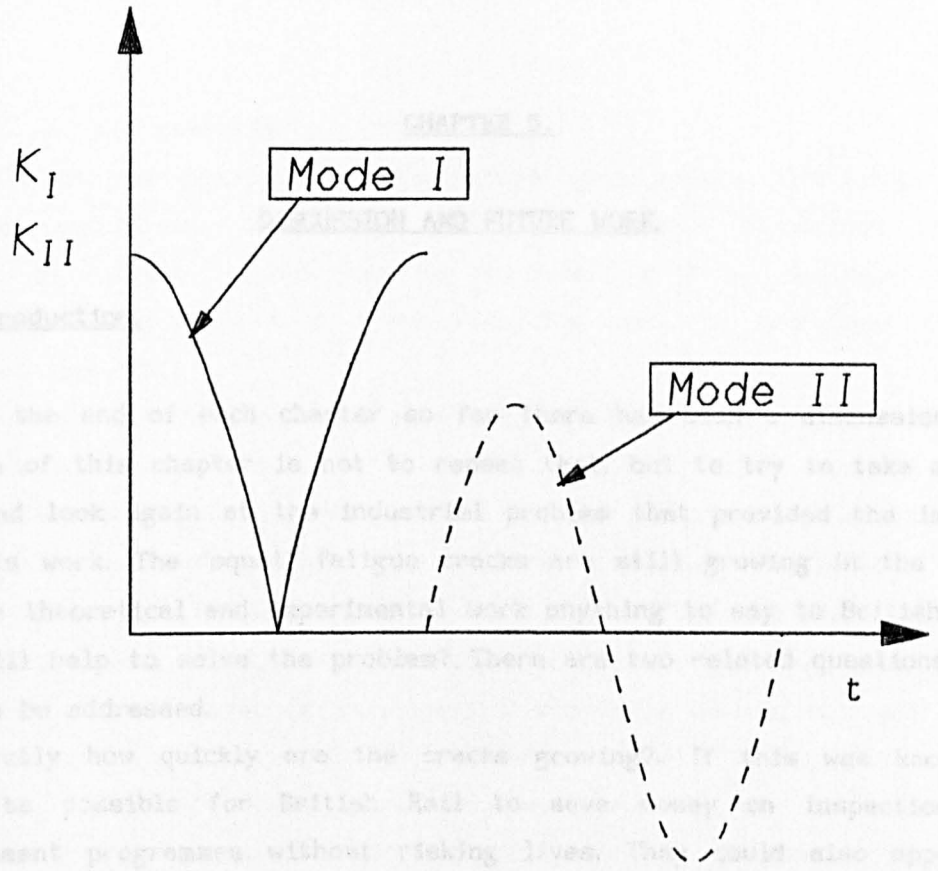

Fig. 4.19 Load Cycles for Co-planar Growth in Type B Tests.

CHAPTER 5.

DISCUSSION AND FUTURE WORK.

5.1 Introduction.

At the end of each chapter so far there has been a discussion. The purpose of this chapter is not to repeat that, but to try to take a step back and look again at the industrial problem that provided the impetus for this work. The 'squat' fatigue cracks are still growing in the rails. Has the theoretical and experimental work anything to say to British Rail, that will help to solve the problem? There are two related questions that need to be addressed.

Firstly how quickly are the cracks growing?. If this was known it would be possible for British Rail to save money on inspection and replacement programmes without risking lives. They could also apportion the cost of damage to the elements of traffic that cause it. At the moment it is not known whether a high speed train does more or less damage than a heavy freight train. They could also assess the financial consequences of changing steel, of grinding the cracks away from the top of the track, or of other policies that might or might not save money.

The second question is, can the fatigue crack growth be stopped? The advantages of doing so are obvious, but no real solution of any form has been suggested so far.

5.2 Crack Growth Rates Under Rolling Contact Fatigue.

To find the crack growth rate in any form of fatigue it is necessary to have both a knowledge of the crack tip conditions, and a knowledge of what effect those conditions will have on the rate of growth. The best work done so far in the calculation of those conditions is that done by Bower [1]. His work, discussed in section 1.3.2, appeared confusing initially because it predicted that the shallow angled crack in 'squats' was predominantly loaded in shear. At the time the vast majority of fatigue tests under in-plane shear had produced only branch crack growth, no crack growth data was available for shear mode growth, and many people thought

that it was not possible to produce any.

This project has produced shear crack growth data. Combining it with Bower's calculations shows that all three possible directions of crack growth in rolling contact can be predicted, that is co-planar growth, branching up to remove a flake from the rail, or branching down to fracture the rail.

However Bower's model was much simpler than a real 'squat'. His model was elastic, whereas there is definitely plasticity under the wheel of a train. His model ignored mean stresses, and yet it is known that there is a compressive mean stress near the surface of a rail, and a tensile mean stress in the longitudinal direction at a few millimetres depth. His model also only covers a very limited range of crack angles and lengths. The biggest problem however is that 'squats' are three dimensional, and Bower's calculations only consider a two dimensional crack. It should be said as well that the reason these approximations were made was that the problem that he solved was still highly complex, and the programme used large amounts of computer time. Bower's approach therefore needs to be repeated to model 'squats' more closely, and to collect enough results to model the various different crack lengths, applied loads, and mean stresses.

Alongside this work, considerably more fatigue crack data needs to be collected. This project only produced co-planar crack growth for one simplification of Bower's calculations. The mean stress, the over lapping of the mode I and mode II cycles, and applying uniaxial rather than equibiaxial mode I loads are all likely to affect the growth rate and, as a consequence, the branching criterion.

5.3 Can the Cracks be Stopped?

The work done so far suggests that it would be very difficult to stop the shallow angled fatigue cracks growing. They do not start from any metallurgical defect or stress concentration. Changing the steel to a stronger steel will not necessarily help because it will yield at a higher load, and therefore reduce the contact patch, and increase the stresses. The crack appears to be driven primarily by the combination of the weight and tractive forces of the train, and the action of water in the crack. The water cannot be removed, and the forces cannot be reduced if the train

speeds and carrying capacities are to be maintained.

However, it is not the shallow angled crack that breaks the rail. The major problem is really due to the branch cracks growing down into the rail. The first two results chapters appeared to contain basically negative results, saying that mode II growth could not be produced, and the mode I branch crack load was much higher than was predicted by the maximum tangential stress criterion. However if this branch crack growth can be stopped in the rails, the rail lives should increase dramatically. The results show that two factors are involved in deciding the branch crack threshold and growth rate. Firstly if the main crack is not opened by a mode I load, frictional forces will reduce the mode II loading at the crack tip which cause branching. In a rail this opening is apparently provided by water entering and being trapped in the crack. This cannot therefore be stopped. The second factor is the mean stress perpendicular to the branch crack. The branch crack growth is essentially a mode I crack. A compressive mean stress increases the threshold, and decreases the growth rate. The equibiaxial mean load applied in the tests of chapter 3, brought the threshold down to that of a mode I crack at that load ratio, and increased the growth rate to that of a normal mode I test.

Currently branch cracks from 'squats' are under a tensile mean load on all but the hottest days of the year, because of the tension required in rails to prevent them from buckling. If that mean load was changed to a compressive load, the branch crack growth should stop. This is supported by the work of Hahn et al, [2], who looked at the rolling contact fatigue of rollers that were shrink fitted onto cylinders before testing. This puts a tensile mean stress in the roller. In these tests the cracks branched down into the roller as occurs in 'squats'. In ordinary fatigue tests the cracks branch up to remove small flakes of metal.

5.4 A Solution.

It would be no good stopping 'squats' branching down into the track, if the rails buckled on hot days instead. However British Rail have considered alternative ways of preventing the rails buckling. In traditional engineering structures are prevented from buckling by using triangulation to make the structure rigid, and by pinning the struts at suitable

intervals to keep their effective length down. In rails this could be achieved by adding diagonal members to the sleepers to provide triangulation, and by pinning the rigid rail structure to the ground at suitable distances, with an appropriate quantity of concrete, as shown in Fig. 5.1. Alternatively concrete slabs might be used as an alternative to the balast and sleeper arrangement. Increasing the second moments of area of the rails would also make them more resistant to buckling enabling the tensile stress to be reduced if not removed.

There are major problems with these approaches. All of them would initially cost more than the current methods, and the triangulation or concrete slab foundation approaches would create enormous problems if the track needed re-aligning due to earth movements. However no other acceptable alternative to track inspection and rail replacement has yet been found.

References.

1. A.F.Bower. 'The Influence of Crack Face Friction and Trapped Fluid on Surface Initiated Rolling Contact Fatigue Cracks.'
Trans. ASME, J. of Lubrication Tech, Vol.110, pp704-711. 1988.

2. G.T.Hahn, V.Bhargava, H.Yoshimura, C.Rubin. 'Analysis of Rolling Contact Fatigue and Fracture.'
6th International Conference on Fracture. New Delhi, India. Dec. 1984.

Figures

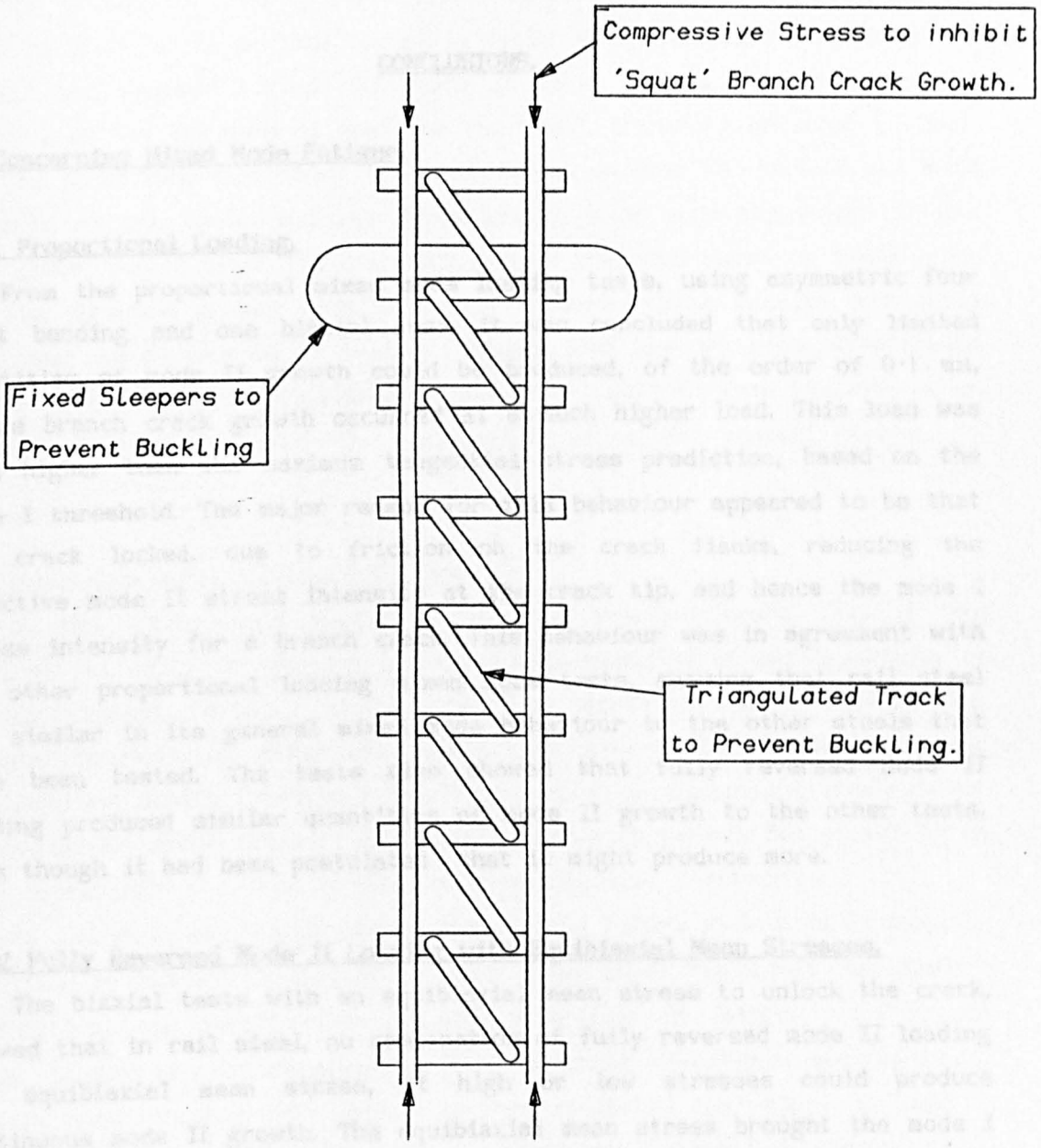

Fig. 5.1 A Possible Solution to the Problem.

CHAPTER 6

CONCLUSIONS.

6.1 Concerning Mixed Mode Fatigue.

6.1.1 Proportional Loading.

From the proportional mixed mode loading tests, using asymmetric four point bending and one biaxial test, it was concluded that only limited quantities of mode II growth could be produced, of the order of 0·1 mm, before branch crack growth occurred at a much higher load. This load was much higher than the maximum tangential stress prediction, based on the mode I threshold. The major reason for this behaviour appeared to be that the crack locked, due to friction on the crack flanks, reducing the effective mode II stress intensity at the crack tip, and hence the mode I stress intensity for a branch crack. This behaviour was in agreement with the other proportional loading mixed mode tests, showing that rail steel was similar in its general mixed mode behaviour to the other steels that have been tested. The tests also showed that fully reversed mode II loading produced similar quantities of mode II growth to the other tests, even though it had been postulated that it might produce more.

6.1.2 Fully Reversed Mode II Loading with Equibiaxial Mean Stresses.

The biaxial tests with an equibiaxial mean stress to unlock the crack, showed that in rail steel, no combination of fully reversed mode II loading and equibiaxial mean stress, at high or low stresses could produce continuous mode II growth. The equibiaxial mean stress brought the mode I thresholds down to the maximum tangential stress criterion prediction, presumably because it unlocked the crack. However it did not prevent the mode II crack arresting. The tests at high stresses, with fully reversed mode II loading and an equibiaxial mean stress showed that a competition occurred between mode I and mode II cracks which the mode I branch cracks won. This supports the proposal that the maximum growth rate criterion is the most appropriate one to use in deciding which mode of crack growth will occur.

6.1.3 Sequential mode I and Mode II Loading.

The sequential loading tests showed that continuous co-planar growth could be produced in a crack loaded in cyclic mode II, if a mode I load was applied and removed before each mode II cycle. If the ratio between the mode I load and the mode II load was too small, branching occurred instead.

The crack rate was shown to be dependent on both the mode I and mode II parts of the cycle, and two crack growth laws were suggested. It was also shown that a branching criterion can be produced based on these laws, and the maximum growth rate criterion. However these results have only scratched the surface of an area of fatigue that has not been investigated before. They have probably produced more new questions than answers, to an area of great importance to the real problem of rolling contact fatigue.

6.2 Concerning Rolling Contact Fatigue.

In the introduction R.A.Smith's comment was mentioned, that it was difficult to apply our greatly increased understanding of metal fatigue, to rolling contact fatigue, because of "the apparent lack of alternating tensile stresses to drive the cracks." He also said "alternating shear stresses are easily found, but the reproduction of continuous crack growth controlled by shear (Mode II in fracture mechanics terms), has proved to be near impossible" [1]. This project has overcome that difficulty.

It has done so by applying a mode I load before each mode II load, as predicted by Bower's calculations [2]. In doing so it has shown that Bower's calculations can permit three possible directions of fatigue crack growth under rolling contact fatigue, the two branching directions, and co-planar growth. Some crack growth data have been collected that might be used in conjunction with Bower's results for rough predictions of growth rates. More importantly though this work has shown that more detailed calculations and further fatigue tests could give much better predictions.

6.3 Concerning 'Squats' in Rails.

As 'squats' are rolling contact fatigue cracks, this work suggests that growth predictions could be made if further calculations and fatigue tests are performed. The required calculations and fatigue tests would be extensive however, because of the complexity of the problem.

The work has also shown that the tension in the rail required to stop buckling is probably the major reason for branch cracks growing into the rail, from the original shallow angled crack. If this tension could be removed, and possibly even be replaced by a compressive mean stress, the branch cracks should stop growing, and the rail lives should increase dramatically. This would obviously require a major change in track design, and alternative methods of preventing the track from buckling.

References.

1. R.A.Smith. 'Contact Fatigue'. Cambridge University Engineering Department. 29 September 1988.

2. A.F.Bower. 'The Influence of Crack Face Friction and Trapped Fluid on Surface Initiated Rolling Contact Fatigue Cracks.'
Trans. ASME, J. of Lubrication Tech, Vol.110, pp704-711. 1988.

APPENDIX 1.

THE BIAXIAL FATIGUE RIGS AND THE SIGNAL GENERATOR.

A1.1 The Biaxial Fatigue Rigs.

A1.1.1 The Requirement For Biaxial Fatigue Rigs.

Traditional fatigue testing has used machines and specimens capable of producing only very limited types of loading, predominantly uniaxial tension and compression, or bending. Real engineering components are subjected to much more complicated stresses. The cracks in rails discussed in this thesis are subject to both tensile and shear stresses. Aircraft components will have stresses in one direction caused by changes in pressure, and in other directions from turning, taking off and landing. A turbine shaft is subject to a bending stress cycle for each revolution, and torsional stresses during changes in loading. In general then it is necessary to consider the effects of these more complicated stresses if crack growth rates and thresholds are to be predicted for real engineering situations. To do this it is necessary to perform experiments under laboratory conditions to measure the effects. The biaxial fatigue rigs were built to enable some such tests to be carried out.

Section 1.4.1.3 gives details of the reasons for the use of biaxial rigs in these projects. Without them it would not have been possible to apply the stresses to the cracks predicted by Bower [1]. Biaxial rigs have also been used in a wide variety of other tests. For example they have been used to show the effect on fatigue crack growth rates of a stress parallel to a crack loaded in mode I, both at room and high temperature [2]. They have been used to look at composite materials whose properties can vary enormously depending on the loading direction [3]. They can be used to look at fretting fatigue where one pair of actuators move a specimen, while the other pair apply the required load to the fretting pads [4].

A1.1.2 The Specification of the Sheffield Mayes Biaxial Rigs.

The machines have four actuators, one pair apply a vertical load, one pair apply a horizontal load, Fig. A1.1. Each actuator has a capacity of +/- 200kN, and a stroke of 50mm. The maximum daylight between the actuators is 550mm.

There are three pairs of pumps supplying oil at a pressure of up to 200 bar. One pair can supply 10 litres/minute to each axis, or 5 litres/minute to each actuator. The other two pairs can each supply 45 litres/minute to each axis, or 22·5 litres/minute to each actuator. The maximum frequency is dependent on both the oil flow rate, the displacement, and the load range. For example with one pair of 45 litres/minute pumps, a dynamic load of 50 kN, and a displacement amplitude of 0·2 mm, a frequency of 18 Hz is possible, whereas a dynamic load of 200 kN, and a displacement amplitude of 2 mm reduces the frequency to 2 Hz. It is possible to link both pairs of pumps to one machine which would roughly double the available maximum frequency. The smaller pump is useful in low frequency or slow fracture tests because it requires much less power to run it.

The machines can run under displacement control, with 5 mm, 10 mm, 25 mm, and 50 mm ranges, load control with 20 kN, 50 kN, 100kN, or 200 kN ranges, or strain control, where the available strain range will depend on the transducer used. In the experiments prior to this project cyclic loads were applied by using a Prosser Scientific Instruments function generator, model D3104. This could produce two outputs in the form of sine waves, square waves or triangular waves, at frequencies between 0.1×10^{-3} Hz to 1000 Hz. The phase angle between these two outputs could then be specified between +/- 180°.

A1.2 A Signal Generator for Non-proportional or variable Amplitude Loading.

The experiments discussed in Chapter 4 required applied load cycles that could not be produced by the Prosser Scientific Instruments function generator. A new signal generator was therefore made from a Viglen I PC compatible computer, and a Blue Chip Technology AOP2 Analogue Output board. The analogue output board was fitted into the standard interface inside the

computer, and programmed using Microsoft's Quick Basic, a compiled basic. The output signal is simply produced by writing the required voltages to the memory addresses associated with the output board.

The type of cycle, load range, frequency, and the number of cycles required were input at the beginning of the programme, and then the cycle could be interrupted by pressing certain keys. The output voltage could be specified as a 12 bit number, or a resolution of 2·5 mV in a 10 V range. The maximum output frequency of the computer was around 250 signal increments to each channel per second.

Any output signal between 0 and 10 volts could be specified in this manner, and so the same system could be used for any another non-proportional load cycle or variable amplitude loading test, with minor modifications to the programme.

A frequency of 2 Hz was used for all the non-proportional sequential tests discussed in chapter 4, as this was the frequency at which the biaxial rigs just began to distort the load cycles in the tests using the highest loads.

References.

1. A.F.Bower. 'The Influence of Crack Face Friction and Trapped Fluid on Surface Initiated Rolling Contact Fatigue Cracks.'
Trans. ASME, J. of Lubrication Tech, Vol.110, pp704-711. 1988.

2. M.W.Brown, K.J.Miller. 'Mode I Fatigue Crack Growth Under Biaxial Stress At Room and Elevated Temperature.'
ASTM STP 853. 'Multiaxial Fatigue.' Eds. M.W.Brown, K.J.Miller. pp135-152. 1985.

3. D.L.Jones, P.K.Poulose, H.Liebowitz. 'Effect of Biaxial Loads on the Static and Fatigue Properties of Composite Materials.'
ASTM STP 853. 'Multiaxial Fatigue.' Eds. M.W.Brown, K.J.Miller. pp413. 1985.

4. Y.Mutoh, T.Satoh, K,Tanaka, E.Tsunoda. 'Fretting Fatigue at Elevated Temperatures in Two Steam Turbine Steels.'
Fatigue and Fract. of Eng. Mater. and Struct. Vol. 12, No.5, pp409-421, 1989.

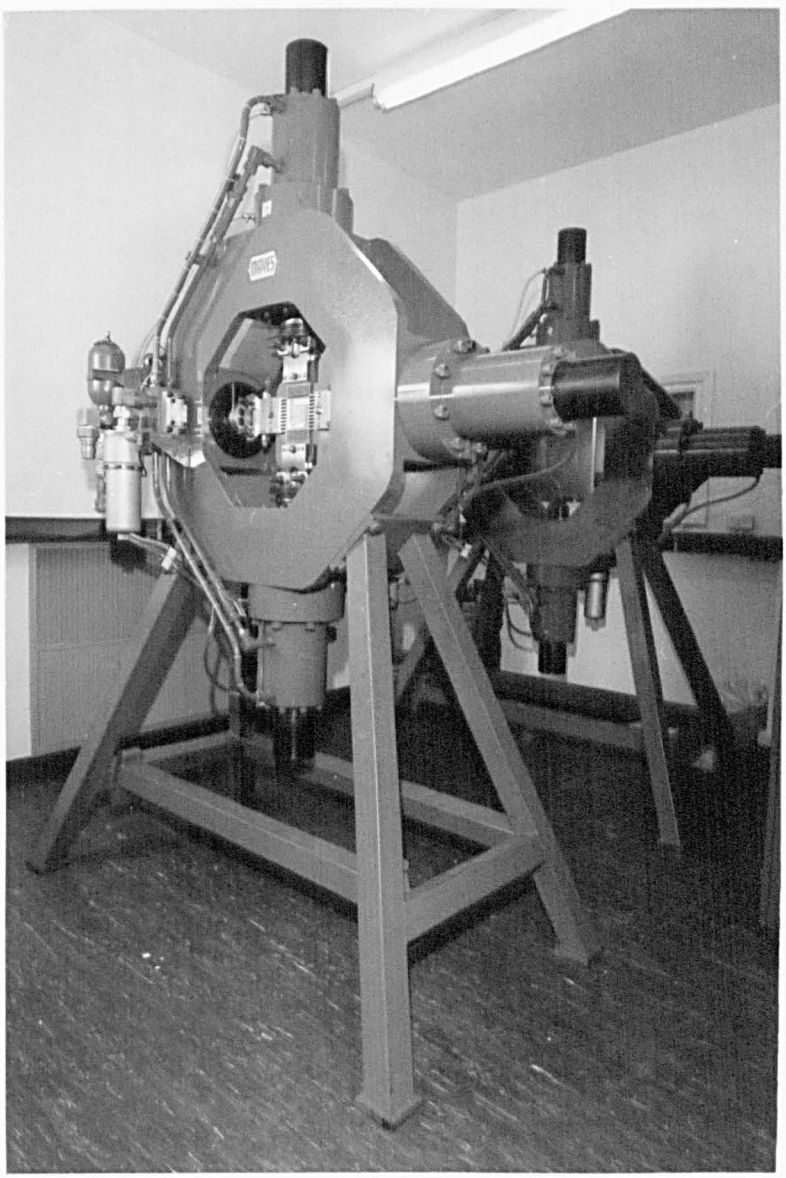

Fig. A1.1 The Biaxial Fatigue Rigs.

APPENDIX 2.

SPECIMEN DESIGN.

A2.1 Specimen Design.

The Biaxial Specimen for the experimental work planned had certain requirements that meant a new design was necessary:

1. It should produce a uniform biaxial stress in its central section, and that section should be as large as possible.
2. It should be possible to load the central section up to yield, without the specimen or grips failing anywhere else by fatigue. Yield was defined as a cyclic plastic deformation of 0.2 %.
3. It should be possible to apply fully reversed loads to the specimen without any backlash effects, or buckling.
4. The specimen must be made out of a rail, so the maximum dimension must be less than or equal to 158mm, the height of a rail; and the thickness must be 16mm or less.
5. The specimen and grips should cost as little as possible to manufacture with the above conditions fulfilled.

No specimen found in the literature [1-20] fulfilled all these conditions, and so a new design was required.

Monch and Galster[1] in 1963 showed that it was necessary to have slots in the arms of the specimen if a uniform stress was going to be applied, as shown in Fig. A2.1. If not each loading arm would restrain the stress in the perpendicular direction, giving a much smaller stress at the edge of the working section than at the centre.

The most common method of loading the arms of the specimen is through a load splitting tree arrangement as shown in Fig. A2.2. This method is of no use for fully reversed loading however, as the tree cannot apply compressive loads. Two other alternatives for loading are obviously available. Firstly to load using friction, ie the specimen is clamped between the loading arms by as many bolts as can be fitted in. Alternatively, the tensile load is applied by loading through pins, the compressive load applied by pushing against the edge of the specimen, and the backlash removed by some sort of screw or wedge tightening mechanism, as shown in Figs. A2.3. The second method was chosen in this case, as it

was not possible to apply enough load through friction to achieve the yield stress.

Because of the problem of these requirements, the limited size of the specimen, and manufacturing costs, it was decided to make the slots in the arms a part of the grips, not part of the specimen. That way they need only be manufactured once, reducing costs, and do not take up such a high proportion of the specimen size. The final design is shown in Figs. A2.3.

A2.2 Photo-Elastic Testing.

The specimen was tested photo-elastically under uniaxial tension, to check that the stress in the central section was uniform, and to check that the stress at the end of the notches in the specimen edges was low enough to prevent fatigue cracks starting from there.

In the two corners in Fig. A2.4, marked A and B, the holes were drilled 1 mm further back than the other holes. This was to reduce the stress at those points, where fatigue cracks were most likely to grow. The holes at corners C and D were drilled at the same distance from the working section as the other holes, so that the effect on the central section of moving the holes back could be investigated.

Fig. A2.4 shows that the central section was all of the same fringe order, and therefore at the same stress. The fringe order was measured using a microscope at points along the centre line, and found to be the same at all points 10 mm in from the edge, to within +/- 3 %. It was shown that drilling the holes at A and B further back had little effect on the stress in the central section, and so these positions were chosen for the final specimen design.

The stresses at the ends of the slots at A and B were calculated, and compared to the stress in the central section:

A=0.94 × stress in central section

B=1.61 × stress in central section.

When a spark machined notch is cut in the central section, the stress at its tip will be much greater than the stress at any of these points, and so the specimen should not fail from any of the edge notches

A2.3 Actual Specimen Performance.

The actual performance of the specimen was in general satisfactory. The uniform nature of the biaxial stress field was indicated by the fact that the final crack lengths from either side of the notch were within 5 mm of each other in all the tests except RSB14. RSB14 was a mode I threshold test, and the initial growth rate on one side was about 25% higher than the other. This difference in growth rate then increased as the longer crack approached the edge of the specimen, producing final crack lengths of about 40 mm and 20 mm when the test stopped. As a 25% difference in crack growth rate just above threshold could be caused by the natural scatter in the material properties, or by a difference in stress level of less than 5% this was not considered to be a great cause for concern.

No backlash effects could be observed by examining the load cell output on an oscilloscope, and only test RSB6 began to buckle. RSB6 had a compressive mean stress of 133 MPa, and a cyclic plasticity range of 0·6 %. As the specimen was only designed for fully reversed shear loading, not for cyclic plasticty with a compressive mean stress, this result was really just an illustration of the limitations of the specimen, not a fault in the basic design.

The grips themselves did not break, and in test RSB4 applied a load range of 206 kN. The only major criticism of them was that a load was needed in order to remove the wedges. This is no problem if the specimen can withstand the required load, but in test RSB3 the specimen broke during testing and some clamps had to be built so that a load could be applied. If the design was modified so that the wedges were angled on both faces rather than just one, then disassembly would be much easier.

The greatest problem with the specimens however was that in some tests fatigue cracks did form at the edges of the specimen causing the test to be finished prematurely. This in general occurred when the angled crack subject to shear loading was not opened by a mode I stress. This would have resulted in friction attenuating the mode II stress intensity at the crack tip, while the mode I stress intensity at the edge notches was not reduced. The problem could be resolved in future tests by using a larger initial notch size, say 8 mm instead of 4 mm. For normal mode I

tests, or non-proportional tests where the crack does not lock up, the specimen should perform adequately.

REFERENCES.

1. E.Monch, D.Galster. 'A Method for Producing a Defined Uniform Biaxial Tensile Stress Field.'
British Journal of Applied Physics. Vol.14, pp810-812. 1963.

2. I.M.H.Charvat, G.C.Garrett. 'The Development of a Closed Loop Servo-Hydraulic Test System for Direct Monotonic and Cyclic Crack propagation Studies, Under Biaxial Loading.'
J. of testing and Evaluation. No.8, pp9-17. 1980.

3. I.H.Wilson, D.J.White. 'Cruciform Specimens For Biaxial Fatigue Tests: An Investigation Using Finite Element Analysis and Photo Elastic Coating Techniques.'
J. of Strain Analysis. Vol.6, No.1, pp27-37. 1971.

4. H.Kitagawa, R.Yuuki, K.Tohgo, M.Tanabe. 'ΔK Dependency of fatigue crack growth of Single and Mixed Mode Cracks under Biaxial Stresses.'
ASTM STP 853. 'Multiaxial Fatigue.' Eds. M.W.Brown, K.J.Miller. pp164. 1985

5. F.Hourlier, H.d'Hondt, M.Truchon, A.Pineau. 'Fatigue Crack Path Behaviour Under Polymodal Fatigue.'
ASTM STP 853. 'Multiaxial Fatigue.' Eds. M.W.Brown, K.J.Miller. pp228-247. 1985.

6. C.D.Hopper. 'Fatigue Crack Propagation Under Biaxial Stresses.'
PhD Thesis. Cambridge University Engineering Department. 1977.

7. C.D.Hopper, K.J.Miller. 'Fatigue Crack Propagation In Biaxial Stress Fields.'
J. of Strain Analysis. Vol.12, No.1, pp23-28. 1977.

8. M.W.Brown. 'Low Cycle fatigue Testing Under multiaxial Stresses at Elevated Temperature.'
'Measurement of High Temperature Mechanical Properties of Materials'. Eds M.S.Loveday, M.F.Day, B.F.Dyson.

9. M.W.Brown, K.J.Miller. 'Mode I Fatigue Crack Growth Under Biaxial Stress At Room and Elevated Temperature.'
ASTM STP 853. 'Multiaxial Fatigue.' Eds. M.W.Brown, K.J.Miller. pp135-152. 1985.

10. W. van Maaren. 'Crack growth Under Biaxial Fatigue Loading.'
B.R.O.S. Fracture Analysis research on Nozzle Intersection. Final Report, Vol.9.

11. G.Terry. 'The Biaxial Tensile Strain Field From a Conventional Loading Splitting Tree.'
Strain. Vol.13, pp110-112.

12. S. Jansson. 'Creep Crack Growth in Austenitic Stainless Steel Under Biaxial Loading.'
International Conference on Creep. Tokyo. 1986.

13. D.L.Jones, P.K.Poulose, H.Liebowitz. 'Effect of Biaxial Loads on the Static and Fatigue Properties of Composite Materials.'
ASTM STP 853. 'Multiaxial Fatigue.' Eds. M.W.Brown, K.J.Miller. pp413. 1985.

14. J.C.Radon, P.S.Leevers, L.E.Culver. 'A Simple Testing Technique for Fracture Under Biaxial Stresses.'
Experimental Mechanics. Vol.17, pp228. 1977.

15. L.Cridland, W.G.Wood. 'A Hydrostatic Tension Test of a Brittle Material.'
The International J. of Fracture Mechanics. Vol.4, pp277. 1968.

16. I.M.Daniel. 'Behaviour of Graphite / Epoxy Plates with Holes Under Biaxial Loading.'
Experimental Mechanics. Vol.20, No.1, pp1-8. 1980

17. I.M.Daniel. 'Biaxial Testing of [O_2/±45] Graphite / Epoxy Plates with Holes.'
Experimental Mechanics. Vol.22, No.5, pp188-195. 1982

18. M.W.Parsons, K.J.Pascoe. 'Development of a Biaxial Fatigue Testing Rig.'
J. of Strain Analysis. Vol.10, pp1-9. 1975.

19. E.W.Smith, K.J.Pascoe. 'Fatigue Crack Initiation and Growth in a High Strength Ductile Steel, Subject to In Plane Biaxial Loading.'
ASTM STP 853. 'Multiaxial Fatigue.' Eds. M.W.Brown, K.J.Miller. pp111-134. 1985

20. E.W.Smith, K.J.Pascoe. 'Fatigue Crack Initiation and Growth in HY100 Steel, Subject to In Plane Biaxial Loading.'
Cambridge University Engineering Department Report. CUED/C-MAT/TR95. 1982.

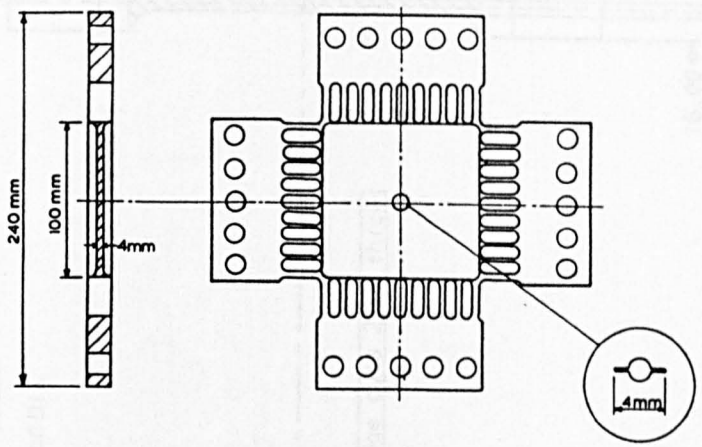

Fig. A2.1 A Biaxial Specimen with Slots in the Loading Arms.

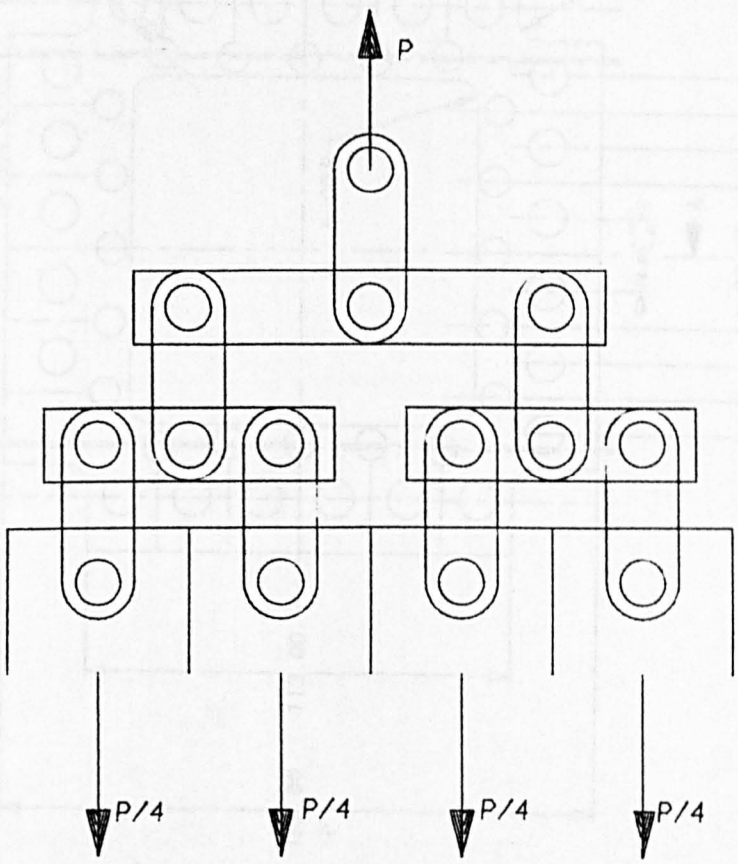

Fig. A2.2 A Load Splitting Tree.

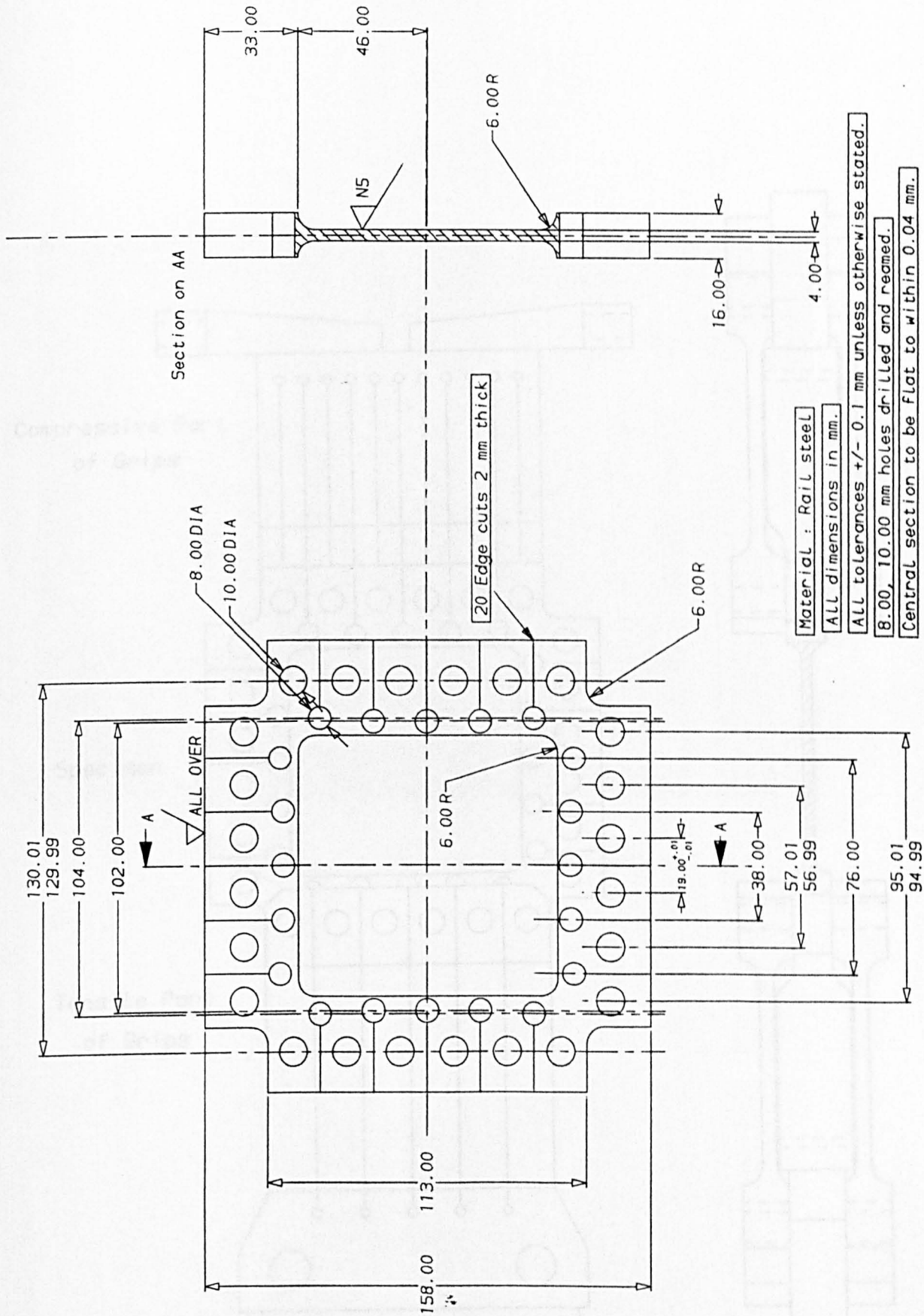

Fig. A2.3 a. The Final Specimen Design.

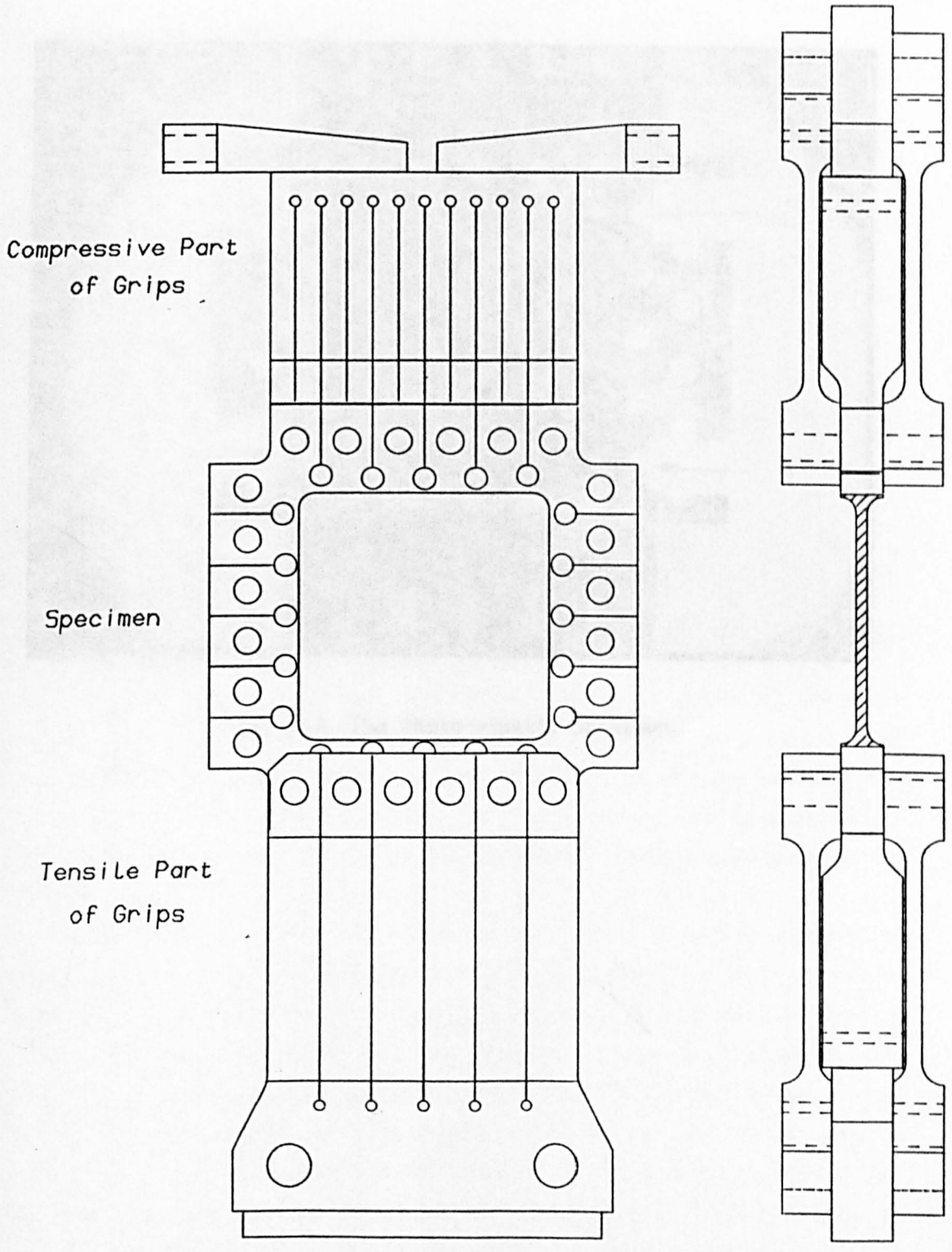

Fig. A2.3 b. Final Grip Design.

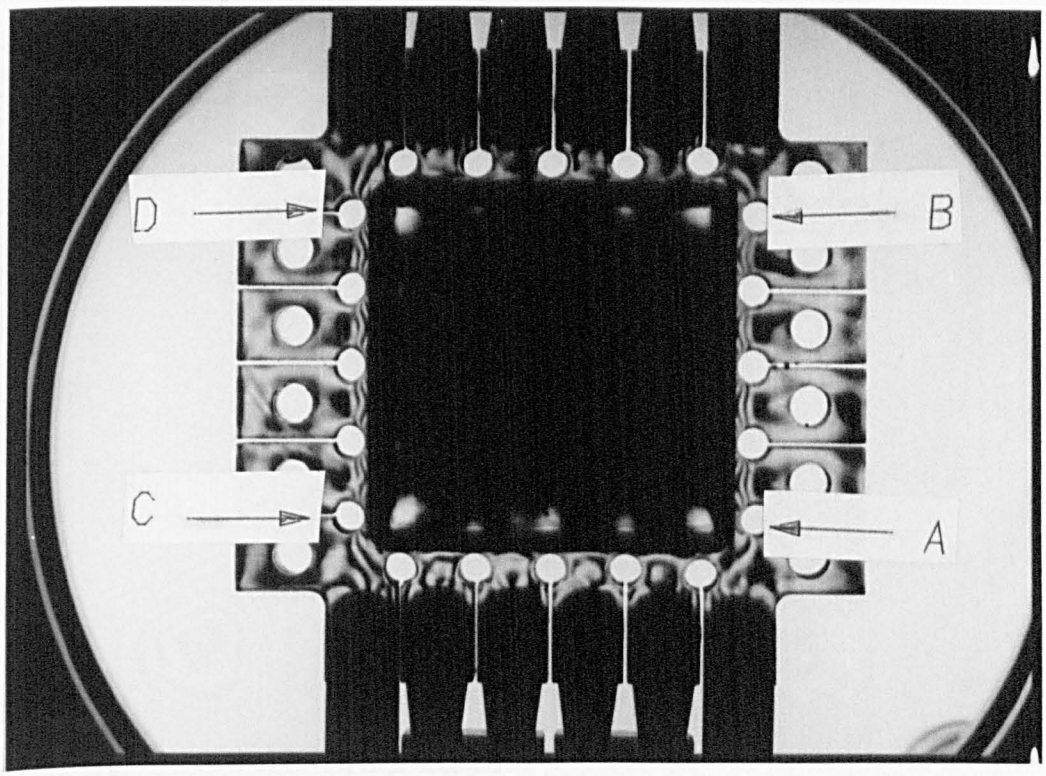

Fig. A2.4. The Photo-elastic Specimen.

APPENDIX 3.

POTENTIAL DIFFERENCE EQUIPMENT AND CALIBRATION.

A3.1 Introduction.

In chapters 2, 3 and 4 it was stated that the potential drop method of crack length measurement was used for the asymmetric four point bending specimens and the cruciform specimens. There are two advantages of this method as opposed to optical microscopy. Firstly, the method gives a measure of the average crack length through the thickness of the whole specimen, rather than just a surface measurement. Secondly, the voltage can be read automatically by a data logger, or chart recorder.

This appendix gives details of the method, of the theory behind it and of the relevant calibrations available in the literature. It also gives a new calibration, for cracks growing at an angle to the current in a finite plate, as occurred in some of the tests recorded in chapter 4.

A3.2 The Potential Difference Method.

The basis of the potential difference method is the fact that the potential difference between two points on a conductor, is a function of its geometry, and in particular of the length of a crack lying between those two points. If that function is found, either by theoretical or experimental means, then the crack length can be found from the potential difference.

It should be noted that the potential difference is also a function of the resistivity of the material, and therefore a function of temperature, and of the applied current. This fact has resulted in the common practice of using two or more pairs of leads, instead of one on a specimen. Any change in current or resistivity will produce the same proportional change in potential drop across each pair of leads, and so the effect can be cancelled out. Also the potential will depend on the exact position of the leads. Spot welding allows them to be positioned to within about 0·5 mm of a marked point, but if the initial and final crack lengths are known, then at those lengths it is possible to treat the lead positions as unknowns, and calculate them.

In the experiments recorded in this project three different sets of potential drop equipment were used. In the tests at British Rail Technical Centre, Derby, a single pair of leads was placed across the crack in the bend specimens, as shown in Fig. A3.1. The output was then recorded on an x-y plotter, where the y axis recorded the potential difference, and the x axis recorded the time. Unfortunately the fact that only one pair of leads was used meant that the output was not constant when the crack was not growing, and so the method was not suitable for the very small amounts of mode II growth measured on the optical microscopes.

In Sheffield, three pairs of leads were placed across the crack on the asymmetric four point bend specimens, Fig. A3.2, and two pairs on the cruciform specimens, Fig. A3.3.

A3.3 Theory.

The electric potential φ along a line of current flow, in a strip of metal of constant composition, with currents flowing only in the plane of the strip, obeys the equation [1]:

$$-\rho(J_x - iJ_y) = \frac{\partial\varphi}{\partial x} - i\frac{\partial\varphi}{\partial y} = \frac{d\Omega}{dz} \qquad \text{A3.1}$$

ρ is the resistivity of the material, J_x and J_y are the current densities in the x and y directions respectively, and Ω is a complex potential function equal to $\varphi(x,y) + i\psi(x,y)$. ψ is a constant along a line current flow, equivalent to a stream line in fluid flow, or along a free surface. Lines of constant ψ are lines across which current does not flow.

The complex variable $z = x + iy$ can be used to denote any position within (x,y) plane, or the z plane, and the real and imaginary parts of any analytical function of z will also be described by equation 1, [1]. The calibration of the potential difference is performed using the method of conformal mapping. Another complex variable, t, is introduced which is a function of z. There is then a t plane in which each point will have a corresponding point in the z plane. The t plane is said to be a transformation of the z plane. A series of such transformations is found so that in the final plane the current is uniform everywhere. The potential of any point in the final plane can then be easily calculated. The

potential of any point in the initial plane can the be found because it will be equal to the potential at the equivalent point in the final plane.

A3.4 Previous Calibrations.

Gilbey and Pearson [2] used this method to calibrate a crack in a plate of finite width, as shown in Fig. A3.4. Their calibration can be expressed as:

$$\frac{V_1}{V_2} = \frac{\cosh^{-1}\left\{\frac{\cosh(\pi y_1/2W)}{\cos(\pi a/2W)}\right\}}{\cosh^{-1}\left\{\frac{\cosh(\pi y_2/2W)}{\cos(\pi a/2W)}\right\}} \qquad \text{A3. 2}$$

Clark and Knott [3] calibrated a crack growing from an elliptical notch in an infinite plate, Fig. A3.5. Their calibration can be expressed as:

$$\frac{V_1}{V_2} = \frac{\lambda(y_1)}{\lambda(y_2)} \qquad \text{A3. 3}$$

where $\lambda(y) = (q^2 + w^2)^{1/2} / q$

$w(y) = \frac{1}{2}(t + 1/t)$

$t(z) = (d+b)^{-1}(z+(z^2+d^2-b^2)^{1/2})$

$q = w(d+s)$

Brown [4] then combined the two calibrations for a crack growing from a notch in a finite plate, where the notch is small compared to the width of the plate, Fig. A3.6.

$$\frac{V_1}{V_2} = \frac{\cosh^{-1}\left\{\cosh\left((\pi(d+b)/4W)(\tau_1-1/\tau_1)\right)\ \sec\left((\pi(d+b)/4W)(T+1/T)\right)\right\}}{\cosh^{-1}\left\{\cosh\left((\pi(d+b)/4W)(\tau_2-1/\tau_2)\right)\ \sec\left((\pi(d+b)/4W)(T+1/T)\right)\right\}} \qquad \text{A3. 4}$$

where:

$\tau = (y + (y^2 - b^2 + d^2)^{1/2} / (a+b)$

$T = (s + (s^2 - b^2 + d^2)^{1/2} / (a+b)$

In the cruciform specimens used in this project, the notch is at an angle of 45° to the current, in a finite plate, as shown in Fig. A3.7. It was thought that Brown's calibration could be adapted to calculate the lengths of cracks growing at an angle to the current, by assuming that the

potential drop was purely dependent on the dimension of the crack perpendicular to the current. This method would therefore also allow branched crack lengths to be estimated, but the accuracy was unknown.

A3.4 The New Calibration.

As an alternative to the modification to Brown's solution given above, a new theoretical calibration was produced. The calibration modelled the starter notch as an ellipse, major axis d, minor axis b. This was assumed to make no difference to the calibration once the crack had grown a small distance away from the notch. As all the specimens were pre-cracked, the calibration for very short cracks was not of interest. The crack and the axes were inclined at an angle of θ to the specimen edges, and therefore to the lines of current flow remote from the crack. The specimen width was 2W.

Using the first of Clark and Knott's transformations, the ellipse can be changed to a unit circle in the t plane, Fig. A3.8, by using:

$$t = \frac{(z + (z^2 - d^2 + b^2)^{1/2})}{(d + b)} \qquad \text{A3.5}$$

Using Clark and Knott's second transformation, the circle is reduced to a line, Fig. A3.9:

$$\omega = \frac{(t + 1/t)}{2} \qquad \text{A3.6}$$

The last transformation can then be used in reverse, to transform the whole of the line back into a circle, Fig. A3.10:

$$\zeta = \left(\frac{\omega}{q}\right) \pm \left\{\left(\frac{\omega}{q}\right)^2 - 1\right\}^{1/2} \qquad \text{A3.7}$$

where q is the transformed distance between the origin and the crack tips.

The axes can then be rotated, Fig. A3.11 using the transformation:

$$\zeta' = \zeta . e^{i\theta} \qquad \text{A3.8}$$

The circle can then be transformed back into a line, but this time perpendicular to the current, using Clark and Knott's transformation, Fig.A3.12:

$$\lambda = \frac{(\zeta' + 1/\zeta')}{2} \qquad \text{A3.9}$$

The line is then transformed to give a line parallel to the current flow, without further distortion of the specimen edges, by using Gilbey and Pearson's transformation, Fig.A3.13:

$$\cos \xi = \cos \left(\frac{\pi\lambda}{2W'}\right) / \cos \left(\frac{\pi q}{2W'}\right) \qquad \text{A3. 10}$$

where: q is the transformed distance from the origin to the crack tip, and is equal to 1.

W' is the transformed half plate width.

Brown went straight from the second to the fifth transformation, as he was not dealing with a crack at an angle.

A solution for a crack at an angle in an infinite plate can be found by using the substitution:

$$\zeta' = \zeta . e^{-i\theta} \qquad \text{A3. 11}$$

instead of equation A3.5. This rotates the axes in the opposite direction, so that the next substitution, A3.6 gives a crack parallel to the current lines. However the solution is exactly the same as Clark and Knott's solution if only the component of current perpendicular to the crack at infinity is considered. This is because the component parallel to the crack will give no potential difference between points on a single line perpendicular to the crack.

The actual calibration equation is then found as follows:

We know that:

$$\frac{d\Omega}{dz} = \frac{d\Omega}{d\xi}\frac{d\xi}{d\lambda}\frac{d\lambda}{d\zeta'}\frac{d\zeta'}{d\zeta}\frac{d\zeta}{d\omega}\frac{d\omega}{dt}\frac{dt}{dz}$$

If we consider a point remote from the notch and crack, where $z \to \infty e^{i\theta}$, we know that:

$$\frac{d\Omega}{dz} = -\rho J e^{i\theta}$$

from equation A3. 1

Also we know that as $z \to \infty e^{i\theta}$

$$\frac{dt}{dz} = \frac{2}{d+b}$$

$$\frac{d\omega}{dt} = \frac{1}{2}$$

$$\frac{d\zeta}{d\omega} = \frac{-2}{q}$$

$$\frac{d\zeta'}{d\zeta} = e^{i\theta}$$

$$\frac{d\lambda}{d\zeta'} = \frac{1}{2}$$

$$\frac{d\xi}{d\lambda} = \frac{e^{\pi/2W'}}{\cos(\pi/2W')}$$

and therefore

$$\frac{d\Omega}{d\xi} = -\rho J \frac{\cos(\pi/2W')}{e^{\pi/2W'}} q(d+b)$$

$$\Omega = -\rho J \frac{\cos(\pi/2W')}{e^{\pi/2W'}} q(d+b).\xi(z)$$

Because the field is uniform in the ξ plane, $d\Omega/d\xi$ will be a constant, and the above two equations will hold for the whole plane. As the potential is the real part of Ω, the ratio between the potentials at points $(0,+/-y_1)$ and $(0,+/-y_2)$, for a crack length s, can then be expressed as:

$$\frac{V_1}{V_2} = \frac{Re\{\xi((s,0),(0,y_1))\}}{Re\{\xi((s,0),(0,y_2))\}}$$

Because of the number of transformations involved, this does not simplify down to a straightforward formula. In this project a computer programme was written to first calculate the values of y_1 and y_2 from the known values of crack lengths at the beginning and end of the tests, and then to calculate the unknown crack lengths from the voltages.

A3.6 Comparison With Experimental Data.

Figs. A3.14 and A3.15 show the new calibration and the modified version of Brown's calibration against the optical microscope readings for tests RSB8, and RSB10. These two tests were ones in which co-planar growth was produced, with a mode I cycle followed by the mode II cycle. In neither case was there a satisfactory correlation between the optical and potential difference calibrations. The reason for this was almost certainly because current was shorting across the crack to some extent. In both tests the potential difference reading dropped as the crack began to grow, suggesting that the crack was not growing but shrinking according to the calibrations. It might have been possible to search through the potential

difference data, collecting the highest values when presumably the crack would have been open, but instead the optical microscope readings were used exclusively in the early stages of growth, and the potential difference values only used to span smaller gaps between optical microscope readings for longer cracks. If the technique is to be used in the future it would be advisable to have a logging system that only measures the potential when a tensile load is applied. This would be possible if the same computer was used to read the signals and send the data, but it was not possible during these tests.

Fig. A3.16 shows the modified version of Brown's calibration against optical microscope readings for branch crack lengths in test RSB16. This time the crack was kept open by the predominantly mode I loading, and the calibration apparently worked well. The only significant difference between the calibration and the optical values occurred during the early stages of growth when the calibration over estimated the crack length by about 0·5mm.

References.

1. E.T.Copson. 'An Introduction to the Theory of Functions of a Complex Variable.'
Oxford University Press. 1935.

2. D.M.Gilbey, S.Pearson. 'Measurement of the Length of a Central or Edge Crack in a Sheet of Metal by an Electrical Resistance Method.'
Royal Aircraft Establishment Technical Report No.66402. 1966.

3 G.Clark, J.F.Knott. 'Measurement of Fatigue Cracks in Notched Specimens by means of Theoretical Electrical Potential Calibrations.'
J. Mech. Phys. Solids. Vol. 23, pp265-276.

4. M.W.Brown. 'Low Cycle Fatigue Testing under Multiaxial Stresses at Elevated Temperature.'
'Measurement of High Temperature Mechanical Properties of Materials.' Eds. M.S.Loveday, M.F.Day, B.F.Dyson.

Figures.

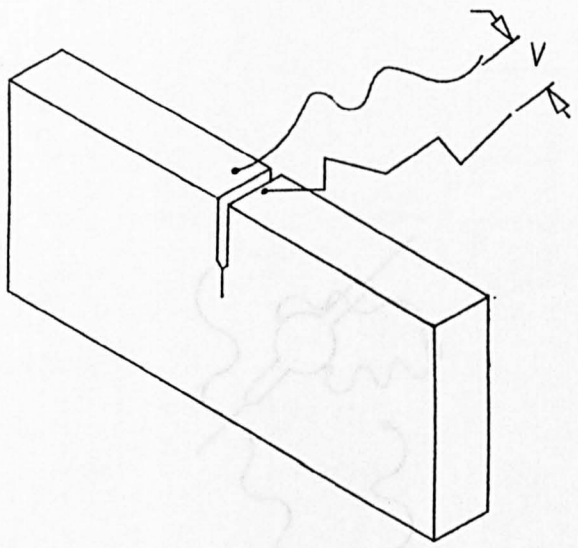

One pair of potential difference leads on a bend specimen.
Fig. A3.1

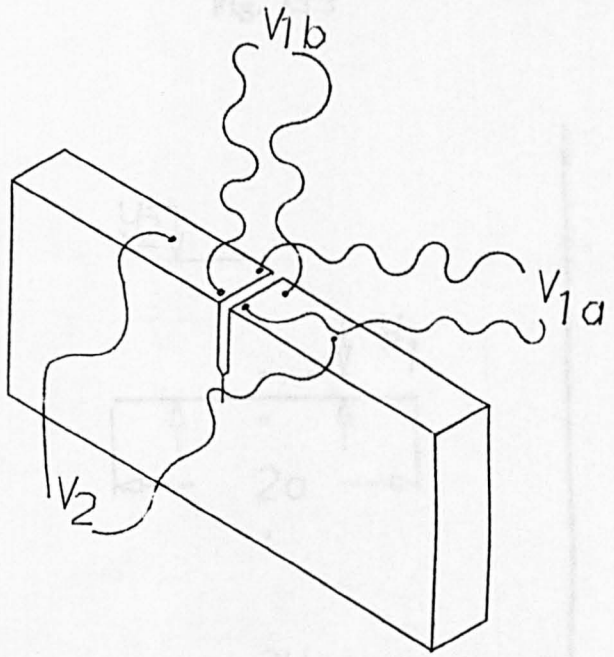

Three pairs of potential difference leads on a bend specimen.
Fig. A3.2

Two pairs of potential difference leads on a cruciform specimen.
Fig. A3.3

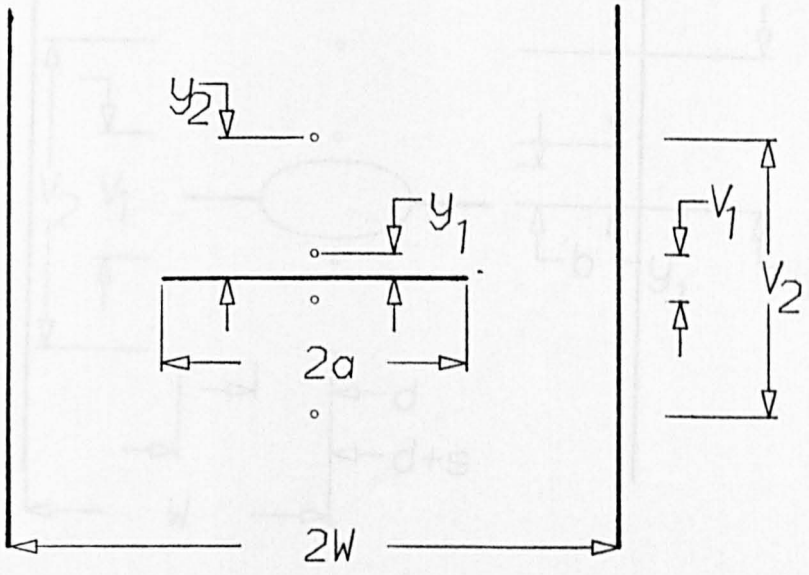

Gilbey and Pearson's model.
Fig. A3.4

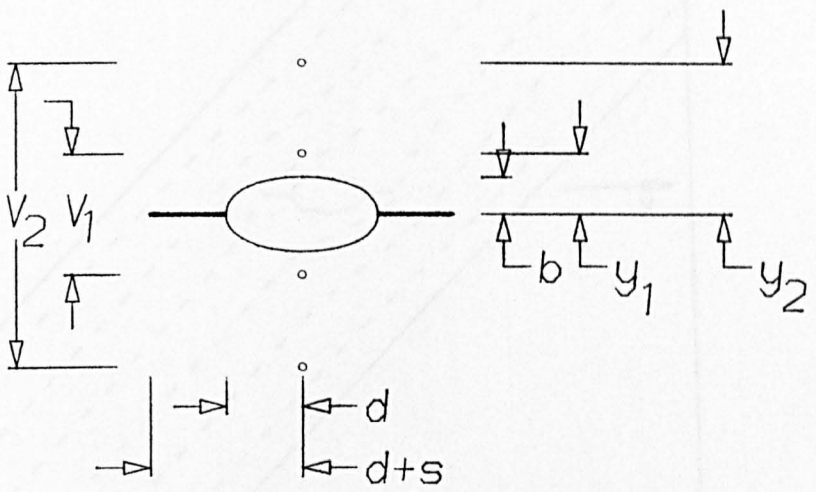

Clark and Knott's model.
Fig. A3.5

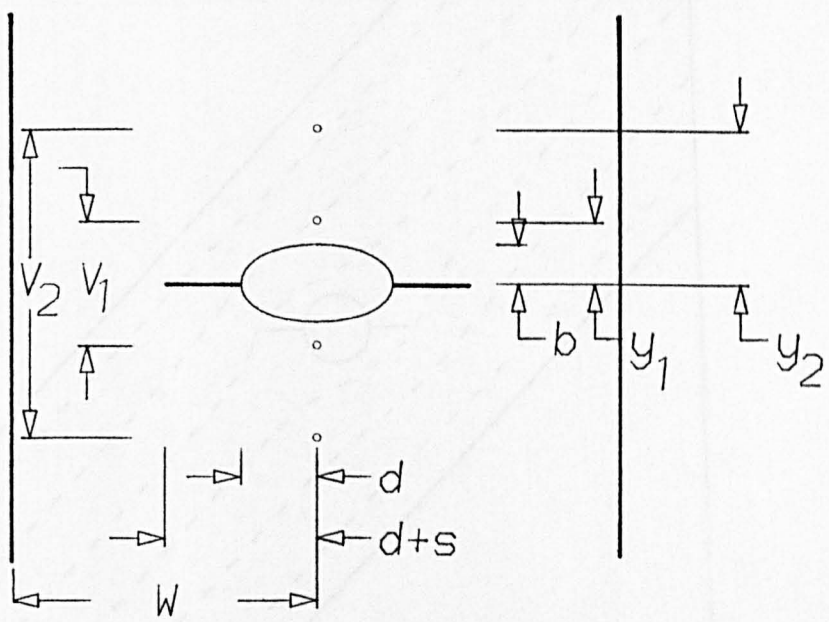

Brown's model.
Fig. A3.6

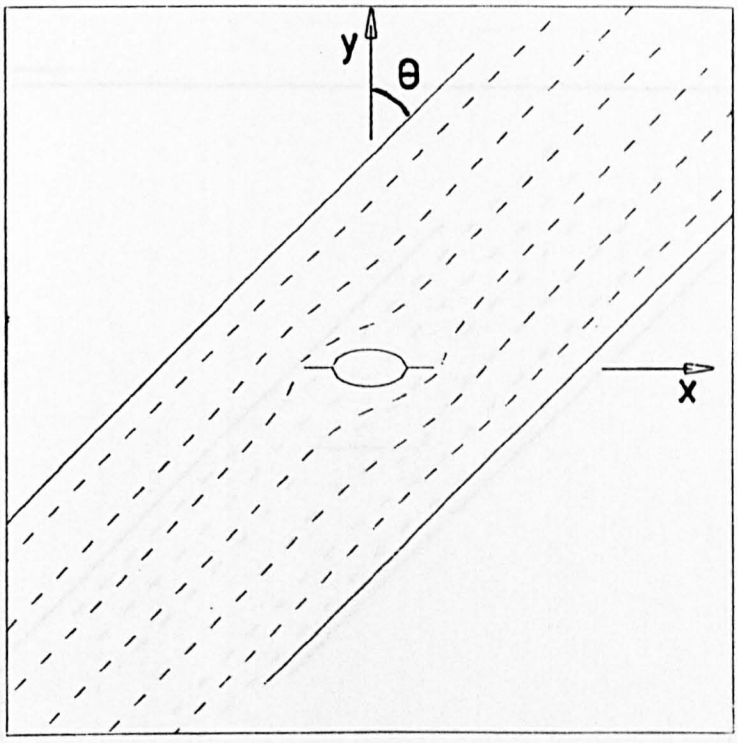

The new model.
Fig. A3.7

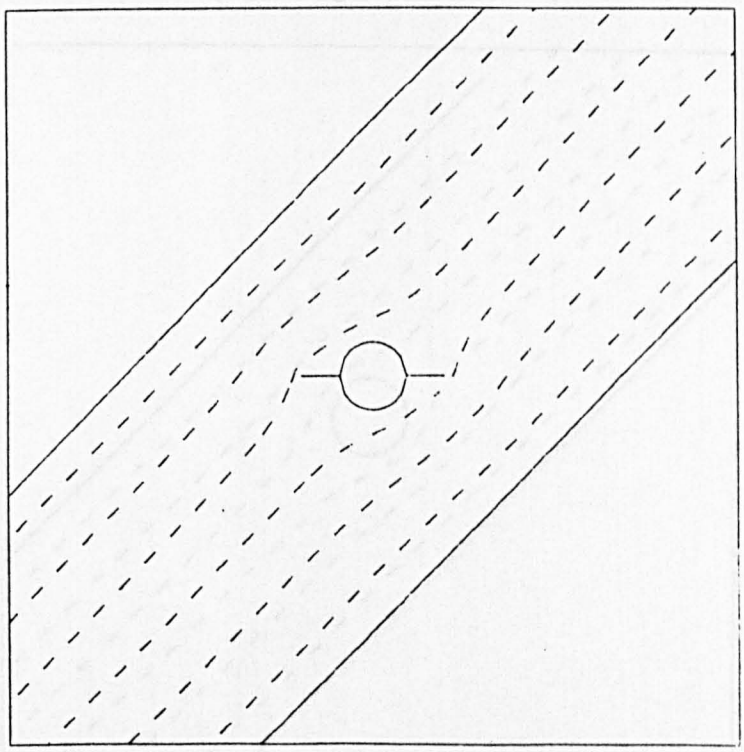

First transformation, z → t
Fig. A3.8

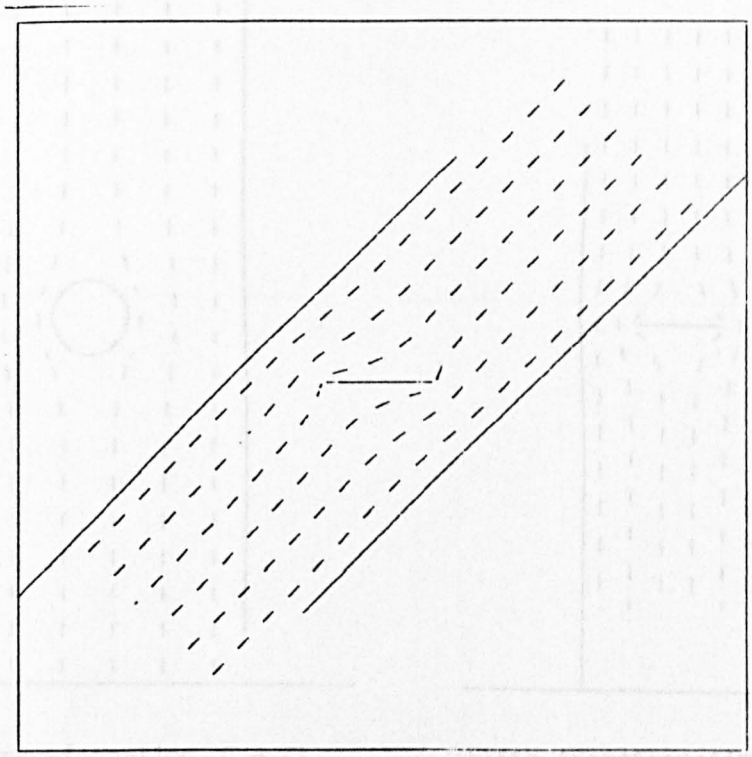

Second transformation, $t \rightarrow \omega$
Fig. A3.9

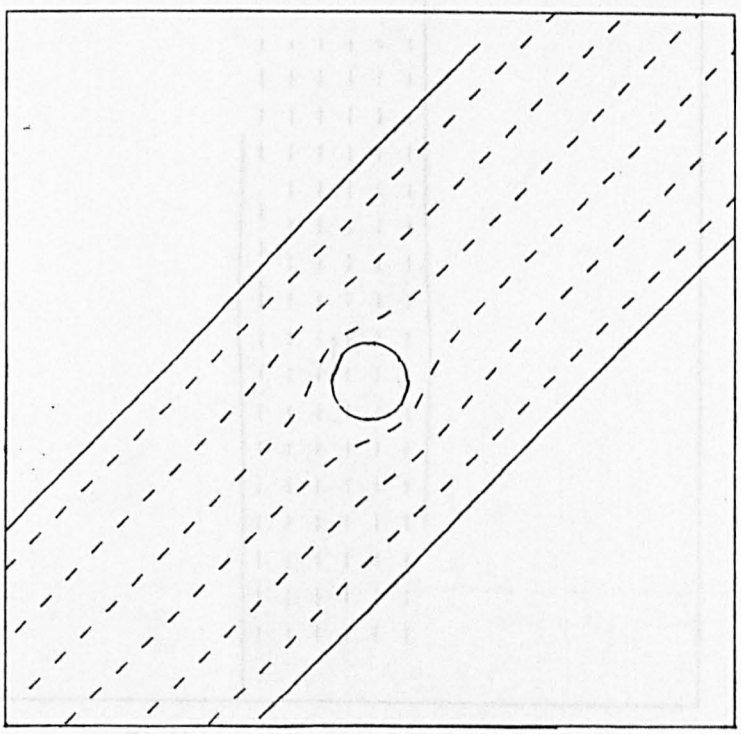

Third transformation, $\omega \rightarrow \zeta$
Fig. A3.10

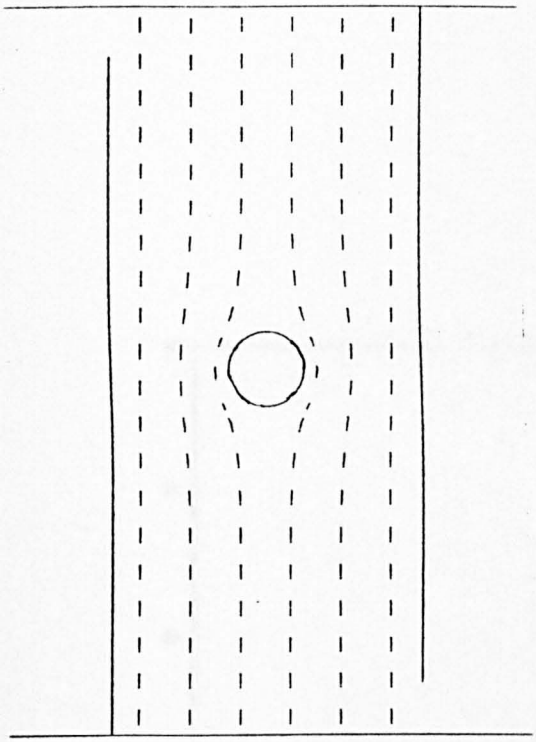

Fourth transformation, $\zeta \rightarrow \zeta'$
Fig. A3.11

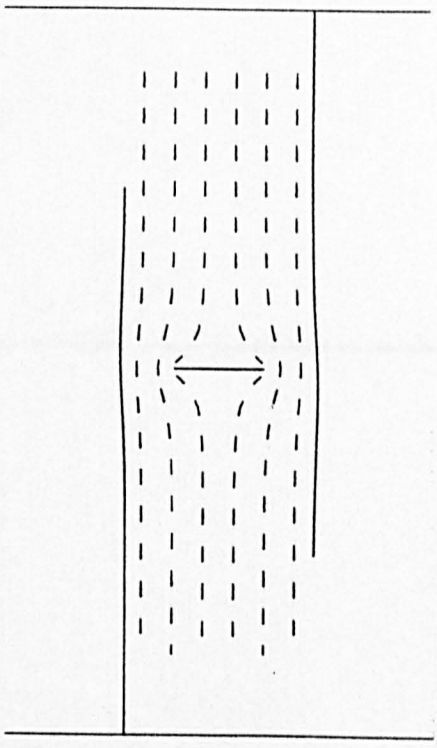

Fifth transformation, $\zeta' \rightarrow \lambda$
Fig. A3.12

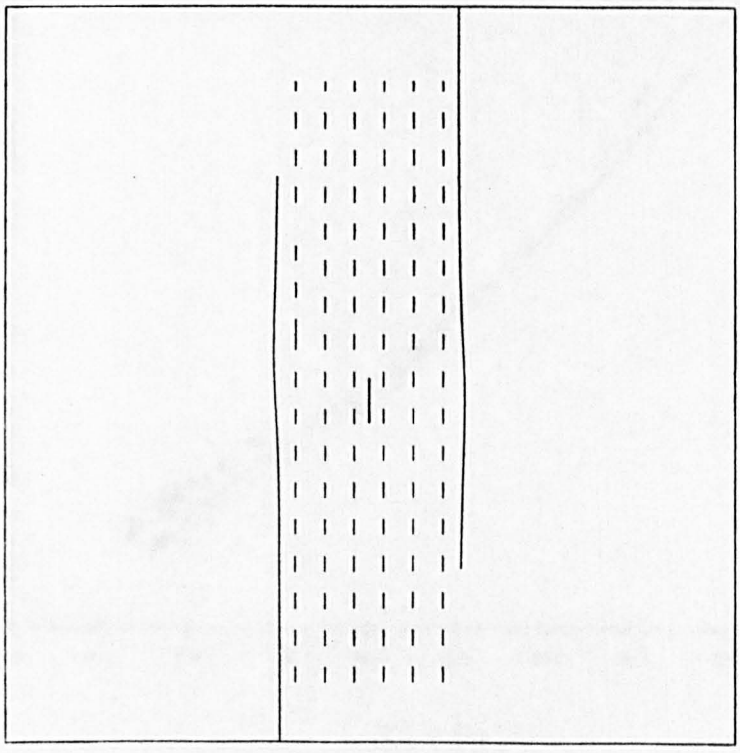

Sixth transformation, $\lambda \rightarrow \xi$
Fig. A3.13

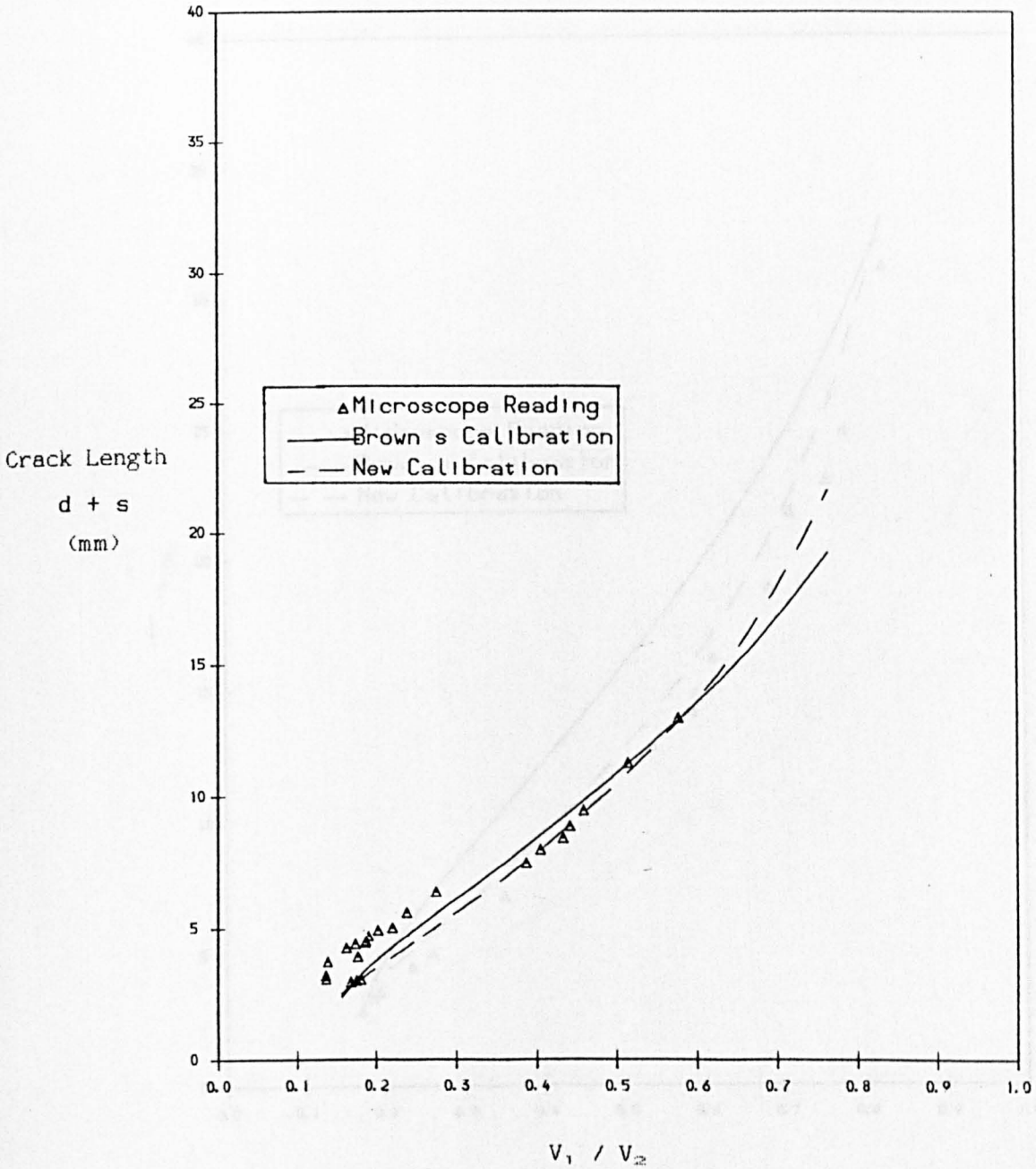

Fig. A3.14 Potential Difference Ratio vs. Crack Length for RSB8.

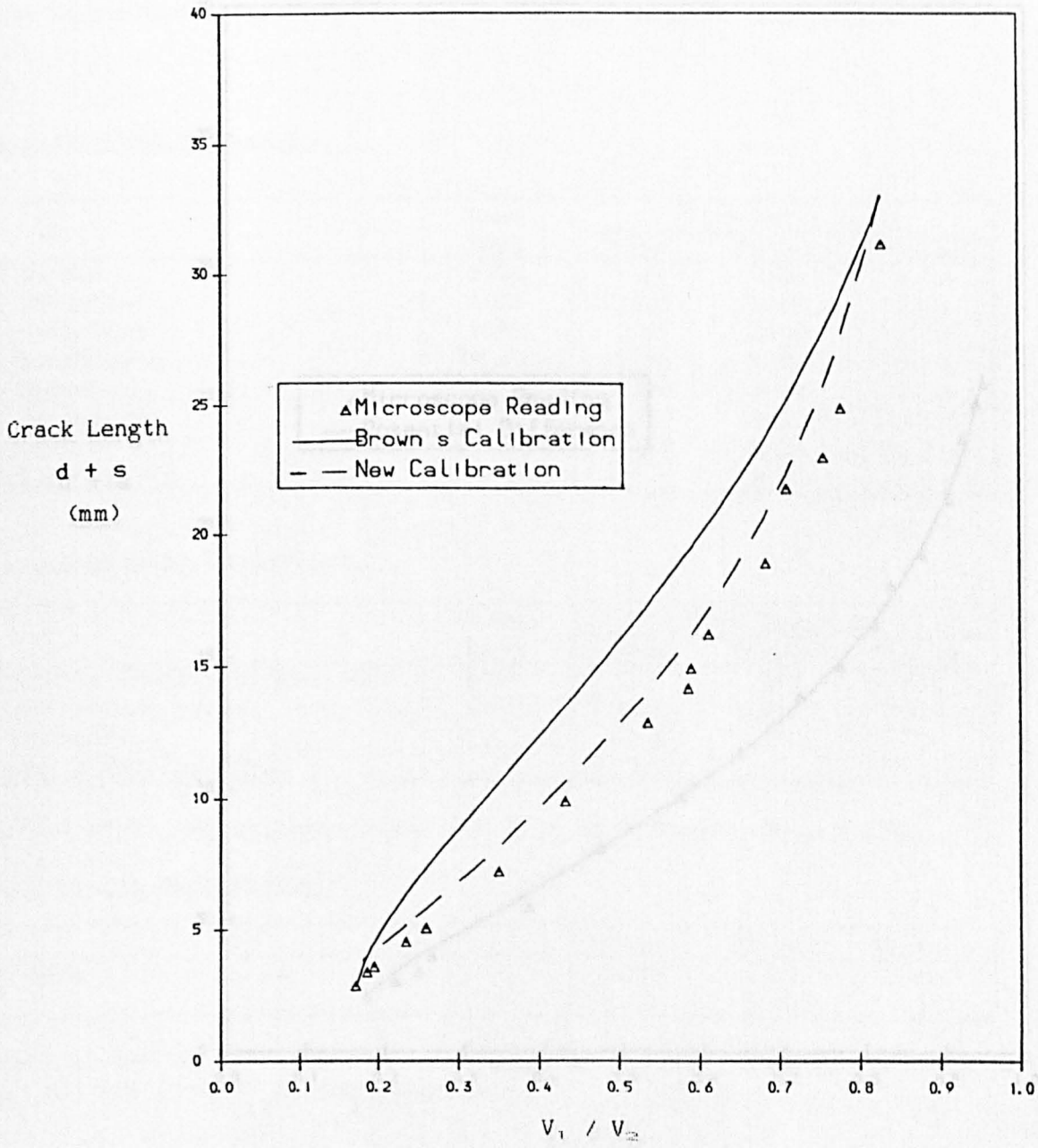

Fig. A3.15 Potential Difference Ratio vs. Crack Length for RSB10.

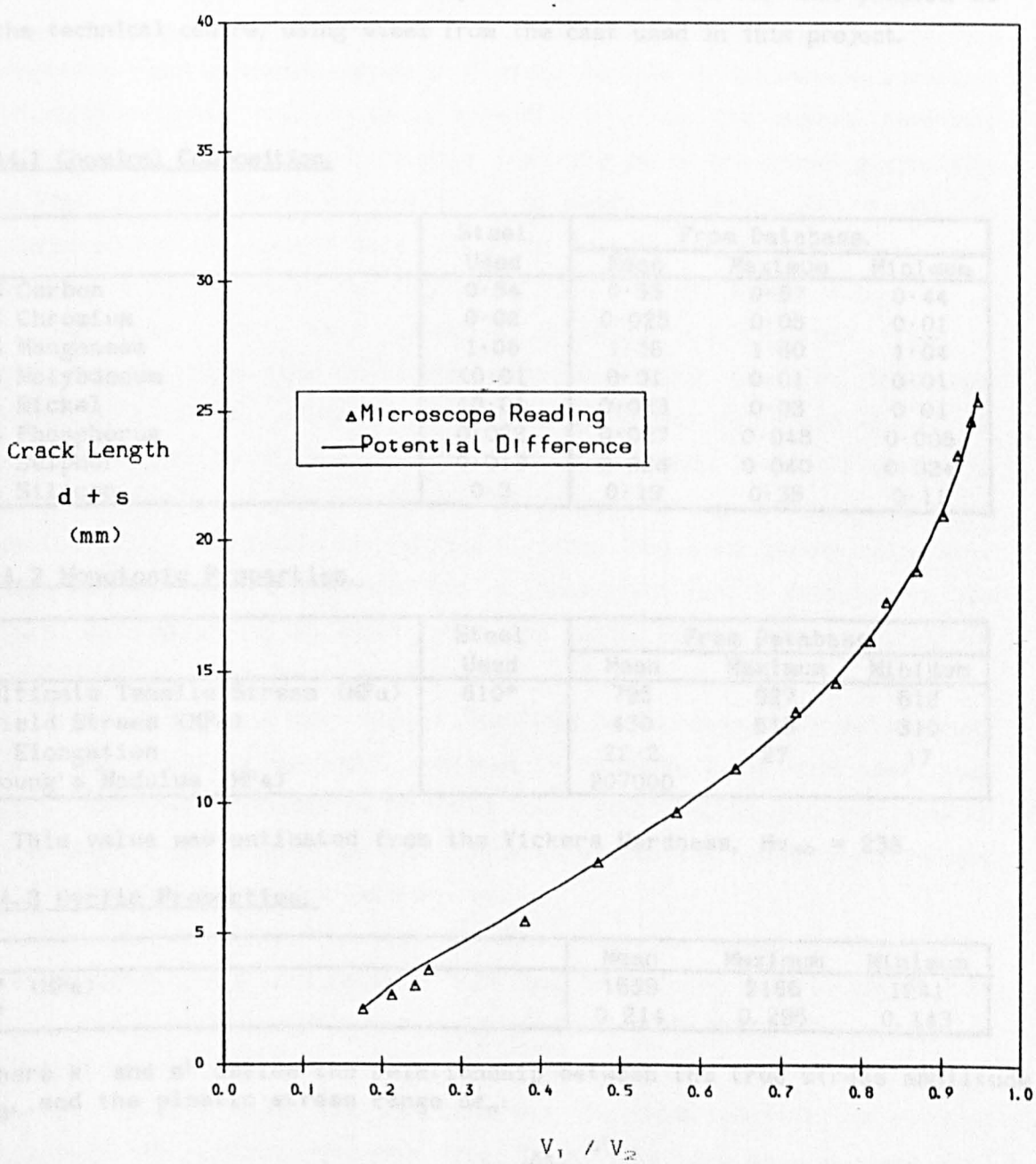

Fig. A3.16 Potential Difference Ratio vs. Crack Length for RSB16.

APPENDIX 4.

COMPOSITION AND PROPERTIES OF RAIL STEEL.

The chemical composition, and static and cyclic stress strain properties quoted here were all either taken from the Database at the British Rail Technical Centre, Derby, or were measured for this project, at the technical centre, using steel from the cast used in this project.

A4.1 Chemical Composition.

	Steel Used	From Database.		
		Mean	Maximum	Minimum
% Carbon	0·54	0·55	0·57	0·44
% Chromium	0·02	0·025	0·08	0·01
% Manganese	1·06	1·16	1·60	1·04
% Molybdenum	<0·01	0·01	0·01	0·01
% Nickel	<0·01	0·023	0·03	0·01
% Phosphorus	0·022	0·027	0·048	0·008
% Sulphur	0·019	0·028	0·040	0·024
% Silicon	0·3	0·19	0·35	0·11

A4.2 Monotonic Properties.

	Steel Used	From Database		
		Mean	Maximum	Minimum
Ultimate Tensile Stress (MPa)	810*	795	927	612
Yield Stress (MPa)		430	515	310
% Elongation		22·2	27	17
Young's Modulus (MPa)		207000		

* This value was estimated from the Vickers Hardness, $Hv_{30} = 238$

A4.3 Cyclic Properties.

	Mean	Maximum	Minimum
k' (MPa)	1659	2166	1241
n'	0.214	0.295	0.143

Where k' and n' define the relationship between the true stress amplitude σ_a, and the plastic stress range $\Delta\varepsilon_p$:

$$\sigma_a = k' \left(\frac{\Delta\varepsilon_p}{2}\right)^{n'}$$

A4.4 Mode I Threshold and Crack Growth Data.

Mode I threshold and crack growth data were collected for comparison with the branch crack growth data produced in the mixed mode tests. The effects of R ratio, and the effect of compressive and tensile stresses parallel to the crack at R=-1 loading were investigated. If there is a compressive load parallel to the crack, as occurs in branch crack growth in shear loading, it is expected to grow more quickly because of the increased plastic strain. Appendix 5 gives details of the strain intensity calculations that predict this. Appendix 6 gives the stress intensity calculations. The crack growth data from the tests are shown graphically in Figs. A4.1 and A4.2, and are given in detail in tables A4.1-8. All the specimens for the mode I data collection, and the mixed mode tests, were manufactured from one of two lengths of rail from the same casting.

The mode I data were collected by using two different types of specimen. The first four tests were done on bending specimens. They were performed by Mr R. Tomlinson, and the crack growth rates and ΔK_I values were calculated by Dr.R.J.Allen, both from British Rail Technical Centre, in Derby. They used an Instron resonance fatigue testing machine, and three point bending, and tested at positive R ratios. The crack growth rates were calculated by using a quadratic fit to three crack length data points. The points were separated by about 0·5 mm to reduce potential errors from the uncertainty in crack length measurement.

Three tests were then done at Sheffield on the Biaxial Mayes machines, using the cruciform specimen described in Appendix 2. In this case crack growth rates were calculated by using the 7 point fitting routine given in ASTM E647. Crack lengths in both tests were measured using the potential drop technique, and optical microscopes.

The scatter in the results was worse than was expected. Two of the bending tests had a load ratio of 0.22, but test 1. had a threshold of 8.34 MPa$\sqrt{m}$, while test 2. had a threshold of about 10·5 MPa$\sqrt{m}$. The thresholds found during the pre-cracking of the mixed mode tests however also varied from 8·0 to 12·1 Mpa$\sqrt{m}$. The threshold was therefore taken as the average, 9·4 MPa$\sqrt{m}$. The growth rate data from these tests also show a great deal of scatter above 1×10^{-8} m/cycle. Both sets of results were therefore plotted when they were compared with branch crack growth data.

The data from the two tests at R=0 and R=-1 under equibiaxial loading appear to be much better, but the test at R=-1, under shear loading started to grow at about the same ΔK value as the equibiaxial test, and then stopped. It would then only start to grow again when the load had been increased. When it did start to grow again, it accelerated back to a growth rate above that of the equibiaxial test, as predicted by the strain intensity calculation. Fig. A4.2 compares the strain intensity calculations for the two tests at R=-1. It shows that for a given strain intensity range the growth rate under shear loading is greater by about 20%, during the stable growth area. For a given stress intensity factor the growth rate under shear loading is greater by about 50%.

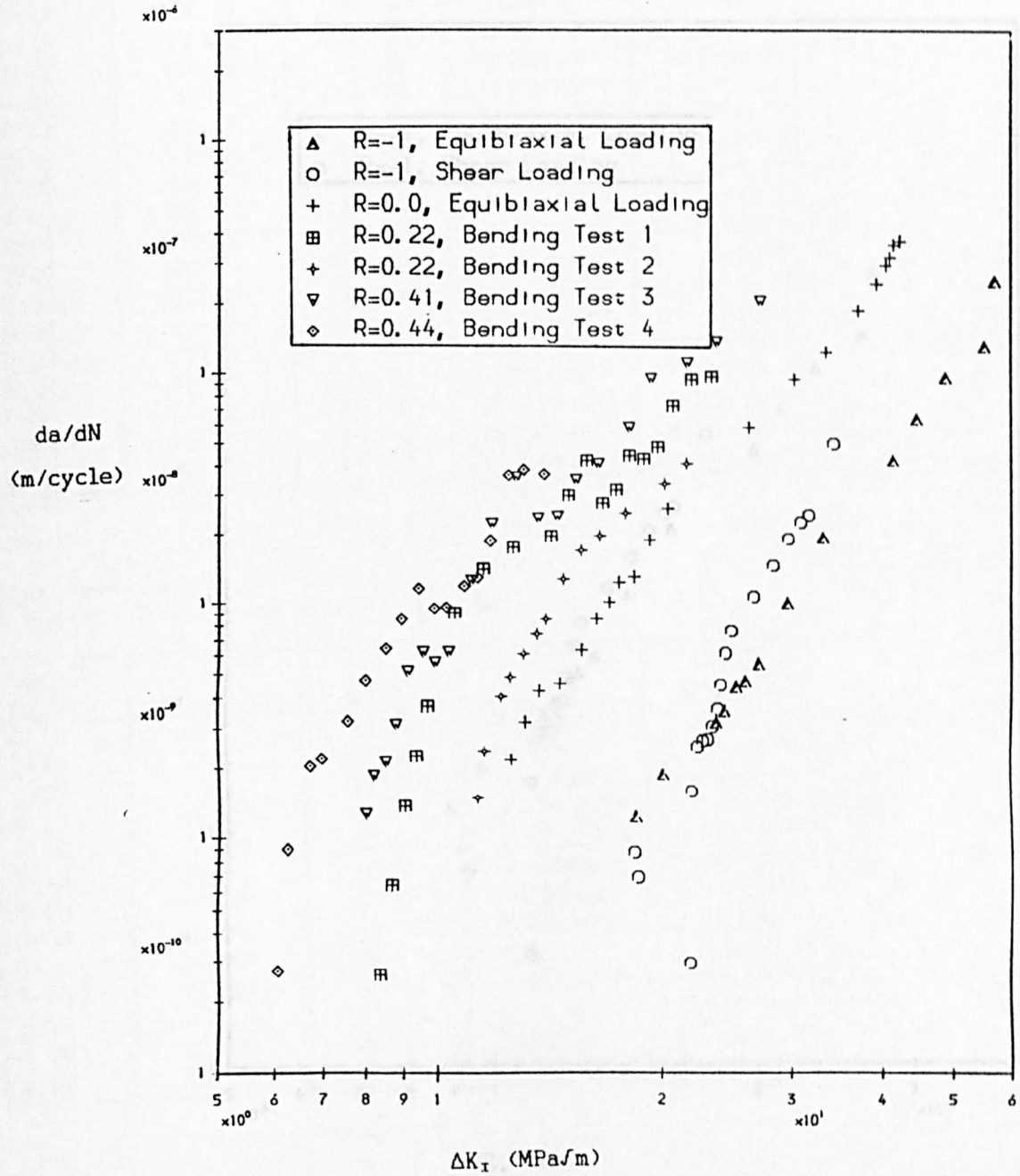

Fig. A4.1 Mode I crack growth data.

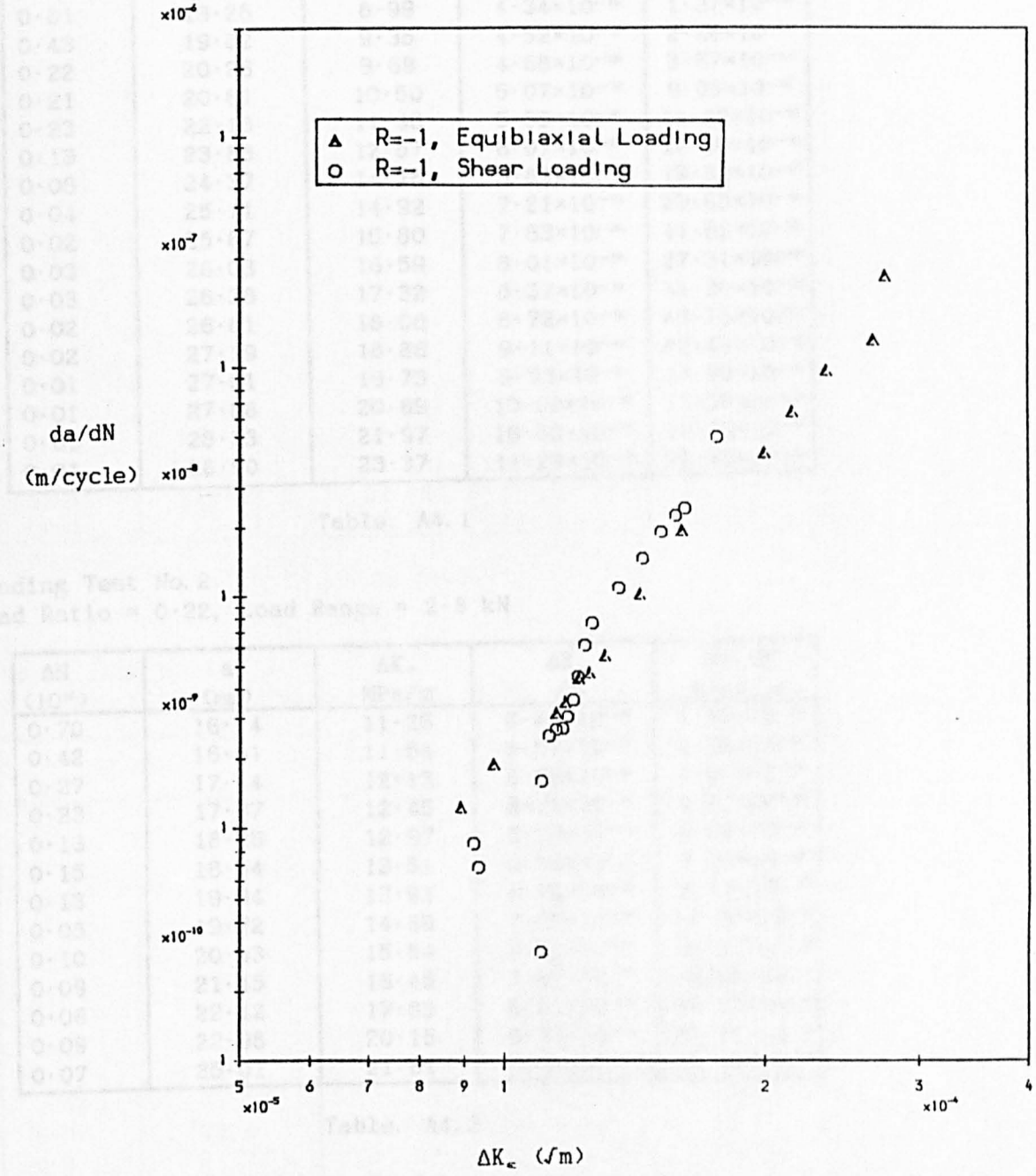

Fig. A4.2 Mode I Growth Data Using Strain Intensities.

Bending Test No. 1.
Load Ratio = 0·22, Load Range = 1·80 kN.

ΔN (10^6)	a (mm)	ΔK_I MPa$\sqrt{m}$	ΔK_{eff} $\sqrt{m}$	da/dN m/cycle
3·36	18·25	8·34	$4·03\times10^{-5}$	$0·26\times10^{-9}$
1·61	18·71	8·66	$4·18\times10^{-5}$	$0·64\times10^{-9}$
0·81	19·28	8·99	$4·34\times10^{-5}$	$1·37\times10^{-9}$
0·43	19·82	9·35	$4·52\times10^{-5}$	$2·26\times10^{-9}$
0·22	20·26	9·69	$4·68\times10^{-5}$	$3·67\times10^{-9}$
0·21	20·61	10·50	$5·07\times10^{-5}$	$9·03\times10^{-9}$
0·23	22·13	11·48	$5·55\times10^{-5}$	$14·22\times10^{-9}$
0·13	23·88	12·57	$6·07\times10^{-5}$	$17·50\times10^{-9}$
0·06	24·37	14·15	$6·84\times10^{-5}$	$19·52\times10^{-9}$
0·04	25·11	14·92	$7·21\times10^{-5}$	$29·55\times10^{-9}$
0·02	25·67	15·80	$7·63\times10^{-5}$	$41·82\times10^{-9}$
0·03	26·03	16·59	$8·01\times10^{-5}$	$27·31\times10^{-9}$
0·03	26·38	17·32	$8·37\times10^{-5}$	$31·20\times10^{-9}$
0·02	26·81	18·06	$8·72\times10^{-5}$	$43·78\times10^{-9}$
0·02	27·19	18·86	$9·11\times10^{-5}$	$42·42\times10^{-9}$
0·01	27·51	19·73	$9·53\times10^{-5}$	$47·59\times10^{-9}$
0·01	27·88	20·69	$10·00\times10^{-5}$	$71·30\times10^{-9}$
0·01	28·33	21·97	$10·60\times10^{-5}$	$92·73\times10^{-9}$
0·01	28·90	23·37	$11·29\times10^{-5}$	$95·45\times10^{-9}$

Table. A4. 1

Bending Test No. 2
Load Ratio = 0·22, Load Range = 2·8 kN

ΔN (10^6)	a (mm)	ΔK_I MPa$\sqrt{m}$	ΔK_{eff} $\sqrt{m}$	da/dN m/cycle
0·70	16·14	11·26	$5·43\times10^{-5}$	$1·48\times10^{-9}$
0·42	16·81	11·54	$5·57\times10^{-5}$	$2·38\times10^{-9}$
0·27	17·14	12·13	$6·05\times10^{-5}$	$4·00\times10^{-9}$
0·23	17·87	12·45	$6·01\times10^{-5}$	$4·82\times10^{-9}$
0·13	18·26	12·97	$6·27\times10^{-5}$	$6·04\times10^{-9}$
0·15	18·64	13·51	$6·53\times10^{-5}$	$7·32\times10^{-9}$
0·13	19·34	13·91	$6·72\times10^{-5}$	$8·47\times10^{-9}$
0·08	19·72	14·69	$7·09\times10^{-5}$	$12·82\times10^{-9}$
0·10	20·43	15·54	$7·51\times10^{-5}$	$16·96\times10^{-9}$
0·09	21·45	16·45	$7·95\times10^{-5}$	$19·65\times10^{-9}$
0·06	22·12	17·83	$8·61\times10^{-5}$	$24·68\times10^{-9}$
0·09	22·98	20·15	$9·73\times10^{-5}$	$33·03\times10^{-9}$
0·07	25·01	21·61	$10·44\times10^{-5}$	$40·46\times10^{-9}$

Table. A4. 2

Bending Test No. 3
load Ratio = 0·41, Load Range = 1·60 kN.

ΔN (10^6)	a (mm)	ΔK_I MPa$\sqrt{m}$	ΔK_{eff} $\sqrt{m}$	da/dN m/cycle
0·68	19·13	7·95	$3·84\times10^{-8}$	$1·26\times10^{-9}$
0·47	19·62	8·17	$3·95\times10^{-8}$	$1·84\times10^{-9}$
0·40	19·99	8·49	$4·10\times10^{-8}$	$2·12\times10^{-9}$
0·30	20·47	8·78	$4·24\times10^{-8}$	$3·09\times10^{-9}$
0·16	20·92	9·09	$4·39\times10^{-8}$	$5·09\times10^{-9}$
0·17	21·31	9·52	$4·60\times10^{-8}$	$6·14\times10^{-9}$
0·20	21·96	9·87	$4·77\times10^{-8}$	$5·55\times10^{-9}$
0·13	22·42	10·31	$4·98\times10^{-8}$	$6·15\times10^{-9}$
0·11	22·76	11·06	$5·34\times10^{-8}$	$12·61\times10^{-9}$
0·10	23·87	11·77	$5·69\times10^{-8}$	$22·11\times10^{-9}$
0·04	24·86	12·68	$6·13\times10^{-8}$	$35·25\times10^{-9}$
0·03	25·28	13·57	$6·56\times10^{-8}$	$23·33\times10^{-9}$
0·04	25·63	14·41	$6·96\times10^{-8}$	$23·78\times10^{-9}$
0·04	26·35	15·28	$7·38\times10^{-8}$	$34·29\times10^{-9}$
0·03	27·07	16·37	$7·91\times10^{-8}$	$40·33\times10^{-9}$
0·02	27·56	18·04	$8·71\times10^{-8}$	$57·50\times10^{-9}$
0·02	28·45	19·33	$9·34\times10^{-8}$	$93·12\times10^{-9}$
0·01	29·05	21·68	$10·50\times10^{-8}$	$109·23\times10^{-9}$
0·01	29·87	23·75	$11·50\times10^{-8}$	$135·45\times10^{-9}$
0·01	30·54	27·24	$13·20\times10^{-8}$	$202·50\times10^{-9}$

Table A4.3

Bending Test No. 4
Load Ratio = 0·44, Load Range = 1·40 kN.

ΔN (10^6)	a (mm)	ΔK_I MPa$\sqrt{m}$	ΔK_{eff} $\sqrt{m}$	da/dN m/cycle
3·16	17·28	6·04	$2·92\times10^{-8}$	$0·27\times10^{-9}$
0·94	17·74	6·22	$3·00\times10^{-8}$	$0·90\times10^{-9}$
0·93	18·13	6·69	$3·23\times10^{-8}$	$2·04\times10^{-9}$
0·96	19·64	6·94	$3·35\times10^{-8}$	$2·20\times10^{-9}$
0·39	20·24	7·56	$3·65\times10^{-8}$	$3·22\times10^{-9}$
0·29	20·89	7·97	$3·85\times10^{-8}$	$4·69\times10^{-9}$
0·24	21·60	8·48	$4·10\times10^{-8}$	$6·40\times10^{-9}$
0·15	22·44	8·90	$4·30\times10^{-8}$	$8·48\times10^{-9}$
0·07	22·83	9·39	$4·54\times10^{-8}$	$11·67\times10^{-9}$
0·11	23·21	9·85	$4·76\times10^{-8}$	$9·45\times10^{-9}$
0·11	23·87	10·24	$4·95\times10^{-8}$	$9·56\times10^{-9}$
0·08	24·30	10·81	$5·22\times10^{-8}$	$12·00\times10^{-9}$
0·07	24·77	11·27	$5·44\times10^{-8}$	$13·09\times10^{-9}$
0·04	25·19	11·72	$5·66\times10^{-8}$	$18·68\times10^{-9}$
0·03	25·48	12·38	$5·98\times10^{-8}$	$36·08\times10^{-9}$
0·03	26·11	12·97	$6·27\times10^{-8}$	$38·10\times10^{-9}$
0·03	26·68	13·83	$6·68\times10^{-8}$	$36·33\times10^{-9}$

Table A4.4

Biaxial Test RSB13.
Load Ratio = 0·0
Equibiaxial loading, Load Range = 58·3 kN.

N (10^6)	a (mm)	ΔK_I MPa$\sqrt{m}$	ΔK_e $\sqrt{m}$	da/dN m/cycle
1·105	3·07	12·50	$6·03\times10^{-5}$	$2·17\times10^{-9}$
1·249	3·37	13·09	$6·32\times10^{-5}$	$3·15\times10^{-9}$
1·393	3·66	13·64	$6·59\times10^{-5}$	$4·20\times10^{-9}$
1·417	4·16	14·54	$7·02\times10^{-5}$	$4·52\times10^{-9}$
1·561	4·75	15·55	$7·51\times10^{-5}$	$6·26\times10^{-9}$
1·651	5·21	16·29	$7·87\times10^{-5}$	$8·54\times10^{-9}$
1·689	5·65	16·96	$8·19\times10^{-5}$	$10·16\times10^{-9}$
1·732	6·01	17·50	$8·45\times10^{-5}$	$12·38\times10^{-9}$
1·768	6·61	18·34	$8·86\times10^{-5}$	$12·93\times10^{-9}$
1·838	7·26	19·23	$9·29\times10^{-5}$	$18·76\times10^{-9}$
1·901	8·12	20·34	$9·83\times10^{-5}$	$25·84\times10^{-9}$
2·107	13·46	26·27	$12·69\times10^{-5}$	$57·57\times10^{-9}$
2·1856	17·86	30·36	$14·67\times10^{-5}$	$93·23\times10^{-9}$
2·2241	21·67	33·57	$16·22\times10^{-5}$	$122·5\times10^{-9}$
2·2531	26·27	37·17	$17·96\times10^{-5}$	$185·8\times10^{-9}$
2·2660	29·20	39·33	$19·00\times10^{-5}$	$240·6\times10^{-9}$
2·2722	30·87	40·54	$19·58\times10^{-5}$	$290·1\times10^{-9}$
2·2745	31·57	41·04	$19·83\times10^{-5}$	$313·1\times10^{-9}$
2·2768	32·32	41·57	$20·08\times10^{-5}$	$354·5\times10^{-9}$
2·2799	33·49	42·40	$20·48\times10^{-5}$	$367·0\times10^{-9}$

Table. A4.5

Biaxial Test RSB14.
Load ratio = -1·0
Equibiaxial Loading, Load Range = 88 kN.

N (10^6)	a (mm)	ΔK_I MPa$\sqrt{m}$	ΔK_e $\sqrt{m}$	da/dN m/cycle
1·611	3·25	18·38	$8·88\times10^{-5}$	$1·24\times10^{-9}$
2·027	3·87	20·07	$9·70\times10^{-5}$	$1·89\times10^{-9}$
2·682	5·43	23·76	$11·48\times10^{-5}$	$3·12\times10^{-9}$
2·761	5·71	24·37	$11·77\times10^{-5}$	$3·48\times10^{-9}$
2·878	6·13	25·25	$12·20\times10^{-5}$	$4·39\times10^{-9}$
2·966	6·47	25·95	$12·54\times10^{-5}$	$4·64\times10^{-9}$
3·087	7·04	27·08	$13·08\times10^{-5}$	$5·49\times10^{-9}$
3·302	8·45	29·67	$14·33\times10^{-5}$	$10·20\times10^{-9}$
3·531	10·56	33·21	$16·04\times10^{-5}$	$19·50\times10^{-9}$
3·793	16·30	41·41	$20·00\times10^{-5}$	$42·30\times10^{-9}$
3·848	18·84	44·61	$21·55\times10^{-5}$	$63·60\times10^{-9}$
3·894	22·44	48·86	$23·60\times10^{-5}$	$96·40\times10^{-9}$
3·9459	28·25	55·21	$26·67\times10^{-5}$	$132·0\times10^{-9}$
3·9511	30·10	57·00	$27·54\times10^{-5}$	$250·0\times10^{-9}$

Table. A4.6

Biaxial Test RSB19.
Load Ratio = -1·0, Load Range = 94·8 kN.
Shear Loading.

N (10^6)	a (mm)	ΔK_I MPa$\sqrt{m}$	ΔK_e $\sqrt{m}$	da/dN m/cycle
0·392	2·46	18·31	$9·20\times10^{-5}$	$0·86\times10^{-9}$
0·490	2·52	18·53	$9·31\times10^{-5}$	$0·68\times10^{-9}$
3·984	3·52	21·92	$11·01\times10^{-5}$	$0·30\times10^{-9}$
4·005	3·55	21·94	$11·02\times10^{-5}$	$1·59\times10^{-9}$
4·037	3·62	22·41	$11·26\times10^{-5}$	$2·49\times10^{-9}$
4·111	3·83	22·80	$11·46\times10^{-5}$	$2·64\times10^{-9}$
4·151	3·95	23·15	$11·66\times10^{-5}$	$2·67\times10^{-9}$
4·202	4·06	23·49	$11·81\times10^{-5}$	$3·00\times10^{-9}$
4·234	4·18	23·83	$11·97\times10^{-5}$	$3·54\times10^{-9}$
4·263	4·25	24·02	$12·07\times10^{-5}$	$4·46\times10^{-9}$
4·292	4·38	24·40	$12·26\times10^{-5}$	$6·05\times10^{-9}$
4·316	4·55	24·87	$12·64\times10^{-5}$	$7·58\times10^{-9}$
4·349	4·78	26·70	$13·42\times10^{-5}$	$10·80\times10^{-9}$
4·373	5·12	28·38	$14·25\times10^{-5}$	$14·62\times10^{-9}$
4·389	5·32	29·74	$14·94\times10^{-5}$	$19·16\times10^{-9}$
4·392	5·42	30·96	$15·55\times10^{-5}$	$22·62\times10^{-9}$
4·406	5·70	31·74	$15·94\times10^{-5}$	$24·26\times10^{-9}$
4·426	6·24	34·34	$17·25\times10^{-5}$	$49·30\times10^{-9}$

Table. A4.7

APPENDIX 5.

STRAIN INTENSITY CALCULATION.

The Paris law for fatigue crack growth is [1]:

$$\frac{da}{dN} = C(\Delta K_I)^m \qquad \text{A5.1}$$

Where

$$\Delta K_I = \Delta\sigma\sqrt{(\pi a)} \qquad \text{A5.2}$$

and C and m are material constants.

However this law does not work when the plastic zone becomes greater than about 1/20 of the crack length. One simple, and widely accepted modification to this law, uses a strain intensity factor instead of the stress intensity factor [2]. This is defined by:

$$\Delta K_\varepsilon = \frac{\Delta K_I}{E_{sec}} \qquad \text{A5.3}$$

where E_{sec} is the secant modulus as defined in Fig. A5.1.

When the loading is purely elastic, E_{sec} is equal to E, Young's modulus, and so the strain intensity is directly proportional to the stress intensity. When the loading becomes elastic-plastic, E_{sec} is found using Von Mises yield criterion:

$$E_{sec} = \frac{\sigma_{eq}}{\varepsilon_{eq}} \qquad \text{A5.4}$$

where:

$$2\sigma_{eq}^2 = (\sigma_1 - \sigma_2)^2 + (\sigma_2 - \sigma_3)^2 + (\sigma_3 - \sigma_1)^2 \qquad \text{A5.5}$$

and:

$$\varepsilon_{eq} = \varepsilon_{el} + \varepsilon_{pl} = \frac{\sigma_{eq}}{E} + \left(\frac{\sigma_{eq}}{k'}\right)^{1/n'} \qquad \text{A5.6}$$

For BS11 rail steel:

k' = 1659 MPa (Mean value)

n' = 0.214 (Mean value)

E = 207000 MPa

The net section stress amplitude was used in the calculation of σ_{eq}, to make some allowance for the finite width of the specimens, though it was recognised that this was only an approximate correction.

An equivalent strain intensity for mode II is defined by:

$$\Delta K_{\gamma} = \frac{\Delta K_{II}}{G_{sec}} \qquad \text{A5.7}$$

where:

$$G_{sec} = \frac{E_{sec}}{2(1 + \nu)}$$

Strictly ν is not a constant, but increases from 0·3 to 0·5 as the stress changes from being elastic to fully plastic. For these tests the value of ν was taken as:

$$\nu = 0{\cdot}3 + \left(0{\cdot}2 * \frac{\varepsilon_{0{\cdot}1}}{\varepsilon_{eq}}\right)$$

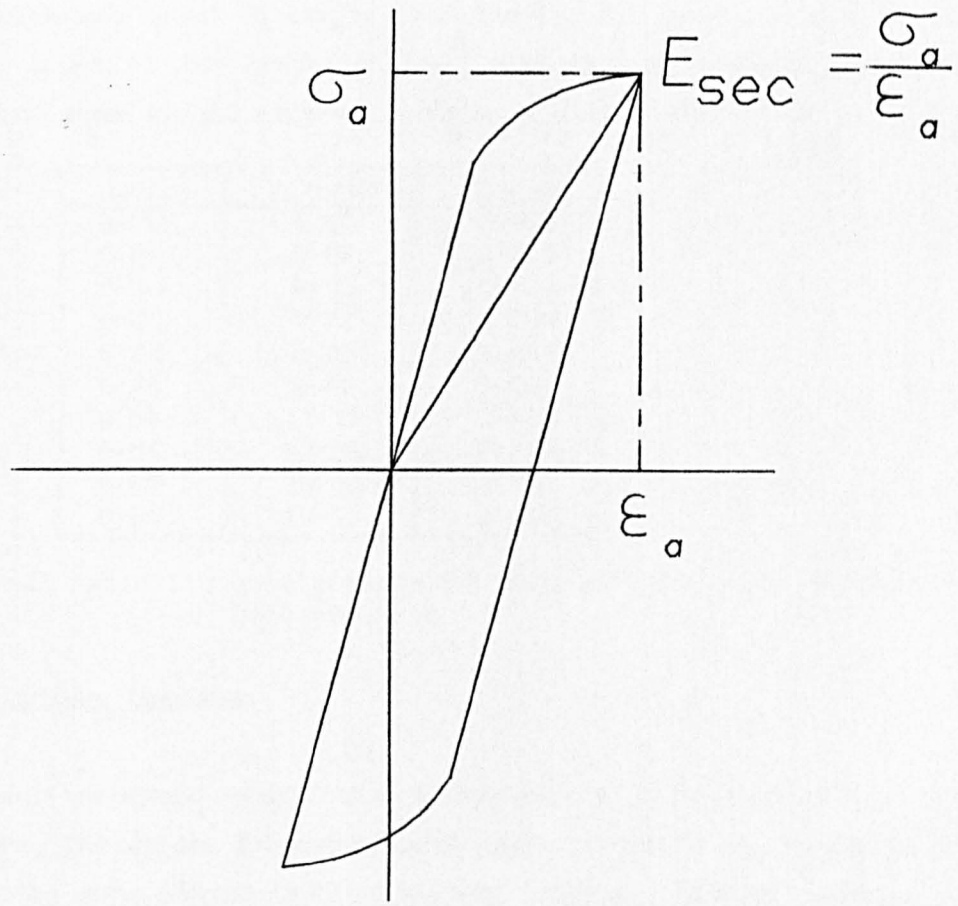

Fig. A5.1 Definition of E_{sec}, from cyclic σ-ε curve.

References:

1. P.C.Paris, F.Erdogan. 'A critical Analysis of Crack Propagation Laws.'
J. of Basic Engineering. Ser. D, Vol. 86, pp528. 1963.

2. R.P.Skelton. 'Growth of Short Cracks During High Strain Fatigue and Thermal Cycling.'
'Low-Cycle Fatigue and Life Prediction.' ASTM STP 770. Eds. C.Amzallag, B.N.Leis, and P.Rabbe. pp337-381. 1982.

APPENDIX 6.

STRESS INTENSITY CALCULATIONS.

A6.1 4 point bending.

For a straight crack in a bending specimen of width W and thickness B, subject to a shearing force Q and a bending moment M, in the plane of the crack, K_I and K_{II} are given by [1]:

$$K_I = \frac{M}{BW^{3/2}} f_b\left(\frac{a}{W}\right)$$
$$K_{II} = \frac{Q}{BW^{1/2}} f_s\left(\frac{a}{W}\right) \qquad \text{A6. 1}$$

where f_s and f_b are given in Table A6·1. It should be noted that as the above formulae are based on simple beam theory, the loading points should not be too close to the crack. In the tests in this project, the inner loading points were always at least a distance W from the crack.

a/W	$f_b(a/W)$	$f_s(a/W)$
0·20	4·97	0·496
0·25	5·67	0·667
0·30	6·45	0·857
0·35	7·32	1·080
0·40	8·35	1·317
0·45	9·60	1·557
0·50	11·12	1·838
0·55	13·09	2·125
0·60	15·06	2·441
0·65	19·17	2·794

Stress intensity coefficients for asymmetric 4 point bending.
Table A6. 1

A6.2 The Cruciform Specimen.

The cruciform specimen described in Appendix 2 is essentially a centre cracked plate. The stress intensity for a crack of length 2a, perpendicular to one of the axes, in an infinitely long uniform plate of width W is given by:

$$K_I = \sigma\sqrt{(\pi a.\sec(\pi a/W))} \qquad \text{A6.2}$$

Two corrections to this formula need to be considered. Firstly solutions have been provided by Isida [2] for the stiffened edges of the specimen, and the stiffness of the fingers. Changing W to 456/4 mm, the equivalent cross sectional area divided by the thickness at the centre, corrects for this where 2a/W ≤ 0·7. This equivalent cross section was calculated during the specimen design to produce the uniform stress field in the working section. The second possible source of error is the finite length of the specimen. Isida again has provided solutions to this problem [3]. Assuming the boundary conditions at the edges of the specimen are those of uniform displacement without transverse shear loading, the required correction is 1.5 % or less for 2a/W ≤ 0.8, and so this was ignored. These boundary conditions were assumed because the fingers in the grips are axially stiff compared to the specimen, and transversely flexible.

The same width correction factors were used for cracks growing at an angle of 45° to the axes, except that W was multiplied by √2 to account for the crack angle. The same procedure was adopted by Gao Hua et al [4].

For a 45° crack in a pure shear stress field, K_{II} is defined by:

$$K_{II} = \tau\sqrt{(\pi a.\sec(\pi a/(\sqrt{2}W)))} \qquad A6.3$$

For a 45° crack in equibiaxial tension, K_I is defined by:

$$K_I = \sigma\sqrt{(\pi a.\sec(\pi a/(\sqrt{2}W)))} \qquad A6.4$$

A6.3 Branch Cracks Under Pure Shear Loading.

In some of the cruciform specimens, the cracks branched under pure shear loading, as shown in Fig. A6.1. They then grew under a mode I mechanism. It was necessary to find a K_I calibration for this loading situation. Unfortunately none of the three standard books of stress intensity calibrations cover this configuration [5-7]. However the addition of the solutions of Vitek, and Kitagawa and Yuuki, [7,8], made a reasonable approximation to the real situation, Fig. A6.2. The difference between the theoretical and the experimental cracks was that the branch cracks in the specimens did not grow out at 45° to the main crack, but started at about

70°, and then curved round slowly tending towards 45°. The result of this is that the addition of the two solutions predicts a mixed mode loading, not a pure mode I load. The mixed mode stress intensities, K_I and K_{II}, were then converted to an equivalent mode I stress intensity, K_σ, by using the maximum tangential stress (MTS) criterion [9]. K_I, K_{II}, K_σ, and the angle the MTS maximum occurs at, θ, are all given in Table A6.2.

The results are plotted in Fig. A6.3, and are compared with the value of K_I found by the MTS criterion or Melin's calculations for a very small crack, [9,10]; and with the simple approach of treating the crack as an equivalent horizontal crack of length 2c, as shown in Fig. A6.1.

In the light of these results, the MTS criterion was used in calculating the initial branching K_I; the combination of Vitek, and Kitagawa and Yuuki's work was used for finite branch lengths up to b/a = 1.0, and the projection method was used for b/a > 1.0.

The dip in the value of K_I as the branch grew was initially thought to be surprising. However Chatterjee's work on cracks in shear fields with a branch at just one end, showed a similar but much larger dip [7,11].

b/a	K_I $\sigma\sqrt{(\pi a)}$	K_{II} $\sigma\sqrt{(\pi a)}$	K_σ $\sigma\sqrt{(\pi a)}$	$\theta°$
0·01	0·99	-0·30	1·11	74°
0·1	0·99	-0·26	1·08	71°
0·2	1·03	-0·23	1·10	68°
0·5	1·16	-0·15	1·19	55°
1·0	1·34	-0·09	1·35	53°

Stress Intensity Factors For Branch Cracks Under Pure Shear Loading.
Table A6.2

A6.4 Branch Cracks Under Uniaxial Tension.

In tests RSB15, RSB16 and RSB17 the branch cracks occurred under approximately pure tension. This type of loading was the same as that used by Vitek, as shown in Fig. A6.2a [8]. It was found that simply using an equivalent crack length c, the length perpendicular to the applied stress, in equation A6.4, gave the same answer as Vitek's calculation. This method was therefore used in these stress intensity calculations.

Figures

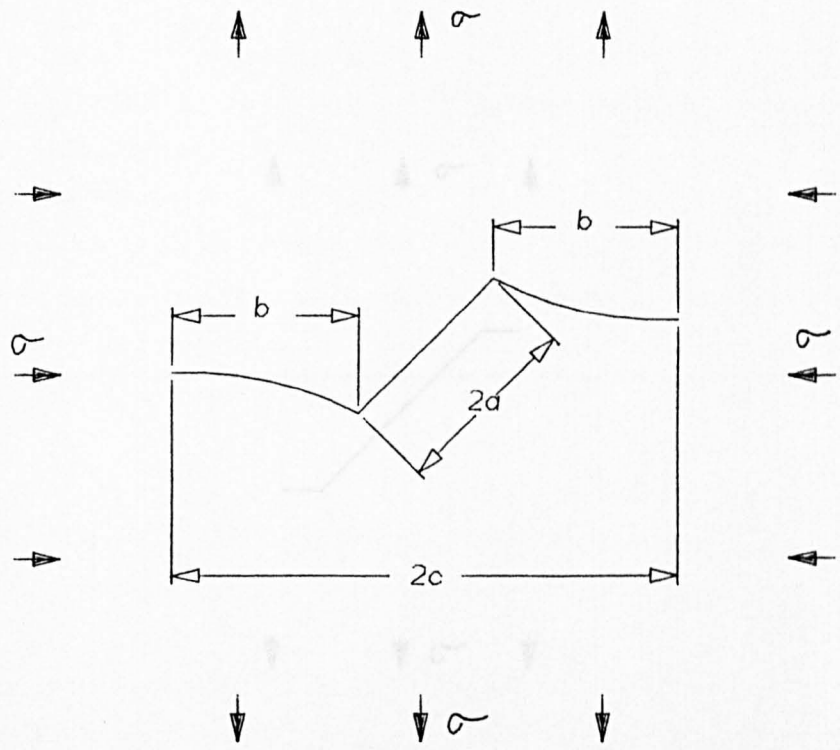

Fig. A6.1 Branch Cracks.

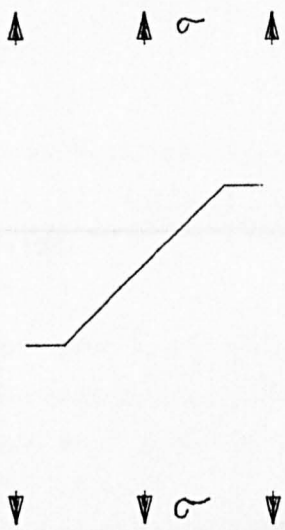

a. Vitek's Model.

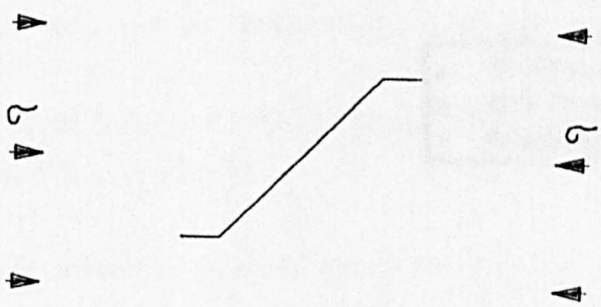

b. Kitagawa and Yuuki's Model.

Fig. A6.2.

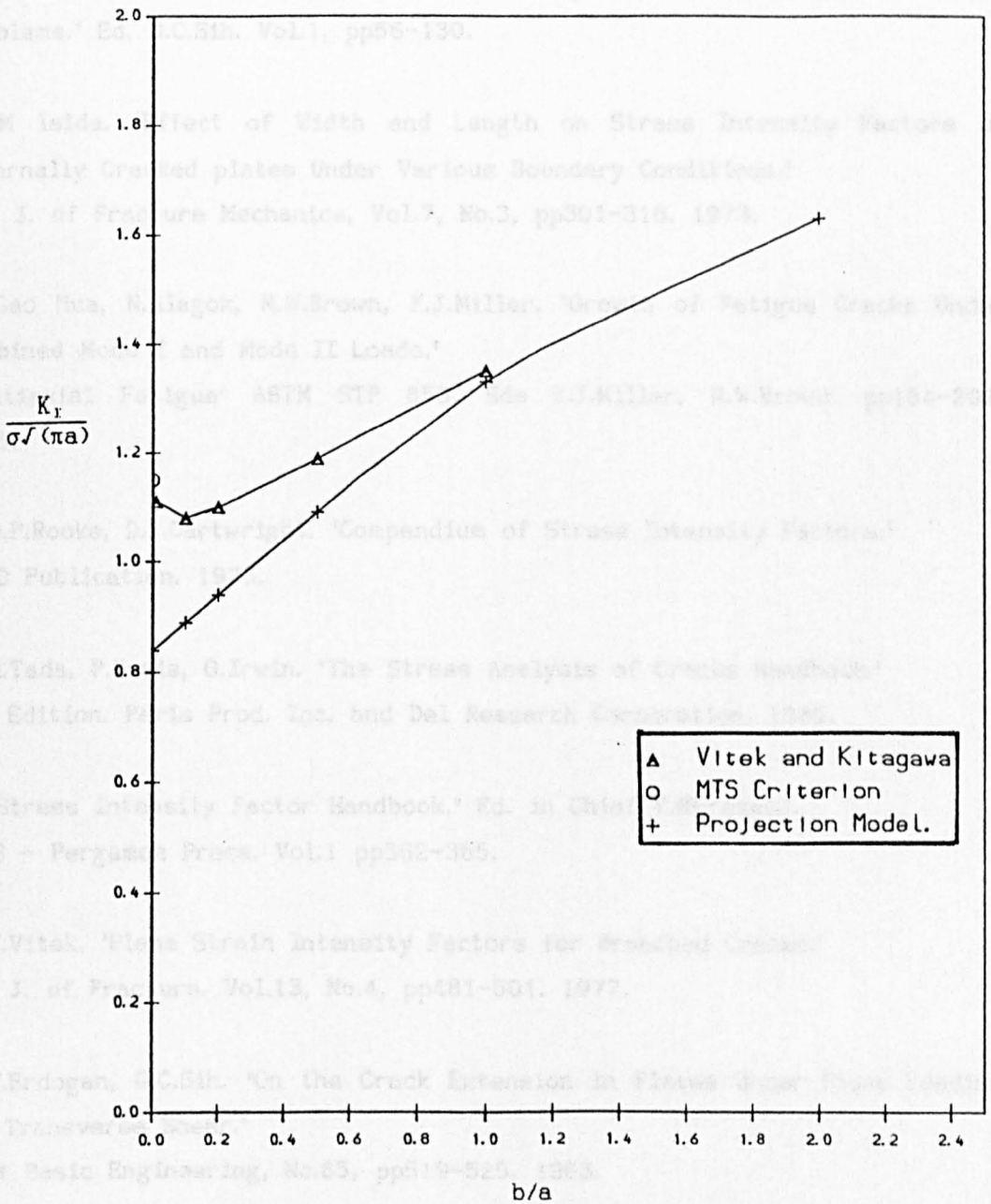

Fig. A6.3 K_I vs. b/a

References.

1. K.J.Wang, C.L.Hsu, Kao Hua. 'Calculation of Stress Intensity Factors for Combined Mode Bend Specimens.'
Proc. ICF 4, Vol.4, pp123-133. 1977.

2. M.Isida. 'Method of Laurent Series Expansion for Internal Crack Problems.' 'Mechanics of Fracture. Methods of Analysis and Solutions of Crack Problems.' Ed. G.C.Sih. Vol.1, pp56-130.

3. M Isida. 'Effect of Width and Length on Stress Intensity Factors of Internally Cracked plates Under Various Boundary Conditions.'
Int. J. of Fracture Mechanics, Vol.7, No.3, pp301-316. 1973.

4. Gao Hua, N.Alagok, M.W.Brown, K.J.Miller. 'Growth of Fatigue Cracks Under Combined Mode I and Mode II Loads.'
'Multiaxial Fatigue' ASTM STP 853. Eds K.J.Miller, M.W.Brown. pp184-202. 1985.

5. D.P.Rooke, D.J.Cartwright. 'Compendium of Stress Intensity Factors.'
HMSO Publication. 1976.

6. H.Tada, P.Paris, G.Irwin. 'The Stress Analysis of Cracks Handbook.'
2nd Edition. Paris Prod. Inc. and Del Research Corporation. 1985.

7. 'Stress Intensity Factor Handbook.' Ed. in Chief Y.Murakami.
JSMS - Pergamon Press. Vol.1 pp362-365.

8. V.Vitek. 'Plane Strain Intensity Factors for Branched Cracks.'
Int. J. of Fracture. Vol.13, No.4, pp481-501. 1977.

9. F.Erdogan, G.C.Sih. 'On the Crack Extension in Plates Under Plane Loading and Transverse Shear.'
J. of Basic Engineering, No.85, pp519-525. 1963.

10. S.Melin. 'Fracture from a Straight Crack Subject to Mixed Mode Loading.'
International Journal of Fracture, No.32, pp257-263. 1987.

11. S.N.Chatterjee. 'The Stress Field in the Neighbourhood of a Branch Crack in an Infinite Elastic Sheet.'
International Journal of Solids and Structures, Vol. 11, p521.

APPENDIX 7.

CRACK GROWTH DATA FROM THE NON_PROPORTIONAL LOADING TESTS.

RSB1.

Equibiaxial mean stress = 50 MPa.

Mode II threshold = 4·0 MPa$\sqrt{m}$

Mode I threshold = 7·3 MPa$\sqrt{m}$

N 10^6	a mm	$\Delta\sigma$ MPa	ΔK_I MPa$\sqrt{m}$	ΔK_e $\sqrt{m}$	da/dN m/cycle
13·779	3·17	53·5	7·3	$3·5\times10^{-8}$	$0·039\times10^{-9}$
14·675	3·19	58·9	7·8	$3·8\times10^{-8}$	$<0·01\times10^{-9}$
15·639	3·19	64·7	8·7	$4·2\times10^{-8}$	$0·031\times10^{-9}$
16·595	3·19	64·7	8·7	$4·2\times10^{-8}$	$<0·01\times10^{-9}$
17·635	3·19	71·2	9·5	$4·6\times10^{-8}$	$<0·01\times10^{-9}$
18·450	3·19	78·3	10·4	$5·0\times10^{-8}$	$0·021\times10^{-9}$
21·931	3·26	78·3	10·4	$5·0\times10^{-8}$	$0·025\times10^{-9}$
23·956	3·31	78·3	10·3	$5·0\times10^{-8}$	$0·014\times10^{-9}$
26·139	3·31	86·2	11·2	$5·4\times10^{-8}$	$<0·01\times10^{-9}$
28·174	3·35	94·8	11·4	$5·5\times10^{-8}$	$0·59\times10^{-9}$
28·444	3.56	94·8	11·4	$5·5\times10^{-8}$	$0·57\times10^{-9}$
28·624	3·63	94·8	11·5	$5·6\times10^{-8}$	$0·78\times10^{-9}$
29·074	4·23	94·8	11·9	$5·7\times10^{-8}$	$1·00\times10^{-9}$
29·524	4·50	94·8	12·1	$5·8\times10^{-8}$	$1·20\times10^{-9}$
29·969	5·21	94·8	12·7	$6·1\times10^{-8}$	$1·73\times10^{-9}$
30. 154	5. 35	94·8	12·8	$6·2\times10^{-8}$	$2·04\times10^{-9}$
30·335	5·77	94·8	13·1	$6·3\times10^{-8}$	$2·38\times10^{-9}$
30·515	6·46	94·8	13·5	$6·5\times10^{-8}$	$2·69\times10^{-9}$
30·695	6·75	94·8	13·8	$6·7\times10^{-8}$	$3·26\times10^{-9}$
30·875	7·41	94·8	14·3	$6·9\times10^{-8}$	$3·80\times10^{-9}$
31·055	8·04	94·8	14·7	$7·1\times10^{-8}$	$4·56\times10^{-9}$
31·235	8·99	94·8	15·5	$7·5\times10^{-8}$	$5·77\times10^{-9}$
31·415	10·03	94·8	16·4	$7·9\times10^{-8}$	$6·73\times10^{-9}$
31·595	11·42	94·8	17·5	$8·5\times10^{-8}$	$8·55\times10^{-9}$

RSB2
Equibiaxial mean stress = 267 MPa
Mode II threshold = 4·4 MPa√m
Mode I threshold = 5·6 MPa√m

N 10^6	a mm	$\Delta\sigma$ MPa	ΔK_I MPa√m	ΔK_{th} √m	da/dN m/cycle
4·123	2·85	43·0	5·6	$2·7\times10^{-8}$	$0·08\times10^{-9}$
6·826	2·95	47·3	5·9	$2·9\times10^{-8}$	$0·07\times10^{-9}$
8·363	3·07	47·3	5·9	$2·9\times10^{-8}$	$0·02\times10^{-9}$
10·561	3·12	52·0	6·4	$3·1\times10^{-8}$	$0·06\times10^{-9}$
11·473	3·15	52.0	6·4	$3·1\times10^{-8}$	$0·12\times10^{-9}$
12·961	3·29	52.0	6·4	$3·1\times10^{-8}$	$0·31\times10^{-9}$
13·394	3·43	52.0	6·4	$3·1\times10^{-8}$	$0·50\times10^{-9}$
16·757	4·25	52.0	6·6	$3·2\times10^{-8}$	$0·75\times10^{-9}$
17·813	4·79	52.0	7·0	$3·4\times10^{-8}$	$1·14\times10^{-9}$
18·176	5·14	52.0	7·1	$3·4\times10^{-8}$	$1·32\times10^{-9}$
19.340	7·19	52.0	7·9	$3·8\times10^{-8}$	$2·44\times10^{-9}$
19·457	7·41	52.0	8·0	$3·9\times10^{-8}$	$2·57\times10^{-9}$
19·718	8·08	52·0	8·3	$4·0\times10^{-8}$	$2·90\times10^{-9}$
20·892	12·31	52·0	10·3	$5·0\times10^{-8}$	$4·86\times10^{-9}$
21·025	12·98	52·0	10·6	$5·1\times10^{-8}$	$6·27\times10^{-9}$
21·128	13·59	52·0	10·8	$5·2\times10^{-8}$	$6·98\times10^{-9}$
21·209	14·03	52·0	11·0	$5·3\times10^{-8}$	$8·44\times10^{-9}$
22·045	21·32	52·0	13·6	$6·6\times10^{-8}$	$10·1\times10^{-9}$
22·162	23·66	52·0	14·4	$6·9\times10^{-8}$	$26·1\times10^{-9}$

RSB3
Equibiaxial Mean Stress = 267 MPa
Mode I Branch Crack Growth, $\Delta\sigma$ = 267 MPa

ΔN	a mm	ΔK_I MPa√m	ΔK_{th} √m	da/dN m/cycle
5200	10·08	55·0	$31·4\times10^{-8}$	$0·845\times10^{-6}$
1300	13·14	59·4	$35·4\times10^{-8}$	$1·33\times10^{-6}$
900	14·91	61·2	$37·6\times10^{-8}$	$2·01\times10^{-6}$
900	17·07	65·9	$42·4\times10^{-8}$	$2·79\times10^{-6}$
900	20·38	73·4	$51·6\times10^{-8}$	$4·58\times10^{-6}$

RSB4
Equibiaxial Mean Stress = 133 MPa
Mode I Branch Crack Growth, $\Delta\sigma$ = 452 MPa

ΔN	a mm	ΔK_I MPa√m	ΔK_{th} √m	da/dN m/cycle
300	4·33	64·0	$56·5\times10^{-8}$	$3·33\times10^{-6}$
45	5·20	66·4	$60·3\times10^{-8}$	$16·4\times10^{-6}$
49	6·07	68·2	$63·8\times10^{-8}$	$20·2\times10^{-6}$
37	6·91	71·7	$69·2\times10^{-8}$	$18·9\times10^{-6}$
67	9·13	79·2	$83·3\times10^{-8}$	$55·8\times10^{-6}$
19	14·12	100·0	$133·5\times10^{-8}$	$328·0\times10^{-6}$

RSB5
Equibiaxial Mean Stress = 0 MPa
Mode I Branch Crack Growth, $\Delta\sigma$ = 452 MPa

ΔN	a mm	ΔK_I MPa$\sqrt{m}$	ΔK_e $\sqrt{m}$	da/dN m/cycle
45	1·78	42·6	$35·6\times10^{-5}$	$4·4\times10^{-6}$
199	1·94	43·0	$36·0\times10^{-5}$	$1·5\times10^{-6}$
181	2·20	44·0	$36·8\times10^{-5}$	$1·2\times10^{-6}$
109	2·45	45·8	$38·3\times10^{-5}$	$2·7\times10^{-6}$
58	2·67	46·4	$38·8\times10^{-5}$	$2·6\times10^{-6}$

RSB6
Equibiaxial Mean Stress = -133 MPa
Mode I Branch Crack Growth, $\Delta\sigma$ = 452 MPa

N	a mm	ΔK_I MPa$\sqrt{m}$	ΔK_e $\sqrt{m}$	da/dN m/cycle
319	1·95	50·2	$39·3\times10^{-5}$	$0·21\times10^{-6}$
1168	2·09	49·5	$38·7\times10^{-5}$	$0·16\times10^{-6}$
1505	2·10	49·5	$38·7\times10^{-5}$	$0·03\times10^{-6}$
1964	2·26	49·9	$39·0\times10^{-5}$	$0·39\times10^{-6}$
2889	2·38	50·4	$39·4\times10^{-5}$	$0·13\times10^{-6}$
3400	2·48	50·8	$39·7\times10^{-5}$	$0·20\times10^{-6}$
4000	2·57	51·2	$40·0\times10^{-5}$	$0·15\times10^{-6}$

RSB7.
Equibiaxial Mean Stress = 0 MPa.
No fatigue crack growth from the crack tips, mode I growth from the notch tip, and from the edge of the specimen.

RSB8.
Sequential Mode I and Mode II loading.
Type 1.
$\Delta\sigma$ = 104 MPa, $\Delta\tau$ = 208 MPa.
Produced co-planar growth.

N 10^3	a mm	ΔK_{II} MPa$\sqrt{m}$	ΔK_{eq} $\sqrt{m}$	da/dN m/cycle
7·2	3·05	20·3	$26·5\times10^{-5}$	$7·51\times10^{-9}$
24·4	3·19	20·8	$27·0\times10^{-5}$	$9·40\times10^{-9}$
71·2	3·73	22·5	$29·4\times10^{-5}$	$12·8\times10^{-9}$
87·2	3·91	23·1	$29·9\times10^{-5}$	$14·5\times10^{-9}$
108·6	4·25	24·0	$31·2\times10^{-5}$	$17·5\times10^{-9}$
116·7	4·41	24·5	$31·7\times10^{-5}$	$13·9\times10^{-9}$
120·6	4·46	24·6	$32·0\times10^{-5}$	$15·0\times10^{-9}$
128·1	4·53	24·8	$32·2\times10^{-5}$	$13·5\times10^{-9}$
137·9	4·71	25·3	$32·8\times10^{-5}$	$16·2\times10^{-9}$
150·9	4·93	25·9	$33·5\times10^{-5}$	$18·0\times10^{-9}$
155·8	5·02	26·1	$34·1\times10^{-5}$	$17·9\times10^{-9}$
186·6	5·60	27·6	$35·9\times10^{-5}$	$20·1\times10^{-9}$
223·9	6·39	29·5	$38·2\times10^{-5}$	$26·1\times10^{-9}$
261·5	7·48	31·9	$41·6\times10^{-5}$	$34·3\times10^{-9}$
274·4	7·98	33·0	$42·9\times10^{-5}$	$39·9\times10^{-9}$
285·8	8·41	33·8	$43·9\times10^{-5}$	$42·5\times10^{-9}$
294·6	8·86	34·7	$45·2\times10^{-5}$	$46·1\times10^{-9}$
308·4	9·45	35·9	$46·8\times10^{-5}$	$52·8\times10^{-9}$
337·0	11·24	39·2	$51·0\times10^{-5}$	$73·8\times10^{-9}$
357·0	14·03	43·8	$58·5\times10^{-5}$	$171·5\times10^{-9}$
385·8	17·28	48·6	$65·6\times10^{-5}$	$368·2\times10^{-9}$
391·0	19·17	51·2	$69·9\times10^{-5}$	$459·5\times10^{-9}$
402·4	25·98	59·6	$87·1\times10^{-5}$	$540·8\times10^{-9}$
414·7	32·74	66·9	$106·2\times10^{-5}$	$618·7\times10^{-9}$

RSB9
Sequential Mode I and Mode II loading
Type 1
$\Delta\sigma$ = 52 MPa, $\Delta\tau$ = 208 MPa
Produced branch crack growth

N 10^3	a mm	ΔK_I MPa$\sqrt{m}$	ΔK_{eq} $\sqrt{m}$	da/dN m/cycle
145·5	3·30	24·4	$12·2\times10^{-5}$	$4·74\times10^{-9}$
211·6	3·63	25·2	$12·6\times10^{-5}$	$6·73\times10^{-9}$
249·3	3·94	25·8	$12·9\times10^{-5}$	$7·45\times10^{-9}$
274·2	4·12	26·0	$13·0\times10^{-5}$	$7·63\times10^{-9}$
315·0	4·44	26·6	$13·3\times10^{-5}$	$8·59\times10^{-9}$
416·6	5·41	28·4	$14·2\times10^{-5}$	$10·0\times10^{-9}$
469·1	5·94	29·5	$14·7\times10^{-5}$	$12·2\times10^{-9}$
494·3	6·19	30·0	$15·0\times10^{-5}$	$11·4\times10^{-9}$
602·7	7·86	33·0	$16·5\times10^{-5}$	$17·2\times10^{-9}$

RSB10
Sequential Mode I and Mode II loading
Type 1
$\Delta\sigma$ = 156 MPa, $\Delta\tau$ = 208 MPa
Produced co-planar growth

N 10^3	a mm	ΔK_{II} MPa$\sqrt{m}$	ΔK_v $\sqrt{m}$	da/dN m/cycle
11·2	3·38	21·4	$27·8\times10^{-8}$	$35·6\times10^{-9}$
18·3	3·58	22·1	$28·6\times10^{-8}$	$28·9\times10^{-9}$
48·3	4·54	24·8	$32·2\times10^{-8}$	$38·7\times10^{-9}$
61·0	5·06	26·2	$34·1\times10^{-8}$	$45·8\times10^{-9}$
98·3	7·23	31·4	$40·8\times10^{-8}$	$76·4\times10^{-9}$
127·2	9·85	36·7	$47·8\times10^{-8}$	$124·6\times10^{-9}$
147·3	12·82	41·9	$55·9\times10^{-8}$	$176·7\times10^{-9}$
154·3	14·14	44·0	$59·3\times10^{-8}$	$179·3\times10^{-9}$
158·7	14·90	45·2	$61·9\times10^{-8}$	$219·0\times10^{-9}$
163.5	16·18	47·2	$64·7\times10^{-8}$	$302·4\times10^{-9}$
171·0	18·85	51·0	$70·8\times10^{-8}$	$421·9\times10^{-9}$
177·0	21·73	54·9	$77·9\times10^{-8}$	$529·9\times10^{-9}$
179·3	22·97	56·6	$81·9\times10^{-8}$	$806·3\times10^{-9}$
181·1	24·85	59·0	$86·0\times10^{-8}$	$1368·0\times10^{-9}$

RSB11
Sequential Mode I and Mode II loading
Type 1
$\Delta\sigma$ = 104 MPa, $\Delta\tau$ = 312 MPa
Produced branch crack growth

N 10^3	a mm	ΔK_I MPa$\sqrt{m}$	ΔK_e $\sqrt{m}$	da/dN m/cycle
27·8	2·28	29·9	$17·2\times10^{-8}$	$19·0\times10^{-9}$
47·8	2·69	31·3	$18·1\times10^{-8}$	$20·5\times10^{-9}$
62·0	3·70	33·8	$19·5\times10^{-8}$	$73·8\times10^{-9}$

RSB12
Sequential Mode I and Mode II loading
Type 1
$\Delta\sigma$ = 104 MPa, $\Delta\tau$ = 156 MPa
Produced co-planar growth

N 10^3	a mm	ΔK_{II} MPa$\sqrt{m}$	ΔK_v $\sqrt{m}$	da/dN m/cycle
11·7	3·15	15·5	$19{\cdot}4\times10^{-8}$	$4{\cdot}7\times10^{-9}$
45·3	3·31	15·9	$20{\cdot}3\times10^{-8}$	$5{\cdot}4\times10^{-9}$
126·3	3·85	17·2	$22{\cdot}1\times10^{-8}$	$8{\cdot}3\times10^{-9}$
140·8	3·98	17·4	$22{\cdot}4\times10^{-8}$	$9{\cdot}3\times10^{-9}$
157·6	4·13	17·8	$22{\cdot}9\times10^{-8}$	$12{\cdot}3\times10^{-9}$
162·2	4·19	17·9	$23{\cdot}0\times10^{-8}$	$12{\cdot}1\times10^{-9}$
174·3	4·34	18·2	$23{\cdot}1\times10^{-8}$	$13{\cdot}1\times10^{-9}$
202·7	4·82	19·2	$23{\cdot}7\times10^{-8}$	$13{\cdot}1\times10^{-9}$
278·2	5·62	20·8	$26{\cdot}5\times10^{-8}$	$16{\cdot}4\times10^{-9}$
296·2	5·91	21·3	$27{\cdot}3\times10^{-8}$	$19{\cdot}3\times10^{-9}$
313·2	6·18	21·7	$27{\cdot}8\times10^{-8}$	$22{\cdot}2\times10^{-9}$
383·6	7·86	24·5	$31{\cdot}5\times10^{-8}$	$30{\cdot}3\times10^{-9}$
386·0	8·40	25·4	$32{\cdot}8\times10^{-8}$	$27{\cdot}3\times10^{-9}$
391·3	8·75	25·9	$33{\cdot}5\times10^{-8}$	$28{\cdot}4\times10^{-9}$
433·0	9·72	27·3	$35{\cdot}4\times10^{-8}$	$27{\cdot}6\times10^{-9}$
516·8	11·66	29·9	$39{\cdot}0\times10^{-8}$	$26{\cdot}8\times10^{-9}$
525·6	11·93	30·3	$39{\cdot}3\times10^{-8}$	$30{\cdot}2\times10^{-9}$
546·9	12·61	31·1	$40{\cdot}6\times10^{-8}$	$41{\cdot}0\times10^{-9}$
562·4	13·05	31·7	$41{\cdot}3\times10^{-8}$	$34{\cdot}0\times10^{-9}$
613·1	15·03	34·1	$44{\cdot}2\times10^{-8}$	$65{\cdot}2\times10^{-9}$
695·3	22·58	42·0	$54{\cdot}9\times10^{-8}$	$145{\cdot}9\times10^{-9}$
702·9	23·82	43·2	$56{\cdot}7\times10^{-8}$	$179{\cdot}0\times10^{-9}$
711·5	25·50	44·8	$59{\cdot}0\times10^{-8}$	$253{\cdot}0\times10^{-9}$
721·3	27·98	47·1	$62{\cdot}9\times10^{-8}$	$336{\cdot}2\times10^{-9}$
727·4	30·23	49·1	$66{\cdot}0\times10^{-8}$	$417{\cdot}6\times10^{-9}$
731·5	32·01	50·7	$68{\cdot}9\times10^{-8}$	$475{\cdot}1\times10^{-9}$
737·1	34·84	53·1	$73{\cdot}1\times10^{-8}$	$559{\cdot}0\times10^{-9}$
738·8	36·11	54·2	$75{\cdot}4\times10^{-8}$	$644{\cdot}7\times10^{-9}$

RSB15
Sequential Mode I and Mode II loading
Type 2
$\Delta\sigma$ = 104 MPa, $\Delta\tau$ = 208 MPa
Produced branch crack growth

N 10^3	a mm	ΔK_I MPa$\sqrt{m}$	ΔK_e $\sqrt{m}$	da/dN m/cycle
13·22	1·99	15·9	$7{\cdot}7\times10^{-8}$	$17{\cdot}4\times10^{-9}$
57·36	2·32	17·1	$8{\cdot}3\times10^{-8}$	$7{\cdot}6\times10^{-9}$
140·46	4·30	21·0	$10{\cdot}1\times10^{-8}$	$17{\cdot}8\times10^{-9}$
147·95	4·70	24·3	$11{\cdot}7\times10^{-8}$	$53{\cdot}4\times10^{-9}$
148·73	4·80	25·3	$12{\cdot}2\times10^{-8}$	$121{\cdot}8\times10^{-9}$

RSB16
Sequential Mode I and Mode II loading
Type 2
$\Delta\sigma$ = 156 MPa, $\Delta\tau$ = 208 MPa
Produced branch crack growth

N 10^3	a mm	ΔK_I MPa$\sqrt{m}$	ΔK_{eff} $\sqrt{m}$	da/dN m/cycle
16·67	2·65	23·7	$11·6\times10^{-5}$	$34·0\times10^{-9}$
26·93	3·01	25·3	$12·4\times10^{-5}$	$59·0\times10^{-9}$
34·51	3·60	27·6	$13·5\times10^{-5}$	$102·5\times10^{-9}$
51·40	5·49	34·1	$16·6\times10^{-5}$	$183·2\times10^{-9}$
62·14	7·73	40·6	$19·9\times10^{-5}$	$278·8\times10^{-9}$
69·11	9·65	45·3	$22·1\times10^{-5}$	$360·8\times10^{-9}$
73·39	11·32	49·2	$24·0\times10^{-5}$	$461·1\times10^{-9}$
77·58	13·49	53·7	$26·3\times10^{-5}$	$623·1\times10^{-9}$
79·77	14·59	55·9	$27·4\times10^{-5}$	$786·2\times10^{-9}$
81·58	16·22	59·0	$28·9\times10^{-5}$	$1·035\times10^{-6}$
82·92	17·69	61·7	$30·2\times10^{-5}$	$1·429\times10^{-6}$
83·90	18·88	63·8	$31·3\times10^{-5}$	$1·906\times10^{-6}$
85·15	21·03	67·5	$33·1\times10^{-5}$	$2·352\times10^{-6}$
85·82	23·39	71·4	$35·0\times10^{-5}$	$4·401\times10^{-6}$
85·98	24·71	73·5	$35·8\times10^{-5}$	$7·411\times10^{-6}$

RSB17
Sequential Mode I and Mode II loading
Type 2
$\Delta\sigma$ = 104 MPa, $\Delta\tau$ = 104 MPa
Produced branch crack growth

N 10^3	a mm	ΔK_I MPa$\sqrt{m}$	ΔK_{II} $\sqrt{m}$	da/dN m/cycle
48·1	1·88	12·0	$5·8\times10^{-8}$	$2·5\times10^{-9}$
145·9	2·14	12·8	$6·2\times10^{-8}$	$2·7\times10^{-9}$
171·1	2·20	13·0	$6·3\times10^{-8}$	$2·9\times10^{-9}$
186·2	2·24	13·1	$6·3\times10^{-8}$	$2·9\times10^{-9}$
253·5	2·42	13·6	$6·6\times10^{-8}$	$3·2\times10^{-9}$
329·0	2·70	14·3	$6·9\times10^{-8}$	$3·6\times10^{-9}$
355·3	2·83	14·7	$7·1\times10^{-8}$	$3·7\times10^{-9}$
468·3	3·24	15·7	$7·6\times10^{-8}$	$5·0\times10^{-9}$
503·1	3·36	16·1	$7·8\times10^{-8}$	$6·5\times10^{-9}$
512·4	3·45	16·2	$7·8\times10^{-8}$	$6·8\times10^{-9}$
561·6	3·84	17·1	$8·3\times10^{-8}$	$8·3\times10^{-9}$
643·4	4·62	18·8	$9·1\times10^{-8}$	$12·6\times10^{-9}$
662·5	4·88	19·3	$9·3\times10^{-8}$	$15·0\times10^{-9}$
679·5	5·08	19·7	$9·5\times10^{-8}$	$16·0\times10^{-9}$
737·6	6·08	21·6	$10·5\times10^{-8}$	$21·5\times10^{-9}$
824·5	8·40	25·4	$12·3\times10^{-8}$	$36·5\times10^{-9}$
838·3	8·88	26·1	$12·6\times10^{-8}$	$41·8\times10^{-9}$
858·6	9·82	27·5	$13·3\times10^{-8}$	$48·6\times10^{-9}$
872·6	10·52	28·4	$13·8\times10^{-8}$	$52·7\times10^{-9}$
895·5	11·84	30·2	$14·7\times10^{-8}$	$61·8\times10^{-9}$
907·0	12·50	31·0	$15·0\times10^{-8}$	$66·2\times10^{-9}$
914·7	13·14	31·8	$15·4\times10^{-8}$	$69·3\times10^{-9}$
922·7	13·68	32·5	$15·8\times10^{-8}$	$73·7\times10^{-9}$
932·2	14·33	33·2	$16·1\times10^{-8}$	$80·8\times10^{-9}$
938·3	14·82	33·8	$16·4\times10^{-8}$	$84·7\times10^{-9}$
947·4	15·65	34·8	$16·9\times10^{-8}$	$93·9\times10^{-9}$
954·5	16·39	35·6	$17·3\times10^{-8}$	$101·5\times10^{-9}$
964·9	17·47	36·8	$17·9\times10^{-8}$	$111·7\times10^{-9}$
969·9	18·00	37·4	$18·2\times10^{-8}$	$121·1\times10^{-9}$
974·2	18·55	37·9	$18·4\times10^{-8}$	$132·5\times10^{-9}$
979·7	19·25	38·7	$18·8\times10^{-8}$	$144·7\times10^{-9}$
983·1	19·81	39·3	$19·2\times10^{-8}$	$154·1\times10^{-9}$
987·4	20·55	40·0	$19·5\times10^{-8}$	$169·6\times10^{-9}$
995·7	21·96	41·4	$20·2\times10^{-8}$	$186·2\times10^{-9}$
1008·4	24·46	43·8	$21·4\times10^{-8}$	$224·2\times10^{-9}$

RSB18
Sequential Mode I and Mode II loading
Type 1
$\Delta\sigma$ = 156 MPa, $\Delta\tau$ = 156 MPa
Produced coplanar crack growth

N 10^3	a mm	ΔK_{II} MPa$\sqrt{m}$	ΔK_v $\sqrt{m}$	da/dN m/cycle
5·4	3·29	15·7	$20·0\times10^{-8}$	$19·8\times10^{-9}$
18·5	3·52	16·2	$20·5\times10^{-8}$	$16·5\times10^{-9}$
99·0	4·70	18·8	$23·9\times10^{-8}$	$23·4\times10^{-9}$
109·8	5·04	19·4	$24·7\times10^{-8}$	$21·3\times10^{-9}$
123·4	5·41	20·1	$25·7\times10^{-8}$	$30·1\times10^{-9}$
131·3	5·63	20·6	$26·3\times10^{-8}$	$29·5\times10^{-9}$
147·2	5·81	20·9	$26·5\times10^{-8}$	$35·0\times10^{-9}$
182·1	7·64	24·0	$30·4\times10^{-8}$	$59·4\times10^{-9}$
192·1	8·20	24·8	$31·7\times10^{-8}$	$63·9\times10^{-9}$
199·7	8·70	25·6	$32·8\times10^{-8}$	$70·1\times10^{-9}$
206·1	9·15	26·2	$33·5\times10^{-8}$	$72·2\times10^{-9}$
227·4	10·82	28·5	$36·4\times10^{-8}$	$95·8\times10^{-9}$
234·7	11·57	29·5	$37·7\times10^{-8}$	$112·2\times10^{-9}$
245·4	12·67	30·9	$39·5\times10^{-8}$	$137·3\times10^{-9}$
252·1	13·66	32·1	$41·1\times10^{-8}$	$156·3\times10^{-9}$
261·9	15·38	34·1	$43·7\times10^{-8}$	$195·0\times10^{-9}$
266·9	16·39	35·2	$45·0\times10^{-8}$	$207·2\times10^{-9}$
272·6	17·60	36·6	$46·8\times10^{-8}$	$312·9\times10^{-9}$

RSB18 continued
Sequential Mode I and Mode II loading
$\Delta\tau$ = 156MPa, $\Delta\sigma$ starts at 156MPa, and is reduced in 10% steps
Type 1
Coplanar growth

N 10^{-3}	a mm	ΔK_I MPa$\sqrt{m}$	ΔK_e MPa$\sqrt{m}$	ΔK_{II} MPa$\sqrt{m}$	ΔK_v $\sqrt{m}$	da/dN m/cycle
274·0	18·09	33·76	$16·4\times10^{-8}$	37·5	$48·9\times10^{-8}$	$138·8\times10^{-9}$
276·2	18·49	30·6	$14·9\times10^{-8}$	37·8	$49·1\times10^{-8}$	$80·5\times10^{-9}$
283·4	18·74	27·8	$13·5\times10^{-8}$	38·1	$49·7\times10^{-8}$	$102·7\times10^{-9}$
290·1	19·07	25·6	$12·4\times10^{-8}$	38·9	$50·7\times10^{-8}$	$91·6\times10^{-9}$
297·3	20·31	23·3	$11·3\times10^{-8}$	39·4	$51·2\times10^{-8}$	$37·8\times10^{-9}$
304·5	20·44	21·0	$10·1\times10^{-8}$	39·5	$51·5\times10^{-8}$	$19·2\times10^{-9}$
318·9	20·75	19·1	$9·2\times10^{-8}$	39·8	$51·7\times10^{-8}$	$27·3\times10^{-9}$

RSB18 continued
Sequential Mode I and Mode II loading
Type 1
$\Delta\sigma$ = 60·4 MPa, $\Delta\tau$ = 156 MPa
Produced branch crack growth

N 10^3	a mm	ΔK_I MPa$\sqrt{m}$	ΔK_e $\sqrt{m}$	da/dN m/cycle
456·5	19·36	52·7	$25·6\times10^{-5}$	$42·2\times10^{-9}$
463·4	19·70	52·7	$25·6\times10^{-5}$	$34·8\times10^{-9}$
468·5	19·84	52·7	$25·6\times10^{-5}$	$27·3\times10^{-9}$
483·4	20·18	52·7	$25·6\times10^{-5}$	$21·9\times10^{-9}$
500·5	20·38	52·7	$25·6\times10^{-5}$	$17·8\times10^{-9}$
507·8	20·58	53·7	$26·2\times10^{-5}$	$17·3\times10^{-9}$
519·4	20·85	54·2	$26·4\times10^{-5}$	$20·7\times10^{-9}$
530·0	20·90	54·2	$26·4\times10^{-5}$	$23·6\times10^{-9}$
543·2	21·16	54·7	$26·7\times10^{-5}$	$36·2\times10^{-9}$
567·4	22·25	56·2	$27·4\times10^{-5}$	$40·9\times10^{-9}$
586·2	22·92	57·2	$28·0\times10^{-5}$	$41·3\times10^{-9}$

RSB20
Sequential Mode I and Mode II loading
Type 1
$\Delta\sigma$ = 156 MPa, $\Delta\tau$ = 312 MPa
Produced coplanar crack growth

N 10^3	a mm	ΔK_{II} MPa$\sqrt{m}$	ΔK_γ $\sqrt{m}$	da/dN m/cycle
2·72	3·20	31·3	$48·5\times10^{-5}$	$74·7\times10^{-9}$
6·96	3·45	32·5	$50·4\times10^{-5}$	$83·2\times10^{-9}$
13·17	4·17	35·7	$55·7\times10^{-5}$	$109·0\times10^{-9}$
17·96	4·44	36·9	$57·6\times10^{-5}$	$139·7\times10^{-9}$
21·50	5·04	39·2	$61·4\times10^{-5}$	$170·5\times10^{-9}$
28·86	6·43	44·4	$70·5\times10^{-5}$	$249·5\times10^{-9}$
33·47	7·66	48·4	$77·8\times10^{-5}$	$320·7\times10^{-9}$
41·45	10·55	56·9	$94·2\times10^{-5}$	$482·1\times10^{-9}$
43·76	11·73	60·1	$101·5\times10^{-5}$	$601·9\times10^{-9}$
45·77	12·93	63·1	$108·0\times10^{-5}$	$728·0\times10^{-9}$
47·11	14·10	66·0	$114·2\times10^{-5}$	$867·8\times10^{-9}$
47·96	14·87	67·8	$119·7\times10^{-5}$	$910·6\times10^{-9}$
48·98	15·77	69·8	$124·9\times10^{-5}$	$1·039\times10^{-6}$
49·71	16·69	71·9	$130·4\times10^{-5}$	$1·175\times10^{-6}$
50·60	17·42	73·5	$136·1\times10^{-5}$	$1·398\times10^{-6}$
51·15	18·45	75·7	$143·0\times10^{-5}$	$1·753\times10^{-6}$
51·88	19·66	78·2	$152·1\times10^{-5}$	$1·745\times10^{-6}$
52·31	20·48	79·9	$157·6\times10^{-5}$	$2·040\times10^{-6}$

RSB20 continued
Sequential Mode I and Mode II loading
Type 1
$\Delta\sigma$ 93·6 MPa, $\Delta\tau$ = 208 MPa
Produced branch crack growth

N 10^3	a mm	ΔK_I MPa$\sqrt{m}$	ΔK_e $\sqrt{m}$	da/dN m/cycle
56·3	23·10	104	104×10^{-3}	$5·57\times10^{-6}$
56·58	25·01	104	115×10^{-3}	$7·47\times10^{-6}$